



Pontificia Universidad Católica del Perú

Escuela de Posgrado

Technische Universität Ilmenau

Department of Computer Science and Automation

Application of Derivative-Free Adaptive Control to a Nanopositioning Machine

Tesis para obtener el grado académico de
Magíster en Ingeniería de Control y Automatización

Presentado por:

Ing. Mario Sebastian Velasquez Elguera

Profesor Responsable en TU Ilmenau: Prof. Dr.-Ing. Johann Reger

Profesor Responsable en PUCP: Dr.-Ing. Carlos Gustavo Pérez Zuñiga

Supervisor en TU Ilmenau: Dr.-Ing. Christoph Weise

Co-Supervisor en TU Ilmenau: M.Sc. Johannes Belkner

Abril, 2023

Informe de Similitud

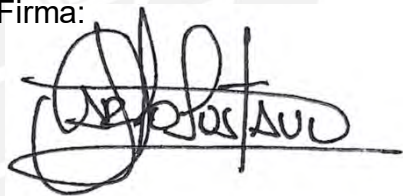
Yo, Carlos Gustavo Pérez Zuñiga, docente de la Escuela de Posgrado de la Pontificia Universidad Católica del Perú, asesor de la tesis titulada: "Application of Derivative-Free Adaptive Control to a Nanopositioning Machine" del autor Mario Sebastian Velasquez Elguera,

dejo constancia de lo siguiente:

- El mencionado documento tiene un índice de puntuación de similitud de 14.%. Así lo consigna el reporte de similitud emitido por el software Turnitin el 18/04/2023.
- He revisado con detalle dicho reporte de la Tesis y no se advierte indicios de plagio.
- Las citas a otros autores y sus respectivas referencias cumplen con las pautas académicas.

Lugar y fecha:

Lima, 18/04/2023

Apellidos y nombres del asesor: <u>Pérez Zuñiga, Carlos Gustavo</u>	
DNI: 41864666	Firma: 
ORCID: 0000-0001-5946-1395	

Abstract

Nanopositioning and nanomeasuring machines are playing an increasingly important role in the evolution of modern technologies in various fields. The Institute of Process Measurement and Sensor Technology at Ilmenau University of Technology has been researching for more than one decade high precision machines. In this direction, the general objective of this master thesis is the development of a derivative-free model reference adaptive control (DFMRAC) algorithm for the vertical axis of a nanopositioning and nanomeasuring machine. Firstly, a nonlinear unknown friction term is included in the adaptation process of a standard model reference adaptive control (MRAC) and the DFMRAC. Then, the MRAC and DFMRAC algorithms are developed theoretically, in which the DFMRAC stability analysis requires a Lyapunov-Krasovskii functional to prove that the error signal and the weight parameters are uniformly ultimately bounded (UUB). Thanks to this characteristic, the DFMRAC algorithm does not have the problem of the weight drifting parameters, as MRAC does. Overall, the new adaptive controllers have significantly better results and fine-tuning in the machine. Regarding the sine reference experimental tests with a fixed amplitude of 1 mm and a frequency from 0.25 Hz to 2 Hz, a reduction of the maximum error and root mean square error (RMSE) of about 95 % is achieved in comparison to a simple PI state-feedback controller and the previously applied MRAC with an adaptation weight matrix of lower order. Referring to the step reference tests, with a step height of 10 mm and different transition times (which are related to the maximum reached velocity from 1 mm/s to 5 mm/s) the maximum error and the RMSE are reduced approximately by 60 % and 75 %, respectively. Furthermore, the corresponding extensions to the unknown input matrix case are developed for the adaptive proposals, however it does not significantly improve the experimental results. The new controllers outperformed the previous ones with DFMRAC being the best one because it does not have the drifting weight parameters problem and it is easier to implement (no need to implement any projection method). Finally, even though, the new adaptive algorithms have extended the size of the weight matrix and added nonlinearities to the computer calculations, the execution time is only increased by around 1 μ s.

Kurzfassung

Nanopositionier- und Nanomessmaschinen spielen eine immer wichtigere Rolle bei der Entwicklung moderner Technologien in verschiedenen Bereichen. Das Institut für Prozessmess- und Sensortechnik der Technischen Universität Ilmenau forscht seit mehr als einem Jahrzehnt an Hochpräzisionsmaschinen. Das allgemeine Ziel dieser Masterarbeit ist die Entwicklung eines ableitungsfreien adaptiven Reglers (DFMRAC) für die vertikale Achse einer Nanopositionier- und Nanomessmaschine. Zunächst wird ein nichtlinearer, unbekannter Reibungsterm in den adaptiven Anteil eines klassischen adaptiven Modellfolgeregler (MRAC) und der DFMRAC einbezogen. Dann werden die MRAC- und DFMRAC-Algorithmen theoretisch entwickelt, wobei die Stabilitätsanalyse des DFMRAC ein Lyapunov-Krasovskii-Funktional erfordert, um zu beweisen, dass das Fehlersignal und die Gewichtsparameter gleichmäßig beschränkt sind. Dank dieser Eigenschaft hat der DFMRAC nicht das Problem, dass die Gewichtsparameter driften, wie es bei MRAC der Fall ist. Insgesamt haben die neuen adaptiven Regler deutlich bessere Ergebnisse in der Maschine erzielt. Bei den experimentellen Tests mit sinusförmiger Anregung mit einer festen Amplitude von 1 mm und einer Frequenz von 0,25 Hz bis 2 Hz wird eine Verringerung des maximalen Fehlers und des mittleren quadratischen Fehlers (RMSE) von etwa 95 % im Vergleich zu einem einfachen PI-Zustandsregler und dem zuvor verwendeten MRAC. Bezogen auf die Stufenreferenztests werden bei einer Stufenhöhe von 10 mm und unterschiedlichen Übergangszeiten (die sich auf die maximal erreichte Geschwindigkeit von 1 mm/s bis 5 mm/s beziehen) der maximale Fehler und der RMSE um etwa 60 % bzw. 75 % reduziert. Darüber hinaus wurden für die adaptiven Vorschläge entsprechende Erweiterungen für den Fall einer unbekanntem Eingangsmatrix entwickelt, die jedoch keine signifikante Verbesserung der experimentellen Ergebnisse zur Folge haben. Die neuen Regler schneiden besser ab als die Bisherigen. Der ableitungsfreie Ansatz erzielt die besten Ergebnisse, da die Gewichtsparameter nicht driften und die Implementierung einfacher ist (es muss keine Projektionsmethode implementiert werden). Obwohl die neuen adaptiven Algorithmen die Größe der Gewichtsmatrix vergrößern und den Computerberechnungen Nichtlinearitäten hinzugefügt haben, ist die Ausführungszeit nur um etwa 1 μ s gestiegen.

Contents

Acronyms	iii
Symbols	iv
List of Tables	viii
List of Figures	ix
1 Introduction	1
1.1 Motivation	1
1.2 Objectives	2
1.3 Limitations and structure	3
1.4 Previous work and new considerations	3
2 Model reference adaptive control	16
2.1 What is model reference adaptive control?	16
2.2 Design of the MRAC	17
2.3 Extensions to the unknown input matrix case - MRAC	25
3 Derivative-free adaptive control	31
3.1 What is derivative-free adaptive control?	31
3.2 Design of the DFMRAC	32
3.3 Extensions to the unknown input matrix case - DFMRAC	41
4 Simulations	53
4.1 Comparison of the adaptive controllers	53
4.2 Comparisons in the noise case	59
4.3 Comparisons in the extensions to the unknown input matrix case	65
5 Experimental results	70
5.1 Sine reference tests	70
5.2 Step reference tests	89
5.3 Execution time test	96
6 Conclusions and Outlook	97
Bibliography	100

A Appendix	104
A.1 Parameter values for the simulations and adaptive controllers	104
A.2 Simulations	107
A.3 Experimental Results	108



Acronyms

DFMRAC	derivative-free model reference adaptive control
MRAC	model reference adaptive control
RMSE	root mean square error
LQR	linear quadratic regulator
NPMDM	nanopositioning and nanomeasuring demonstration machine
IPMS	Institute of Process Measurement and Sensor Technology
TUIL	Ilmenau University of Technology
IRDS	International Roadmap for Devices and Systems
ITRS	International Technology Roadmap for Semiconductors
UUB	uniformly ultimately boundedness
DOB	disturbance observer
SNR-DOB	simple noise reduction disturbance observer
PI-SFC	PI state-feedback controller

Symbols

\mathbf{A}	System matrix
\mathbf{A}_s	System matrix for simulations
$\tilde{\mathbf{A}}$	System matrix of the extended system
\mathbf{A}_m	System matrix of the reference model
\mathbf{B}	Input matrix
\mathbf{B}_s	Input matrix for simulations
$\tilde{\mathbf{B}}$	Input matrix of the extended system
\mathbf{B}_m	Input matrix of the reference model
\mathbf{B}_{mf}	Input matrix of the reference model considering feed-forward control
$\beta_s(x)$	Vector of known system parameters of the MRAC or the DFMRAC
$\tilde{\beta}(\cdot)$	Extended vector of known system parameters of the MRAC for the unknown input matrix case
$\tilde{\beta}_f(\cdot)$	Extended vector of known system parameters of the MRAC for the unknown input matrix case considering feed-forward control
$\beta_e(x)$	Extended vector of known parameters of the DFMRAC for the unknown input matrix case
$\tilde{\beta}_e(x)$	Extended vector of known parameters of the DFMRAC for the unknown input matrix case considering feed-forward control
c	Spring constant
\mathbf{C}	Output matrix
$\tilde{\mathbf{C}}$	Output matrix of the extended system
\mathbf{C}_m	Output matrix of the reference model
d	Damping constant
δ	Stribeck shape factor
$\Delta(x)$	Unknown matched uncertainty of the system
$\Delta(t, x)$	Unknown time dependent matched uncertainty of the system
$e(t)$	Measure error
F_c	Coulomb friction force

$F_e(t)$	Electromagnetic force
$F_f(t)$	Friction force
F_s	Static friction force
\mathbf{F}	Friction matrix
$\tilde{\mathbf{F}}$	Friction extended matrix
$G_a(s)$	Transfer function of the linear differentiator for the velocity estimation
Γ	Adaptation gain of the MRAC
Γ_u	Adaptation gain of the MRAC for the unknown input matrix case
\mathbf{J}	Quadratic cost function
k_m	Motor constant
k_I	Integrator parameter of the PI state-feedback control
k_p	Proportional parameter of the PI state-feedback control
k_r	Electrical resistance coefficient
k_2	Constant gain parameter of the DFMRAC (unknown input matrix)
\mathbf{k}^T	Gain parameter of the PI state-feedback control
$\tilde{\mathbf{k}}^T$	Extended gain parameter of the PI state-feedback control
\mathbf{K}_f	Gain matrix of the feed-forward control
$\tilde{\mathbf{K}}_f$	Extended gain matrix corresponding to the feed-forward control
\mathbf{K}_2	Constant gain parameter of the DFMRAC
\mathbf{K}_3	Constant gain parameter of the DFMRAC (unknown input matrix)
\mathbf{K}_{1e}	Constant parameter of the DFMRAC (unknown input matrix)
\mathbf{K}_{2e}	Constant parameter of the DFMRAC (unknown input matrix)
$\hat{\mathbf{K}}_{1e}(t)$	Estimated parameter of the DFMRAC (unknown input matrix)
$\hat{\mathbf{K}}_{2e}(t)$	Estimated parameter of the DFMRAC (unknown input matrix)
\mathcal{K}_e	Extended constant gain parameter of the DFMRAC (unknown input matrix)
λ	Unknown input matrix constant
m	Mass of the vertical system
Ω_1	Constant parameter of the DFMRAC
$\Omega_2(t)$	Parameter of the DFMRAC

$\hat{\Omega}_2(t)$	Estimated parameter of the DFMRAC
$\hat{\Omega}_{21}(t)$	Estimated parameter of the DFMRAC (unknown input matrix)
Ω_{1e}	Constant parameter of the DFMRAC (unknown input matrix)
$\Omega_{2e}(t)$	Parameter of the DFMRAC (unknown input matrix)
P	Matrix of the Lyapunov equation
P _{lqr}	Matrix of the LQR controller
Ψ_1	Parameter of the DFMRAC
Ψ_2	Parameter of the DFMRAC
Ψ_3	Parameter of the DFMRAC
ϕ	Constant parameter corresponding to the unknown input matrix
Q	Matrix of the Lyapunov equation
Q _{lqr}	Weighting matrix of the LQR controller
$r(t)$	Target or reference position
$\dot{r}(t)$	Target or reference velocity
$\ddot{r}(t)$	Target or reference acceleration
R	Matrix corresponding to the reference
$\tilde{\mathbf{R}}$	Extended matrix corresponding to the reference
R _{lqr}	Weighting matrix of the LQR controller
ρ	Parameter for the Lyapunov candidate function
$\tilde{\mathbf{S}}$	Controllability matrix
σ	Viscous friction force coefficient
t	time
τ	Filter time constant
$u(t)$	Controller output signal
$u_{ad}(t)$	Adaptive controller output signal
$u_{dob}(t)$	DOB-based controller output signal
$u_n(t)$	Nominal controller output signal
$u_{nf}(t)$	Nominal controller output signal considering feed-forward control
$u_{opt}(t)$	Optimal controller
$u_{pi,1}(t)$	PI state-feedback controller output signal

$u_{\text{pi},2}(t)$	PI state-feedback controller output signal considering feed-forward control
$u_{\text{fwd}}(t)$	Feed-forward controller output signal
v_s	Stribeck velocity
\mathcal{V}	Lyapunov function
\mathbf{W}_s	Unknown constant weight matrix of the system
\mathbf{W}	Extended unknown constant weight matrix of the system
\mathbf{W}_e	Extended unknown constant weight matrix of the system for DFMRAC considering the unknown input matrix case
$\hat{\mathbf{W}}_s(t)$	Estimated unknown constant weight matrix of the system
$\hat{\mathbf{W}}(t)$	Extended estimated unknown constant weight matrix of the system
$\hat{\mathbf{W}}_e(t)$	Estimated extended unknown constant weight matrix of the system for DFMRAC considering the unknown input matrix case
$\mathbf{x}(t)$	State vector
$x_1(t)$	Additional state
$\tilde{\mathbf{x}}(t)$	Extended state vector
$\mathbf{x}_m(t)$	State vector of the reference model
$\mathbf{\Xi}_{11}$	Constant gain parameter of the DFMRAC (unknown input matrix)
$\hat{\mathbf{\Xi}}_{12}(t)$	Parameter of the DFMRAC (unknown input matrix)
$\mathbf{\Xi}_{21}$	Constant gain parameter of the DFMRAC (unknown input matrix)
$\hat{\mathbf{\Xi}}_{22}(t)$	Parameter of the DFMRAC (unknown input matrix)
$y(t)$	Output value, actual vertical position
$\tilde{\mathbf{Y}}(t)$	Desired vector reference
$z(t)$	Position of the vertical axis
$\dot{z}(t)$	Velocity of the vertical axis
$\ddot{z}(t)$	Acceleration of the vertical axis

List of Tables

1	Parameters of the system. Adapted from [19].	6
2	RMSE and maximum error of the sine simulation.	54
3	RMSE and maximum error of the noise case simulation.	60
4	Maximum error values in nm of the changing sine amplitude test. . .	78
5	RMSE values in nm of the changing sine amplitude test.	80
6	Maximum error values of the sine reference test with different fre- quencies and a fixed 100 nm amplitude.	85
7	RMSE values of the sine reference test with different frequencies and a fixed 100 nm amplitude.	86
8	Maximum error values of the sine reference test with different fre- quencies and a fixed 1 mm amplitude.	87
9	RMSE values of the sine reference test with different frequencies and a fixed 1 mm amplitude.	88
10	Parameters of the system for the simulations	104
11	PI state control parameters.	105
12	Gain parameters of the adaptive controllers	106
13	RMSE and maximum error for the extensions to the unknown input matrix.	108
14	Maximum error values in nm of the changing sine amplitude test. . .	108
15	RMSE values in nm of the changing sine amplitude test.	108
16	Maximum error values in nm from step experiment.	123
17	RMSE values in nm from step experiment.	123
18	Maximum error in nm when testing a step reference at different ve- locities.	125
19	RMSE in nm when testing a step reference at different velocities. . . .	125

List of Figures

1	Vertical axis of the NPMDM.	4
2	Mass-spring-damper system.	5
3	Friction force with the Stribeck effect. Extracted from [6].	7
4	Friction force with a sign function approximation.	7
5	Bode diagram of the 2 nd Order linear differentiator.	8
6	Classical disturbance observer scheme.	14
7	MRAC scheme adopted to the nanopositioning machine.	16
8	DFMRAC scheme adopted to the nanopositioning machine.	31
9	Output response to a sine reference when applying the old MRAC, new MRAC and DFMRAC.	53
10	Error, $e(t) = r(t) - x_1(t)$, when applying the old MRAC, new MRAC and DFMRAC.	54
11	Estimated weight $\hat{\mathbf{W}}_s(t)$ of the old MRAC.	55
12	Estimated weight $\hat{\mathbf{W}}_s(t)$ of the new MRAC.	56
13	Estimated weight $\hat{\mathbf{W}}_s(t)$ of the DFMRAC.	57
14	Ideal vs estimated matched uncertainty of the simulated controllers.	58
15	Output response to a pulse reference when applying the old MRAC, new MRAC and DFMRAC considering sensor noise.	59
16	Error, $e(t) = r(t) - x_1(t)$, when applying the old MRAC, new MRAC and DFMRAC considering sensor noise.	59
17	Estimated weight $\hat{\mathbf{W}}_s(t)$ of the old MRAC considering sensor noise.	60
18	Estimated weight $\hat{\mathbf{W}}_s(t)$ of the new MRAC considering sensor noise.	61
19	Estimated weight $\hat{\mathbf{W}}_s(t)$ of the DFMRAC considering sensor noise.	62
20	Ideal vs estimated matched uncertainty term of the new MRAC and DFMRAC considering sensor noise.	63
21	Nominal and adaptive control output of the old MRAC, new MRAC and DFMRAC considering sensor noise.	64
22	Output response to a sine reference when applying the “MRAC un” and “DFMRAC un” and sensor noise.	65
23	Error, $e(t) = r(t) - x_1(t)$, when applying the “MRAC un” and “DFM- RAC un” and sensor noise to a sine reference.	65
24	Estimated weights $\hat{\mathbf{W}}_s(t)$ of the “MRAC un”.	66
25	Estimated weight of the “DFMRAC un”.	67
26	Ideal vs estimated matched uncertainties of the “MRAC un” and “DFMRAC un”.	68

27	Nominal and adaptive control output of the “MRAC un” and “DFM-RAC un” considering sensor noise.	69
28	Output response to a $r(t) = 100 \sin(0.2\pi t)$ nm reference when applying the DFMRAC.	70
29	Error, $e(t) = r(t) - x_1(t)$, to a sine reference of 100 nm amplitude. . .	71
30	Estimated weight $\hat{\mathbf{W}}_s(t)$ of the old MRAC.	72
31	Estimated weight $\hat{\mathbf{W}}_s(t)$ of the new MRAC.	73
32	Estimated weight $\hat{\mathbf{W}}_s(t)$ of the DFMRAC.	74
33	Error comparisons to a $r(t) = 1000 \sin(0.2\pi t)$ nm reference.	75
34	Error comparisons to a $r(t) = 1 \sin(0.2\pi t)$ mm reference.	75
35	Error comparisons to a $r(t) = 4 \sin(0.2\pi t)$ mm.	76
36	Sine references with different amplitudes from 50 nm to 5 mm with a fixed frequency of 0.2 Hz.	77
37	Maximum error of the sine reference test with different amplitudes and a fixed frequency of 0.2 Hz.	77
38	Maximum error of the sine reference test with different amplitudes and a fixed frequency of 0.2 Hz (zoomed version).	78
39	RMSE of the sine reference test with different amplitudes and a fixed frequency of 0.2 Hz.	79
40	Control output comparison regarding the changing sine amplitude test with a 5 mm amplitude and a 0.2 Hz frequency.	81
41	Nominal, adaptive and DOB-based control output comparisons regarding the changing sine amplitude test with a 5 mm amplitude and a 0.2 Hz frequency.	82
42	Maximum error and RMSE comparison for the reduced adaptive controllers regarding the changing sine amplitude test with a 5 mm amplitude and a 0.2 Hz frequency.	83
43	Maximum error of the sine reference test with different frequencies and a fixed 100 nm amplitude.	84
44	RMSE of the sine reference test with different frequencies and a fixed 100 nm amplitude.	85
45	Maximum error of the sine reference test with different frequencies and a fixed 1 mm amplitude.	86
46	RMSE of the sine reference test with different frequencies and a fixed 1 mm amplitude.	87
47	RMSE of the sine reference test with different frequencies and a fixed 1 mm amplitude (zoomed version).	88

48	Output response to a 10 μm step height reference with DFMRAC. . .	89
49	Error, $e(t) = r(t) - x_1(t)$, regarding a 10 μm step height reference. . .	90
50	Error, $e(t) = r(t) - x_1(t)$, regarding a 1 mm step height reference. . .	91
51	Output response to a multi-step reference with DFMRAC.	91
52	Comparison of the error $e(t) = r(t) - x_1(t)$ of a multi-step reference in the NPMDM.	92
53	Step references with a fixed height of 10 mm and different transition times.	92
54	Different velocities plot for a 10 mm step height.	93
55	Maximum error and RMSE regarding a step reference at different velocities.	93
56	Nominal, adaptive and DOB-based control output comparison of the new MRAC and DFMRAC regarding the changing step maximum velocity test at 5 mm/s velocity.	94
57	Maximum error and RMSE comparison for the reduced adaptive con- trollers regarding the changing step maximum velocity test at 5 mm/s velocity.	95
58	Execution time when applying different controllers.	96
59	Noise reduction disturbance observer-based controller scheme. Ex- tracted from [10].	98
60	Output response and error, $e(t) = r(t) - x_1(t)$, comparison between DOB and SNR-DOB.	99
61	Simulink blocks of the system	107
62	Output response to a $r(t) = 1000 \sin(0.2\pi t)$ nm reference when ap- plying DFMRAC.	109
63	Output response to a $r(t) = 1 \sin(0.2\pi t)$ mm reference when applying DFMRAC.	109
64	Output response to a $r(t) = 4 \sin(0.2\pi t)$ mm reference when applying DFMRAC.	110
65	Error comparison regarding the changing sine test with a 5 mm am- plitude and a 0.2 Hz frequency.	111
66	Adaptive control output comparison of the old MRAC, DFMRAC, “DFMRAC un” regarding the changing sine amplitude test with a 5 mm amplitude and a 0.2 Hz frequency.	111
67	Adaptive control terms of the old MRAC regarding the changing sine amplitude test with a 5 mm amplitude and a 0.2 Hz frequency. . . .	112

68	Adaptive control terms of the new MRAC regarding the changing sine amplitude test with a 5 mm amplitude and a 0.2 Hz frequency.	113
69	Adaptive control terms of the “MRAC un” regarding the changing sine amplitude test with a 5 mm amplitude and a 0.2 Hz frequency. . .	114
70	Adaptive control terms of the DFMRAC regarding the changing sine amplitude test with a 5 mm amplitude and a 0.2 Hz frequency.	115
71	Adaptive control terms of the “DFMRAC un” regarding the changing sine amplitude test with a 5 mm amplitude and a 0.2 Hz frequency. . .	116
72	Adaptive control terms of the “DFMRAC un” regarding the changing sine amplitude test with a 5 mm amplitude and a 0.2 Hz frequency. . .	117
73	Adaptive control terms of the old MRAC regarding the changing step maximum velocity test at 5 mm/s velocity.	118
74	Adaptive control terms of the new MRAC regarding the changing step maximum velocity test at 5 mm/s velocity.	119
75	Adaptive control terms of the DFMRAC regarding the changing step maximum velocity test at 5 mm/s velocity.	120
76	Adaptive control terms of the “DFMRAC un” regarding the changing step maximum velocity test at 5 mm/s velocity.	121
77	Adaptive control terms of the “DFMRAC un” regarding the changing step maximum velocity test at 5 mm/s velocity.	122
78	Output response to a 1 mm step height reference with DFMRAC. . .	123
79	Velocity of the double step reference test with a step height of 10 μm . . .	124
80	Velocity of the double step reference test with a step height of 1 mm. . .	124
81	Velocity for the multi-step reference test.	124

1 Introduction

This chapter first describes the motivation and the context in which this master's thesis is developed. Secondly, the main objective is established. Thirdly, the limitations and structure of this thesis are outlined. Finally, the principle of operation of the machine, the control strategies that were previously implemented and the new considerations that will be taken are described.

1.1 Motivation

High-precision nanopositioning and nanomeasuring machines (NPM-machines) are playing an increasingly important role in the evolution of modern technologies in various fields, such as microscopy, semiconductors, optics and materials science, among others. The International Roadmap for Devices and Systems (IRDS), successor of the International Technology Roadmap for Semiconductors (ITRS), has already set its projections regarding the development of electronic devices and systems. In Chapter Metrology, device feature sizes are projected to decrease to less than 5 nm within the next 10 years. They are also expected to reach soon its physical limits or get to a point where cost and reliability issues far outweigh the benefits. It is reported that device structures will evolve from FinFETs (fin-shaped field-effect transistor) to GAA (gate-all-around) based on nanowires. That will cause a reduction in the “node range” labelling in the logic industry to 2.1 nm by 2025 and other considerations such as new metrology techniques, structures and materials. Transistors for chips at the 5 – 2 nm nodes have already been demonstrated [11].

To meet technological demands, the Institute of Process Measurement and Sensor Technology (IPMS) at Ilmenau University of Technology (TUIL) has been researching and developing NPM-machines for several years providing high-precision measurement and positioning of objects, from 20 pm resolution up to 200 mm measuring range [21]. In 2000, the NPMM-1 machine was built in partnership with SIOS Meßtechnik GmbH, with a measuring range of 25 mm × 25 mm × 5 mm [13]. Due to the limitation of its measuring ranges, in 2010 the nanopositioning and nanomeasuring demonstration machine (NPMDM) was produced with a measurement range of 200 mm × 200 mm [1]. On this background, the next generation, the NPMM-200 with a measuring range of 200 mm × 200 mm × 25 mm and a resolution of 20 pm based on SIOS fibre-coupled laser interferometry and other technologies, was launched in 2016 [14].

Lately, the vertical axis for the NPMDM has been built and since that new control algorithms and parameter identification techniques have been applied in order to improve the machine in terms of repeatability, precision, accuracy and robustness. The last control algorithm, implemented for the vertical axis for the NPMDM, is the model reference adaptive control (MRAC) in [19]. It shows under certain conditions an average error of approximately 10 nm and peak errors of 35 nm. However, the resolution of the interferometer, sensor that measures the distance, is 5 pm. Therefore, there is still room for improvement. Furthermore, recent research in the NPMDM suggest the addition of a nonlinear friction term in the adaptive control algorithm to improve the error [19]. In this context, the motivation for the development of the present thesis was born, which proposes the application of a derivative-free model reference adaptive control (DFMRAC) algorithm that includes the nonlinear friction force in the system dynamics and further considerations.

1.2 Objectives

The main objective is the development of a derivative-free adaptive control algorithm for the vertical axis of the nanopositioning and nanomeasuring demonstration machine of the Institute of Process Measurement and Sensor Technology at Ilmenau University of Technology.

The specific objectives of this thesis are:

1. Review the principle of operation of the machine, the sensors and actuators involved, the system parameters and the current control algorithms already implemented for the vertical axis of the NPMDM.
2. Investigate and develop the MRAC and DFMRAC control algorithms, which both consider the friction force in the system dynamics. It is a desire to implement their respective extensions to the unknown input matrix.
3. Implement and test the control algorithms (MRAC and DFMRAC), first in the Matlab and Simulink environment, and then in the real NPMDM.
4. Compare and analyse the root mean square error (RMSE) and maximum error in the output obtained by the previous MRAC algorithm and the new proposed controllers. It is a desire to apply other methods to analyze the error.

1.3 Limitations and structure

This research is limited to the development of the DFMRAC algorithm and its application only for the vertical axis of the NPMDM. In addition, this thesis does not study system identification techniques to obtain the parameters of the system, however it considers the model values obtained previously in [19]. Finally, the redesign of mechanical parts or sensors of the current NPMDM machine is not part of the scope of the thesis.

The content of this thesis will cover the study of the MRAC and DFMRAC algorithms with their respective computational simulations, and finally both algorithms will be implemented and tested in the real NPMDM. The structure of this thesis is as follows: In Chapter 2, the MRAC algorithm is presented but including the nonlinear friction in the model. It is also given its extension to the unknown input matrix case. In Chapter 3, it is described the DFMRAC which also includes the nonlinear friction and its extension to the unknown input matrix case. Chapter 4 shows the simulations of the algorithms in the Matlab-Simulink environment, whereas Chapter 5 shows the experiments performed in the real NPMDM. Finally, at the end of the document, the conclusions are described and some proposals for future work are provided.

1.4 Previous work and new considerations

In this section, first it is explained the principle of operation of the vertical axis of the NPMDM. Secondly, it is recalled the system dynamics given in [19], but now with the new friction considerations. Thirdly, it is explained the velocity estimation of the system, which is already developed in the machine. In fourth place, the PI state-feedback, feed-forward and disturbance observer-based controllers are explained. The mentioned controllers were implemented in a similar approach in [19]. Finally, the performance criteria for the simulations and the experiments are outlined.

1.4.1 Principle of operation

This document will briefly describe the principle of operation of the system, more information and details about sensors, actuators and hardware are given in [19]. Figure 1 shows the structure and principal components of the vertical axis of the NPMDM. The mechanism is assembled to a stainless steel structure. The actuator of the system is a plunger coil actuator manufactured by Moticont (3). In order

to compensate the weight force, it has been coupled a compression spring (4). To measure the length, a Michelson interferometer type SP 120 (based on a frequency stabilized He-Ne laser with a length resolution of 5 pm) from SIOS Messtechnik GmbH is employed. At the top, it is placed the measuring head of the interferometer (1) and in (2) it is situated the measuring mirror. Below, the target header (6) is adjusted in a vertical cage. The cage is guided by three linear ball bearings (5), which minimizes friction and tilting.

The controller of the NPMDM is implemented using the rapid-prototyping-system from dSPACE and the DS1006 processor board allows its execution in real time. In addition, DS4003 digital I/O boards are used for the communication between sensors and actuators. DS4003 board is connected to the evaluation unit of the interferometer to obtain the length measurement in the form of digital 32 bits through the parallel data transmission. DS2102 D/A card controls the plunger coil actuator using the power amplifier. It converts the digital value read by the interferometers to voltage in the power output stage. Then, the power output stage converges the voltage signal in the range ± 10 V to the current signal in the range ± 3 A. The control algorithm is developed using Matlab and Simulink. The sample time for the Simulink blocks code is set at 0.0001 s. Also, the output of the controller

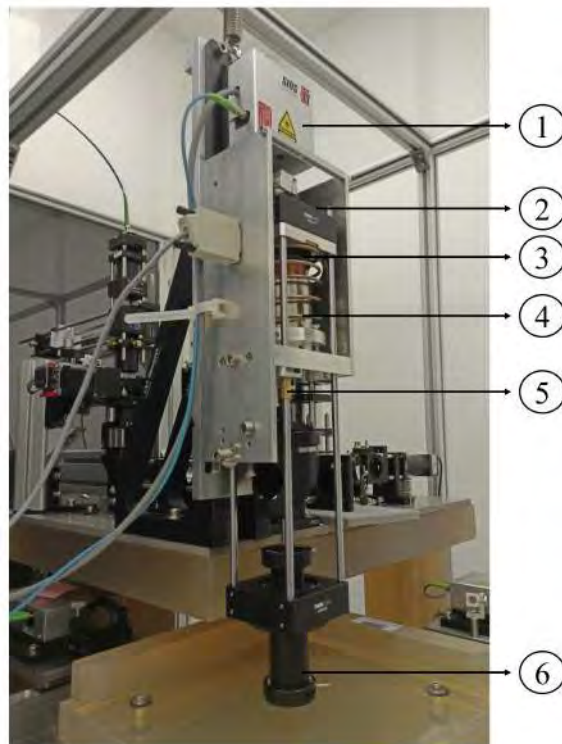


Figure 1: Vertical axis of the NPMDM.

is saturated between -0.4 and 0.75 , which was determined by previous experiences [19]. The real-time interface block from dSPACE allows that the Simulink sequential language can be overlaid as ANSI C. Additionally, there is a supporting software ControlDesk from dSPACE, which is used to change the control parameters online and also to observe and save the reading signals.

1.4.2 System dynamics

The vertical axis of the NPMDM can be simplified as a mass-spring-damper system, see Figure 2. The corresponding dynamic equation can be obtained using the Newton's second law:

$$m\ddot{z}(t) + d\dot{z}(t) + cz(t) = F_e(t) - F_r(t), \quad (1)$$

where m is mass, d is damping constant, c is spring constant, $z(t)$ is the position of the vertical axis, $F_e(t)$ is the electromagnetic force and $F_r(t)$ corresponds to the friction force. The electromagnetic force is approximated as proportional to the current magnitude $F_e(t) = k_m i(t)$, where k_m is a motor constant. The current signal is controlled by the dSPACE-Machine, which can be represented by $u(t) = (1/k_r)i(t)$, where k_r is the electrical resistance coefficient. The values of the system parameters are extracted from a previous study performed in the NPMDM, master thesis of Phattaradanai Kiratiwudhikul [19]. Table 1 shows the values of the mentioned parameters.

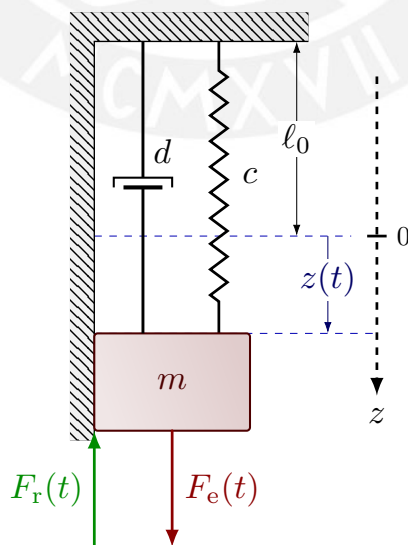


Figure 2: Mass-spring-damper system.

Table 1: Parameters of the system. Adapted from [19].

Parameter	Value	Unit
Mass and objective m	1.875	kg
Spring stiffness c	299	N/m
Damping constant d	10.34	N _s /m
Motor constant k_m	7	N/A
Electrical resistance coefficient k_r	1	unitless

Finally, is possible to represent Equation (1) in the form of a state space equation:

$$\underbrace{\begin{bmatrix} \dot{z}(t) \\ \ddot{z}(t) \end{bmatrix}}_{\dot{\mathbf{x}}(t)} = \underbrace{\begin{bmatrix} 0 & 1 \\ -\frac{c}{m} & -\frac{d}{m} \end{bmatrix}}_{\mathbf{A}} \underbrace{\begin{bmatrix} z(t) \\ \dot{z}(t) \end{bmatrix}}_{\mathbf{x}(t)} + \underbrace{\begin{bmatrix} 0 \\ \frac{k_m k_r}{m} \end{bmatrix}}_{\mathbf{B}} u(t) - \underbrace{\begin{bmatrix} 0 \\ \frac{1}{m} \end{bmatrix}}_{\mathbf{F}} F_r(t), \quad (2a)$$

$$y(t) = \underbrace{\begin{bmatrix} 1 & 0 \end{bmatrix}}_{\mathbf{C}} \mathbf{x}(t), \quad (2b)$$

where $\mathbf{x} \in \mathbb{R}^{2 \times 1}$ is the state vector, $\mathbf{A} \in \mathbb{R}^{2 \times 2}$ is the system matrix, $\mathbf{B} \in \mathbb{R}^{2 \times 1}$ input matrix, $\mathbf{F} \in \mathbb{R}^{2 \times 1}$ is the friction vector and $\mathbf{C} \in \mathbb{R}^{1 \times 2}$ is the output matrix. Until now, the same approach was described in [19]. However, in the previous research the friction force was considered as $F_r(t) = 0$ and now it is defined as the static friction model considering the Stribeck effect [6], as shown below:

$$F_r(t) = \left[F_c + (F_s - F_c) \exp \left(- \left| \frac{\dot{z}(t)}{v_s} \right|^\delta \right) \right] \text{sign}(\dot{z}(t)) + \sigma \dot{z}(t), \quad (3)$$

where F_c denoted the Coulomb friction force, F_s is the maximum static friction force, σ is the coefficient of viscous friction, v_s represented the Stribeck velocity and δ is the Stribeck shape factor.

Figure 3 shows the shape of the friction force respect to velocity. It also shows the effects of each mentioned parameter on the previous function. As stated before, no identifications techniques will be implemented in this master thesis. Nevertheless, it will be explained later that for the proposed adaptive algorithms it is not necessary to known all the friction parameters, but v_s and δ . However, as shown in Figure 3, both have only influence on the slope of the viscous friction and could therefore be roughly estimated. The friction force parameters considered for the simulations can be found in Appendix A.1. In addition, it is found that $\text{sign}(x_2)$ function causes problems in the computational simulations and also in the implementation in the real

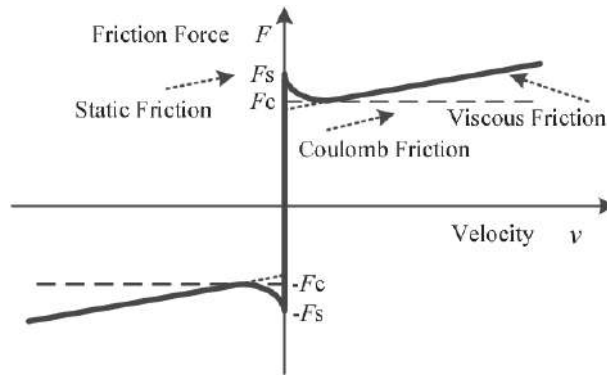


Figure 3: Friction force with the Stribeck effect. Extracted from [6].

system due to its discontinuity near zero velocity. For that reason, an approximation using a continuous $\text{atan}(k_{\text{atg}}x_2)$ function is proposed, where the gain k_{atg} adjusts the curve approximation, see Figure 4.

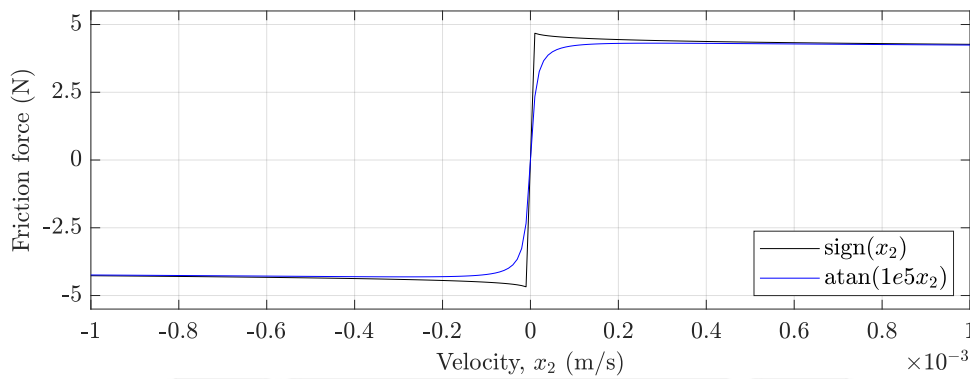


Figure 4: Friction force with a sign function approximation.

1.4.3 Estimation of the velocity

The position in the NPMDM is measured by the interferometer. However, there is no sensor available to measure the velocity and the acceleration. Consequently, the velocity is estimated using the derivative of the position with the second order linear filter with a cutoff frequency $(1/\tau)$ set at 1 kHz, whereas the acceleration is estimated using the second derivative. This approach was previously explained and implemented in [19]. The transfer function of the differentiator is shown below:

$$G_a(s) = \frac{s}{(\tau s + 1)^2} . \quad (4)$$

The bode diagram of $G_a(s)$ can be shown in Figure 5.

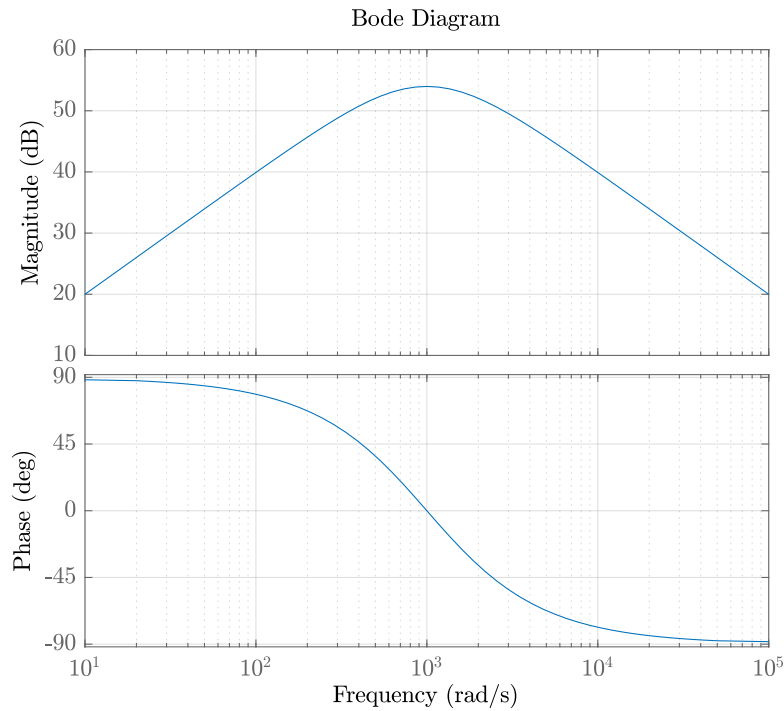


Figure 5: Bode diagram of the 2nd Order linear differentiator.

1.4.4 PI state-feedback controller

In this subsection the PI state-feedback controller (PI-SFC) will be developed. This document divide the PI-SFC equations without considering the feed-forward control and when it is considered. To begin with, the nominal control $u_n(t)$ is defined as:

$$u_n(t) = u_{pi,1}(t) + u_{fwd}(t) . \quad (5)$$

In this first approach, it is consider $u_{fwd}(t) = 0$. Later, the feed-forward control and its considerations will be added and explained. The procedure followed to build this controller can be found in [22]. Therefore, $u_n(t) = u_{pi,1}(t)$ is as follows:

Remark 1. *PI state-feedback controller output signal:*

$$u_{pi,1}(t) = -\mathbf{k}^T \mathbf{x}(t) + k_p e(t) + k_I \int_{t_o}^t e(\tau) d\tau . \quad (6)$$

Then, the error equation is:

$$e(t) = r(t) - y(t) = r(t) - \mathbf{C}\mathbf{x}(t) . \quad (7)$$

The integral part can be defined as another state variable

$$x_I(t) := \int_{t_o}^t e(\tau) d\tau , \quad (8)$$

which derivative is:

$$\dot{x}_I(t) = e(t) = r(t) - \mathbf{C}\mathbf{x}(t) . \quad (9)$$

The new state $x_I(t)$ is added to the system in (2a) to obtain the extended matrix $\tilde{\mathbf{A}}$ as follows:

$$\underbrace{\begin{bmatrix} \dot{\mathbf{x}} \\ \dot{x}_I \end{bmatrix}}_{\dot{\tilde{\mathbf{x}}}(t)} = \underbrace{\begin{bmatrix} \mathbf{A} & \mathbf{0} \\ -\mathbf{C} & \mathbf{0} \end{bmatrix}}_{\tilde{\mathbf{A}}} \underbrace{\begin{bmatrix} \mathbf{x} \\ x_I \end{bmatrix}}_{\tilde{\mathbf{x}}(t)} + \underbrace{\begin{bmatrix} \mathbf{B} \\ \mathbf{0} \end{bmatrix}}_{\tilde{\mathbf{B}}} u(t) - \underbrace{\begin{bmatrix} \mathbf{F} \\ 0 \end{bmatrix}}_{\tilde{\mathbf{F}}} F_r(t) + \underbrace{\begin{bmatrix} \mathbf{0} \\ 1 \end{bmatrix}}_{\tilde{\mathbf{R}}} r(t) . \quad (10)$$

Then, equations (7) and (8) are replaced in (6):

$$\begin{aligned} u_n(t) &= k_p(r(t) - \mathbf{C}\mathbf{x}(t)) + \begin{bmatrix} -\mathbf{k}^T & k_I \end{bmatrix} \begin{bmatrix} \mathbf{x}(t) \\ x_I(t) \end{bmatrix} \\ &= k_p r(t) - \underbrace{\begin{bmatrix} \mathbf{k}^T + k_p \mathbf{C} & -k_I \end{bmatrix}}_{\tilde{\mathbf{k}}^T(t)} \underbrace{\begin{bmatrix} \mathbf{x}(t) \\ x_I(t) \end{bmatrix}}_{\tilde{\mathbf{x}}(t)} . \end{aligned} \quad (11)$$

Finally, Equation (12) is obtained after grouping some terms into a extended gain parameter $\tilde{\mathbf{k}}^T$.

Remark 2. *Nominal controller output signal without feed-forward control:*

$$u_n(t) = -\tilde{\mathbf{k}}^T \tilde{\mathbf{x}}(t) + k_p r(t) . \quad (12)$$

The control law $u_n(t)$ shown in (12) will be used to study the stability of the closed loop. Referring to [22] and common literature, all the roots (poles) of the characteristic polynomial of a linear system must have negative real parts in order to be stable. Thus, it must be ensured that the roots of the closed loop system,

$$\dot{\tilde{\mathbf{x}}}(t) = (\tilde{\mathbf{A}} - \tilde{\mathbf{B}}\tilde{\mathbf{k}}^T)\tilde{\mathbf{x}}(t) , \quad (13)$$

are negative. The parameters related to the extended matrices $\tilde{\mathbf{A}}$ and $\tilde{\mathbf{B}}$ are shown below:

$$\underbrace{\begin{bmatrix} \dot{x}_1(t) \\ \dot{x}_2(t) \\ \dot{x}_I(t) \end{bmatrix}}_{\dot{\tilde{\mathbf{x}}}(t)} = \underbrace{\begin{bmatrix} 0 & 1 & 0 \\ -\frac{c}{m} & -\frac{d}{m} & 0 \\ -1 & 0 & 0 \end{bmatrix}}_{\tilde{\mathbf{A}}} \underbrace{\begin{bmatrix} x_1(t) \\ x_2(t) \\ x_I(t) \end{bmatrix}}_{\tilde{\mathbf{x}}(t)} + \underbrace{\begin{bmatrix} 0 \\ \frac{k_m k_r}{m} \\ 0 \end{bmatrix}}_{\tilde{\mathbf{B}}} u(t) - \underbrace{\begin{bmatrix} 0 \\ \frac{1}{m} \\ 0 \end{bmatrix}}_{\tilde{\mathbf{F}}} F_r(t) + \underbrace{\begin{bmatrix} 0 \\ 0 \\ 1 \end{bmatrix}}_{\tilde{\mathbf{R}}} r(t). \quad (14)$$

Firstly, there is a need to check the controllability of the system, in order to ensure that the state variables can be controlled to achieve the desired output. The controllability matrix $\tilde{\mathbf{S}}$ is:

$$\tilde{\mathbf{S}} = \begin{bmatrix} \tilde{\mathbf{B}} & \tilde{\mathbf{A}}\tilde{\mathbf{B}} & \tilde{\mathbf{A}}^2\tilde{\mathbf{B}} \end{bmatrix}. \quad (15)$$

To achieved a controllable closed loop system, the matrix $\tilde{\mathbf{S}}$ should have full rank or analogously $\det(\tilde{\mathbf{S}}) \neq 0$. The system is found to be controllable, due to $\text{rank}(\tilde{\mathbf{S}})=3$.

Secondly, the $\tilde{\mathbf{k}}$ extended gain can be determined as a solution of the linear quadratic regulator (LQR) problem, also called the H_2 problem, the procedure could be found in [2]. The aim is to determine $u_{\text{opt}}(t)$, which minimizes the quadratic cost in time $t \geq 0$:

$$\mathbf{J}(u) = \frac{1}{2} \int_0^\infty \tilde{\mathbf{x}}^T(t) \mathbf{Q}_{\text{lqr}} \tilde{\mathbf{x}}(t) + u_{\text{opt}}^T(t) \mathbf{R}_{\text{lqr}} u_{\text{opt}}(t) dt, \quad (16)$$

with \mathbf{Q}_{lqr} , \mathbf{R}_{lqr} real, symmetric ($\mathbf{Q}_{\text{lqr}} = \mathbf{Q}_{\text{lqr}}^T$, $\mathbf{R}_{\text{lqr}} = \mathbf{R}_{\text{lqr}}^T$) and $\mathbf{Q}_{\text{lqr}} \geq 0$, $\mathbf{R}_{\text{lqr}} > 0$ matrices.

The optimal control is determined as:

$$u_{\text{opt}}(t) = -(\mathbf{R}_{\text{lqr}})^{-1} \tilde{\mathbf{B}}^T \mathbf{P}_{\text{lqr}} \tilde{\mathbf{x}}(t) = -\tilde{\mathbf{k}}^T \tilde{\mathbf{x}}(t). \quad (17)$$

The values for the matrices \mathbf{Q}_{lqr} and \mathbf{R}_{lqr} are shown below:

$$\mathbf{Q}_{\text{lqr}} = \text{diag}(10^8, 10^3, 4 \times 10^{13}), \quad (18)$$

$$\mathbf{R}_{\text{lqr}} = 10, \quad (19)$$

which were studied and proposed before for this plant in [19]. Finally, it is important to replace $\tilde{\mathbf{k}}^T$ in Equation (13) and check that the roots of the closed loop system

are all negative, which is fulfilled in this case. Afterwards, it is possible to determine \mathbf{k}^T , k_p and k_I , since $\tilde{\mathbf{k}}^T$ is defined in (11). If $\tilde{\mathbf{k}}^T = [\tilde{k}_1, \dots, \tilde{k}_{n+1}]$, then \mathbf{k}^T and k_I could be written as:

$$\mathbf{k}^T = (\tilde{k}_1, \dots, \tilde{k}_n) - k_p \mathbf{C}, \quad (20)$$

$$k_I = -\tilde{k}_{n+1}. \quad (21)$$

To obtain k_p , Equation (12) is replaced in (2a). Then, the result is evaluated in $t \rightarrow \infty$, where $e(\tau) = 0$ and \mathbf{x}_s is a stationary point of the state vector. Therefore, the following also applies: $x_I = \int e(\tau) d\tau = 0$, $y = r(t)$ and

$$\begin{aligned} \dot{\mathbf{x}}_s &= 0 = \mathbf{A}\mathbf{x}_s + \mathbf{B}(-(\mathbf{k}^T + k_p \mathbf{C})\mathbf{x}_s + k_I x_I + k_p r(t)) \\ 0 &= \mathbf{A}\mathbf{x}_s + \mathbf{B}\left(-(\tilde{k}_1, \dots, \tilde{k}_n)\mathbf{x}_s + k_p r(t)\right) \\ 0 &= \left(\mathbf{A} - \mathbf{B}(\tilde{k}_1, \dots, \tilde{k}_n)\right)\mathbf{x}_s + \mathbf{B}k_p r(t) \\ \mathbf{x}_s &= -\left(\mathbf{A} - \mathbf{B}(\tilde{k}_1, \dots, \tilde{k}_n)\right)^{-1} \mathbf{B}k_p r(t). \end{aligned} \quad (22)$$

Replacing (22) in (2a) and equaling to $r(t)$:

$$\begin{aligned} y &= \mathbf{C}\mathbf{x}_s = r(t) \\ &= -\mathbf{C}\left(\mathbf{A} - \mathbf{B}(\tilde{k}_1, \dots, \tilde{k}_n)\right)^{-1} \mathbf{B}k_p r(t) = r(t). \end{aligned} \quad (23)$$

Finally, k_p is:

$$k_p = -\frac{1}{\mathbf{C}\left(\mathbf{A} - \mathbf{B}(\tilde{k}_1, \dots, \tilde{k}_n)\right)^{-1} \mathbf{B}}. \quad (24)$$

1.4.5 Feed-forward controller

Feed-forward control is plenty used in the literature to control the effects of measurable disturbances, leaving the incompletely feed-forward controlled parts and the effect of not measurable disturbances on the controlled variable to feedback control [12]. However, in this document the approach of using the feed-forward control is that the output variable could ideally follows the reference variable $\tilde{\mathbf{Y}}(t)$. It is important to remark that the feed-forward control does not influence the stability of a control loop in the case of linear processes. In consequence, it can be added after the feedback controllers are tuned [12]. To build the feed-forward controller, the system state equations shown in (2a) are now equal to the ideal reference:

$$\begin{aligned}
x_1(t) &= r(t) \\
\dot{x}_1(t) &= x_2(t) = \dot{r}(t) \\
\dot{x}_2(t) &= -\frac{c}{m}x_1(t) - \frac{d}{m}x_2(t) + \frac{k_m k_r}{m}u_{\text{fwd}}(t) = \ddot{r}(t) .
\end{aligned} \tag{25}$$

In the last differential equation $\dot{x}_2(t)$, the variables $x_1(t)$, $x_2(t)$ could be replaced with $r(t)$ and $\dot{r}(t)$ respectively. Finally, the equation is solved for $u_{\text{fwd}}(t)$:

$$\begin{aligned}
u_{\text{fwd}}(t) &= \frac{m}{k_m k_r} \left(\frac{c}{m}r(t) + \frac{d}{m}\dot{r}(t) + \ddot{r}(t) \right) \\
&= \underbrace{\begin{bmatrix} \frac{c}{k_m k_r} & \frac{d}{k_m k_r} & \frac{m}{k_m k_r} \end{bmatrix}}_{\mathbf{K}_f} \underbrace{\begin{bmatrix} r(t) \\ \dot{r}(t) \\ \ddot{r}(t) \end{bmatrix}}_{\tilde{\mathbf{Y}}(t)} .
\end{aligned} \tag{26}$$

It is important to note that it is necessary to previously calculate the derivatives. To achieve that, the second order linear filter explained in section 1.4.3 is applied.

Remark 3. *Feed-forward controller output signal:*

$$u_{\text{fwd}}(t) = \mathbf{K}_f \tilde{\mathbf{Y}}(t) . \tag{27}$$

1.4.6 PI state-feedback controller with feed-forward control

Because the stability of the control loop system is not affected by adding the feed-forward control, the same parameters for $\tilde{\mathbf{k}}^T$ and consequently \mathbf{k}^T , k_p and k_I could be use. However, it is important to point out the difference between this new PI-SFC and the last proposed in Equation (6). The PI-SFC considering feed-forward control is the following:

Remark 4. *PI state-feedback controller output signal with feed-forward control:*

$$u_{\text{pi},2}(t) = -\mathbf{k}^T (\mathbf{x}(t) - \tilde{\mathbf{y}}(t)) + k_p e(t) + k_I \int_{t_o}^t e(\tau) d\tau , \tag{28}$$

where $\tilde{\mathbf{y}}(t) = \begin{bmatrix} r(t) & \dot{r}(t) \end{bmatrix}^T$. Precisely, $e(t)$ should be $e(t) = \text{ref} - (x_1(t) - r(t))$, but $\text{ref} = 0$. Therefore, $e(t)$ could be define as before $e(t) = r(t) - x_1(t)$.

Defining x_I as before, $x_I(t) := \int_{t_o}^t e(\tau) d\tau$, it can be seen that the procedure to obtain

the extended state space equations could be done in a similar way as it was done for (10), however now with a different nominal controller. The nominal control considering feed-forward control is defined as:

$$u_{\text{nf}}(t) = u_{\text{pi},2}(t) + u_{\text{fwd}}(t) . \quad (29)$$

Replacing (28) and (27) in (29), $u_{\text{nf}}(t)$ can be obtained:

$$\begin{aligned} u_{\text{nf}}(t) &= -\mathbf{k}^T (\mathbf{x}(t) - \tilde{\mathbf{y}}(t)) + k_p e(t) + k_I x_I(t) + \mathbf{K}_f \tilde{\mathbf{Y}}(t) \\ &= k_p (r(t) - \mathbf{C}\mathbf{x}(t)) + \begin{bmatrix} -\mathbf{k}^T & k_I \end{bmatrix} \begin{bmatrix} \mathbf{x}(t) \\ x_I(t) \end{bmatrix} + \mathbf{k}^T \tilde{\mathbf{y}}(t) + \mathbf{K}_f \tilde{\mathbf{Y}}(t) \\ &= - \underbrace{\begin{bmatrix} \mathbf{k}^T + k_p \mathbf{C} & -k_I \end{bmatrix}}_{\tilde{\mathbf{k}}^T(t)} \underbrace{\begin{bmatrix} \mathbf{x}(t) \\ x_I(t) \end{bmatrix}}_{\tilde{\mathbf{x}}(t)} + k_p r(t) + \mathbf{k}^T \tilde{\mathbf{y}}(t) + \mathbf{K}_f \tilde{\mathbf{Y}}(t) \\ &= -\tilde{\mathbf{k}}^T \tilde{\mathbf{x}}(t) + k_p r(t) + \mathbf{k}^T \tilde{\mathbf{y}}(t) + \mathbf{K}_f \tilde{\mathbf{Y}}(t) , \end{aligned} \quad (30)$$

with the reminder that $\tilde{\mathbf{Y}}$ was defined above in Equation (26).

Remark 5. *Nominal control output signal considering feed-forward control:*

$$u_{\text{nf}}(t) = -\tilde{\mathbf{k}}^T \tilde{\mathbf{x}}(t) + \tilde{\mathbf{K}}_f \tilde{\mathbf{Y}}(t) , \quad (31)$$

where $\tilde{\mathbf{K}}_f = \begin{bmatrix} k_p & 0 & 0 \end{bmatrix} + \begin{bmatrix} \mathbf{k}^T & 0 \end{bmatrix} + \mathbf{K}_f$.

1.4.7 Classical disturbance observer-based controller

The disturbance observer (DOB)-based controller has been extensively study and used in several applications due to its ability to reject sensor noise, compensate plant uncertainties and to help the real plant to behave almost like the nominal plant by attenuating external disturbances [10], [4], [5]. Because of these advantages, a DOB-based controller was also implemented in the nanopositioning machine in [19]. Figure 6 shows the scheme of the mentioned controller. Parameter P is the plant with uncertainties and parameter P_n represents the ideal plant. The NPMDM is idealized as a second order system, which transfer function is shown below:

$$P_n(s) = \frac{k_m}{ms^2 + ds + c} . \quad (32)$$

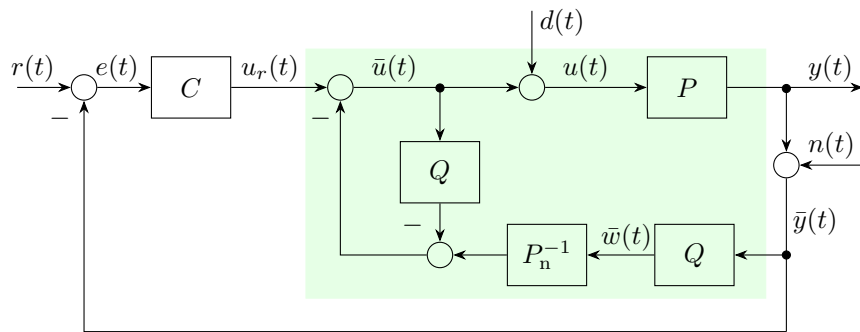


Figure 6: Classical disturbance observer scheme.

Parameter C is the controller of the system, which include the PI-SFC, feed-forward and adaptive controller. The entries $r(t)$, $d(t)$ and $n(t)$ represent the reference input, input disturbance and sensor noise, respectively. The Q-filter, which is represented by the parameter Q , is a second order low-pass filter:

$$Q(s) = \frac{1}{(\tau s + 1)^2}, \quad (33)$$

where $\tau = 1/w_c$ with a cutoff frequency w_c of 1000 rad/s. It is also important to remark, that noise suppression could be adjusted by the chose of the Q-filter.

The controller considers among others two particular assumptions. On one hand, it is assumed that in the low frequency range ($w < w_c$), the reference signal $r(s)$ and the disturbance $d(s)$ are significant, while the noise $n(s)$ is approximately zero. On the other hand, it is assumed that in the high frequency range ($w > w_c$), the noise $n(s)$ is significant, but the reference signal $r(s)$ and the disturbance $d(s)$ are approximately zero. The selected Q-filter behaves as:

$$|Q(s)| \approx \begin{cases} 1, & \text{if } w < w_c \\ 0, & \text{if } w > w_c. \end{cases} \quad (34)$$

It is explained in several articles such as [15], that in the low frequency range, the plant output is approximated to the nominal plant without the DOB, which means that the noise suppression is satisfactory. However, in the high frequency range, the system performs the same as the closed loop system without the DOB, which means that the DOB-based controller does not provide any improvement with respect to noise suppression.

1.4.8 Performance criteria

To evaluate the results of the simulations and experiments, the same approach as [19] is chosen. The first criterion is the RMSE.

Remark 6. *Root mean square error (RMSE):*

$$\text{RMSE} = \sqrt{\sum_{i=1}^N \frac{(r_i - x_{1,i})^2}{N}}, \quad (35)$$

where $r(t)$ is the reference trajectory, $x_1(t)$ is the measure trajectory and N is the number of samples.

The second criterion is the maximum error because it is desirable that the controller avoids peak errors.

Remark 7. *Maximum error:*

$$e_{\max} = \max_{i=0, \dots, N} |r_i - x_{1,i}|. \quad (36)$$

2 Model reference adaptive control

In this chapter, first it is explained what means model reference adaptive control (MRAC). Secondly, it is presented the development of its algorithm. Finally, it is shown the MRAC considering the extension to the unknown input matrix case.

2.1 What is model reference adaptive control?

Adaptive control systems can be divided in two classes: direct and indirect. According to [17], direct or implicit adaptive controllers are those in which there is no need to identify the plant parameters. The control law is directly tuned to decrease the error between the plant and the desired output. On the other hand, in indirect or explicit adaptive controllers, there is an on-line estimation of the plant parameters which are used for the control law adjustment. Inside the direct adaptive control class, MRAC can be founded. The main idea of this controller is that the response of the real system should match the response of an ideal reference model plant [3]. This ideal plant behaves in such a way that, an input step will gives an output with the desired rise time, overshoot, settling time, etc. Referring to [17], MRAC is helpful when there is a limited knowledge of the parameters of the controlled plant. Also, it allows to make on-line changes to reduce the effects of the unknown parameters with a satisfactory performance. Over the years, MRAC have been widely study and use in different applications such as vehicle suspension [27], aerial manipulation [23]

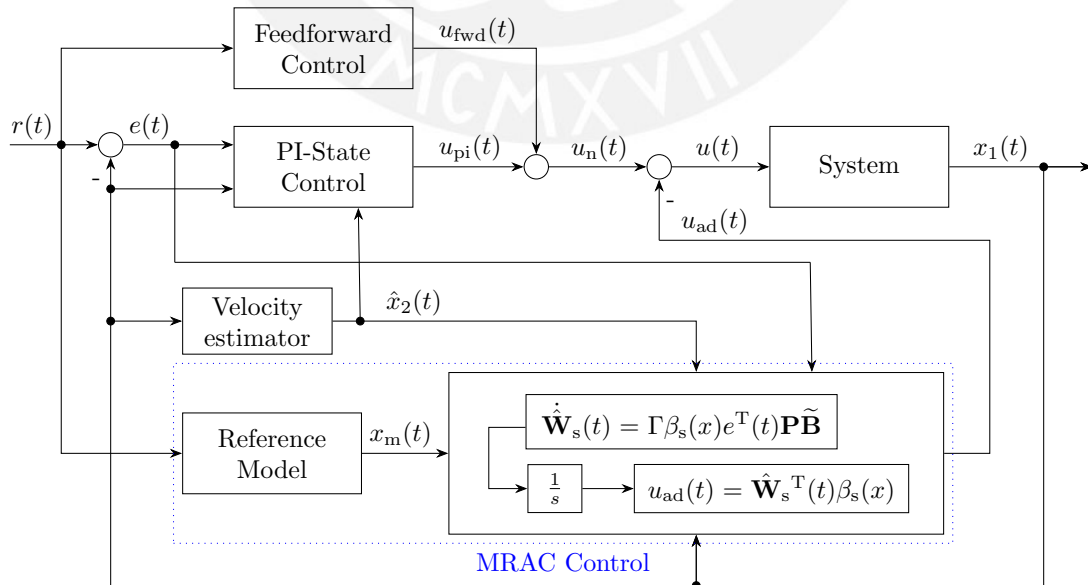


Figure 7: MRAC scheme adopted to the nan positioning machine.

or others [20], [29]. The MRAC developed in this master thesis uses the Lyapunov stability theory as shown in [32], [28]. Figure 7 shows the MRAC scheme adopted to the nanopositioning machine.

2.2 Design of the MRAC

In this section, the MRAC without unknown parameters in the extended input matrix $\tilde{\mathbf{B}}$ is shown. It is important to remark, that ideally the only parameters that could be unknown in this case could be c (spring constant) and d (damping constant). Notice that if m (mass), k_m (motor constant) or k_r (electrical resistance coefficient) are unknown, there will always remain a constant unknown parameter in the matrix $\tilde{\mathbf{B}}$, which can not be grouped into the matrix $\mathbf{W}_s'^T$. Therefore, there is a need to build the extended method, which is shown in Section 2.3. The system with the allowed unknown parameters is presented below:

$$\underbrace{\begin{bmatrix} \dot{x}_1 \\ \dot{x}_2 \\ \dot{x}_I \end{bmatrix}}_{\dot{\tilde{x}}(t)} = \underbrace{\begin{bmatrix} 0 & 1 & 0 \\ -\frac{\bar{c}}{m} & -\frac{\bar{d}}{m} & 0 \\ -1 & 0 & 0 \end{bmatrix}}_{\tilde{\mathbf{A}}} \underbrace{\begin{bmatrix} x_1 \\ x_2 \\ x_I \end{bmatrix}}_{\tilde{x}(t)} + \underbrace{\begin{bmatrix} 0 \\ \frac{k_m k_r}{m} \\ 0 \end{bmatrix}}_{\tilde{\mathbf{B}}} u(t) + \underbrace{\begin{bmatrix} 0 \\ 0 \\ 1 \end{bmatrix}}_{\tilde{\mathbf{R}}} r(t) \quad (37)$$

$$+ \underbrace{\begin{bmatrix} 0 \\ -\frac{1}{m} \\ 0 \end{bmatrix}}_{\tilde{\mathbf{F}}} F_r(t) + \underbrace{\begin{bmatrix} 0 \\ \frac{k_m k_r}{m} \\ 0 \end{bmatrix}}_{\tilde{\mathbf{B}}} \underbrace{\begin{bmatrix} \frac{m}{k_m k_r} \left(-\frac{\Delta c}{m}\right) \\ \frac{m}{k_m k_r} \left(-\frac{\Delta d}{m}\right) \\ 0 \end{bmatrix}}_{\mathbf{W}_s'^T} \underbrace{\begin{bmatrix} x_1 \\ x_2 \\ 1 \end{bmatrix}}_{\beta'_s(x)},$$

where $\bar{c} = c + \Delta c$, $\bar{d} = d + \Delta d$ and $F_r(t)$ was previously defined in (3). Note that an unknown parameter is represented by a bar over it and Δ is used to represent the difference from its real value.

Recalling that $F_r(t)$ is a scalar, it can be noticed the following:

$$\begin{aligned} \tilde{\mathbf{F}} F_r(t) &= \tilde{\mathbf{B}} \left(\frac{-1}{k_m k_r} \right) F_r(t) \\ &= \tilde{\mathbf{B}} \left(\underbrace{\begin{bmatrix} -\frac{1}{k_m k_r} F_c \\ -\frac{1}{k_m k_r} F_s \end{bmatrix}}_{\mathbf{W}_s''^T} \underbrace{\begin{bmatrix} \left(1 - e^{-|\frac{x_2}{v_s}|^\delta}\right) \text{sign}(x_2) \\ \left(e^{-|\frac{x_2}{v_s}|^\delta}\right) \text{sign}(x_2) \end{bmatrix}}_{\beta''_s(x)} + \underbrace{\left(\frac{-1}{k_m k_r} \right) \sigma x_2}_{(i)} \right). \end{aligned} \quad (38)$$

Because $\mathbf{W}_s'^T \beta'_s(x)$ and $\mathbf{W}_s''^T \beta''_s(x)$ terms are scalars, both can be grouped. Term (i) can be summed to the $\mathbf{W}_{s,2}'^T \beta'_{s,2}(x) = \frac{m}{k_m k_r} \left(-\frac{\Delta d}{m}\right) x_2$ expression. Then, is possible to rewrite the equation (37) as:

Remark 8. *State space representation of the system with a known input matrix:*

$$\underbrace{\begin{bmatrix} \dot{x}_1 \\ \dot{x}_2 \\ \dot{x}_I \end{bmatrix}}_{\dot{\mathbf{x}}(t)} = \underbrace{\begin{bmatrix} 0 & 1 & 0 \\ -\frac{\bar{c}}{m} & -\frac{\bar{d}}{m} & 0 \\ -1 & 0 & 0 \end{bmatrix}}_{\tilde{\mathbf{A}}} \underbrace{\begin{bmatrix} x_1 \\ x_2 \\ x_I \end{bmatrix}}_{\tilde{\mathbf{x}}(t)} + \underbrace{\begin{bmatrix} 0 \\ \frac{k_m k_r}{m} \\ 0 \end{bmatrix}}_{\tilde{\mathbf{B}}} u(t) + \underbrace{\begin{bmatrix} 0 \\ 0 \\ 1 \end{bmatrix}}_{\tilde{\mathbf{R}}} r(t) + \underbrace{\begin{bmatrix} 0 \\ \frac{k_m k_r}{m} \\ 0 \end{bmatrix}}_{\tilde{\mathbf{B}}} + \underbrace{\begin{bmatrix} \frac{m}{k_m k_r} \left(-\frac{\Delta c}{m}\right) \\ \frac{m}{k_m k_r} \left(-\frac{\Delta d}{m}\right) - \frac{1}{k_m k_r} \sigma \\ 0 \\ -\frac{1}{k_m k_r} F_c \\ -\frac{1}{k_m k_r} F_s \end{bmatrix}^T}_{\mathbf{W}_s^T} \underbrace{\begin{bmatrix} x_1 \\ x_2 \\ 1 \\ \left(1 - e^{-\left|\frac{x_2}{v_s}\right|^\delta}\right) \text{sign}(x_2) \\ \left(e^{-\left|\frac{x_2}{v_s}\right|^\delta}\right) \text{sign}(x_2) \end{bmatrix}}_{\beta_s(x)}, \quad (39)$$

where $\bar{c} = c + \Delta c$, $\bar{d} = d + \Delta d$.

The control law $u(t)$ is defined as:

$$u(t) = u_n(t) - u_{ad}(t), \quad (40)$$

where the nominal control will be at first $u_n(t)$, without the feed-forward control, as shown in (12). At the end of the section, the control law considering feed-forward control will be applied.

Then, the reference model is presented:

$$\dot{\mathbf{x}}_m(t) = \mathbf{A}_m \mathbf{x}_m(t) + \mathbf{B}_m r(t). \quad (41)$$

The parameters of the reference model are chosen from the close loop, so the system can have the desired response:

$$\mathbf{A}_m = \tilde{\mathbf{A}} - \tilde{\mathbf{B}} \tilde{\mathbf{k}}^T, \quad (42)$$

$$\mathbf{B}_m = \tilde{\mathbf{B}} k_p + \tilde{\mathbf{R}}. \quad (43)$$

The Lyapunov equation of the reference model system is the following:

$$0 = \mathbf{A}_m^T \mathbf{P} + \mathbf{P} \mathbf{A}_m + \mathbf{Q} . \quad (44)$$

The unknown matched uncertainty is defined as:

$$\Delta(x) = \mathbf{W}_s^T \beta_s(x) , \quad (45)$$

where \mathbf{W}_s^T is the unknown constant weight matrix and β_s is a known vector of functions of the form $\beta_s = [\beta_{s,1}(x), \beta_{s,2}(x), \beta_{s,3}(x), \beta_{s,4}(x), \beta_{s,5}(x)]^T$, already defined in (39). On one hand, it is important to remark that nonlinearities are added to the system due to the exponential and sign functions. This can be found precisely in:

$$\beta_{s,4}(x) = \left(1 - e^{-|\frac{x_2}{v_s}|^\delta} \right) \text{sign}(x_2) , \quad (46)$$

$$\beta_{s,5}(x) = \left(e^{-|\frac{x_2}{v_s}|^\delta} \right) \text{sign}(x_2) . \quad (47)$$

On the other hand, now it is clear what it was stated before: the only parameters that need to be known are the Stribeck velocity v_s and the Stribeck shape factor δ . It can be seen that the other friction parameters are inside the unknown constant weight matrix \mathbf{W}_s^T and therefore, they are not required to build the adaptive controller. The values for the mentioned friction parameters can be found in Appendix A.1. To build the MRAC, the first step is to replace the control law from (40) and the matched uncertainty from (45) in (39):

$$\dot{\tilde{\mathbf{x}}}(t) = \tilde{\mathbf{A}}\tilde{\mathbf{x}}(t) + \tilde{\mathbf{B}} [u_n(t) - u_{ad}(t) + \Delta(x)] + \tilde{\mathbf{R}}r(t) . \quad (48)$$

Then, replacing $u_n(t)$ from (12), and grouping conveniently with \mathbf{A}_m and \mathbf{B}_m from (42) and (43) respectively, the following is obtained:

$$\begin{aligned} \dot{\tilde{\mathbf{x}}}(t) &= \tilde{\mathbf{A}}\tilde{\mathbf{x}}(t) + \tilde{\mathbf{B}} \left[-\tilde{\mathbf{k}}^T \tilde{\mathbf{x}}(t) + k_p r(t) - u_{ad}(t) + \Delta(x) \right] + \tilde{\mathbf{R}}r(t) \\ &= \underbrace{(\tilde{\mathbf{A}} - \tilde{\mathbf{B}}\tilde{\mathbf{k}}^T)}_{\mathbf{A}_m} \tilde{\mathbf{x}}(t) + \underbrace{(\tilde{\mathbf{B}}k_p + \tilde{\mathbf{R}})}_{\mathbf{B}_m} r(t) + \tilde{\mathbf{B}} [-u_{ad}(t) + \Delta(x)] \\ &= \mathbf{A}_m \tilde{\mathbf{x}}(t) + \mathbf{B}_m r(t) + \tilde{\mathbf{B}} [-u_{ad}(t) + \Delta(x)] . \end{aligned} \quad (49)$$

In order to achieve a system equal to the model reference, shown in (41), the adaptive control should be defined as:

$$u_{ad}(t) = \hat{\Delta}(x) = \hat{\mathbf{W}}_s^T(t) \beta_s(x) , \quad (50)$$

where $\hat{\mathbf{W}}_s^T(t)$ is the estimated unknown constant weight matrix. Then $\tilde{\mathbf{W}}_s(t)$ is defined as:

$$\tilde{\mathbf{W}}_s(t) = \mathbf{W}_s - \hat{\mathbf{W}}_s(t) . \quad (51)$$

After that, equations (45) and (51) are replaced in (49), which results in:

$$\dot{\tilde{\mathbf{x}}}(t) = \mathbf{A}_m \tilde{\mathbf{x}}(t) + \mathbf{B}_m r(t) + \tilde{\mathbf{B}} \tilde{\mathbf{W}}_s^T(t) \beta_s(x) . \quad (52)$$

To fully define the adaptive control $u_{\text{ad}}(t)$, it is necessary to determine the evolution of the estimated weight matrix of the system $\hat{\mathbf{W}}_s(t)$. Barbălat's Lemma allows to find $\dot{\hat{\mathbf{W}}}_s(t)$ and also to prove that the error of the system $e(t)$ asymptotically goes to zero. But first the error is defined:

$$e(t) = \tilde{\mathbf{x}}(t) - \mathbf{x}_m(t) . \quad (53)$$

Deriving (53) and with $\dot{\mathbf{x}}_m$ from (41), the error state dynamics can be obtained:

$$\begin{aligned} \dot{e}(t) &= \dot{\tilde{\mathbf{x}}}(t) - \dot{\mathbf{x}}_m(t) \\ &= \mathbf{A}_m \tilde{\mathbf{x}}(t) + \mathbf{B}_m r(t) + \tilde{\mathbf{B}} \tilde{\mathbf{W}}_s^T(t) \beta_s(x) - \mathbf{A}_m \mathbf{x}_m(t) - \mathbf{B}_m r(t) \\ &= \mathbf{A}_m (\tilde{\mathbf{x}}(t) - \mathbf{x}_m(t)) + \tilde{\mathbf{B}} \tilde{\mathbf{W}}_s^T(t) \beta_s(x) \\ &= \mathbf{A}_m e(t) + \tilde{\mathbf{B}} \tilde{\mathbf{W}}_s^T(t) \beta_s(x) . \end{aligned} \quad (54)$$

Barbălat's Lemma is presented at the Lemma 1, which is extracted from the book Nonlinear Control by Hassan K. Khalil [18].

Lemma 1. Barbălat's Lemma: Consider the differentiable function $f : \mathbb{R}_0^+ \rightarrow \mathbb{R}$ with

$$(i) \lim_{t \rightarrow \infty} f(t) = c, \quad \text{where } |c| < \infty ,$$

(ii) \dot{f} is uniformly continuous.

If both conditions are satisfied, then the following applies: $\lim_{t \rightarrow \infty} \dot{f}(t) = 0$.

Note: If \ddot{f} bounded, then (ii) holds.

Remark 9 outlines a Lyapunov-like lemma, which can be derived from Barbălat's Lemma. In fact, it can be seen that, condition (i) from Remark 1 is equivalent to condition (i) and (ii) from this new approach. Meanwhile condition (ii) from Remark 1 is equivalent to the last one (iii).

Remark 9. Lyapunov-like lemma: *If a scalar function $\mathcal{V}(t, x) : \mathbb{R}_+ \times \mathbb{R}^n \rightarrow \mathbb{R}$ satisfies the conditions:*

(i) $\mathcal{V}(t, x)$ is lower bounded,

(ii) $\dot{\mathcal{V}}(t, x) \leq 0$ and

(iii) $\dot{\mathcal{V}}(t, x)$ is uniformly continuous in time t

then the following applies: $\lim_{t \rightarrow \infty} \dot{\mathcal{V}}(t, x) = 0$.

If $\ddot{\mathcal{V}}(t, x)$ is bounded, the condition (iii) is satisfied.

The conditions established in Remark 9 will be consider to prove the stability and to find the $\dot{\tilde{\mathbf{W}}}_s(t)$ term. First, to satisfy condition (i), the following Lyapunov-like candidate function is proposed:

Remark 10. *The proposed Lyapunov-like candidate function:*

$$\mathcal{V}(e(t), \tilde{\mathbf{W}}_s(t)) = e^T(t) \mathbf{P} e(t) + \tilde{\mathbf{W}}_s^T(t) \mathbf{\Gamma}^{-1} \tilde{\mathbf{W}}_s(t), \quad \mathbf{\Gamma} > 0. \quad (55)$$

\mathcal{V} is lower bounded because it is positive definite. Then, to check if it satisfies the second condition, Equation (55) is derived:

$$\dot{\mathcal{V}} = \dot{e}^T(t) \mathbf{P} e(t) + e^T(t) \mathbf{P} \dot{e}(t) + \underbrace{\dot{\tilde{\mathbf{W}}}_s^T(t) \mathbf{\Gamma}^{-1} \tilde{\mathbf{W}}_s(t)}_a + \underbrace{\tilde{\mathbf{W}}_s^T(t) \mathbf{\Gamma}^{-1} \dot{\tilde{\mathbf{W}}}_s(t)}_a. \quad (56)$$

It can be noticed that a terms are scalars. Therefore, $a = a^T$ satisfies and both terms can be summed. Then, replacing $\dot{e}(t)$ from (54) in (56) and recalling that $\dot{\tilde{\mathbf{W}}}_s(t) = -\dot{\hat{\mathbf{W}}}_s(t)$ from (51) yields:

$$\begin{aligned} \dot{\mathcal{V}} &= \left[\mathbf{A}_m e(t) + \tilde{\mathbf{B}} \tilde{\mathbf{W}}_s^T(t) \beta_s(x) \right]^T \mathbf{P} e(t) \\ &\quad + e^T(t) \mathbf{P} \left[\mathbf{A}_m e(t) + \tilde{\mathbf{B}} \tilde{\mathbf{W}}_s^T(t) \beta_s(x) \right] + 2 \tilde{\mathbf{W}}_s^T(t) \mathbf{\Gamma}^{-1} \dot{\tilde{\mathbf{W}}}_s(t) \\ &= \underbrace{e^T(t) \mathbf{A}_m^T \mathbf{P} e(t)}_b + \underbrace{\left[\tilde{\mathbf{B}} \tilde{\mathbf{W}}_s^T(t) \beta_s(x) \right]^T \mathbf{P} e(t)}_c + \underbrace{e^T(t) \mathbf{P} \mathbf{A}_m e(t)}_b \\ &\quad + \underbrace{e^T(t) \mathbf{P} \left[\tilde{\mathbf{B}} \tilde{\mathbf{W}}_s^T(t) \beta_s(x) \right]}_c - 2 \tilde{\mathbf{W}}_s^T(t) \mathbf{\Gamma}^{-1} \dot{\tilde{\mathbf{W}}}_s(t). \end{aligned} \quad (57)$$

Notice that c terms are also scalars. Then, summing c terms and grouping b terms

leads to:

$$\begin{aligned} \dot{\mathcal{V}} = & \underbrace{e^T(t) [\mathbf{A}_m^T \mathbf{P} + \mathbf{P} \mathbf{A}_m] e(t)}_{\text{(I)}} \\ & + \underbrace{2e^T(t) \mathbf{P} \tilde{\mathbf{B}} \tilde{\mathbf{W}}_s^T(t) \beta_s(x) - 2\tilde{\mathbf{W}}_s^T(t) \mathbf{\Gamma}^{-1} \dot{\tilde{\mathbf{W}}}_s(t)}_{\text{(II)}} . \end{aligned} \quad (58)$$

From (I) is obtained:

$$\text{(I)} = e^T(t) \underbrace{[\mathbf{A}_m^T \mathbf{P} + \mathbf{P} \mathbf{A}_m]}_{-\mathbf{Q}=-\mathbf{I}} e(t) = -e^T(t)e(t) = -\|e(t)\|_2^2 . \quad (59)$$

From (II) is obtained:

$$\text{(II)} = 2 \underbrace{e^T(t) \mathbf{P} \tilde{\mathbf{B}}}_d \underbrace{\tilde{\mathbf{W}}_s^T(t) \beta_s(x)}_e - 2\tilde{\mathbf{W}}_s^T(t) \mathbf{\Gamma}^{-1} \dot{\tilde{\mathbf{W}}}_s(t) , \quad (60)$$

where d and e terms are scalars and therefore, because of commutative property of multiplication, $de = ed$ is satisfied and yields:

$$\begin{aligned} \text{(II)} &= 2\tilde{\mathbf{W}}_s^T(t) \beta_s(x) e^T(t) \mathbf{P} \tilde{\mathbf{B}} - 2\tilde{\mathbf{W}}_s^T(t) \mathbf{\Gamma}^{-1} \dot{\tilde{\mathbf{W}}}_s(t) \\ &= 2 \left[\tilde{\mathbf{W}}_s^T(t) \mathbf{\Gamma}^{-1} \left(\mathbf{\Gamma} \beta_s(x) e^T(t) \mathbf{P} \tilde{\mathbf{B}} - \dot{\tilde{\mathbf{W}}}_s(t) \right) \right] . \end{aligned} \quad (61)$$

Then, it is possible to define $\dot{\tilde{\mathbf{W}}}_s(t)$ as:

$$\dot{\tilde{\mathbf{W}}}_s(t) = \mathbf{\Gamma} \beta_s(x) e^T(t) \mathbf{P} \tilde{\mathbf{B}} , \quad (62)$$

Therefore, the following applies:

$$\dot{\mathcal{V}} = -\|e(t)\|_2^2 \leq 0 , \quad (63)$$

where $\dot{\mathcal{V}}$ is negative semi-definite and thereby satisfies condition (ii) from Remark 9. The final step is to calculate $\ddot{\mathcal{V}}$ to check if condition (iii) is satisfied, $\dot{e}(t)$ from Equation (54),

$$\begin{aligned} \ddot{\mathcal{V}} &= -2e^T(t) \dot{e}(t) \\ &= -2e^T(t) \left(\mathbf{A}_m e(t) + \tilde{\mathbf{B}} \tilde{\mathbf{W}}_s^T(t) \beta_s(x) \right) . \end{aligned} \quad (64)$$

In the equation shown in (64), terms $e(t)$ and $\tilde{\mathbf{W}}_s(t)$ are bounded since conditions (i) and (ii) are satisfied, which means that \mathcal{V} approaches a finite limit as $t \rightarrow \infty$. Then, it is only necessary to prove that $\beta_s(x)$ is bounded. $\beta_s(x)$ depends on x_1 and x_2 , see Equation (39). Terms x_1 and x_2 can be found in the extended state vector

$\tilde{\mathbf{x}}$, which satisfies $\tilde{\mathbf{x}} = e(t) + \mathbf{x}_m$. The model reference vector \mathbf{x}_m , previously defined in (41), is bounded because \mathbf{A}_m is a Hurwitz matrix and $r(t)$ is a bounded entry. Therefore, all terms are bounded and the last condition is satisfied:

$$\begin{aligned} \lim_{t \rightarrow \infty} -\|e(t)\|_2^2 &= 0 \\ \lim_{t \rightarrow \infty} e(t) &= 0. \end{aligned} \quad (65)$$

Finally, it is guaranteed that $e(t)$ asymptotically goes to zero.

2.2.1 MRAC with feed-forward control

In this subsection, the feed-forward control is added to the algorithm. First, it is important to build a new reference model that includes this new considerations. The reference model dynamics considering feed-forward control is shown below:

$$\dot{\mathbf{x}}_m(t) = \mathbf{A}_m \mathbf{x}_m(t) + \mathbf{B}_{mf} \tilde{\mathbf{Y}}(t) + \tilde{\mathbf{R}}r(t), \quad (66)$$

where \mathbf{A}_m was previously defined in (42) and

$$\mathbf{B}_{mf} = \tilde{\mathbf{B}}\tilde{\mathbf{K}}_f, \quad (67)$$

with $\tilde{\mathbf{K}}_f$ from (31).

The differential equation for the system was shown in (48). However, in this case the nominal control is the corresponding to $u_{nf}(t)$ shown in (31), so the expression is as follows:

$$\dot{\tilde{\mathbf{x}}}(t) = \tilde{\mathbf{A}}\tilde{\mathbf{x}}(t) + \tilde{\mathbf{B}} [u_{nf}(t) - u_{ad}(t) + \Delta(x)] + \tilde{\mathbf{R}}r(t). \quad (68)$$

Replacing $u_{nf}(t)$ from (31) in (68) and grouping certain terms,

$$\begin{aligned} \dot{\tilde{\mathbf{x}}}(t) &= \tilde{\mathbf{A}}\tilde{\mathbf{x}}(t) + \tilde{\mathbf{B}} \left[-\tilde{\mathbf{k}}^T \tilde{\mathbf{x}}(t) + \tilde{\mathbf{K}}_f \tilde{\mathbf{Y}}(t) - u_{ad}(t) + \Delta(x) \right] + \tilde{\mathbf{R}}r(t) \\ &= \underbrace{(\tilde{\mathbf{A}} - \tilde{\mathbf{B}}\tilde{\mathbf{k}}^T)}_{\mathbf{A}_m} \tilde{\mathbf{x}}(t) + \underbrace{\tilde{\mathbf{B}}\tilde{\mathbf{K}}_f}_{\mathbf{B}_{mf}} \tilde{\mathbf{Y}}(t) + \tilde{\mathbf{R}}r(t) + \tilde{\mathbf{B}} [-u_{ad}(t) + \Delta(x)] \\ &= \mathbf{A}_m \tilde{\mathbf{x}}(t) + \mathbf{B}_{mf} \tilde{\mathbf{Y}}(t) + \tilde{\mathbf{R}}r(t) + \tilde{\mathbf{B}} [-u_{ad}(t) + \Delta(x)], \end{aligned} \quad (69)$$

then, replacing $u_{ad}(t)$ from (50) and $\tilde{\mathbf{W}}_s(t)$ from (51) in (69), yields:

$$\dot{\tilde{\mathbf{x}}}(t) = \mathbf{A}_m \tilde{\mathbf{x}}(t) + \mathbf{B}_{mf} \tilde{\mathbf{Y}}(t) + \tilde{\mathbf{R}}r(t) + \tilde{\mathbf{B}}\tilde{\mathbf{W}}_s^T(t)\beta_s(x). \quad (70)$$

Finally, recalling $\tilde{\mathbf{x}}_m(t)$ from (66), the error of the system $e(t) = \tilde{\mathbf{x}}(t) - \tilde{\mathbf{x}}_m(t)$ is derived:

$$\begin{aligned}
\dot{e}(t) &= \dot{\tilde{\mathbf{x}}}(t) - \dot{\tilde{\mathbf{x}}}_m(t) \\
&= \mathbf{A}_m \tilde{\mathbf{x}}(t) + \mathbf{B}_{mf} \tilde{\mathbf{Y}}(t) + \tilde{\mathbf{R}} r(t) + \tilde{\mathbf{B}} \tilde{\mathbf{W}}_s^T(t) \beta_s(x) \\
&\quad - \left[\mathbf{A}_m \tilde{\mathbf{x}}_m(t) + \mathbf{B}_{mf} \tilde{\mathbf{Y}}(t) + \tilde{\mathbf{R}} r(t) \right] \\
&= \mathbf{A}_m (\tilde{\mathbf{x}}(t) - \tilde{\mathbf{x}}_m(t)) + \tilde{\mathbf{B}} \tilde{\mathbf{W}}_s^T(t) \beta_s(x) \\
&= \mathbf{A}_m e(t) + \tilde{\mathbf{B}} \tilde{\mathbf{W}}_s^T(t) \beta_s(x) .
\end{aligned} \tag{71}$$

It can be noticed that Equation (71) is equivalent to (54). Therefore, considering the theory of Remark 9 and with the Lyapunov candidate function proposed in (55), it can be stated that $\dot{\tilde{\mathbf{W}}}_s(t)$ is determined as in Equation (62) and that the system error $e(t)$ asymptotically goes to zero by applying the same procedure.



2.3 Extensions to the unknown input matrix case - MRAC

This section considers that all parameters in the nanopositioning machine can be unknown. When the parameters m (mass and objective), k_m (motor constant) or k_r (electrical resistance) are unknown, then there exists unknown terms in the input matrix $\tilde{\mathbf{B}}$ and therefore, it is needed to apply the unknown input matrix case. The MRAC considering an unmodeled or unknown input matrix, have been widely study through the years as seen for example in [30], [24], [25]. Also, modifications were applied to the MRAC considering this extension to achieve higher robustness to time delays [8]. Finally, many applications can be found in adaptive flight control systems for unmanned aerial vehicles (UAVs) [9], [7]. In this thesis, the input matrix will be modeled in a multiplicative way because all the unknown parameters can be grouped into a positive constant λ . The system dynamics can be expressed as:

Remark 11. *State space representation of the system with an unknown input matrix:*

$$\begin{aligned}
 \underbrace{\begin{bmatrix} \dot{x}_1(t) \\ \dot{x}_2(t) \\ \dot{x}_I(t) \end{bmatrix}}_{\dot{\mathbf{x}}(t)} &= \underbrace{\begin{bmatrix} 0 & 1 & 0 \\ -\frac{c}{m} & -\frac{d}{m} & 0 \\ -1 & 0 & 0 \end{bmatrix}}_{\tilde{\mathbf{A}}} \underbrace{\begin{bmatrix} x_1(t) \\ x_2(t) \\ x_I(t) \end{bmatrix}}_{\tilde{\mathbf{x}}(t)} + \underbrace{\begin{bmatrix} 0 \\ 0 \\ 1 \end{bmatrix}}_{\tilde{\mathbf{R}}} r(t) \\
 &+ \underbrace{\begin{bmatrix} 0 \\ \frac{k_m k_r}{m} \\ 0 \end{bmatrix}}_{\tilde{\mathbf{B}}} \underbrace{\left[\frac{m}{k_m k_r} \left(\frac{(k_m) k_r}{\bar{m}} \right) \right]}_{\lambda} u(t) \\
 &+ \tilde{\mathbf{B}} \underbrace{\begin{bmatrix} \frac{m}{k_m k_r} \left(-\Delta \left[\frac{c}{m} \right] \right) \\ \frac{m}{k_m k_r} \left(-\Delta \left[\frac{d}{m} \right] \right) - \frac{m}{k_m k_r} \left(\frac{1}{\bar{m}} \right) \sigma \\ 0 \\ -\frac{m}{k_m k_r} \left(\frac{1}{\bar{m}} \right) F_c \\ -\frac{m}{k_m k_r} \left(\frac{1}{\bar{m}} \right) F_s \end{bmatrix}}_{\mathbf{W}_s^T} \underbrace{\begin{bmatrix} x_1 \\ x_2 \\ 1 \\ \left(1 - e^{-\left| \frac{x_2}{v_s} \right|^\delta} \right) \text{sign}(x_2) \\ \left(e^{-\left| \frac{x_2}{v_s} \right|^\delta} \right) \text{sign}(x_2) \end{bmatrix}}_{\beta_s(\mathbf{x})}, \tag{72}
 \end{aligned}$$

where $\bar{\frac{c}{m}} = \frac{c}{m} + \Delta \left[\frac{c}{m} \right]$, $\bar{\frac{d}{m}} = \frac{d}{m} + \Delta \left[\frac{d}{m} \right]$ and $\lambda > 0$.

The system dynamics with all unknown parameters is presented below:

$$\dot{\tilde{\mathbf{x}}}(t) = \tilde{\mathbf{A}}\tilde{\mathbf{x}}(t) + \tilde{\mathbf{B}}\lambda [u(t) + \lambda^{-1}\mathbf{W}_s^T\beta_s(x)] + \tilde{\mathbf{R}}r(t). \quad (73)$$

The procedure for building the controller and proving its stability is analogous to the one in Section 2.2. The control law $u(t)$ was determined in (40) and then some terms are strategically added and subtracted:

$$\begin{aligned} \dot{\tilde{\mathbf{x}}}(t) &= \tilde{\mathbf{A}}\tilde{\mathbf{x}}(t) + \tilde{\mathbf{B}}\lambda [u_n(t) - u_{\text{ad}}(t) + \lambda^{-1}\mathbf{W}_s^T\beta_s(x)] + \tilde{\mathbf{R}}r(t) \\ &\quad \tilde{\mathbf{B}}\lambda\lambda^{-1}\tilde{\mathbf{k}}^T\tilde{\mathbf{x}}(t) - \tilde{\mathbf{B}}\tilde{\mathbf{k}}^T\tilde{\mathbf{x}}(t) + \tilde{\mathbf{B}}k_p r(t) - \tilde{\mathbf{B}}\lambda\lambda^{-1}k_p r(t). \end{aligned} \quad (74)$$

Grouping conveniently with the consideration that \mathbf{A}_m and \mathbf{B}_m were defined previously in (42) and (43), respectively, results in:

$$\begin{aligned} \dot{\tilde{\mathbf{x}}}(t) &= \underbrace{(\tilde{\mathbf{A}} - \tilde{\mathbf{B}}\tilde{\mathbf{k}}^T)}_{\mathbf{A}_m}\tilde{\mathbf{x}}(t) + \underbrace{(\tilde{\mathbf{B}}k_p + \tilde{\mathbf{R}})}_{\mathbf{B}_m}r(t) + \tilde{\mathbf{B}}\lambda [u_n(t) - u_{\text{ad}}(t) \\ &\quad + \lambda^{-1}\mathbf{W}_s^T\beta_s(x) - \lambda^{-1}\underbrace{(-\tilde{\mathbf{k}}^T\tilde{\mathbf{x}}(t) + k_p r(t))}_{u_n(t)}] \\ &= \mathbf{A}_m\tilde{\mathbf{x}}(t) + \mathbf{B}_m r(t) + \tilde{\mathbf{B}}\lambda \left[\underbrace{(1 - \lambda^{-1})u_n(t) + \lambda^{-1}\mathbf{W}_s^T\beta_s(x) - u_{\text{ad}}(t)}_{\mathbf{W}^T\tilde{\beta}(x, u_n)} \right], \end{aligned} \quad (75)$$

where:

$$\mathbf{W}^T = \left[\lambda^{-1}\mathbf{W}_s^T, (1 - \lambda^{-1}) \right], \quad (76)$$

$$\tilde{\beta}(x, u_n) = \begin{bmatrix} \beta_s(x) \\ u_n(t) \end{bmatrix}. \quad (77)$$

$u_{\text{ad}}(t)$ is chosen such that:

$$u_{\text{ad}}(t) = \hat{\mathbf{W}}^T(t) \underbrace{\tilde{\beta}(x, u_n)}_{\tilde{\beta}(\cdot)}. \quad (78)$$

Defining

$$\tilde{\mathbf{W}}(t) = \mathbf{W} - \hat{\mathbf{W}}(t) \quad (79)$$

and replacing (78) and (79) in (75), yields:

$$\dot{\tilde{\mathbf{x}}}(t) = \mathbf{A}_m \tilde{\mathbf{x}} + \mathbf{B}_m r(t) + \tilde{\mathbf{B}} \lambda \tilde{\mathbf{W}}^T(t) \tilde{\beta}(\cdot). \quad (80)$$

Same as before, Remark 9 allows to find $\dot{\tilde{\mathbf{W}}}(t)$ and also to prove that the system error, $e(t)$, asymptotically goes to zero. Analogously, the error equation is defined:

$$e(t) = \tilde{\mathbf{x}}(t) - \mathbf{x}_m(t). \quad (81)$$

Deriving (81) and with \mathbf{x}_m from (41), the error state dynamics can be obtained:

$$\begin{aligned} \dot{e}(t) &= \dot{\tilde{\mathbf{x}}}(t) - \dot{\mathbf{x}}_m(t) \\ &= \mathbf{A}_m \tilde{\mathbf{x}}(t) + \mathbf{B}_m r(t) + \tilde{\mathbf{B}} \lambda \tilde{\mathbf{W}}^T(t) \tilde{\beta}(\cdot) - \mathbf{A}_m \mathbf{x}_m(t) - \mathbf{B}_m r(t) \\ &= \mathbf{A}_m (\tilde{\mathbf{x}}(t) - \mathbf{x}_m(t)) + \tilde{\mathbf{B}} \lambda \tilde{\mathbf{W}}^T(t) \tilde{\beta}(\cdot) \\ &= \mathbf{A}_m e(t) + \tilde{\mathbf{B}} \lambda \tilde{\mathbf{W}}^T(t) \tilde{\beta}(\cdot). \end{aligned} \quad (82)$$

To meet condition (i) from Remark 9, a positive definite (lower bounded) Lyapunov function is proposed:

Remark 12. *The proposed Lyapunov-like candidate function:*

$$\mathcal{V}(e(t), \tilde{\mathbf{W}}(t)) = e^T(t) \mathbf{P} e(t) + \lambda \left[\tilde{\mathbf{W}}(t)^T \Gamma_u^{-1} \tilde{\mathbf{W}}(t) \right], \quad \Gamma_u > 0. \quad (83)$$

Deriving (83), $\dot{e}(t)$ from (82) and recalling that $\dot{\tilde{\mathbf{W}}}(t) = -\dot{\mathbf{W}}(t)$ from (79), yields:

$$\begin{aligned} \dot{\mathcal{V}} &= \dot{e}^T(t) \mathbf{P} e(t) + e^T(t) \mathbf{P} \dot{e}(t) + 2\lambda \left[\tilde{\mathbf{W}}^T(t) \Gamma_u^{-1} \dot{\tilde{\mathbf{W}}}(t) \right] \\ &= e^T(t) \mathbf{A}_m^T \mathbf{P} e(t) + \lambda \left[\tilde{\mathbf{B}} \tilde{\mathbf{W}}^T(t) \tilde{\beta}(\cdot) \right]^T \mathbf{P} e(t) + e^T(t) \mathbf{P} \mathbf{A}_m e(t) \\ &\quad + \lambda e^T(t) \mathbf{P} \left[\tilde{\mathbf{B}} \tilde{\mathbf{W}}^T(t) \tilde{\beta}(\cdot) \right] - 2\lambda \left[\tilde{\mathbf{W}}^T(t) \Gamma_u^{-1} \dot{\tilde{\mathbf{W}}}(t) \right] \\ &= \underbrace{e^T(t) \left[\mathbf{A}_m^T \mathbf{P} + \mathbf{P} \mathbf{A}_m \right] e(t)}_{\text{(I)}} \\ &\quad + \underbrace{2\lambda e^T(t) \mathbf{P} \tilde{\mathbf{B}} \tilde{\mathbf{W}}^T(t) \tilde{\beta}(\cdot) - 2\lambda \left[\tilde{\mathbf{W}}^T(t) \Gamma_u^{-1} \dot{\tilde{\mathbf{W}}}(t) \right]}_{\text{(II)}}. \end{aligned} \quad (84)$$

Part (I) was explained in (59). Also, recognizing the scalar terms and using the commutative property of multiplication, (II) can be expressed as:

$$\begin{aligned}
 (\text{II}) &= 2\lambda \underbrace{e^T(t)\mathbf{P}\tilde{\mathbf{B}}}_a \underbrace{\tilde{\mathbf{W}}^T(t)\tilde{\beta}(\cdot)}_b - 2\lambda \left[\tilde{\mathbf{W}}^T(t)\Gamma_u^{-1}\dot{\hat{\mathbf{W}}}(t) \right] \\
 &= 2\lambda \left[\tilde{\mathbf{W}}^T(t)\tilde{\beta}(\cdot)e^T(t)\mathbf{P}\tilde{\mathbf{B}} \right] - 2\lambda \left[\tilde{\mathbf{W}}^T(t)\Gamma_u^{-1}\dot{\hat{\mathbf{W}}}(t) \right] \\
 &= 2\lambda \left[\tilde{\mathbf{W}}^T(t)\Gamma_u^{-1} \left(\Gamma_u\tilde{\beta}(\cdot)e^T(t)\mathbf{P}\tilde{\mathbf{B}} - \dot{\hat{\mathbf{W}}}(t) \right) \right] .
 \end{aligned} \tag{85}$$

Then, $\dot{\hat{\mathbf{W}}}(t)$ is defined as:

$$\dot{\hat{\mathbf{W}}}(t) = \Gamma_u\tilde{\beta}(\cdot)e^T(t)\mathbf{P}\tilde{\mathbf{B}} . \tag{86}$$

Therefore, the following applies:

$$\dot{\mathcal{V}} = -\|e(t)\|_2^2 \leq 0 , \tag{87}$$

where $\dot{\mathcal{V}}$ is negative semi-definite, thereby satisfies condition (ii) from Remark 9. Then, to check if condition (iii) is satisfied, (87) is derived:

$$\begin{aligned}
 \ddot{\mathcal{V}} &= -2e^T(t)\dot{e}(t) \\
 &= -2e^T(t) \left(\mathbf{A}_m e(t) + \tilde{\mathbf{B}}\lambda\tilde{\mathbf{W}}^T(t)\tilde{\beta}(\cdot) \right) .
 \end{aligned} \tag{88}$$

Same as before, in Equation (88), $e(t)$ and $\tilde{\mathbf{W}}(t)$ are bounded, since the conditions (i) and (ii) from Remark 9 are satisfied, which means that \mathcal{V} approaches a finite limit as $t \rightarrow \infty$. Moreover, $\tilde{\beta}(x, u_n)$ is bounded since $\tilde{\mathbf{x}}$ and $u_n(t)$, which depends of $\mathbf{x}(t)$, $e(t)$ and $r(t)$, are bounded. Therefore, all terms are bounded and condition (iii) from Remark 9 is satisfied:

$$\begin{aligned}
 \lim_{t \rightarrow \infty} -\|e(t)\|_2^2 &= 0 \\
 \lim_{t \rightarrow \infty} e(t) &= 0 .
 \end{aligned} \tag{89}$$

Finally, it is guaranteed that $e(t)$ asymptotically goes to zero.

2.3.1 MRAC for the unknown input matrix case with feed-forward control

The procedure is analogous to the one developed in Subsection 2.2.1. The differential equation for this case is analog to (73) with the consideration that now the nominal control is the corresponding to $u_{\text{nf}}(t)$ shown in (31). The system is defined below:

$$\dot{\tilde{\mathbf{x}}}(t) = \tilde{\mathbf{A}}\tilde{\mathbf{x}}(t) + \tilde{\mathbf{B}}\lambda [u_{\text{nf}}(t) - u_{\text{ad}}(t) + \lambda^{-1}\mathbf{W}_s^T\beta_s(x)] + \tilde{\mathbf{R}}r(t). \quad (90)$$

Then, same as before, certain terms are added and subtracted:

$$\begin{aligned} \dot{\tilde{\mathbf{x}}}(t) &= \tilde{\mathbf{A}}\tilde{\mathbf{x}}(t) + \tilde{\mathbf{B}}\lambda [u_{\text{nf}}(t) - u_{\text{ad}}(t) + \lambda^{-1}\mathbf{W}_s^T\beta_s(x)] + \tilde{\mathbf{R}}r(t) \\ &\quad + \tilde{\mathbf{B}}\lambda\lambda^{-1}\tilde{\mathbf{k}}^T\tilde{\mathbf{x}}(t) - \tilde{\mathbf{B}}\tilde{\mathbf{k}}^T\tilde{\mathbf{x}}(t) + \tilde{\mathbf{B}}\tilde{\mathbf{K}}_f\tilde{\mathbf{Y}}(t) - \tilde{\mathbf{B}}\lambda\lambda^{-1}\tilde{\mathbf{K}}_f\tilde{\mathbf{Y}}(t). \end{aligned} \quad (91)$$

Grouping conveniently to build \mathbf{A}_m and \mathbf{B}_{mf} , which were previously defined in (42) and (67), respectively, yields:

$$\begin{aligned} \dot{\tilde{\mathbf{x}}}(t) &= \underbrace{(\tilde{\mathbf{A}} - \tilde{\mathbf{B}}\tilde{\mathbf{k}}^T)}_{\mathbf{A}_m}\tilde{\mathbf{x}}(t) + \underbrace{(\tilde{\mathbf{B}}\tilde{\mathbf{K}}_f)}_{\mathbf{B}_{\text{mf}}}\tilde{\mathbf{Y}}(t) + \tilde{\mathbf{R}}r(t) \\ &\quad + \tilde{\mathbf{B}}\lambda \left[u_{\text{nf}}(t) - u_{\text{ad}}(t) + \lambda^{-1}\mathbf{W}_s^T\beta_s(x) - \lambda^{-1} \underbrace{(-\tilde{\mathbf{k}}\tilde{\mathbf{x}}(t) + \tilde{\mathbf{K}}_f\tilde{\mathbf{Y}}(t))}_{u_{\text{nf}}(t)} \right] \\ &= \mathbf{A}_m\tilde{\mathbf{x}}(t) + \mathbf{B}_{\text{mf}}\tilde{\mathbf{Y}}(t) + \tilde{\mathbf{R}}r(t) \\ &\quad + \tilde{\mathbf{B}}\lambda \left[\underbrace{(1 - \lambda^{-1})u_{\text{nf}}(t) + \lambda^{-1}\mathbf{W}_s^T\beta_s(x) - u_{\text{ad}}(t)}_{\mathbf{W}^T\tilde{\beta}_f(x, u_{\text{nf}})} \right], \end{aligned} \quad (92)$$

where:

$$\mathbf{W}^T = \left[\lambda^{-1}\mathbf{W}_s^T, \quad (1 - \lambda^{-1}) \right], \quad (93)$$

$$\tilde{\beta}_f(x, u_{\text{nf}}) = \begin{bmatrix} \beta_s(x) \\ u_{\text{nf}}(t) \end{bmatrix}. \quad (94)$$

Then, $u_{\text{ad}}(t)$ is chosen such that:

$$u_{\text{ad}}(t) = \hat{\mathbf{W}}^T(t) \underbrace{\tilde{\beta}_f(x, u_{\text{nf}})}_{\tilde{\beta}_f(\cdot)}. \quad (95)$$

Replacing (95) and $\tilde{\mathbf{W}}(t)$, previously defined in (79), in (92), results in:

$$\dot{\tilde{\mathbf{x}}}(t) = \mathbf{A}_m \tilde{\mathbf{x}} + \mathbf{B}_{mf} \tilde{\mathbf{Y}}(t) + \tilde{\mathbf{R}}r(t) + \tilde{\mathbf{B}}\lambda\tilde{\mathbf{W}}^T(t)\tilde{\beta}_f(\cdot). \quad (96)$$

Finally, recalling $\mathbf{x}_m(t)$ from (66), the error of the system $e(t) = \tilde{\mathbf{x}}(t) - \mathbf{x}_m(t)$ is derived:

$$\begin{aligned} \dot{e}(t) &= \dot{\tilde{\mathbf{x}}}(t) - \dot{\mathbf{x}}_m(t) \\ &= \mathbf{A}_m \tilde{\mathbf{x}}(t) + \mathbf{B}_{mf} \tilde{\mathbf{Y}}(t) + \tilde{\mathbf{R}}r(t) + \tilde{\mathbf{B}}\lambda\tilde{\mathbf{W}}^T(t)\tilde{\beta}_f(\cdot) \\ &\quad - \left[\mathbf{A}_m \mathbf{x}_m(t) + \mathbf{B}_{mf} \tilde{\mathbf{Y}}(t) + \tilde{\mathbf{R}}r(t) \right] \\ &= \mathbf{A}_m (\tilde{\mathbf{x}}(t) - \mathbf{x}_m(t)) + \tilde{\mathbf{B}}\lambda\tilde{\mathbf{W}}^T(t)\tilde{\beta}_f(\cdot) \\ &= \mathbf{A}_m e(t) + \tilde{\mathbf{B}}\lambda\tilde{\mathbf{W}}^T(t)\tilde{\beta}_f(\cdot). \end{aligned} \quad (97)$$

It can be noticed that Equation (97) is equivalent to (82). Therefore, considering the theory of Remark 9 and with the Lyapunov candidate function proposed in (83), it can be stated that $\hat{\mathbf{W}}(t)$ is determined similarly to Equation (86). Then, the system error, $e(t)$, goes asymptotically to zero, as explained before.

3 Derivative-free adaptive control

In this chapter, first the definition of derivative-free model reference adaptive control (DFMRAC) is given. Secondly, the DFMRAC algorithm is presented and finally, there is shown the considerations related to the unknown input matrix case.

3.1 What is derivative-free adaptive control?

The DFMRAC was proposed by Dr. Yucelen in his dissertation entitled Advances in Adaptive Control Theory: Gradient- and Derivative-free Approaches [33], which it is also a direct adaptive control but with a slightly different approach. In the last chapter, the MRAC assumes that there exists a constant, but unknown, ideal set of uncertainties weights \mathbf{W}_s , see (45). However, the DFMRAC considers that \mathbf{W}_s could be a time-varying weights $\mathbf{W}_s(t)$. For that reason, according to [33] it has a better performance for applications that can undergo a sudden change in dynamics, reconfiguration, deployment of a payload, docking or structural damage. Furthermore, the DFMRAC does not use an integration in its weight update law, as does the MRAC. This integration, found in the MRAC algorithm, is disadvantageous because it causes drifting in the estimated parameters $\hat{\mathbf{W}}_s(t)$, which can be seen in the simulations presented in Chapter 4 and in the real experiments in Chapter 5. Moreover, it is stated that the DFMRAC is particularly well suited for maintaining stability, error transient performance, fast upset recovery and preserving to the ex-

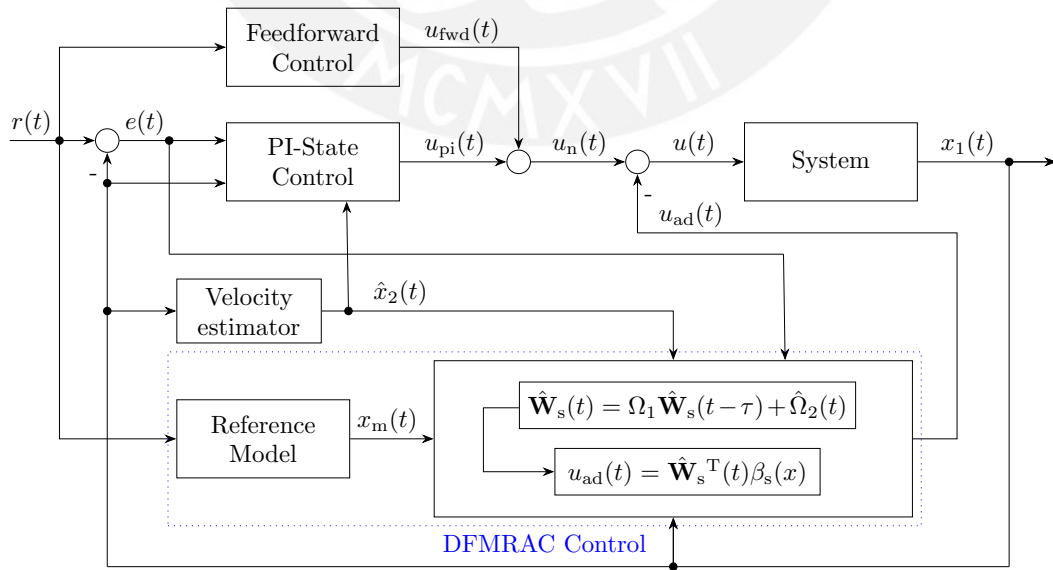


Figure 8: DFMRAC scheme adopted to the nanopositioning machine.

tent possible the time delay margins of the nominal design [33]. Subsequent work demonstrated the advantages of using DFMRAC over MRAC in relation to robustness against unmodeled dynamics [34]. Additionally, some applications related to aerial control has been developed [16], [31] and other topics [35]. The present thesis uses the DFMRAC algorithm proposed in [28] adapted to the nanopositioning machine, whose scheme is shown in Figure 8.

3.2 Design of the DFMRAC

In this subsection, it is presented the development of the DFMRAC algorithm without unknown parameters in the input matrix. In the same manner, the nominal control is first considered without feed-forward control, $u_n(t)$, and then considering it, $u_{nf}(t)$. As stated before, the ideal uncertainty weights can change in time in the DFMRAC algorithm. In that sense, the state space representation of the system is the same as in (39), however the matched uncertainty $\Delta(x)$ is redefined as:

$$\Delta(t, x) = \mathbf{W}_s^T(t)\beta_s(x(t)) , \quad (98)$$

where $\mathbf{W}_s(t)$ is an unknown time-varying weight matrix, which satisfies $\|\mathbf{W}_s(t)\| \leq w^*$. Then, the differential equation of the system is as follows:

$$\dot{\tilde{\mathbf{x}}}(t) = \tilde{\mathbf{A}}\tilde{\mathbf{x}}(t) + \tilde{\mathbf{B}}[u(t) + \Delta(t, x)] + \tilde{\mathbf{R}}r(t) . \quad (99)$$

The same procedure from (48) to (49) is applied, so $u_{ad}(t)$ is defined as:

$$u_{ad}(t) = \hat{\Delta}(t, x) = \hat{\mathbf{W}}_s^T(t)\beta_s(x(t)) . \quad (100)$$

The state error dynamics and the procedure to obtain it are equivalent to (54), then the following is obtained:

$$\dot{e}(t) = \mathbf{A}_m e(t) + \tilde{\mathbf{B}}\tilde{\mathbf{W}}_s^T(t)\beta_s(x(t)) . \quad (101)$$

To fully define the adaptive controller $u_{ad}(t)$, $\hat{\mathbf{W}}_s(t)$ is now determined as:

$$\hat{\mathbf{W}}_s(t) = \Omega_1 \hat{\mathbf{W}}_s(t - \tau) + \hat{\Omega}_2(t) , \quad (102)$$

where:

$$0 \leq \Omega_1^T \Omega_1 < \mathbf{I} \quad (103)$$

$$\hat{\Omega}_2(t) = \mathbf{K}_2 \beta_s(x(t)) e^T(t) \mathbf{P} \tilde{\mathbf{B}} , \quad \mathbf{K}_2 > 0 . \quad (104)$$

The derivative-free adaptive control algorithm is now completed because the $\hat{\mathbf{W}}_s(t)$ term has been defined. However, what remains to be demonstrated is its stability. The stability of the system is analysed by applying the uniformly ultimately boundedness (UUB) theory extracted from the book Nonlinear Control [18]. Remark 13 summarizes the theory from [18].

Remark 13. *Lyapunov in uniform ultimate boundedness (UUB):*

Consider a continuously differentiable, positive definite function $\mathcal{V}(x)$ and suppose that the set $\{\mathcal{V}(x) \leq c\}$ is compact, for some $c > 0$. Let

$$\Lambda = \{\varepsilon \leq \mathcal{V}(x) \leq c\}$$

for some positive constant $\varepsilon < c$. Suppose the derivative of $\mathcal{V}(x)$ along the trajectories of the system $\dot{x} = f(t, x)$ satisfies:

$$\dot{\mathcal{V}}(t, x) \leq -W_3(x), \quad \forall x \in \Lambda, \quad \forall t \geq t_0,$$

where $W_3(x)$ is a continuous positive definite function. The sets $\Omega_c = \{\mathcal{V}(x) \leq c\}$ and $\Omega_\varepsilon = \{\mathcal{V}(x) \leq \varepsilon\}$ are positively invariant since on the boundaries $\partial\Omega_c$ and $\partial\Omega_\varepsilon$, the derivative $\dot{\mathcal{V}}$ is negative. Since $\dot{\mathcal{V}}$ is negative in Λ , a trajectory starting in Λ must move in a direction decreasing $\mathcal{V}(x(t))$. Therefore, the trajectory behaves as if the origin was uniformly asymptotically stable and satisfies an inequality of the form:

$$\|x(t)\| \leq \beta(\|x(t_0)\|, t - t_0),$$

for some class \mathcal{KL} function β . The function $\mathcal{V}(x(t))$ will continue decreasing until the trajectory enters the set Ω_ε in finite time and stays therein for all future time.

First of all, it is already known that \mathbf{P} satisfies the Lyapunov equation (44). Therefore, it is just necessary to prove that $e(t)$ and $\hat{\mathbf{W}}_s(t)$ are uniformly ultimately bounded. To begin with, $\Omega_2(t)$ is defined as:

$$\Omega_2(t) \equiv \mathbf{W}_s(t) - \Omega_1 \mathbf{W}_s(t - \tau), \quad (105)$$

where $\|\Omega_2(t)\| \leq \delta^*$, $\delta^* = w^*(1 + \|\Omega_1\|)$. Also, adding equations (102) and (105), with the consideration that $\tilde{\mathbf{W}}_s(t) = \mathbf{W}_s(t) - \hat{\mathbf{W}}_s(t)$ and analogously $\tilde{\mathbf{W}}_s(t - \tau) = \mathbf{W}_s(t - \tau) - \hat{\mathbf{W}}_s(t - \tau)$, $\tilde{\mathbf{W}}_s(t)$ can be written as:

$$\tilde{\mathbf{W}}_s(t) = \Omega_1 \tilde{\mathbf{W}}_s(t - \tau) + \Omega_2(t) - \hat{\Omega}_2(t). \quad (106)$$

Then, replacing (106) in (101), the error dynamics is now:

$$\dot{e}(t) = \mathbf{A}_m e(t) + \tilde{\mathbf{B}} \left[\Omega_1 \tilde{\mathbf{W}}_s(t - \tau) + \Omega_2(t) - \hat{\Omega}_2(t) \right]^T \beta_s(x(t)). \quad (107)$$

Following the procedure from Remark 13, a Lyapunov-Krasovskii functional candidate (continuously differentiable and positive definite) is proposed:

Remark 14. *The proposed Lyapunov-Krasovskii functional candidate:*

$$\mathcal{V}(e(t), \tilde{\mathbf{W}}_t) = e^T(t) \mathbf{P} e(t) + \rho \left[\int_{t-\tau}^t \tilde{\mathbf{W}}_s^T(s) \tilde{\mathbf{W}}_s(s) ds \right], \quad (108)$$

where $\rho > 0$ and $\tilde{\mathbf{W}}_t$ represents $\tilde{\mathbf{W}}_s(t)$ over the time interval $t - \tau$ to t .

It can be observed that the integral part of the Lyapunov-Krasovskii functional in (108) is always positive, because its integrand is a squared term and the limits of integration are related to time (positive). As a reminder, the Second Fundamental Theorem of Calculus is outlined, because it is useful for deriving the function above. The theorem was extracted from [26].

Theorem 1. *Second Fundamental Theorem of Calculus: If f is continuous on $[a, b]$, then*

$$\int_a^b f(x) dx = F(b) - F(a),$$

where F is any anti-derivative of f , in other words, a function such that $F' = f$.

Deriving (108) and using Theorem 1, yields:

$$\dot{\mathcal{V}} = \dot{e}^T(t) \mathbf{P} e(t) + e^T(t) \mathbf{P} \dot{e}(t) + \rho \left[\tilde{\mathbf{W}}_s^T(t) \tilde{\mathbf{W}}_s(t) - \tilde{\mathbf{W}}_s^T(t - \tau) \tilde{\mathbf{W}}_s(t - \tau) \right]. \quad (109)$$

Then, replacing $\dot{e}(t)$ from (101) in (109), results in:

$$\begin{aligned}
 \dot{\nu} &= e^T(t) \mathbf{A}_m^T \mathbf{P} e(t) + \left[\tilde{\mathbf{B}} \tilde{\mathbf{W}}_s^T(t) \beta_s(x) \right]^T \mathbf{P} e(t) + e^T(t) \mathbf{P} \mathbf{A}_m e(t) \\
 &\quad + e^T(t) \mathbf{P} \left[\tilde{\mathbf{B}} \tilde{\mathbf{W}}_s^T(t) \beta_s(x) \right] \\
 &\quad + \rho \left[\tilde{\mathbf{W}}_s^T(t) \tilde{\mathbf{W}}_s(t) - \tilde{\mathbf{W}}_s^T(t - \tau) \tilde{\mathbf{W}}_s(t - \tau) \right] \\
 &= \underbrace{e^T(t) \left[\mathbf{A}_m^T \mathbf{P} + \mathbf{P} \mathbf{A}_m \right] e(t)}_{\text{(I)}} + 2e^T(t) \mathbf{P} \tilde{\mathbf{B}} \underbrace{\tilde{\mathbf{W}}_s^T(t)}_{\text{(II)}} \beta_s(x(t)) \\
 &\quad + \rho \left[\underbrace{\tilde{\mathbf{W}}_s^T(t) \tilde{\mathbf{W}}_s(t)}_{\text{(III)}} - \tilde{\mathbf{W}}_s^T(t - \tau) \tilde{\mathbf{W}}_s(t - \tau) \right].
 \end{aligned} \tag{110}$$

Part **(I)** was explained in (59). Then, for part **(II)** replace Equation (106) in (110). For part **(III)** consider that $\Upsilon = \mathbf{I} + \mathcal{E}$ with $\mathcal{E} \geq 0$ and \mathcal{E} a diagonal matrix (note that it is also true that Υ is a positive diagonal matrix). These operations result in:

$$\begin{aligned}
 \dot{\nu} &= -e^T(t) e(t) + 2e^T(t) \mathbf{P} \tilde{\mathbf{B}} \left[\Omega_1 \tilde{\mathbf{W}}_s(t - \tau) \right]^T \beta_s(x(t)) \\
 &\quad - 2e^T(t) \mathbf{P} \tilde{\mathbf{B}} \hat{\Omega}_2^T(t) \beta_s(x(t)) + 2e^T(t) \mathbf{P} \tilde{\mathbf{B}} \Omega_2^T(t) \beta_s(x(t)) \\
 &\quad + \rho \left[-\tilde{\mathbf{W}}_s^T(t) \mathcal{E} \tilde{\mathbf{W}}_s(t) + \underbrace{\tilde{\mathbf{W}}_s^T(t) \Upsilon \tilde{\mathbf{W}}_s(t)}_{\text{(I)}} - \tilde{\mathbf{W}}_s^T(t - \tau) \tilde{\mathbf{W}}_s(t - \tau) \right].
 \end{aligned} \tag{111}$$

Replacing (106) in (111), only for the term **(I)**, yields:

$$\begin{aligned}
 \dot{\nu} &= -e^T(t) e(t) + 2e^T(t) \mathbf{P} \tilde{\mathbf{B}} \left[\Omega_1 \tilde{\mathbf{W}}_s(t - \tau) \right]^T \beta_s(x(t)) \\
 &\quad - 2e^T(t) \mathbf{P} \tilde{\mathbf{B}} \hat{\Omega}_2^T(t) \beta_s(x(t)) + 2e^T(t) \mathbf{P} \tilde{\mathbf{B}} \Omega_2^T(t) \beta_s(x(t)) \\
 &\quad + \rho \left[-\tilde{\mathbf{W}}_s^T(t) \mathcal{E} \tilde{\mathbf{W}}_s(t) - \tilde{\mathbf{W}}_s^T(t - \tau) \tilde{\mathbf{W}}_s(t - \tau) \right. \\
 &\quad \left. + \tilde{\mathbf{W}}_s^T(t - \tau) \Omega_1^T \Upsilon \Omega_1 \tilde{\mathbf{W}}_s(t - \tau) \right] \boxed{+ \tilde{\mathbf{W}}_s^T(t - \tau) \Omega_1^T \Upsilon \Omega_2(t)}^{(i_1)} \\
 &\quad \boxed{- \tilde{\mathbf{W}}_s^T(t - \tau) \Omega_1^T \Upsilon \hat{\Omega}_2(t)}^{(i_2)} \boxed{+ \Omega_2^T(t) \Upsilon \Omega_1 \tilde{\mathbf{W}}_s(t - \tau)}^{(i_1)} \\
 &\quad \left. + \Omega_2^T(t) \Upsilon \Omega_2(t) \boxed{- \Omega_2^T(t) \Upsilon \hat{\Omega}_2(t)}^{(i_3)} \boxed{- \hat{\Omega}_2^T(t) \Upsilon \Omega_1 \tilde{\mathbf{W}}_s(t - \tau)}^{(i_2)} \right. \\
 &\quad \left. \boxed{- \hat{\Omega}_2^T(t) \Upsilon \Omega_2(t)}^{(i_3)} + \hat{\Omega}_2^T(t) \Upsilon \hat{\Omega}_2(t) \right].
 \end{aligned} \tag{112}$$

In Equation (112), it is possible to sum the terms in the boxes with the same upper indices (i_1) , (i_2) and (i_3) because they are equivalent. Notice, that the terms are scalars, therefore for term (i_1) yields $\tilde{\mathbf{W}}_s^T(t - \tau)\Omega_1^T\Upsilon\Omega_2(t) = [\tilde{\mathbf{W}}_s^T(t - \tau)\Omega_1^T\Upsilon\Omega_2(t)]^T = [\Upsilon\Omega_2(t)]^T[\tilde{\mathbf{W}}_s^T(t - \tau)\Omega_1^T]^T = \Omega_2^T(t)\Upsilon\Omega_1\tilde{\mathbf{W}}_s(t - \tau)$. Analogously, the same procedure can be applied for (i_2) and (i_3) , which results:

$$\begin{aligned}
 \dot{\mathcal{V}} = & -e^T(t)e(t) + 2e^T(t)\mathbf{P}\tilde{\mathbf{B}} \left[\Omega_1\tilde{\mathbf{W}}_s(t - \tau) \right]^T \beta_s(x(t)) \\
 & - 2e^T(t)\mathbf{P}\tilde{\mathbf{B}}\hat{\Omega}_2^T(t)\beta_s(x(t)) + 2e^T(t)\mathbf{P}\tilde{\mathbf{B}}\Omega_2^T(t)\beta_s(x(t)) \\
 & + \rho \left[-\tilde{\mathbf{W}}_s^T(t)\mathcal{E}\tilde{\mathbf{W}}_s(t) - \tilde{\mathbf{W}}_s^T(t - \tau)\tilde{\mathbf{W}}_s(t - \tau) \right. \\
 & + \tilde{\mathbf{W}}_s^T(t - \tau)\Omega_1^T\Upsilon\Omega_1\tilde{\mathbf{W}}_s(t - \tau) + \hat{\Omega}_2^T(t)\Upsilon\hat{\Omega}_2(t) + \Omega_2^T(t)\Upsilon\Omega_2(t) \\
 & \left. - 2\hat{\Omega}_2^T(t)\Upsilon\Omega_1\tilde{\mathbf{W}}_s(t - \tau) + \boxed{2\tilde{\mathbf{W}}_s^T(t - \tau)\Omega_1^T\Upsilon\Omega_2(t)}^{(a)} \right. \\
 & \left. - 2\hat{\Omega}_2^T(t)\Upsilon\Omega_2(t) \right].
 \end{aligned} \tag{113}$$

The following property of Young's inequality generalized to matrices, which was extracted from [28], is highlighted below:

Remark 15. *Young's inequality generalized to matrices*

$$\begin{aligned}
 \text{tr} [A^T B] &= \text{vec}(A)^T \text{vec}(B) \\
 &\leq \gamma \text{vec}(A)^T \text{vec}(A) + \text{vec}(B)^T \text{vec}(B) / (4\gamma) = \text{tr} [A^T \mathcal{Z} A] \\
 &\quad + \text{tr} [B^T \mathcal{Z}^{-1} B] / 4,
 \end{aligned}$$

where $\mathcal{Z} > 0$. And also $\mathcal{Z} = \gamma \mathbf{I}$, γ is a scalar.

Using Remark 15, the term with the upper index (a) from (113) could be expressed as:

$$\begin{aligned}
 2\tilde{\mathbf{W}}_s^T(t - \tau)\Omega_1^T\Upsilon\Omega_2(t) &\leq \tilde{\mathbf{W}}_s^T(t - \tau)\Omega_1^T\mathcal{Z}\Omega_1\tilde{\mathbf{W}}_s(t - \tau) \\
 &\quad + \Omega_2^T(t)\Upsilon\mathcal{Z}^{-1}\Upsilon\Omega_2(t), \quad \mathcal{Z} > 0.
 \end{aligned} \tag{114}$$

Replacing (114) and $\hat{\Omega}_2(t)$ from (104) in (113), yields:

$$\begin{aligned}
 \dot{\mathcal{V}} = & -e^T(t)e(t) \boxed{+2e^T(t)\mathbf{P}\tilde{\mathbf{B}} \left[\Omega_1 \tilde{\mathbf{W}}_s(t-\tau) \right]^T \beta_s(x(t))}^{(a_1)} \\
 & \boxed{-2e^T(t)\mathbf{P}\tilde{\mathbf{B}} \left[\mathbf{K}_2 \beta_s(x(t)) e^T(t)\mathbf{P}\tilde{\mathbf{B}} \right]^T \beta_s(x(t))}^{(b_1)} \\
 & \boxed{+2e^T(t)\mathbf{P}\tilde{\mathbf{B}} \Omega_2^T(t) \beta_s(x(t))}^{(c_1)} \\
 & + \rho \left[-\tilde{\mathbf{W}}_s^T(t) \mathcal{E} \tilde{\mathbf{W}}_s(t) \boxed{-\tilde{\mathbf{W}}_s^T(t-\tau) \tilde{\mathbf{W}}_s(t-\tau)}^{(d_1)} \right. \\
 & \left. + \tilde{\mathbf{W}}_s^T(t-\tau) \Omega_1^T \Upsilon \Omega_1 \tilde{\mathbf{W}}_s(t-\tau) \right]^{(d_2)} \\
 & \left. + \left[\mathbf{K}_2 \beta_s(x(t)) e^T(t)\mathbf{P}\tilde{\mathbf{B}} \right]^T \Upsilon \left[\mathbf{K}_2 \beta_s(x(t)) e^T(t)\mathbf{P}\tilde{\mathbf{B}} \right] \right]^{(b_2)} \\
 & \boxed{+\Omega_2^T(t) \Upsilon \Omega_2(t)}^{(e_1)} \boxed{-2 \left[\mathbf{K}_2 \beta_s(x(t)) e^T(t)\mathbf{P}\tilde{\mathbf{B}} \right]^T \Upsilon \Omega_1 \tilde{\mathbf{W}}_s(t-\tau)}^{(a_2)} \\
 & \boxed{+\tilde{\mathbf{W}}_s^T(t-\tau) \Omega_1^T \mathcal{Z} \Omega_1 \tilde{\mathbf{W}}_s(t-\tau)}^{(d_3)} \boxed{+\Omega_2^T(t) \Upsilon \mathcal{Z}^{-1} \Upsilon \Omega_2(t)}^{(e_2)} \\
 & \left. -2 \left[\mathbf{K}_2 \beta_s(x(t)) e^T(t)\mathbf{P}\tilde{\mathbf{B}} \right]^T \Upsilon \Omega_2(t) \right]^{(c_2)} \Bigg] .
 \end{aligned} \tag{115}$$

Then, considering that $\mathbf{K}_2 = (1/\rho)\Upsilon^{-1}$, the terms with the upper indices (a_1) , (a_2) , (c_1) and (c_2) are cancelled. To begin with, the following proof $\rho(a_2) + (a_1) = 0$ is performed (notice that (i) and (ii) terms in (116) are scalars):

$$\begin{aligned}
 0 & = \rho \left(-2 \left[\mathbf{K}_2 \beta_s(x(t)) e^T(t)\mathbf{P}\tilde{\mathbf{B}} \right]^T \Upsilon \Omega_1 \tilde{\mathbf{W}}_s(t-\tau) \right) + (a_1) \\
 & = \rho \left(-2 \left[\beta_s(x(t)) e^T(t)\mathbf{P}\tilde{\mathbf{B}} \right]^T \mathbf{K}_2 \Upsilon \Omega_1 \tilde{\mathbf{W}}_s(t-\tau) \right) + (a_1) \\
 & = -2 \left[\beta_s(x(t)) e^T(t)\mathbf{P}\tilde{\mathbf{B}} \right]^T \Omega_1 \tilde{\mathbf{W}}_s(t-\tau) + (a_1) \\
 & = -2 \underbrace{\left[e^T(t)\mathbf{P}\tilde{\mathbf{B}} \right]^T}_{(i)} \underbrace{\beta_s(x(t)) \Omega_1 \tilde{\mathbf{W}}_s(t-\tau)}_{(ii)} + (a_1) \\
 & = -2e^T(t)\mathbf{P}\tilde{\mathbf{B}} \left[\Omega_1 \tilde{\mathbf{W}}_s(t-\tau) \right]^T \beta_s(x(t)) + (a_1) = 0 .
 \end{aligned} \tag{116}$$

The proof for $\rho(c_2) + (c_1) = 0$ is shown below (notice that (i) and (ii) terms in (117) are scalars):

$$\begin{aligned}
 0 &= \rho \left(-2 \left[\mathbf{K}_2 \beta_s(x(t)) e^T(t) \mathbf{P} \tilde{\mathbf{B}} \right]^T \Upsilon \Omega_2(t) \right) + (c_1) \\
 &= \rho \left(-2 \left[\beta_s(x(t)) e^T(t) \mathbf{P} \tilde{\mathbf{B}} \right]^T \mathbf{K}_2 \Upsilon \Omega_2(t) \right) + (c_1) \\
 &= -2 \left[\beta_s(x(t)) e^T(t) \mathbf{P} \tilde{\mathbf{B}} \right]^T \Omega_2(t) + (c_1) \\
 &= -2 \underbrace{\left[e^T(t) \mathbf{P} \tilde{\mathbf{B}} \right]^T}_{(i)} \underbrace{\beta_s(x(t)) \Omega_2(t)}_{(ii)} + (c_1) \\
 &= -2 e^T(t) \mathbf{P} \tilde{\mathbf{B}} \Omega_2^T(t) \beta_s(x(t)) + (c_1) = 0.
 \end{aligned} \tag{117}$$

Then, it is possible to group the remaining terms. Grouping $\rho(d_1)$, $\rho(d_2)$ and $\rho(d_3)$, results in:

$$\begin{aligned}
 \rho \sum_{i=1}^3 (d_i) &= \rho \left[-\tilde{\mathbf{W}}_s^T(t-\tau) \tilde{\mathbf{W}}_s(t-\tau) + \tilde{\mathbf{W}}_s^T(t-\tau) \Omega_1^T \Upsilon \Omega_1 \tilde{\mathbf{W}}_s(t-\tau) \right. \\
 &\quad \left. + \tilde{\mathbf{W}}_s^T(t-\tau) \Omega_1^T \mathcal{Z} \Omega_1 \tilde{\mathbf{W}}_s(t-\tau) \right] \\
 &= -\rho \left[\tilde{\mathbf{W}}_s^T(t-\tau) \tilde{\mathbf{W}}_s(t-\tau) - \tilde{\mathbf{W}}_s^T(t-\tau) \Omega_1^T \Upsilon \Omega_1 \tilde{\mathbf{W}}_s(t-\tau) \right. \\
 &\quad \left. - \tilde{\mathbf{W}}_s^T(t-\tau) \Omega_1^T \mathcal{Z} \Omega_1 \tilde{\mathbf{W}}_s(t-\tau) \right] \\
 &= -\rho \left[\tilde{\mathbf{W}}_s^T(t-\tau) \left[\mathbf{I} - \Omega_1^T (\Upsilon + \mathcal{Z}) \Omega_1 \right] \tilde{\mathbf{W}}_s(t-\tau) \right].
 \end{aligned} \tag{118}$$

Grouping $\rho(e_1)$ and $\rho(e_2)$, yields:

$$\begin{aligned}
 \rho(e_1) + \rho(e_2) &= \rho \left[\Omega_2^T(t) \Upsilon \Omega_2(t) + \Omega_2^T(t) \Upsilon \mathcal{Z}^{-1} \Upsilon \Omega_2(t) \right] \\
 &= \rho \left[\Omega_2^T(t) (\Upsilon + \Upsilon \mathcal{Z}^{-1} \Upsilon) \Omega_2(t) \right] \\
 &= \rho \left[\Omega_2^T(t) \left(\Upsilon + \frac{\Upsilon^2}{\gamma} \right) \Omega_2(t) \right].
 \end{aligned} \tag{119}$$

Terms (b_1) and $\rho(b_2)$ can also be grouped. Notice that (i) and (ii) terms in (120) are scalars and recalling that $\mathbf{K}_2 = (1/\rho)\Upsilon^{-1}$, the following is obtained:

$$\begin{aligned}
 \rho(b_2) + (b_1) &= \rho \left(\left[\mathbf{K}_2 \beta_s(x(t)) e^T(t) \mathbf{P} \tilde{\mathbf{B}} \right]^T \Upsilon \mathbf{K}_2 \beta_s(x(t)) e^T(t) \mathbf{P} \tilde{\mathbf{B}} \right) + (b_1) \\
 &= \rho \left(\left[\beta_s(x(t)) e^T(t) \mathbf{P} \tilde{\mathbf{B}} \right]^T \mathbf{K}_2 \Upsilon \mathbf{K}_2 \beta_s(x(t)) e^T(t) \mathbf{P} \tilde{\mathbf{B}} \right) + (b_1) \\
 &= \left[\beta_s(x(t)) e^T(t) \mathbf{P} \tilde{\mathbf{B}} \right]^T \mathbf{K}_2 \beta_s(x(t)) e^T(t) \mathbf{P} \tilde{\mathbf{B}} + (b_1) \\
 &= \underbrace{\left[e^T(t) \mathbf{P} \tilde{\mathbf{B}} \right]^T}_{(i)} \underbrace{\beta_s(x(t))^T \mathbf{K}_2 \beta_s(x(t)) e^T(t) \mathbf{P} \tilde{\mathbf{B}}}_{(ii)} + (b_1) \\
 &= e^T(t) \mathbf{P} \tilde{\mathbf{B}} \left[\mathbf{K}_2 \beta_s(x(t)) e^T(t) \mathbf{P} \tilde{\mathbf{B}} \right]^T \beta_s(x(t)) + (b_1) \\
 &= -e^T(t) \mathbf{P} \tilde{\mathbf{B}} \left[\mathbf{K}_2 \beta_s(x(t)) e^T(t) \mathbf{P} \tilde{\mathbf{B}} \right]^T \beta_s(x(t)) \\
 &= -e^T(t) \mathbf{P} \tilde{\mathbf{B}} \tilde{\mathbf{B}}^T \mathbf{P} e(t) \beta_s(x(t))^T \mathbf{K}_2 \beta_s(x(t)) .
 \end{aligned} \tag{120}$$

Finally, replacing (120), (118) and (119) in (115), yields:

$$\begin{aligned}
 \dot{\mathcal{V}} &= -e^T(t)e(t) - e^T(t) \mathbf{P} \tilde{\mathbf{B}} \tilde{\mathbf{B}}^T \mathbf{P} e(t) \beta_s(x(t))^T \mathbf{K}_2 \beta_s(x(t)) \\
 &\quad - \rho \left[\tilde{\mathbf{W}}_s^T(t) \mathcal{E} \tilde{\mathbf{W}}_s(t) \right] \\
 &\quad - \rho \left[\tilde{\mathbf{W}}_s^T(t - \tau) \left[\mathbf{I} - \Omega_1^T (\Upsilon + \mathcal{Z}) \Omega_1 \right] \tilde{\mathbf{W}}_s(t - \tau) \right] \\
 &\quad + \rho \left[\Omega_2^T(t) \left(\Upsilon + \frac{\Upsilon^2}{\gamma} \right) \Omega_2(t) \right] .
 \end{aligned} \tag{121}$$

Taking (103) into consideration and defining $\mathbf{K}_1 \triangleq (\Upsilon + \mathcal{Z})^{-1} < \mathbf{I}$ for Ω_1 , yields:

$$\dot{\mathcal{V}} \leq -\|e(t)\|^2 - c_2 \left\| \tilde{\mathbf{W}}_s(t) \right\|^2 - c_3 \left\| \tilde{\mathbf{W}}_s(t - \tau) \right\|^2 + \zeta , \tag{122}$$

where the constants c_2 , c_3 , and ζ are:

$$c_2 = \rho \lambda_{\min}(\mathcal{E}) \geq 0 , \tag{123}$$

$$c_3 = \rho \lambda_{\min}(\mathbf{I} - \Omega_1^T \mathbf{K}_1^{-1} \Omega_1) > 0 , \tag{124}$$

$$\zeta = \rho \lambda_{\min} \left(\Upsilon + \frac{\Upsilon^2}{\gamma} \right) \delta^{*2} \geq 0 . \tag{125}$$

If $\mathcal{E} > 0$, then since $\Upsilon = \mathbf{K}_1^{-1} - \mathcal{Z} = 1 + \mathcal{E}$, $0 < \mathbf{K}_1 < \mathbf{I}$, and $\mathcal{Z} > 0$, it can be deduced that Υ should be in the open interval $(1, \mathbf{K}_1^{-1})$. Notice that, either $\|e(t)\| > \Psi_1$, $\|\tilde{\mathbf{W}}_s(t)\| > \Psi_2$ or $\|\tilde{\mathbf{W}}_s(t - \tau)\| > \Psi_3$ renders $\dot{\mathcal{V}} < 0$, where $\Psi_1 = \sqrt{\zeta}$, $\Psi_2 = \sqrt{\zeta/c_2}$ and $\Psi_3 = \sqrt{\zeta/c_3}$, or also:

$$\Psi_1 = \delta^* \sqrt{\rho \lambda_{\min} \left(\Upsilon + \frac{\Upsilon^2}{\gamma} \right)}, \quad (126)$$

$$\Psi_2 = \Psi_1 \sqrt{\frac{1}{c_2}} = \Psi_1 \sqrt{\frac{1}{\rho \lambda_{\min}(\mathcal{E})}}, \quad (127)$$

$$\Psi_3 = \Psi_1 \sqrt{\frac{1}{c_3}} = \Psi_1 \sqrt{\frac{1}{\rho \lambda_{\min}(\mathbf{I} - \Omega_1^T \mathbf{K}_1^{-1} \Omega_1)}}. \quad (128)$$

Therefore, it follows that $e(t)$ and $\tilde{\mathbf{W}}(t)$ are uniformly ultimately bounded.

Remark 16. *DFMRAC with feed-forward control:*

The considerations to build the adaptive control considering feed-forward control has already been explained. Notice that the error dynamics, $\dot{e}(t)$, for the MRAC controller with feed-forward control (71) is equivalent to (101) with the exception that now the uncertainty weights can change in time. Therefore, it is possible to use the proposed Lyapunov-Krasovskii functional in (108) and ensure that $e(t)$ and $\tilde{\mathbf{W}}(t)$ are uniformly ultimately bounded with a procedure similar to the above.

3.3 Extensions to the unknown input matrix case - DFMRAC

Same as in Section 2.3, the DFMRAC considering the unknown input matrix case is derived. This extension case can be found in [33] and also an application in adaptive flight control is shown in [28]. According to [34], it is proved that DFMRAC is inherently robust to unmodeled dynamics (including an unknown input matrix), which robustness can be improved by simply adjusting the adaptation gain. The state space representation of the system for this case is:

Remark 17. *State space representation of the system with an unknown input matrix using DFMRAC:*

$$\begin{aligned}
 \underbrace{\begin{bmatrix} \dot{x}_1(t) \\ \dot{x}_2(t) \\ \dot{x}_I(t) \end{bmatrix}}_{\tilde{\dot{x}}(t)} &= \underbrace{\begin{bmatrix} 0 & 1 & 0 \\ -\frac{c}{m} & -\frac{d}{m} & 0 \\ -1 & 0 & 0 \end{bmatrix}}_{\mathbf{A}} \underbrace{\begin{bmatrix} x_1(t) \\ x_2(t) \\ x_I(t) \end{bmatrix}}_{\tilde{x}(t)} + \underbrace{\begin{bmatrix} 0 \\ 0 \\ 1 \end{bmatrix}}_{\tilde{\mathbf{R}}} r(t) \\
 &+ \underbrace{\begin{bmatrix} 0 \\ \frac{k_m k_r}{m} \\ 0 \end{bmatrix}}_{\tilde{\mathbf{B}}} \underbrace{\left[\frac{m}{k_m k_r} \left(\frac{(k_m) k_r}{m} \right) \right]}_{\lambda} u(t) \\
 &+ \tilde{\mathbf{B}} \lambda \underbrace{\begin{bmatrix} \frac{\bar{m}}{(k_m) k_r} (-\Delta \left[\frac{c}{m} \right]) \\ \frac{\bar{m}}{(k_m) k_r} (-\Delta \left[\frac{d}{m} \right]) - \frac{\bar{m}}{(k_m) k_r} \left(\frac{1}{m} \right) \sigma \\ 0 \\ -\frac{\bar{m}}{(k_m) k_r} \left(\frac{1}{m} \right) F_c \\ -\frac{\bar{m}}{(k_m) k_r} \left(\frac{1}{m} \right) F_s \end{bmatrix}}_{\mathbf{W}_s^T} \underbrace{\begin{bmatrix} x_1 \\ x_2 \\ 1 \\ \left(1 - e^{-\left| \frac{x_2}{v_s} \right|^\delta} \right) \text{sign}(x_2) \\ \left(e^{-\left| \frac{x_2}{v_s} \right|^\delta} \right) \text{sign}(x_2) \end{bmatrix}}_{\beta_s(x)}, \tag{129}
 \end{aligned}$$

where $\frac{\bar{c}}{\bar{m}} = \frac{c}{m} + \Delta \left[\frac{c}{m} \right]$, $\frac{\bar{d}}{\bar{m}} = \frac{d}{m} + \Delta \left[\frac{d}{m} \right]$ and $\lambda > 0$.

The matched uncertainty is defined as:

$$\Delta(t, x(t)) = \mathbf{W}_s^T(t) \beta_s(x(t)). \tag{130}$$

Therefore, the system is now defined as:

$$\dot{\tilde{\mathbf{x}}}(t) = \tilde{\mathbf{A}}\tilde{\mathbf{x}}(t) + \tilde{\mathbf{B}}\lambda [u(t) + \Delta(t, x(t))] + \tilde{\mathbf{R}}r(t) . \quad (131)$$

Adding and subtracting terms with the same strategy as in (74) and taking $u_n(t)$ from (12), leads to

$$\begin{aligned} \dot{\tilde{\mathbf{x}}}(t) &= \mathbf{A}_m\tilde{\mathbf{x}}(t) + \mathbf{B}_m r(t) \\ &\quad + \tilde{\mathbf{B}}\lambda \left[(1 - \lambda^{-1}) u_n(t) + \mathbf{W}_s^T(t)\beta_s(x(t)) - u_{\text{ad}}(t) \right] \\ &= \mathbf{A}_m\tilde{\mathbf{x}}(t) + \mathbf{B}_m r(t) \\ &\quad + \tilde{\mathbf{B}}\lambda \left[(1 - \lambda^{-1}) \left(-\tilde{\mathbf{k}}\tilde{\mathbf{x}}(t) + k_p r(t) \right) + \mathbf{W}_s^T(t)\beta_s(x(t)) - u_{\text{ad}}(t) \right] . \end{aligned} \quad (132)$$

Grouping some terms conveniently, results in:

$$\begin{aligned} \dot{\tilde{\mathbf{x}}}(t) &= \mathbf{A}_m\tilde{\mathbf{x}}(t) + \mathbf{B}_m r(t) + \underbrace{\tilde{\mathbf{B}}\lambda (1 - \lambda^{-1}) (-\tilde{\mathbf{k}})}_{\mathbf{K}_{1e}^T} \tilde{\mathbf{x}}(t) \\ &\quad + \underbrace{\tilde{\mathbf{B}}\lambda (1 - \lambda^{-1}) k_p}_{k_{2e}} r(t) + \tilde{\mathbf{B}}\lambda \left[\mathbf{W}_s^T(t)\beta_s(x(t)) - u_{\text{ad}}(t) \right] \\ &= \mathbf{A}_m\tilde{\mathbf{x}}(t) + \mathbf{B}_m r(t) \\ &\quad + \tilde{\mathbf{B}}\lambda \left[\mathbf{W}_s^T(t)\beta_s(x(t)) - u_{\text{ad}}(t) + \mathbf{K}_{1e}^T \tilde{\mathbf{x}}(t) + k_{2e} r(t) \right] . \end{aligned} \quad (133)$$

The model following error dynamics, $\dot{e}(t) = \dot{\tilde{\mathbf{x}}}(t) - \dot{\mathbf{x}}_m(t)$ with $\dot{\mathbf{x}}_m(t)$ from (41), is:

$$\dot{e}(t) = \mathbf{A}_m e(t) + \tilde{\mathbf{B}}\lambda \left[-u_{\text{ad}}(t) + \mathbf{W}_s^T(t)\beta_s(x(t)) + \mathbf{K}_{1e}^T \tilde{\mathbf{x}}(t) + k_{2e} r(t) \right] . \quad (134)$$

In order to cancel all the right terms, $u_{\text{ad}}(t)$ is defined as:

$$u_{\text{ad}}(t) = \hat{\mathbf{W}}_s^T(t)\beta_s(x(t)) + \hat{\mathbf{K}}_{1e}^T(t)\tilde{\mathbf{x}}(t) + \hat{k}_{2e}(t)r(t) , \quad (135)$$

where the derivative-free weight update of $\hat{\mathbf{W}}_s(t)$, $\hat{\mathbf{K}}_{1e}(t)$ and $\hat{k}_{2e}(t)$ have the form:

$$\hat{\mathbf{W}}_s(t) = \Omega_1 \hat{\mathbf{W}}_s(t - \tau) + \hat{\Omega}_2(t), \quad 0 \leq \Omega_1^T \Omega_1 < \mathbf{I} , \quad (136)$$

$$\hat{\mathbf{K}}_{1e}(t) = \Xi_{11} \hat{\mathbf{K}}_{1e}(t - \tau) + \hat{\Xi}_{12}(t), \quad 0 \leq \Xi_{11}^T \Xi_{11} < \mathbf{I} , \quad (137)$$

$$\hat{k}_{2e}(t) = \xi_{21} \hat{k}_{2e}(t - \tau) + \hat{\xi}_{22}(t), \quad 0 \leq \xi_{21}^2 < 1 , \quad (138)$$

where:

$$\hat{\Omega}_2(t) = \mathbf{K}_2 \beta_s(x(t)) e^T(t) \mathbf{P} \tilde{\mathbf{B}}, \quad \mathbf{K}_2 > 0 , \quad (139)$$

$$\hat{\mathbf{\Xi}}_{12}(t) = \mathbf{K}_3 \tilde{\mathbf{x}}(t) e^T(t) \mathbf{P} \tilde{\mathbf{B}}, \quad \mathbf{K}_3 > 0, \quad (140)$$

$$\hat{\xi}_{22}(t) = k_2 r(t) e^T(t) \mathbf{P} \tilde{\mathbf{B}}, \quad k_2 > 0. \quad (141)$$

The following is also defined:

$$\tilde{\mathbf{W}}_s(t) = \mathbf{W}_s(t) - \hat{\mathbf{W}}_s(t), \quad (142)$$

$$\tilde{\mathbf{K}}_{1e}(t) \equiv \mathbf{K}_{1e} - \hat{\mathbf{K}}_{1e}(t), \quad (143)$$

$$\tilde{k}_{2e}(t) \equiv k_{2e} - \hat{k}_{2e}(t). \quad (144)$$

The derivative-free adaptive control algorithm considering the input with uncertainties case is now completed because the estimated terms $\hat{\mathbf{W}}_s$, $\hat{\mathbf{K}}_{1e}(t)$ and $\hat{k}_{2e}(t)$ have been already defined. However, what remains to be demonstrated is the stability in the sense of uniform ultimately boundedness. Same as before, it is known that matrix \mathbf{P} satisfies (44) and it is just necessary to prove that $e(t)$, $\tilde{\mathbf{W}}_s(t)$, $\tilde{\mathbf{K}}_{1e}(t)$ and $\tilde{k}_{2e}(t)$ are uniformly ultimately bounded. In order to prove it, first the parameters $\mathbf{W}_e^T(t) = [\mathbf{W}_s^T(t), \mathbf{K}_{1e}^T, k_{2e}]^T$ and $\hat{\mathbf{W}}_e^T(t) = [\hat{\mathbf{W}}_s^T(t), \hat{\mathbf{K}}_{1e}^T(t), \hat{k}_{2e}(t)]^T$ are defined. Then, it is also true that:

$$\tilde{\mathbf{W}}_e(t) = \mathbf{W}_e(t) - \hat{\mathbf{W}}_e(t), \quad (145)$$

$$\beta_e(\cdot) = \begin{bmatrix} \beta_s(x(t)) \\ \tilde{\mathbf{x}}(t) \\ r(t) \end{bmatrix}. \quad (146)$$

Replacing (135) in (134) and considering (145) and (146), the error state dynamics can be represented as:

$$\dot{e}(t) = \mathbf{A}_m e(t) + \tilde{\mathbf{B}} \lambda \tilde{\mathbf{W}}_e^T(t) \beta_e(\cdot). \quad (147)$$

Also Equations (136), (137) and (138) can be grouped into:

$$\hat{\mathbf{W}}_e(t) = \Omega_{1e} \hat{\mathbf{W}}_e(t - \tau) + \hat{\Omega}_{21}(t), \quad (148)$$

where $\Omega_{1e} \equiv \text{diag} [\Omega_1, \mathbf{\Xi}_{11}, \xi_{21}]$ and $\hat{\Omega}_{21}(t) \equiv [\hat{\Omega}_2^T(t), \hat{\mathbf{\Xi}}_{12}^T(t), \hat{\xi}_{22}^T(t)]^T$.

It is important to remark that Ω_{1e} stays in the following limits

$$0 \leq \Omega_{1e}^T \Omega_{1e} < \mathbf{I}. \quad (149)$$

Then, $\Omega_{2e}(t)$ is defined as:

$$\Omega_{2e}(t) \equiv \mathbf{W}_e(t) - \Omega_{1e} \mathbf{W}_e(t - \tau), \quad (150)$$

where $\|\Omega_{2e}(t)\| \leq \delta_e^*$. Subsequently, summing equations (148) and (150), with (145) into consideration, $\tilde{\mathbf{W}}_e(t)$ can be expressed as:

$$\tilde{\mathbf{W}}_e(t) = \Omega_{1e} \tilde{\mathbf{W}}_e(t - \tau) + \Omega_{2e}(t) - \hat{\Omega}_{21}(t). \quad (151)$$

Finally, the error dynamics can be rewritten as:

$$\dot{e}(t) = \mathbf{A}_m e(t) + \tilde{\mathbf{B}} \lambda \left[\Omega_{1e} \tilde{\mathbf{W}}_e(t - \tau) + \Omega_{2e}(t) - \hat{\Omega}_{21}(t) \right]^T \beta_e(\cdot). \quad (152)$$

In order to follow the procedure from Remark 13, the Lyapunov-Krasovskii functional candidate (continuously differentiable and positive definite) is proposed:

Remark 18. *The proposed Lyapunov-Krasovskii functional candidate:*

$$\mathcal{V}(e(t), \tilde{\mathbf{W}}_{et}) = e^T(t) \mathbf{P} e(t) + \rho \left[\int_{t-\tau}^t \tilde{\mathbf{W}}_e^T(s) \tilde{\mathbf{W}}_e(s) (\lambda + \varepsilon) ds \right], \quad (153)$$

where $\rho > 0$, $\tilde{\mathbf{W}}_{et}$ represents $\tilde{\mathbf{W}}_e(t)$ over the time interval $t - \tau$ to t and $\varepsilon > 0$ is sufficiently small.

To simplify the following calculations, $(\lambda + \varepsilon)$ will be written as a scalar ϕ . Then, deriving (153) and using Theorem 1, leads to

$$\begin{aligned} \dot{\mathcal{V}} &= \underbrace{\dot{e}^T(t) \mathbf{P} e(t) + e^T(t) \mathbf{P} \dot{e}(t)}_{\text{(I)}} \\ &= + \rho \phi \underbrace{\left[\tilde{\mathbf{W}}_e^T(t) \tilde{\mathbf{W}}_e(t) - \tilde{\mathbf{W}}_e^T(t - \tau) \tilde{\mathbf{W}}_e(t - \tau) \right]}_{\text{(II)}}. \end{aligned} \quad (154)$$

Replacing (152) in (154) for term (I), yields:

$$\begin{aligned} \text{(I)} &= e^T(t) \mathbf{A}_m^T \mathbf{P} e(t) + \lambda \beta_e^T(\cdot) \left[\Omega_{1e} \tilde{\mathbf{W}}_e(t - \tau) + \Omega_{2e}(t) - \hat{\Omega}_{21}(t) \right] \tilde{\mathbf{B}}^T \mathbf{P} e(t) \\ &\quad + e^T(t) \mathbf{P} \mathbf{A}_m e(t) + e^T(t) \mathbf{P} \tilde{\mathbf{B}} \lambda \left[\Omega_{1e} \tilde{\mathbf{W}}_e(t - \tau) + \Omega_{2e}(t) - \hat{\Omega}_{21}(t) \right]^T \beta_e(\cdot) \\ &= \boxed{e^T(t) [\mathbf{A}_m^T \mathbf{P} + \mathbf{P} \mathbf{A}_m] e(t)}^{(i)} + 2e^T(t) \mathbf{P} \tilde{\mathbf{B}} \lambda \left[\Omega_{1e} \tilde{\mathbf{W}}_e(t - \tau) \right]^T \beta_e(\cdot) \\ &\quad + 2e^T(t) \mathbf{P} \tilde{\mathbf{B}} \lambda \Omega_{2e}^T(t) \beta_e(\cdot) - 2e^T(t) \mathbf{P} \tilde{\mathbf{B}} \lambda \hat{\Omega}_{21}^T(t) \beta_e(\cdot). \end{aligned} \quad (155)$$

Term (i) was previously calculated in (59). Then, Equation (155) is simplified:

$$\begin{aligned} (\mathbf{I}) = & -e^T(t)e(t) + 2e^T(t)\mathbf{P}\tilde{\mathbf{B}}\lambda \left[\Omega_{1e}\tilde{\mathbf{W}}_e(t-\tau) \right]^T \beta_e(\cdot) \\ & + 2e^T(t)\mathbf{P}\tilde{\mathbf{B}}\lambda\Omega_{2e}^T(t)\beta_e(\cdot) - 2e^T(t)\mathbf{P}\tilde{\mathbf{B}}\lambda\hat{\Omega}_{21}^T(t)\beta_e(\cdot). \end{aligned} \quad (156)$$

Considering $\Upsilon = \mathbf{I} + \mathcal{E}$ (with $\mathcal{E} \geq 0$ and \mathcal{E} a diagonal matrix, note that it is also true that Υ is also a positive diagonal matrix) for term (II) of Equation (154), yields:

$$\begin{aligned} (\mathbf{II}) = & \rho\phi \left[\tilde{\mathbf{W}}_e^T(t)\tilde{\mathbf{W}}_e(t) - \tilde{\mathbf{W}}_e^T(t-\tau)\tilde{\mathbf{W}}_e(t-\tau) \right] \\ = & \rho\phi \left[-\tilde{\mathbf{W}}_e^T(t)\mathcal{E}\tilde{\mathbf{W}}_e(t) + \underbrace{\tilde{\mathbf{W}}_e^T(t)\Upsilon\tilde{\mathbf{W}}_e(t)}_{(ii)} - \tilde{\mathbf{W}}_e^T(t-\tau)\tilde{\mathbf{W}}_e(t-\tau) \right]. \end{aligned} \quad (157)$$

Replacing $\tilde{\mathbf{W}}_e(t)$ from (151) in term (ii), it is obtained:

$$\begin{aligned} (\mathbf{II}) = & \rho\phi \left[-\tilde{\mathbf{W}}_e^T(t)\mathcal{E}\tilde{\mathbf{W}}_e(t) + \left[\Omega_{1e}\tilde{\mathbf{W}}_e(t-\tau) + \Omega_{2e}(t) \right. \right. \\ & \left. \left. - \hat{\Omega}_{21}(t) \right]^T \Upsilon \left[\Omega_{1e}\tilde{\mathbf{W}}_e(t-\tau) + \Omega_{2e}(t) - \hat{\Omega}_{21}(t) \right] \right. \\ & \left. - \tilde{\mathbf{W}}_e^T(t-\tau)\tilde{\mathbf{W}}_e(t-\tau) \right] \\ = & \rho\phi \left[-\tilde{\mathbf{W}}_e^T(t)\mathcal{E}\tilde{\mathbf{W}}_e(t) + \left[\tilde{\mathbf{W}}_e^T(t-\tau)\Omega_{1e}^T + \Omega_{2e}^T(t) \right. \right. \\ & \left. \left. - \hat{\Omega}_{21}^T(t) \right] \Upsilon \left[\Omega_{1e}\tilde{\mathbf{W}}_e(t-\tau) + \Omega_{2e}(t) - \hat{\Omega}_{21}(t) \right] \right. \\ & \left. - \tilde{\mathbf{W}}_e^T(t-\tau)\tilde{\mathbf{W}}_e(t-\tau) \right] \quad (158) \\ = & \rho\phi \left[-\tilde{\mathbf{W}}_e^T(t)\mathcal{E}\tilde{\mathbf{W}}_e(t) - \tilde{\mathbf{W}}_e^T(t-\tau)\tilde{\mathbf{W}}_e(t-\tau) \right. \\ & + \tilde{\mathbf{W}}_e^T(t-\tau)\Omega_{1e}^T\Upsilon\Omega_{1e}\tilde{\mathbf{W}}_e(t-\tau) \boxed{+\tilde{\mathbf{W}}_e^T(t-\tau)\Omega_{1e}^T\Upsilon\Omega_{2e}(t)}^{(i_1)} \\ & \boxed{-\tilde{\mathbf{W}}_e^T(t-\tau)\Omega_{1e}^T\Upsilon\hat{\Omega}_{21}(t)}^{(i_2)} \boxed{+\Omega_{2e}^T(t)\Upsilon\Omega_{1e}\tilde{\mathbf{W}}_e(t-\tau)}^{(i_1)} \\ & + \Omega_{2e}^T(t)\Upsilon\Omega_{2e}(t) \boxed{-\Omega_{2e}^T(t)\Upsilon\hat{\Omega}_{21}(t)}^{(i_3)} \boxed{-\hat{\Omega}_{21}^T(t)\Upsilon\Omega_{1e}\tilde{\mathbf{W}}_e^T(t-\tau)}^{(i_2)} \\ & \left. \boxed{-\hat{\Omega}_{21}^T(t)\Upsilon\Omega_{2e}(t)}^{(i_3)} + \hat{\Omega}_{21}^T(t)\Upsilon\hat{\Omega}_{21}(t) \right]. \end{aligned}$$

As explained before in the case with a known input matrix, it is possible to sum the terms in the boxes with the same upper indices (i_1) , (i_2) and (i_3) because they are equivalent. Then, Equation (158) simplifies to:

$$\begin{aligned}
 (\mathbf{II}) = & \rho\phi \left[-\tilde{\mathbf{W}}_e^T(t)\mathcal{E}\tilde{\mathbf{W}}_e(t) - \tilde{\mathbf{W}}_e^T(t-\tau)\tilde{\mathbf{W}}_e(t-\tau) \right. \\
 & + \tilde{\mathbf{W}}_e^T(t-\tau)\Omega_{1e}^T\Upsilon\Omega_{1e}\tilde{\mathbf{W}}_e(t-\tau) + \Omega_{2e}^T(t)\Upsilon\Omega_{2e}(t) + \hat{\Omega}_{21}^T(t)\Upsilon\hat{\Omega}_{21}(t) \\
 & - 2\hat{\Omega}_{21}^T(t)\Upsilon\Omega_{1e}\tilde{\mathbf{W}}_e(t-\tau) + \boxed{2\tilde{\mathbf{W}}_e^T(t-\tau)\Omega_{1e}^T\Upsilon\Omega_{2e}(t)} \quad (a) \\
 & \left. - 2\hat{\Omega}_{21}^T(t)\Upsilon\Omega_{2e}(t) \right] .
 \end{aligned} \tag{159}$$

Then, applying the Young's inequality property (see Remark 15) for term (a) , yields:

$$\begin{aligned}
 2\tilde{\mathbf{W}}_e^T(t-\tau)\Omega_{1e}^T\Upsilon\Omega_{2e}(t) & \leq \tilde{\mathbf{W}}_e^T(t-\tau)\Omega_{1e}^T\mathcal{Z}\Omega_{1e}\tilde{\mathbf{W}}_e(t-\tau) \\
 & + \Omega_{2e}^T(t)\Upsilon\mathcal{Z}^{-1}\Upsilon\Omega_{2e}(t), \quad \mathcal{Z} > 0 .
 \end{aligned} \tag{160}$$

Replacing (160) in (159), results in:

$$\begin{aligned}
 (\mathbf{II}) = & \rho\phi \left[-\tilde{\mathbf{W}}_e^T(t)\mathcal{E}\tilde{\mathbf{W}}_e(t) - \tilde{\mathbf{W}}_e^T(t-\tau)\tilde{\mathbf{W}}_e(t-\tau) \right. \\
 & + \tilde{\mathbf{W}}_e^T(t-\tau)\Omega_{1e}^T\Upsilon\Omega_{1e}\tilde{\mathbf{W}}_e(t-\tau) + \Omega_{2e}^T(t)\Upsilon\Omega_{2e}(t) \\
 & + \hat{\Omega}_{21}^T(t)\Upsilon\hat{\Omega}_{21}(t) - 2\hat{\Omega}_{21}^T(t)\Upsilon\Omega_{1e}\tilde{\mathbf{W}}_e(t-\tau) \\
 & + \tilde{\mathbf{W}}_e^T(t-\tau)\Omega_{1e}^T\mathcal{Z}\Omega_{1e}\tilde{\mathbf{W}}_e(t-\tau) + \Omega_{2e}^T(t)\Upsilon\mathcal{Z}^{-1}\Upsilon\Omega_{2e}(t) \\
 & \left. - 2\hat{\Omega}_{21}^T(t)\Upsilon\Omega_{2e}(t) \right] .
 \end{aligned} \tag{161}$$

Then, replacing (161) and (156) in (154), the following is obtained:

$$\begin{aligned}
 \mathcal{V} = & -e^T(t)e(t) + 2e^T(t)\mathbf{P}\tilde{\mathbf{B}}\lambda \left[\Omega_{1e}\tilde{\mathbf{W}}_e(t-\tau) \right]^T \beta_e(\cdot) \\
 & + 2e^T(t)\mathbf{P}\tilde{\mathbf{B}}\lambda\Omega_{2e}^T(t)\beta_e(\cdot) - 2e^T(t)\mathbf{P}\tilde{\mathbf{B}}\lambda\hat{\Omega}_{21}^T(t)\beta_e(\cdot) \\
 & + \rho\phi \left[-\tilde{\mathbf{W}}_e^T(t)\mathcal{E}\tilde{\mathbf{W}}_e(t) - \tilde{\mathbf{W}}_e^T(t-\tau)\tilde{\mathbf{W}}_e(t-\tau) \right. \\
 & + \tilde{\mathbf{W}}_e^T(t-\tau)\Omega_{1e}^T\Upsilon\Omega_{1e}\tilde{\mathbf{W}}_e(t-\tau) + \Omega_{2e}^T(t)\Upsilon\Omega_{2e}(t) \\
 & + \hat{\Omega}_{21}^T(t)\Upsilon\hat{\Omega}_{21}(t) - 2\hat{\Omega}_{21}^T(t)\Upsilon\Omega_{1e}\tilde{\mathbf{W}}_e(t-\tau) \\
 & + \tilde{\mathbf{W}}_e^T(t-\tau)\Omega_{1e}^T\mathcal{Z}\Omega_{1e}\tilde{\mathbf{W}}_e(t-\tau) + \Omega_{2e}^T(t)\Upsilon\mathcal{Z}^{-1}\Upsilon\Omega_{2e}(t) \\
 & \left. - 2\hat{\Omega}_{21}^T(t)\Upsilon\Omega_{2e}(t) \right] .
 \end{aligned} \tag{162}$$

The next step is to recognize that $\hat{\Omega}_{21}(t)$ can be expressed as:

$$\begin{aligned}
 \hat{\Omega}_{21}(t) &= \begin{bmatrix} \hat{\Omega}_2(t) \\ \hat{\Xi}_{12}(t) \\ \hat{\xi}_{22}(t) \end{bmatrix} = \begin{bmatrix} \mathbf{K}_2 \beta_s(x(t)) e^T(t) \mathbf{P} \tilde{\mathbf{B}} \\ \mathbf{K}_3 \tilde{\mathbf{x}}(t) e^T(t) \mathbf{P} \tilde{\mathbf{B}} \\ k_2 r(t) e^T(t) \mathbf{P} \tilde{\mathbf{B}} \end{bmatrix} \\
 &= \underbrace{\begin{bmatrix} \mathbf{K}_2 & 0 & 0 \\ 0 & \mathbf{K}_3 & 0 \\ 0 & 0 & k_2 \end{bmatrix}}_{\mathcal{K}_e} \underbrace{\begin{bmatrix} \beta_s(x(t)) \\ \tilde{\mathbf{x}}(t) \\ r(t) \end{bmatrix}}_{\beta_e(\cdot)} e^T(t) \mathbf{P} \tilde{\mathbf{B}} \\
 &= \mathcal{K}_e \beta_e(\cdot) e^T(t) \mathbf{P} \tilde{\mathbf{B}}.
 \end{aligned} \tag{163}$$

Replacing $\hat{\Omega}_{21}(t)$ from (163) in (161), yields:

$$\begin{aligned}
 \mathcal{V} &= -e^T(t) e(t) \left[+2\lambda e^T(t) \mathbf{P} \tilde{\mathbf{B}} \left[\Omega_{1e} \tilde{\mathbf{W}}_e(t - \tau) \right]^T \beta_e(\cdot) \right]^{(a_1)} \\
 &\quad \left[-2\lambda e^T(t) \mathbf{P} \tilde{\mathbf{B}} \left[\mathcal{K}_e \beta_e(\cdot) e^T(t) \mathbf{P} \tilde{\mathbf{B}} \right]^T \beta_e(\cdot) \right]^{(b_1)} \\
 &\quad \left[+2\lambda e^T(t) \mathbf{P} \tilde{\mathbf{B}} \Omega_{2e}^T(t) \beta_e(\cdot) \right]^{(c_1)} \\
 &\quad + \rho \phi \left[-\tilde{\mathbf{W}}_e^T(t) \mathcal{E} \tilde{\mathbf{W}}_e(t) \left[-\tilde{\mathbf{W}}_e^T(t - \tau) \tilde{\mathbf{W}}_e(t - \tau) \right] \right]^{(d_1)} \\
 &\quad \left[+\tilde{\mathbf{W}}_e^T(t - \tau) \Omega_{1e}^T \Upsilon \Omega_{1e} \tilde{\mathbf{W}}_e(t - \tau) \right]^{(d_2)} \\
 &\quad \left[+ \left[\mathcal{K}_e \beta_e(\cdot) e^T(t) \mathbf{P} \tilde{\mathbf{B}} \right]^T \Upsilon \left[\mathcal{K}_e \beta_e(\cdot) e^T(t) \mathbf{P} \tilde{\mathbf{B}} \right] \right]^{(b_2)} \\
 &\quad \left[+\Omega_{2e}^T(t) \Upsilon \Omega_{2e}(t) \right]^{(e_1)} \left[-2 \left[\mathcal{K}_e \beta_e(\cdot) e^T(t) \mathbf{P} \tilde{\mathbf{B}} \right]^T \Upsilon \Omega_{1e} \tilde{\mathbf{W}}_e(t - \tau) \right]^{(a_2)} \\
 &\quad \left[+\tilde{\mathbf{W}}_e^T(t - \tau) \Omega_{1e}^T \mathcal{Z} \Omega_{1e} \tilde{\mathbf{W}}_e(t - \tau) \right]^{(d_3)} \left[+\Omega_{2e}^T(t) \Upsilon \mathcal{Z}^{-1} \Upsilon \Omega_{2e}(t) \right]^{(e_2)} \\
 &\quad \left[-2 \left[\mathcal{K}_e \beta_e(\cdot) e^T(t) \mathbf{P} \tilde{\mathbf{B}} \right]^T \Upsilon \Omega_{2e}(t) \right]^{(c_2)} \Big].
 \end{aligned} \tag{164}$$

Then, considering that $\mathcal{K}_e = (1/\rho)\Upsilon^{-1}$, the terms with the upper indices (a_1) , (a_2) , (c_1) and (c_2) are cancelled.

To begin with, it is proven that $\rho\phi(a_2) + (a_1) = 0$ (notice that (i) and (ii) terms in (165) are scalars, and recalling that $\phi = \lambda + \varepsilon$ with ε sufficiently small):

$$\begin{aligned}
 0 &= \rho\phi \left(-2 \left[\mathcal{K}_e \beta_e(\cdot) e^T(t) \mathbf{P}\tilde{\mathbf{B}} \right]^T \Upsilon \Omega_{1e} \tilde{\mathbf{W}}_e(t - \tau) \right) + (a_1) \\
 &= \rho\phi \left(-2 \left[\beta_e(\cdot) e^T(t) \mathbf{P}\tilde{\mathbf{B}} \right]^T \mathcal{K}_e \Upsilon \Omega_{1e} \tilde{\mathbf{W}}_e(t - \tau) \right) + (a_1) \\
 &= -2\phi \left[\beta_e(\cdot) e^T(t) \mathbf{P}\tilde{\mathbf{B}} \right]^T \Omega_{1e} \tilde{\mathbf{W}}_e(t - \tau) + (a_1) \\
 &= -2\phi \underbrace{\left[e^T(t) \mathbf{P}\tilde{\mathbf{B}} \right]^T}_{(i)} \underbrace{\beta_e(\cdot)^T \Omega_{1e} \tilde{\mathbf{W}}_e(t - \tau)}_{(ii)} + (a_1) \\
 &= -2(\lambda + \varepsilon) e^T(t) \mathbf{P}\tilde{\mathbf{B}} \left[\Omega_{1e} \tilde{\mathbf{W}}_e(t - \tau) \right]^T \beta_e(\cdot) + (a_1) \\
 &= -2\varepsilon e^T(t) \mathbf{P}\tilde{\mathbf{B}} \left[\Omega_{1e} \tilde{\mathbf{W}}_e(t - \tau) \right]^T \beta_e(\cdot) \approx 0.
 \end{aligned} \tag{165}$$

The proof for $\rho\phi(c_2) + (c_1) = 0$ is shown below (notice that (i) and (ii) terms in (166) are scalars, and recalling that $\phi = \lambda + \varepsilon$ with ε sufficiently small):

$$\begin{aligned}
 0 &= \rho\phi \left(-2 \left[\mathcal{K}_e \beta_e(\cdot) e^T(t) \mathbf{P}\tilde{\mathbf{B}} \right]^T \Upsilon \Omega_{2e}(t) \right) + (c_1) \\
 &= \rho\phi \left(-2 \left[\beta_e(\cdot) e^T(t) \mathbf{P}\tilde{\mathbf{B}} \right]^T \mathcal{K}_e \Upsilon \Omega_{2e}(t) \right) + (c_1) \\
 &= -2\phi \left[\beta_e(\cdot) e^T(t) \mathbf{P}\tilde{\mathbf{B}} \right]^T \Omega_{2e}(t) + (c_1) \\
 &= -2\phi \underbrace{\left[e^T(t) \mathbf{P}\tilde{\mathbf{B}} \right]^T}_{(i)} \underbrace{\beta_e(\cdot)^T \Omega_{2e}(t)}_{(ii)} + (c_1) \\
 &= -2(\lambda + \varepsilon) e^T(t) \mathbf{P}\tilde{\mathbf{B}} \Omega_{2e}^T(t) \beta_e(\cdot) + (c_1) \\
 &= -2\varepsilon e^T(t) \mathbf{P}\tilde{\mathbf{B}} \Omega_{2e}^T(t) \beta_e(\cdot) \approx 0.
 \end{aligned} \tag{166}$$

Then, it can be noted that the other terms can be grouped. Grouping $\rho\phi(d_1)$, $\rho\phi(d_2)$ and $\rho\phi(d_3)$, results in:

$$\begin{aligned}
 \rho\phi \sum_{i=1}^3 (d_i) &= \rho\phi \left[-\tilde{\mathbf{W}}_e^T(t - \tau) \tilde{\mathbf{W}}_e(t - \tau) + \tilde{\mathbf{W}}_e^T(t - \tau) \Omega_{1e}^T \Upsilon \Omega_{1e} \tilde{\mathbf{W}}_e(t - \tau) \right. \\
 &\quad \left. + \tilde{\mathbf{W}}_e^T(t - \tau) \Omega_{1e}^T \mathcal{Z} \Omega_{1e} \tilde{\mathbf{W}}_e(t - \tau) \right] \\
 &= -\rho\phi \left[\tilde{\mathbf{W}}_e^T(t - \tau) \left[\mathbf{I} - \Omega_{1e}^T (\Upsilon + \mathcal{Z}) \Omega_{1e} \right] \tilde{\mathbf{W}}_e(t - \tau) \right].
 \end{aligned} \tag{167}$$

Grouping $\rho\phi(e_1)$ and $\rho\phi(e_2)$, yields:

$$\begin{aligned}
 \rho\phi(e_1) + \rho\phi(e_2) &= \rho\phi \left[\Omega_{2e}^T(t) \Upsilon \Omega_{2e}(t) + \Omega_{2e}^T(t) \Upsilon \mathcal{Z}^{-1} \Upsilon \Omega_{2e}(t) \right] \\
 &= \rho\phi \left[\Omega_{2e}^T(t) (\Upsilon + \Upsilon \mathcal{Z}^{-1} \Upsilon) \Omega_{2e}(t) \right] \\
 &= \rho\phi \left[\Omega_{2e}^T(t) \left(\Upsilon + \frac{\Upsilon^2}{\gamma} \right) \Omega_{2e}(t) \right].
 \end{aligned} \tag{168}$$

Terms (b_1) and $\rho\phi(b_2)$ can also be grouped. Noticing that (i) and (ii) terms in (169) are scalars, and recalling that $\mathcal{K}_e = (1/\rho)\Upsilon^{-1}$, it is obtained:

$$\begin{aligned}
 (b_1) + \rho\phi(b_2) &= \rho\phi \left(\left[\mathcal{K}_e \beta_e(\cdot) e^T(t) \mathbf{P} \tilde{\mathbf{B}} \right]^T \Upsilon \mathcal{K}_e \beta_e(\cdot) e^T(t) \mathbf{P} \tilde{\mathbf{B}} \right) + (b_1) \\
 &= \rho\phi \left(\left[\beta_e(\cdot) e^T(t) \mathbf{P} \tilde{\mathbf{B}} \right]^T \mathcal{K}_e \Upsilon \mathcal{K}_e \beta_e(\cdot) e^T(t) \mathbf{P} \tilde{\mathbf{B}} \right) + (b_1) \\
 &= \phi \left[\beta_e(\cdot) e^T(t) \mathbf{P} \tilde{\mathbf{B}} \right]^T \mathcal{K}_e \beta_e(\cdot) e^T(t) \mathbf{P} \tilde{\mathbf{B}} + (b_1) \\
 &= \phi \left[\underbrace{e^T(t) \mathbf{P} \tilde{\mathbf{B}}}_{(i)} \right]^T \underbrace{\beta_e(\cdot)^T \mathcal{K}_e \beta_e(\cdot) e^T(t) \mathbf{P} \tilde{\mathbf{B}}}_{(ii)} + (b_1) \\
 &= \phi e^T(t) \mathbf{P} \tilde{\mathbf{B}} \left[\beta_e(\cdot)^T \mathcal{K}_e \beta_e(\cdot) e^T(t) \mathbf{P} \tilde{\mathbf{B}} \right]^T + (b_1) \\
 &= (\lambda + \varepsilon) e^T(t) \mathbf{P} \tilde{\mathbf{B}} \left[\mathcal{K}_e \beta_e(\cdot) e^T(t) \mathbf{P} \tilde{\mathbf{B}} \right]^T \beta_e(\cdot) + (b_1) \\
 &\approx -\lambda e^T(t) \mathbf{P} \tilde{\mathbf{B}} \left[\mathcal{K}_e \beta_e(\cdot) e^T(t) \mathbf{P} \tilde{\mathbf{B}} \right]^T \beta_e(\cdot) \\
 &\approx -\lambda e^T(t) \mathbf{P} \tilde{\mathbf{B}} \tilde{\mathbf{B}}^T \mathbf{P} e(t) \beta_e(\cdot)^T \mathcal{K}_e \beta_e(\cdot).
 \end{aligned} \tag{169}$$

Finally, replacing (169), (167) and (168) in (164), results in:

$$\begin{aligned}
 \mathcal{V} &= -e^T(t) e(t) - \lambda e^T(t) \mathbf{P} \tilde{\mathbf{B}} \tilde{\mathbf{B}}^T \mathbf{P} e(t) \beta_e(\cdot)^T \mathcal{K}_e \beta_e(\cdot) \\
 &\quad - \rho\phi \left[\tilde{\mathbf{W}}_e^T(t) \mathcal{E} \tilde{\mathbf{W}}_e(t) \right] \\
 &\quad - \rho\phi \left[\tilde{\mathbf{W}}_e^T(t - \tau) \left[\mathbf{I} - \Omega_{1e}^T(\Upsilon + \mathcal{Z}) \Omega_{1e} \right] \tilde{\mathbf{W}}_e(t - \tau) \right] \\
 &\quad + \rho\phi \left[\Omega_{2e}^T(t) \left(\Upsilon + \frac{\Upsilon^2}{\gamma} \right) \Omega_{2e}(t) \right].
 \end{aligned} \tag{170}$$

Taking (149) into consideration and defining $\mathbf{K}_1 \triangleq (\Upsilon + \mathcal{Z})^{-1} < \mathbf{I}$, for Ω_{1e} yields:

$$\mathcal{V} \leq -\|e(t)\|^2 - \bar{c}_2 \left\| \tilde{\mathbf{W}}(t) \right\|^2 - \bar{c}_3 \left\| \tilde{\mathbf{W}}(t - \tau) \right\|^2 + \zeta_e, \tag{171}$$

where the constants \bar{c}_2 , \bar{c}_3 and ζ_e are:

$$\bar{c}_2 = \rho\phi\lambda_{\min}(\mathcal{E}) \geq 0, \quad (172)$$

$$\bar{c}_3 = \rho\phi\lambda_{\min}(\mathbf{I} - \Omega_{1e}^T(\Upsilon + \mathcal{Z})\Omega_{1e}) > 0, \quad (173)$$

$$\zeta_e = \rho\phi\lambda_{\min}\left(\Upsilon + \frac{\Upsilon^2}{\gamma}\right)\delta_e^{*2} \geq 0. \quad (174)$$

Same as before, if $\mathcal{E} > 0$, then since $\Upsilon = \mathbf{K}_1^{-1} - \mathcal{Z} = 1 + \mathcal{E}$, $0 < \mathbf{K}_1 < \mathbf{I}$, and $\mathcal{Z} > 0$, it can be deduced that Υ should be in the open interval $(1, \mathbf{K}_1^{-1})$. Notice that, either $\|e(t)\| > \Psi_1$ or $\|\tilde{\mathbf{W}}_s(t)\| > \Psi_2$ or $\|\tilde{\mathbf{W}}_s(t - \tau)\| > \Psi_3$ renders $\dot{\mathcal{V}} < 0$, where $\Psi_1 = \sqrt{\zeta_e}$, $\Psi_2 = \sqrt{\zeta_e/\bar{c}_2}$ and $\Psi_3 = \sqrt{\zeta_e/\bar{c}_3}$, or also:

$$\Psi_1 = \delta_e^* \sqrt{\rho\phi\lambda_{\min}(\Upsilon + \Upsilon\mathcal{Z}^{-1}\Upsilon)}, \quad (175)$$

$$\Psi_2 = \Psi_1 \sqrt{\frac{1}{\bar{c}_2}} = \Psi_1 \sqrt{\frac{1}{\rho\phi\lambda_{\min}(\mathcal{E})}} \quad (176)$$

$$\Psi_3 = \Psi_1 \sqrt{\frac{1}{\bar{c}_3}} = \Psi_1 \sqrt{\frac{1}{\rho\phi\lambda_{\min}(\mathbf{I} - \Omega_{1e}^T(\Upsilon + \mathcal{Z})\Omega_{1e})}}. \quad (177)$$

Therefore, it follows that $e(t)$ and $\tilde{\mathbf{W}}_e(t)$ are uniformly ultimately bounded.

3.3.1 DFMRAC for the unknown input matrix case with feed-forward control

In this subsection, the feed-forward control is included in the algorithm. The state space representation of the system was already defined in (131), however, now the nominal control is the corresponding to $u_{mf}(t)$ shown in (31).

$$\dot{\tilde{\mathbf{x}}}(t) = \tilde{\mathbf{A}}\tilde{\mathbf{x}}(t) + \tilde{\mathbf{B}}\lambda [u_{mf}(t) + \Delta(t, x(t))] + \tilde{\mathbf{R}}r(t). \quad (178)$$

Adding and subtracting terms in (178), with the same strategy as (92), results in:

$$\begin{aligned} \dot{\tilde{\mathbf{x}}}(t) &= \mathbf{A}_m\tilde{\mathbf{x}}(t) + \mathbf{B}_{mf}\tilde{\mathbf{Y}}(t) + \tilde{\mathbf{R}}r(t) \\ &\quad + \tilde{\mathbf{B}}\lambda [(1 - \lambda^{-1})u_{mf}(t) + \mathbf{W}_s(t)^T\beta_s(x(t)) - u_{ad}(t)] \\ &= \mathbf{A}_m\tilde{\mathbf{x}}(t) + \mathbf{B}_{mf}\tilde{\mathbf{Y}}(t) + \tilde{\mathbf{R}}r(t) \\ &\quad + \tilde{\mathbf{B}}\lambda \left[(1 - \lambda^{-1}) (-\tilde{\mathbf{k}}^T\tilde{\mathbf{x}}(t) + \tilde{\mathbf{K}}_f\tilde{\mathbf{Y}}(t)) + \mathbf{W}_s(t)^T\beta_s(x(t)) - u_{ad}(t) \right] \\ &= \mathbf{A}_m\tilde{\mathbf{x}}(t) + \mathbf{B}_{mf}\tilde{\mathbf{Y}}(t) + \tilde{\mathbf{R}}r(t) \\ &\quad + \tilde{\mathbf{B}}\lambda \underbrace{(1 - \lambda^{-1}) (-\tilde{\mathbf{k}}^T)}_{\mathbf{K}_{1e}^T} \tilde{\mathbf{x}}(t) + \tilde{\mathbf{B}}\lambda \underbrace{(1 - \lambda^{-1}) (\tilde{\mathbf{K}}_f)}_{\mathbf{K}_{2e}^T} \tilde{\mathbf{Y}}(t) \\ &\quad + \tilde{\mathbf{B}}\lambda [\mathbf{W}_s^T(t)\beta_s(x(t)) - u_{ad}(t)] \\ &= \mathbf{A}_m\tilde{\mathbf{x}}(t) + \mathbf{B}_{mf}\tilde{\mathbf{Y}}(t) + \tilde{\mathbf{R}}r(t) \\ &\quad + \tilde{\mathbf{B}}\lambda \left[-u_{ad}(t) + \mathbf{W}_s^T(t)\beta_s(x(t)) + \mathbf{K}_{1e}^T\tilde{\mathbf{x}}(t) + \mathbf{K}_{2e}^T\tilde{\mathbf{Y}}(t) \right]. \end{aligned} \quad (179)$$

To cancel all the right terms corresponding to the parameters with uncertainties, $u_{ad}(t)$ is defined as:

$$u_{ad}(t) = \hat{\mathbf{W}}_s^T(t)\beta_s(x(t)) + \hat{\mathbf{K}}_{1e}^T(t)\tilde{\mathbf{x}}(t) + \hat{\mathbf{K}}_{2e}^T(t)\tilde{\mathbf{Y}}(t), \quad (180)$$

where, the derivative-free weight update of $\hat{\mathbf{W}}_s(t)$ and $\hat{\mathbf{K}}_{1e}(t)$ have the form of (136) and (137). Meanwhile $\hat{\mathbf{K}}_{2e}(t)$ is defined as:

$$\hat{\mathbf{K}}_{2e}(t) = \mathbf{\Xi}_{21}\hat{\mathbf{K}}_{2e}(t - \tau) + \hat{\mathbf{\Xi}}_{22}(t), \quad 0 \leq \mathbf{\Xi}_{21}^T\mathbf{\Xi}_{21} < \mathbf{I}, \quad (181)$$

where:

$$\hat{\mathbf{\Xi}}_{22}(t) = \mathbf{K}_4\tilde{\mathbf{Y}}(t)e^T(t)\mathbf{P}\tilde{\mathbf{B}}, \quad \mathbf{K}_4 > 0. \quad (182)$$

Analogously, $\tilde{\mathbf{W}}_s$ and $\tilde{\mathbf{K}}_{1e}(t)$ were defined in (142) and (143). Term $\tilde{\mathbf{K}}_{2e}(t)$ is defined as $\tilde{\mathbf{K}}_{2e}(t) \equiv \mathbf{K}_{2e}(t) - \hat{\mathbf{K}}_{2e}(t)$. Same as before, the DFMRAC algorithm is completed and the stability in the sense of uniform ultimately boundedness remains to be proved. Following the previous steps, $\mathbf{W}_e^T(t) = [\mathbf{W}_s^T(t), \mathbf{K}_{1e}^T, \mathbf{K}_{2e}^T]^T$ and $\hat{\mathbf{W}}_e^T(t) = [\hat{\mathbf{W}}_s^T(t), \hat{\mathbf{K}}_{1e}^T(t), \hat{\mathbf{K}}_{2e}^T(t)]^T$ can be defined such as:

$$\tilde{\mathbf{W}}_e(t) = \mathbf{W}_e(t) - \hat{\mathbf{W}}_e(t), \quad (183)$$

$$\tilde{\beta}_e(\cdot) = \begin{bmatrix} \beta_s(x(t)) \\ \tilde{\mathbf{x}}(t) \\ \tilde{\mathbf{Y}}(t) \end{bmatrix}. \quad (184)$$

Then, the model following error dynamics $\dot{e}(t) = \dot{\tilde{\mathbf{x}}}(t) - \dot{\mathbf{x}}_m(t)$, can be defined, $\dot{\mathbf{x}}_m(t)$ from (66).

$$\dot{e}(t) = \mathbf{A}_m e(t) + \tilde{\mathbf{B}} \lambda \tilde{\mathbf{W}}_e^T(t) \tilde{\beta}_e(\cdot). \quad (185)$$

It can be seen that the error dynamics (185) is equivalent to the above (147). Therefore, using the proposed Lyapunov-Krasovskii functional in (153) and a similar procedure as before, it can be proven that $e(t)$ and $\tilde{\mathbf{W}}_e(t)$ are uniformly ultimately bounded.

4 Simulations

In this chapter, the computational simulations with the MRAC and DFMRAC algorithms are presented. Firstly, a comparison between the latest MRAC algorithm implemented in the machine (without considering friction force), and the new MRAC and DFMRAC (both consider the Stribeck friction) is discussed. From now on, the term “old MRAC” will be used, to refer the latest MRAC implemented in NPMDM, which does not consider the friction force. Meanwhile, “new MRAC” refers to the MRAC controller considering the friction force. Secondly, a comparison of the MRAC and DFMRAC algorithm considering the unknown input matrix case is shown. Finally, Gaussian measurement noise is given. In all cases, the nominal control incorporates the PI-SFC in combination with the feed-forward control. The main Simulink diagram can be found in Appendix A.2.

4.1 Comparison of the adaptive controllers

The state space matrices of the system, the reference model, the gain parameters for the PI-SFC and feed-forward control, and the gain values for the adaptive controllers are given in Appendix A.1. It is important to remark again, that the friction coefficients were estimated and no identification techniques were applied to know the real values. Figure 9 shows the output position when using the old MRAC, the new MRAC and DFMRAC. The desired trajectory is a sine function of the form $r(t) = 100 \sin(5t)$ in nm. It can be seen also in Figure 9, that the output can follow the desired reference for the three adaptive controllers, even though the real system used in the simulations has unknown parameters including in the input matrix, see parameters in Appendix A.1.

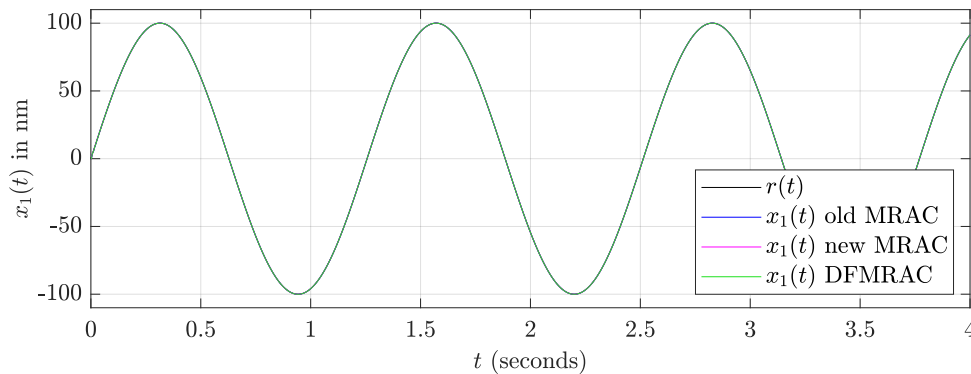


Figure 9: Output response to a sine reference when applying the old MRAC, new MRAC and DFMRAC.

Figure 10 shows the comparison between the error, $e(t) = r(t) - x_1(t)$, for the three controllers. At the bottom, the image is zoomed to show the stationary error.

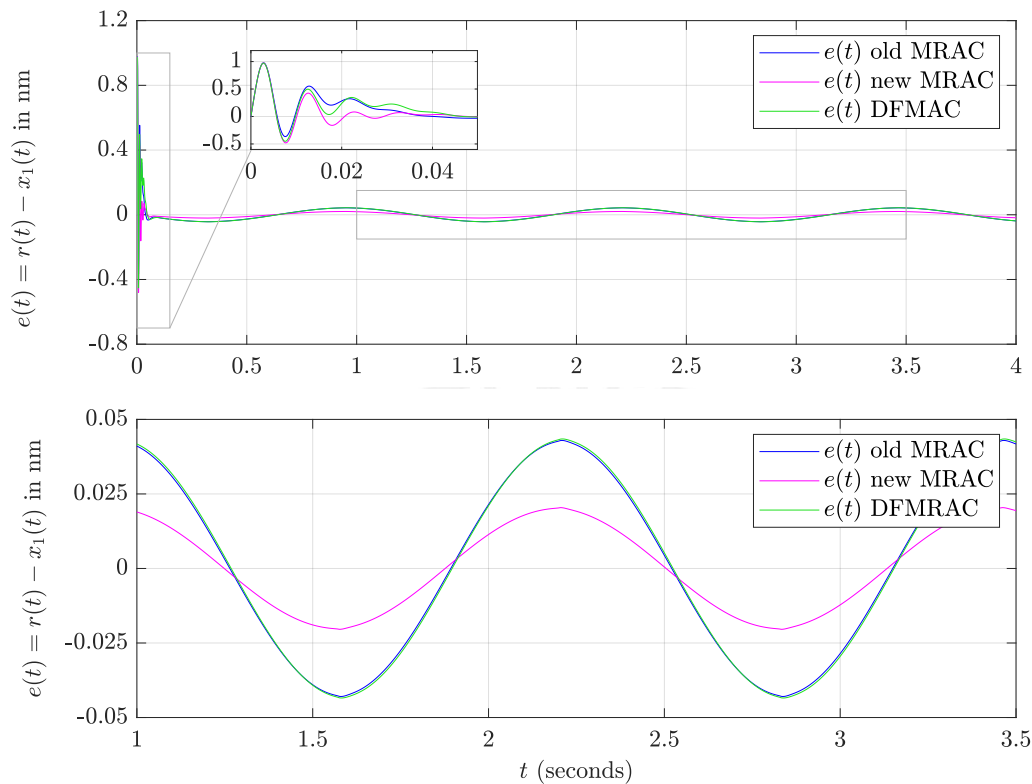


Figure 10: Error, $e(t) = r(t) - x_1(t)$, when applying the old MRAC, new MRAC and DFMRAC.

Table 2 lists the RMSE and maximum error. As expected, the new MRAC and DFMRAC lead to a lower RMSE and a lower peak error. Nevertheless, it can be seen that they are not significantly better. The lower RMSE and peak error can be found by the new MRAC. When the friction parameters are increased, the performance of the adaptive controllers without considering the friction, significantly decreases.

Table 2: RMSE and maximum error of the sine simulation.

Adaptive controller	RMSE (nm)	Maximum error (nm)
old MRAC	0.046	0.977
new MRAC	0.033	0.975
DFMRAC	0.045	0.972

Figure 11 shows the estimated weights for the old MRAC. As intuited, it can be seen that the weights $\hat{\mathbf{W}}_{s,1}(t)$ and $\hat{\mathbf{W}}_{s,2}(t)$ increase indefinitely in time. This behaviour is referred to as drifting parameters, which was previously mentioned in Section 3.1. This occurs because the MRAC algorithm obtains in fact $\dot{\hat{\mathbf{W}}}_s(t)$ and then considers an integration to determine $\hat{\mathbf{W}}_s(t)$, see (62), which causes the parameters to accumulate. Furthermore, it is observed that $\hat{\mathbf{W}}_{s,1}(t)$ and $\hat{\mathbf{W}}_{s,2}(t)$ have a really low value (around 10^{-17}) compared to $\hat{\mathbf{W}}_{s,3}(t)$, which remains around 10^{-7} . However, $\hat{\mathbf{W}}_{s,1}(t)$ and $\hat{\mathbf{W}}_{s,2}(t)$ will increase after a long time and that will cause numerical problems. As a consequence, the performance of the closed loop will drop, which is critical if the machine runs without resetting for a long period of time.

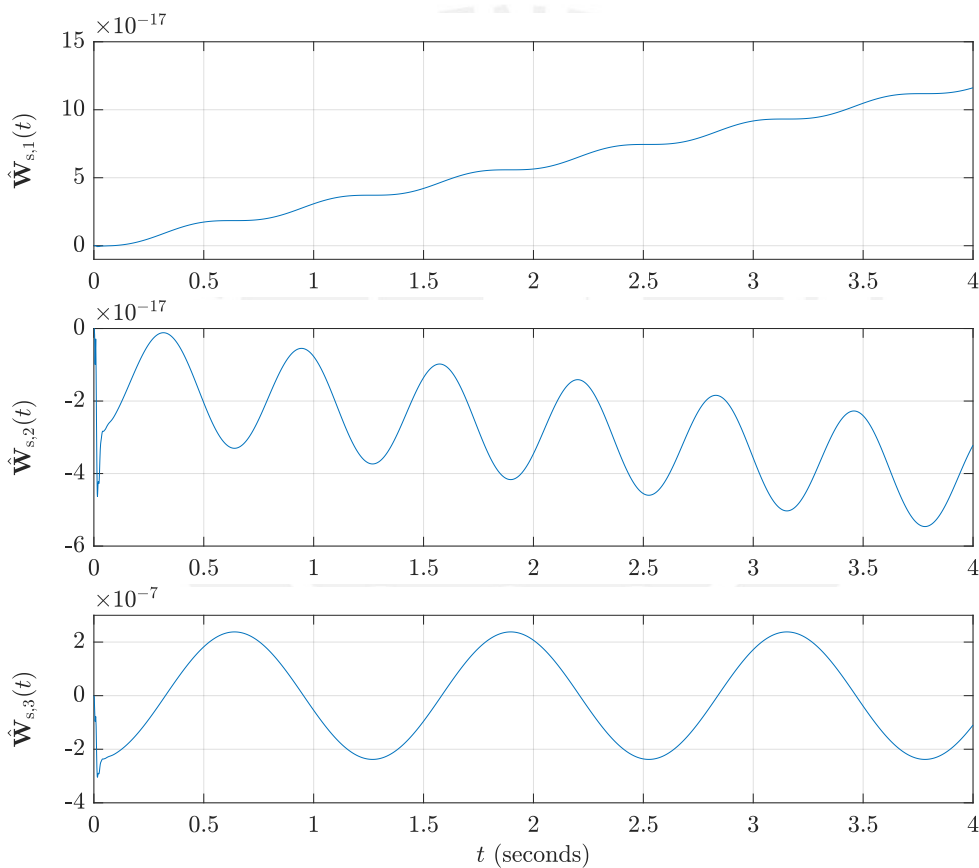


Figure 11: Estimated weight $\hat{\mathbf{W}}_s(t)$ of the old MRAC.

Figure 12 shows the estimated weights for the new MRAC. Same as before, it can be noted that the weights parameters $\hat{\mathbf{W}}_{s,1}(t)$, $\hat{\mathbf{W}}_{s,2}(t)$, $\hat{\mathbf{W}}_{s,4}(t)$ and $\hat{\mathbf{W}}_{s,5}(t)$ increase indefinitely in time. All of them have a low value (less than 10^{-14}) compared to $\hat{\mathbf{W}}_{s,3}(t)$, $\approx 10^{-5}$. Therefore, is not possible to see a drop in the performance in a 4s simulation.

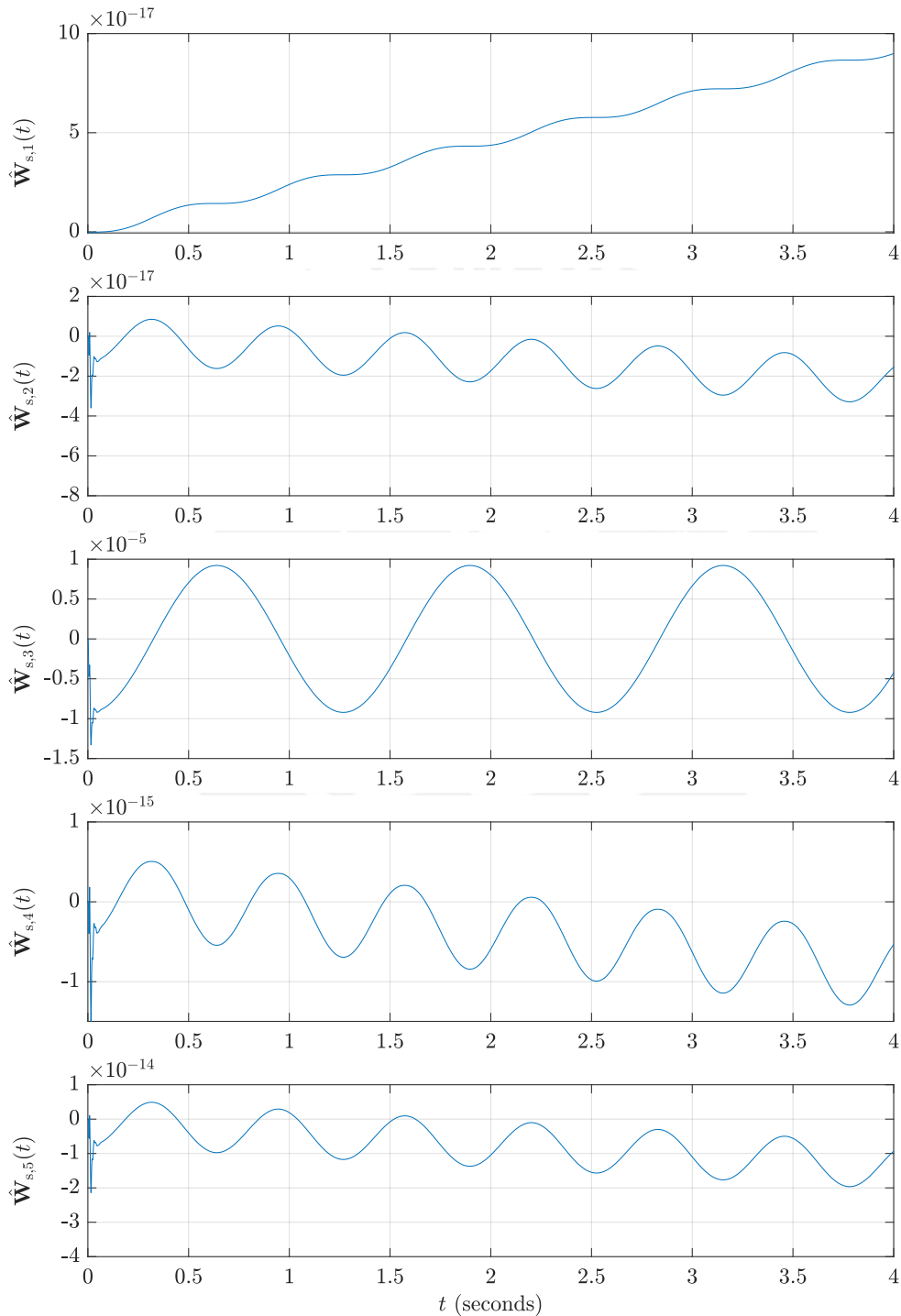


Figure 12: Estimated weight $\hat{\mathbf{W}}_s(t)$ of the new MRAC.

Figure 13 shows the estimated weight uncertainties for the DFMRAC algorithm. It can be seen that none of the parameters increases in time. This is due to the fact that the DFMRAC does not need an integration to calculate $\hat{\mathbf{W}}_s(t)$, see equations (102), (103) and (104). This also proves that $\hat{\mathbf{W}}_s(t)$ is in fact UUB, as demonstrated in the previous chapter.

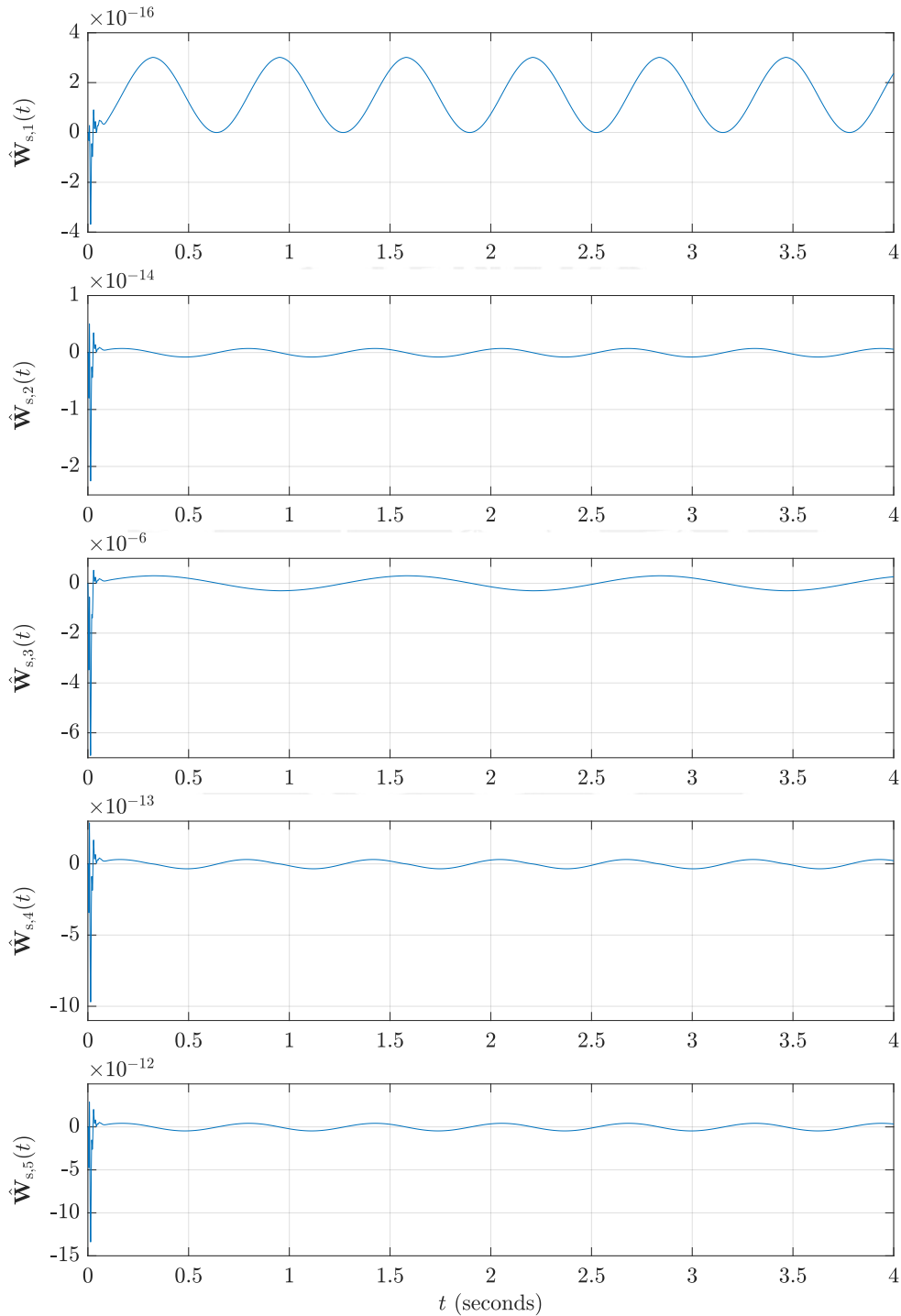


Figure 13: Estimated weight $\hat{\mathbf{W}}_s(t)$ of the DFMRAC.

Figure 14 shows the ideal matched uncertainty $\mathbf{W}_s^T \beta(x)$ and the adaptive control $u_{\text{ad}}(t) = \hat{\mathbf{W}}_s^T \beta(x)$ for the controllers. Ideally, a perfect estimation will follow the ideal matched uncertainty, which means that the adaptive control is capable of cancelling all the uncertainties in the system (from the unknown terms) and also the friction force. However, it is important to remark that, it is not possible to achieve this because the velocity of the system, $x_2(t)$, is estimated and not measured directly. Furthermore, the ideal matched uncertainty $\mathbf{W}_s^T \beta(x)$ signal can not be the same for the three controllers because \mathbf{W}_s and $\beta(x)$ depends on $x_1(t)$, which value depends on the simulated controller. It can be noted in Figure 14 that only for the new MRAC the two signals are in phase.

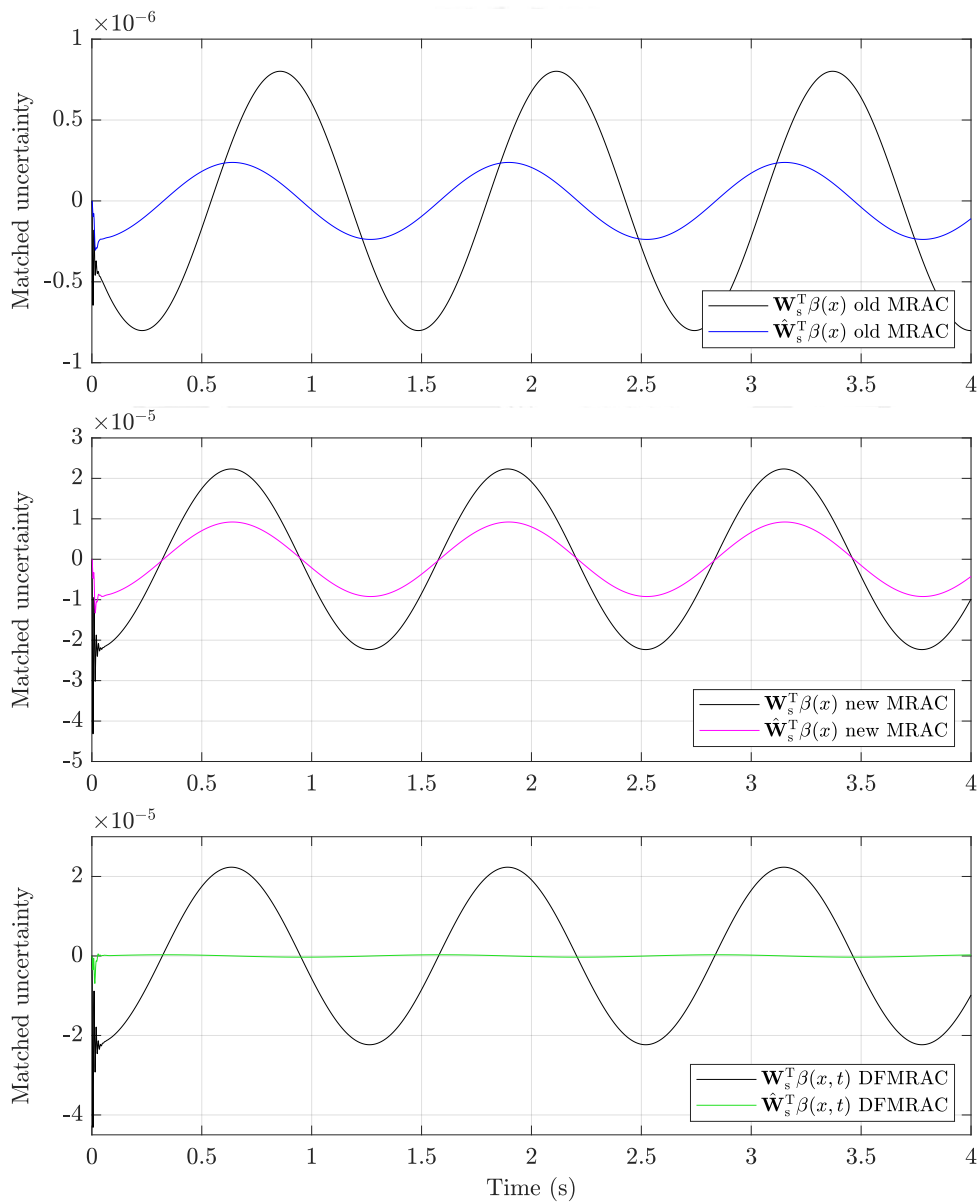


Figure 14: Ideal vs estimated matched uncertainty of the simulated controllers.

4.2 Comparisons in the noise case

The noise on the position signal of the NPMDM is a limiting factor regarding the controller performance. Therefore, to test the new adaptive algorithms, a Gaussian noise ($\mu = 0$ and $\sigma^2 = 10^{-18}$) is added to the output of the simulations. It can be seen in Figure 15, that despite the noise, the controller is capable of following the desired trajectory.

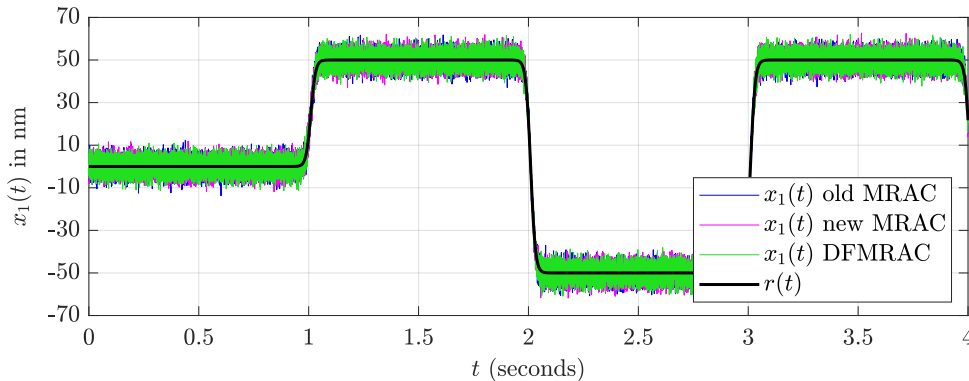


Figure 15: Output response to a pulse reference when applying the old MRAC, new MRAC and DFMRAC considering sensor noise.

Figure 16 shows the error of the closed loop and Table 3 shows the RMSE and maximum error. All the adaptive controllers obtain similar results. The maximum error remains around 12 nm, whereas the RMSE around 3.3 nm.

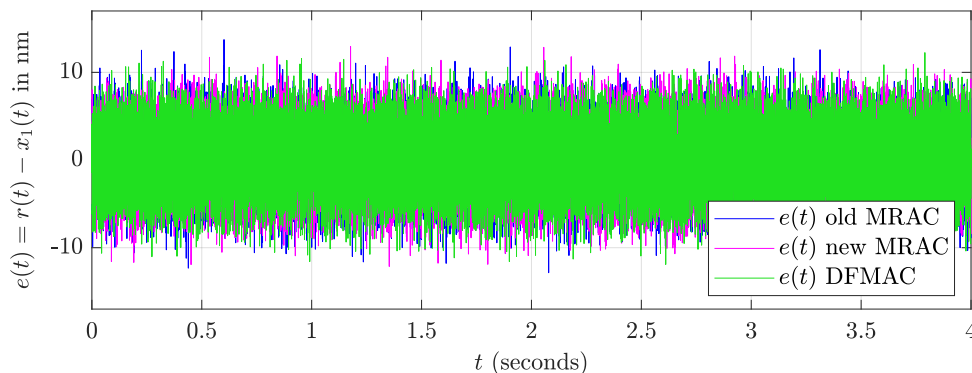


Figure 16: Error, $e(t) = r(t) - x_1(t)$, when applying the old MRAC, new MRAC and DFMRAC considering sensor noise.

Table 3: RMSE and maximum error of the noise case simulation.

Adaptive controller	RMSE (nm)	Maximum error (nm)
old MRAC	3.266	12.508
new MRAC	3.281	12.836
DFMRAC	3.315	12.136

Figure 17 shows the estimated weights for the old MRAC considering sensor noise. As expected, parameters $\hat{\mathbf{W}}_{s,1}(t)$ and $\hat{\mathbf{W}}_{s,2}(t)$ increase indefinitely in time.

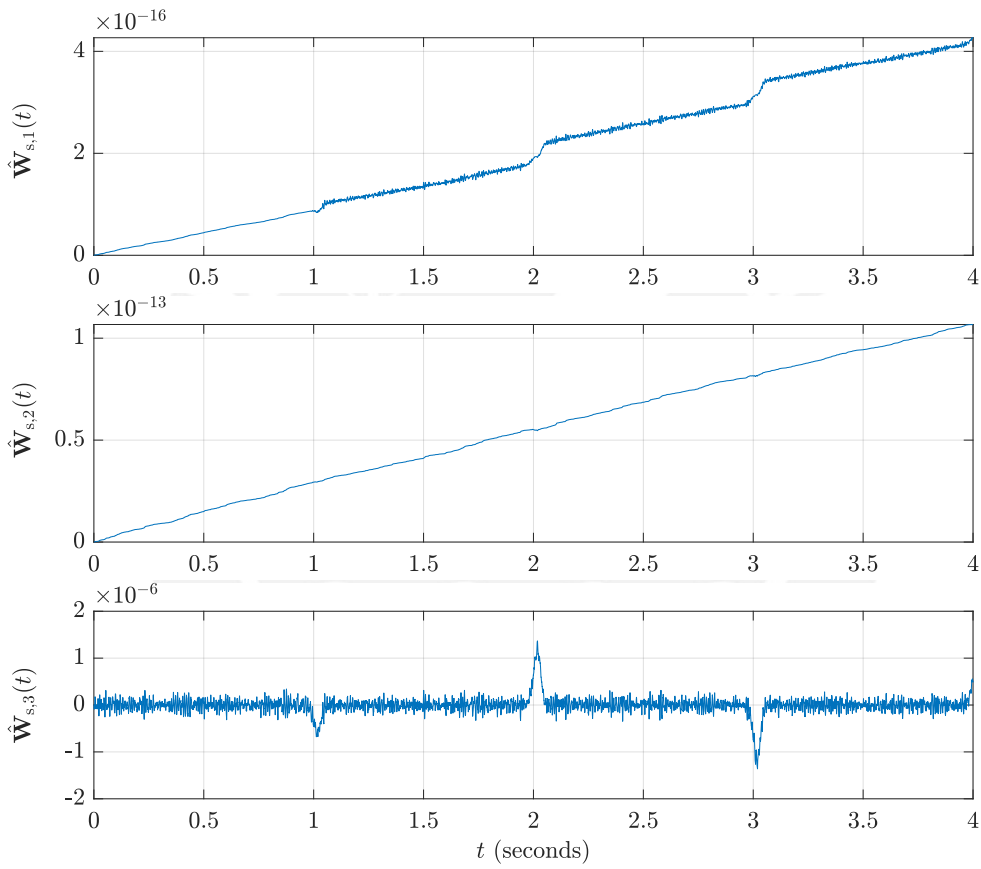
Figure 17: Estimated weight $\hat{\mathbf{W}}_s(t)$ of the old MRAC considering sensor noise.

Figure 18 shows the estimated weights for the new MRAC considering sensor noise. Also for this case, the $\hat{\mathbf{W}}_{s,1}(t)$, $\hat{\mathbf{W}}_{s,2}(t)$, $\hat{\mathbf{W}}_{s,4}(t)$ and $\hat{\mathbf{W}}_{s,5}(t)$ parameters increase indefinitely in time.

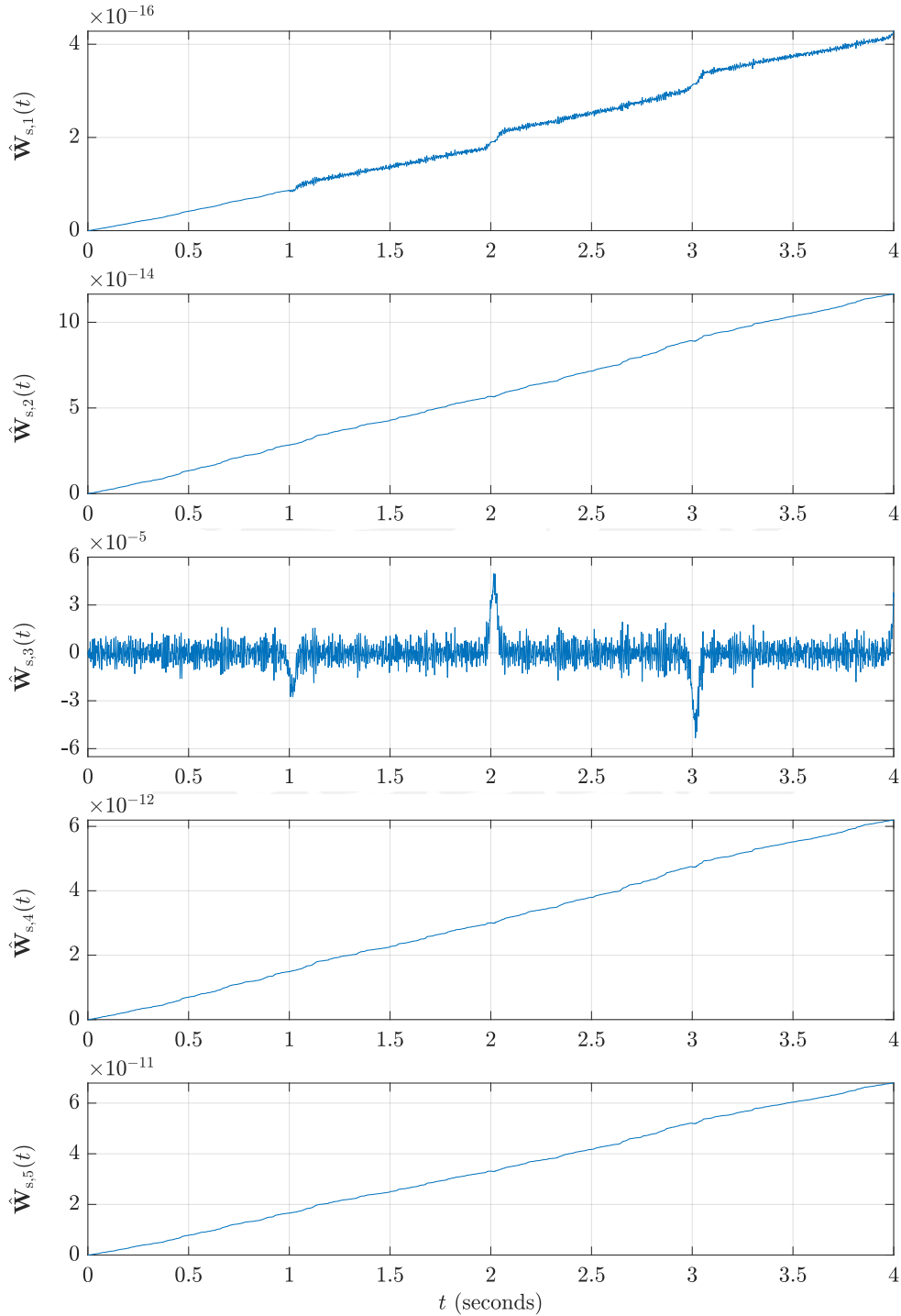


Figure 18: Estimated weight $\hat{\mathbf{W}}_s(t)$ of the new MRAC considering sensor noise.

Figure 19 shows the estimated weights for the DFMRAC considering sensor noise. For this controller, the estimated parameters do not increase in time.

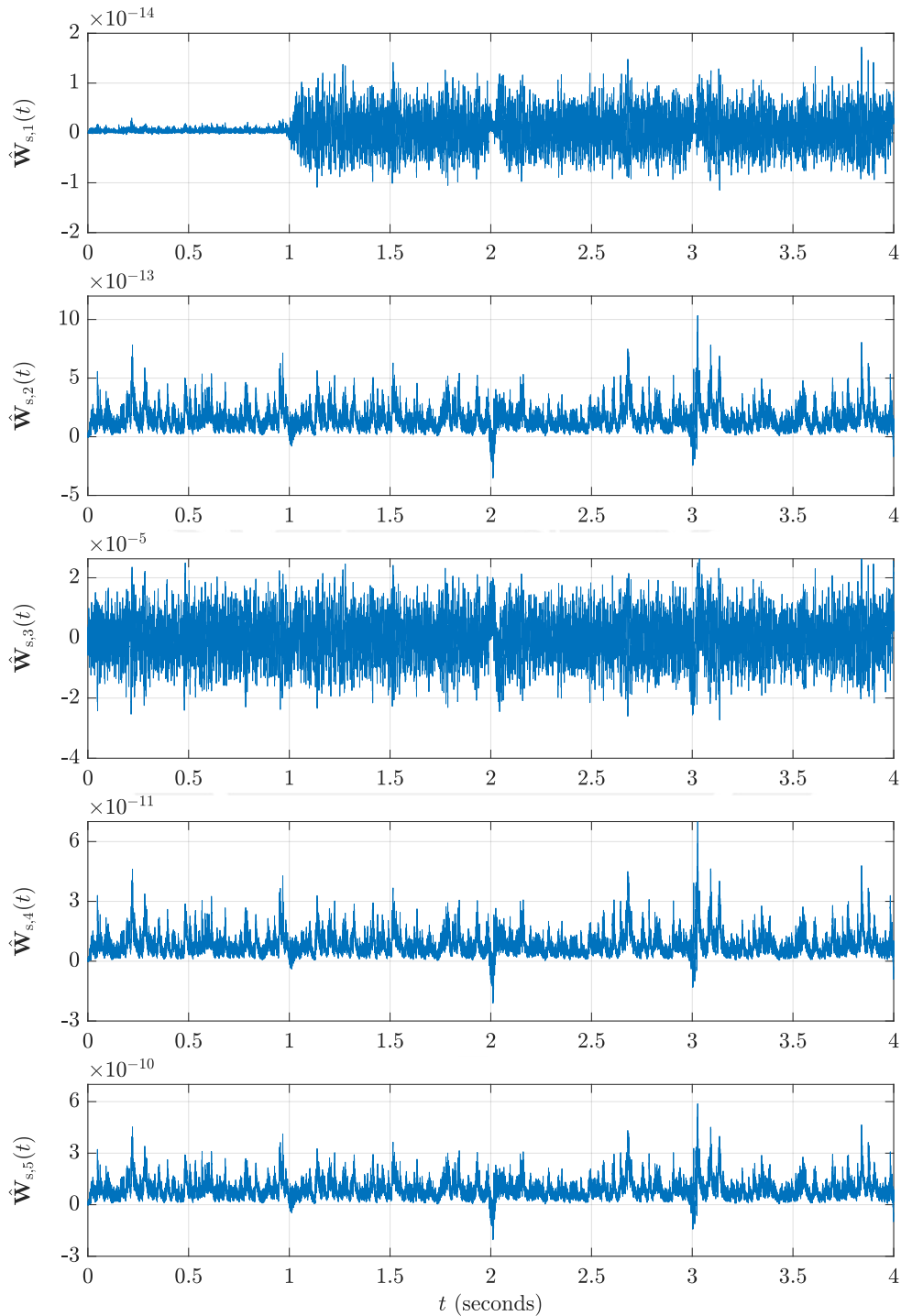


Figure 19: Estimated weight $\hat{\mathbf{W}}_s(t)$ of the DFMRAC considering sensor noise.

Figure 20 shows the ideal matched uncertainty, $\mathbf{W}_s^T \beta(x)$, and the adaptive control $u_{ad}(t) = \hat{\mathbf{W}}_s^T \beta(x)$ for the new MRAC and DFMRAC. Even in spite of the noise, both controllers attempt to estimate the ideal matched uncertainty. At $t = 2$ s, see

zoomed versions, the DFMRAC does not react the same way as the MRAC.

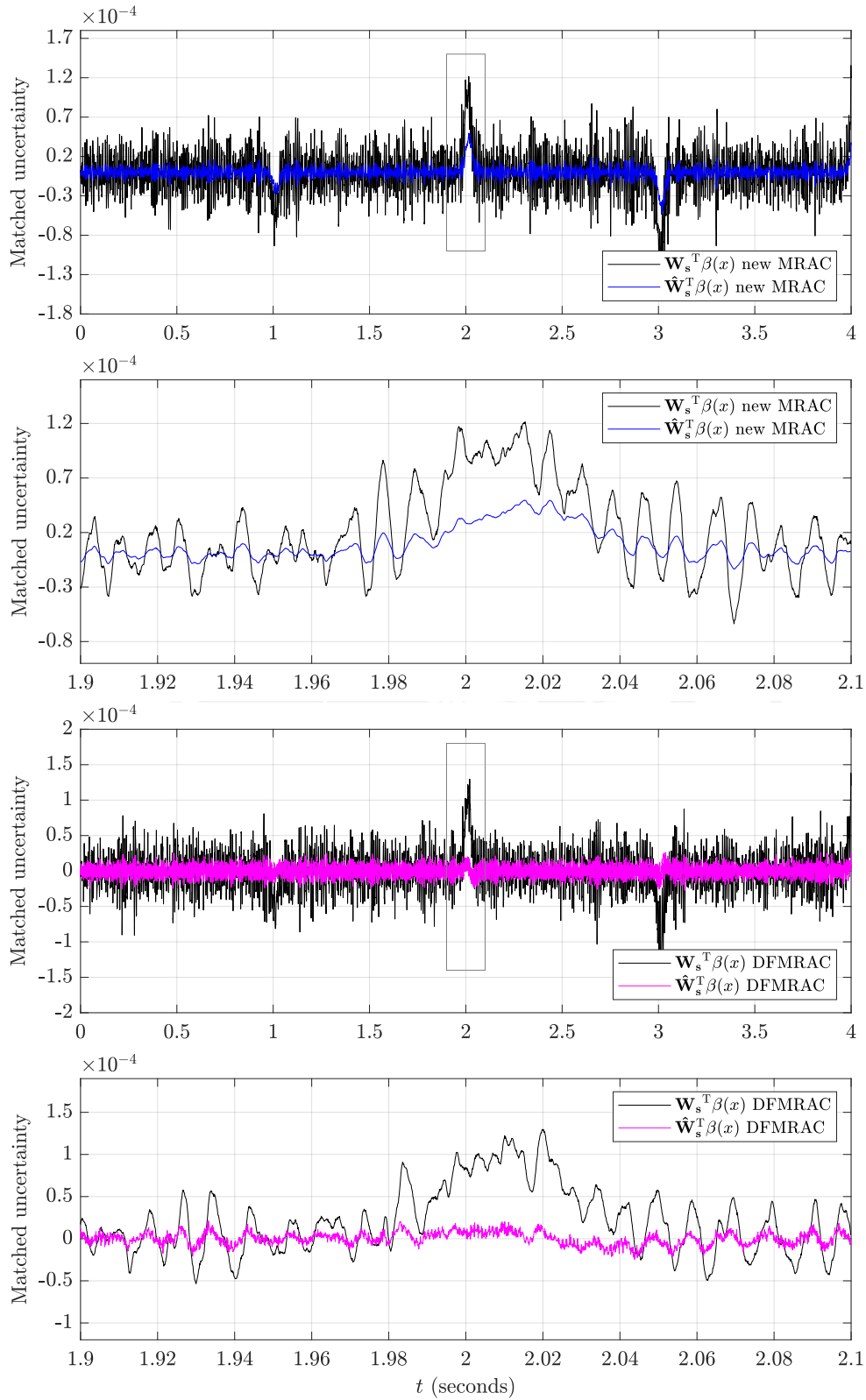


Figure 20: Ideal vs estimated matched uncertainty term of the new MRAC and DFMRAC considering sensor noise.

Figure 21 shows the nominal and adaptive control output of the simulated controllers. At $t = 1$ s, $t = 2$ s and $t = 3$ s the output of the new MRAC algorithm has more presence in the total control output than the other controllers.

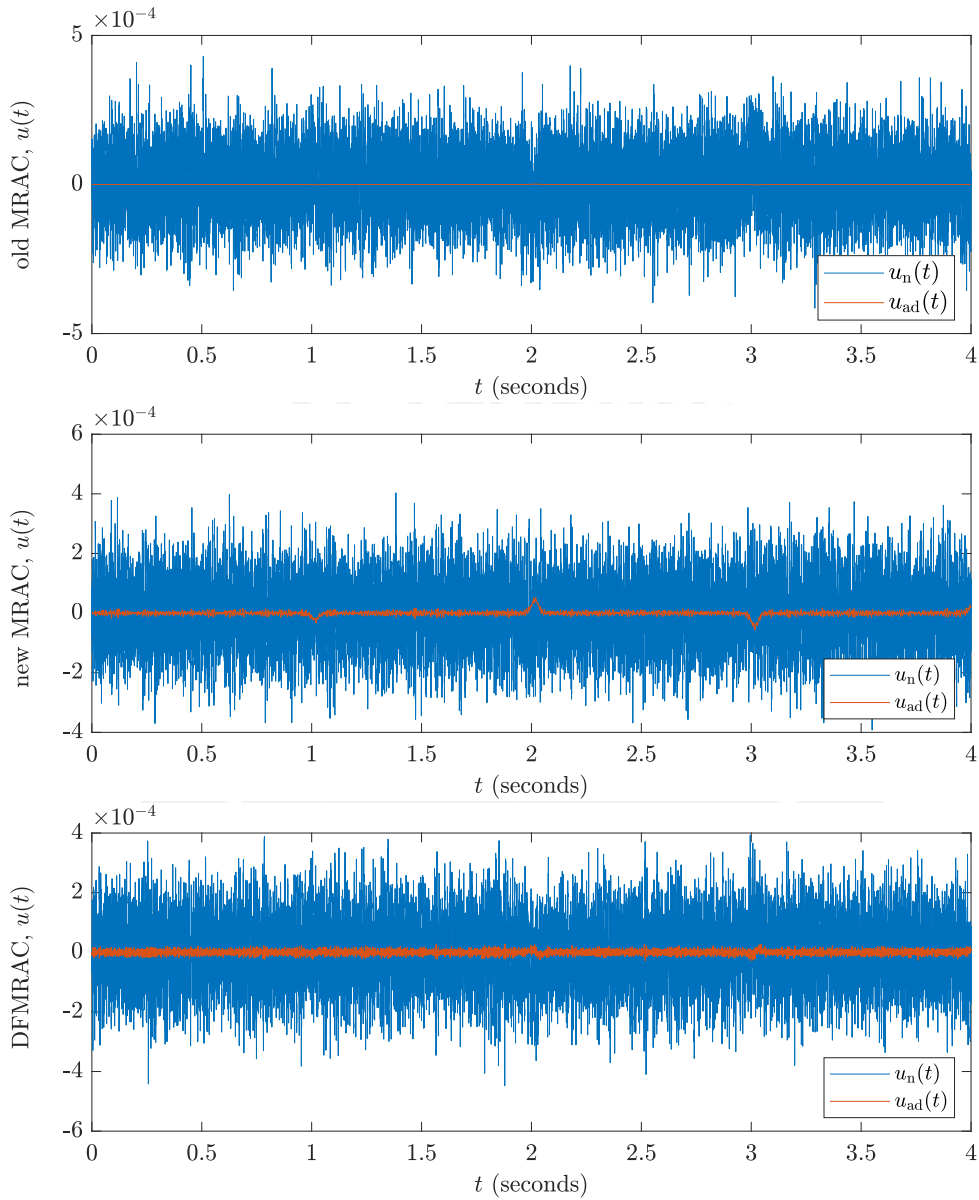


Figure 21: Nominal and adaptive control output of the old MRAC, new MRAC and DFMRAC considering sensor noise.

4.3 Comparisons in the extensions to the unknown input matrix case

This section shows the simulations related to the adaptive algorithms considering their extensions to the unknown input matrix case. “MRAC un” refers to the MRAC considering the unknown input matrix case, whereas “DFMRAC un” refers to the DFMRAC extension. Both controllers consider the friction force in their algorithms and their corresponding gain parameters can be found in Appendix A.1. The sine reference trajectory and the sensor noise are the same as defined in Section 4.1. Figure 22 shows that both controllers are capable of following the corresponding reference despite of the noise.

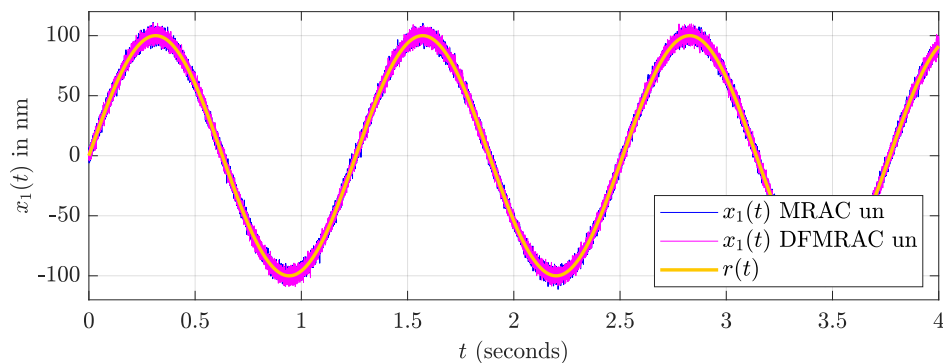


Figure 22: Output response to a sine reference when applying the “MRAC un” and “DFMRAC un” and sensor noise.

Figure 23 shows that the error is mostly influenced by sensor noise. In Appendix A.2, Table 13 shows the RMSE and the maximum error for both controllers. The results are very similar (RMSE around 3.3 nm and maximum error around 14 nm).

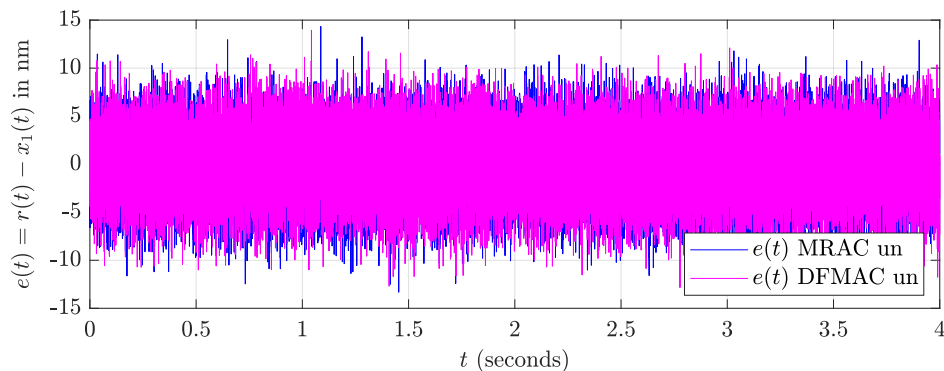


Figure 23: Error, $e(t) = r(t) - x_1(t)$, when applying the “MRAC un” and “DFMRAC un” and sensor noise to a sine reference.

Figure 24 shows the estimated weights for the “MRAC un”. Similar as before, parameters $\hat{\mathbf{W}}_{s,1}(t)$, $\hat{\mathbf{W}}_{s,2}(t)$, $\hat{\mathbf{W}}_{s,4}(t)$ and $\hat{\mathbf{W}}_{s,5}(t)$ increase indefinitely in time and have a lower value compared to $\hat{\mathbf{W}}_{s,3}(t)$.

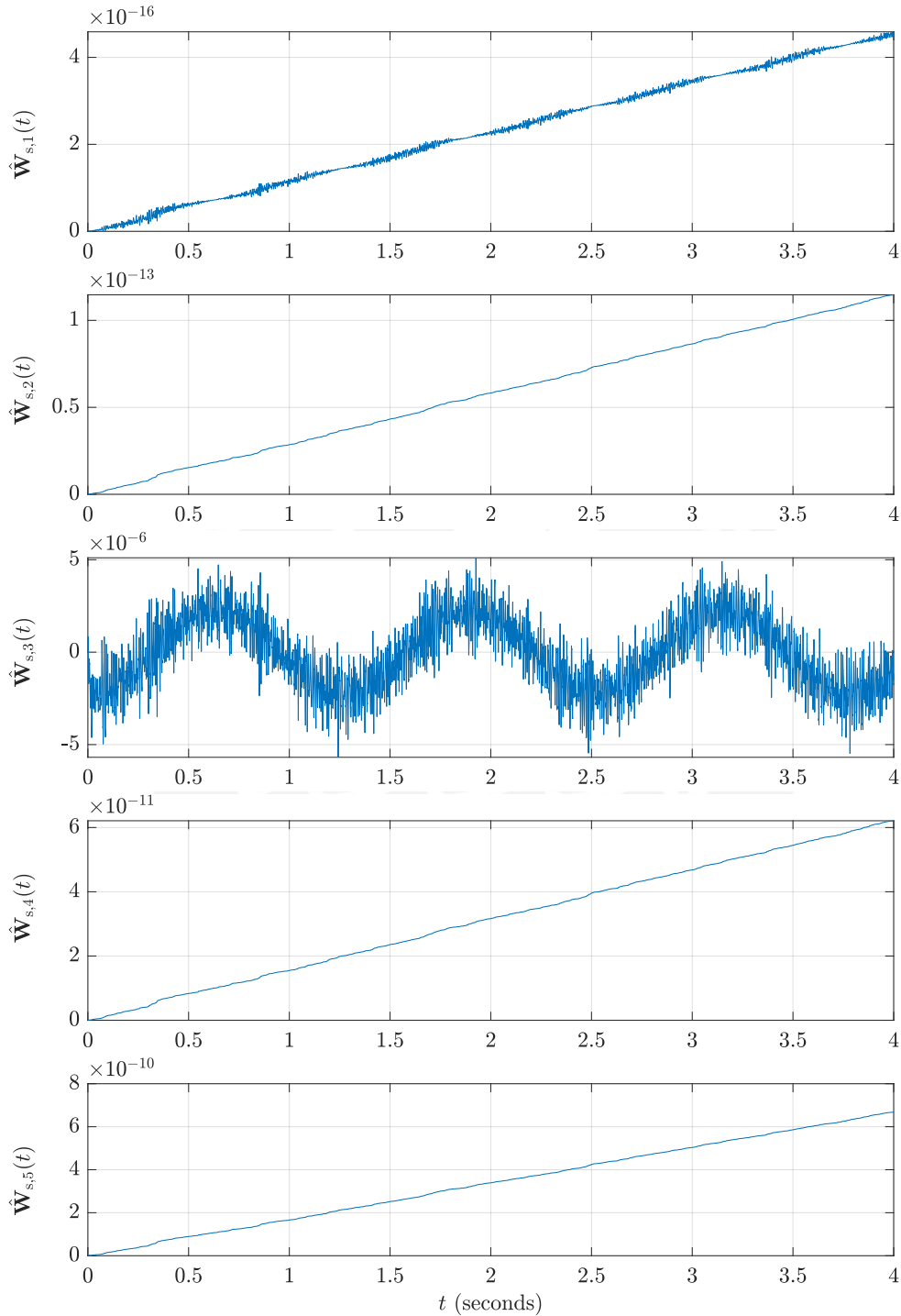


Figure 24: Estimated weights $\hat{\mathbf{W}}_s(t)$ of the “MRAC un”.

Figure 25 shows the estimated weights for the “DFMRAC un”. As expected, estimated parameters do not increase in time because they are all UUB. The weight parameter $\hat{W}_{s,3}(t)$ has a higher value in comparison to the others.

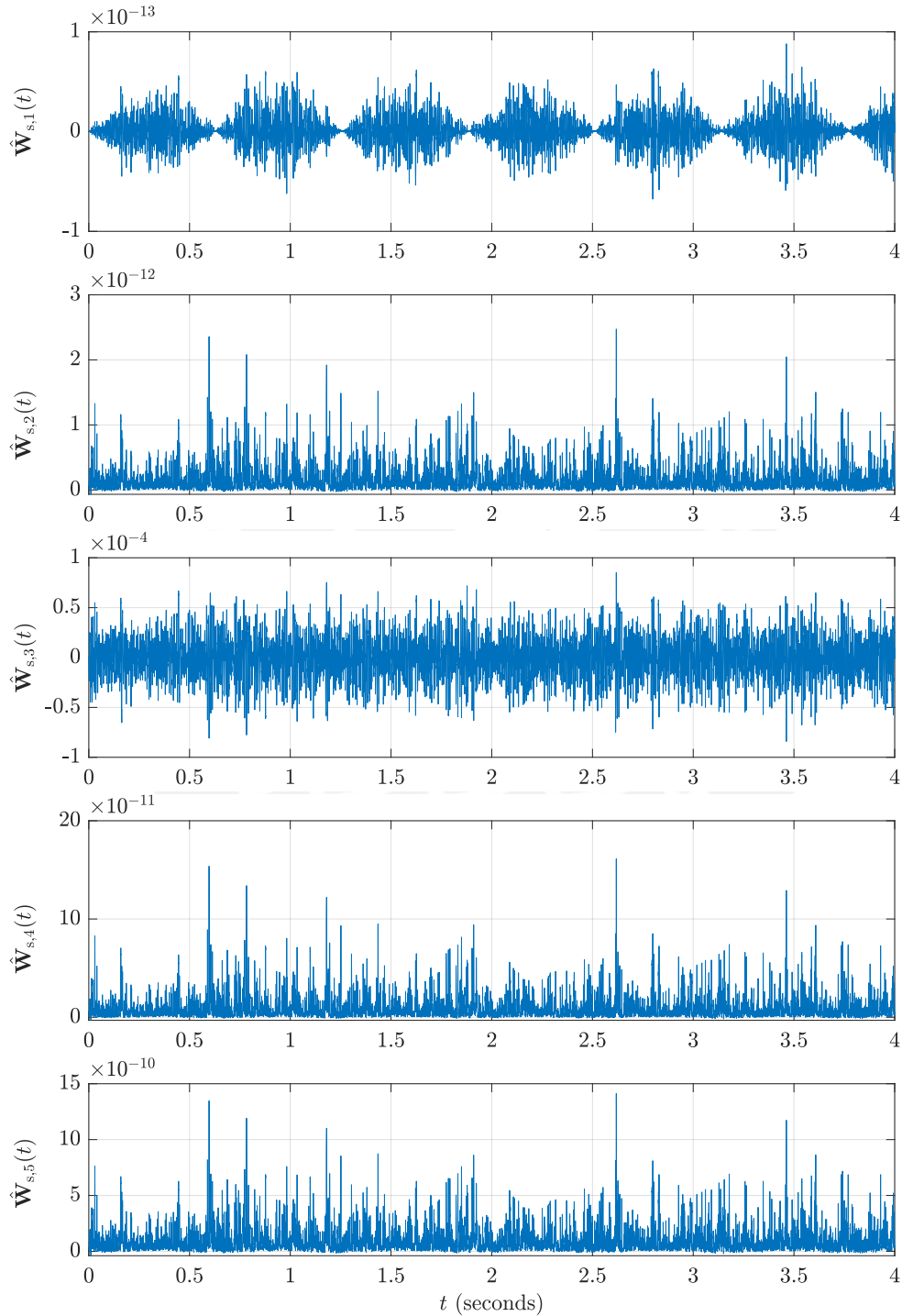


Figure 25: Estimated weight of the “DFMRAC un”.

Figure 26 shows the ideal matched uncertainty, $\mathbf{W}^T\beta(\cdot)$, and the adaptive control $u_{\text{ad}}(t) = \hat{\mathbf{W}}^T\beta(\cdot)$ for the “MRAC un” and “DFMRAC un”. At $t = 2\text{s}$, see zoomed versions, the “DFMRAC un” has a better approximation to the ideal matched uncertainty compared to “MRAC un”.

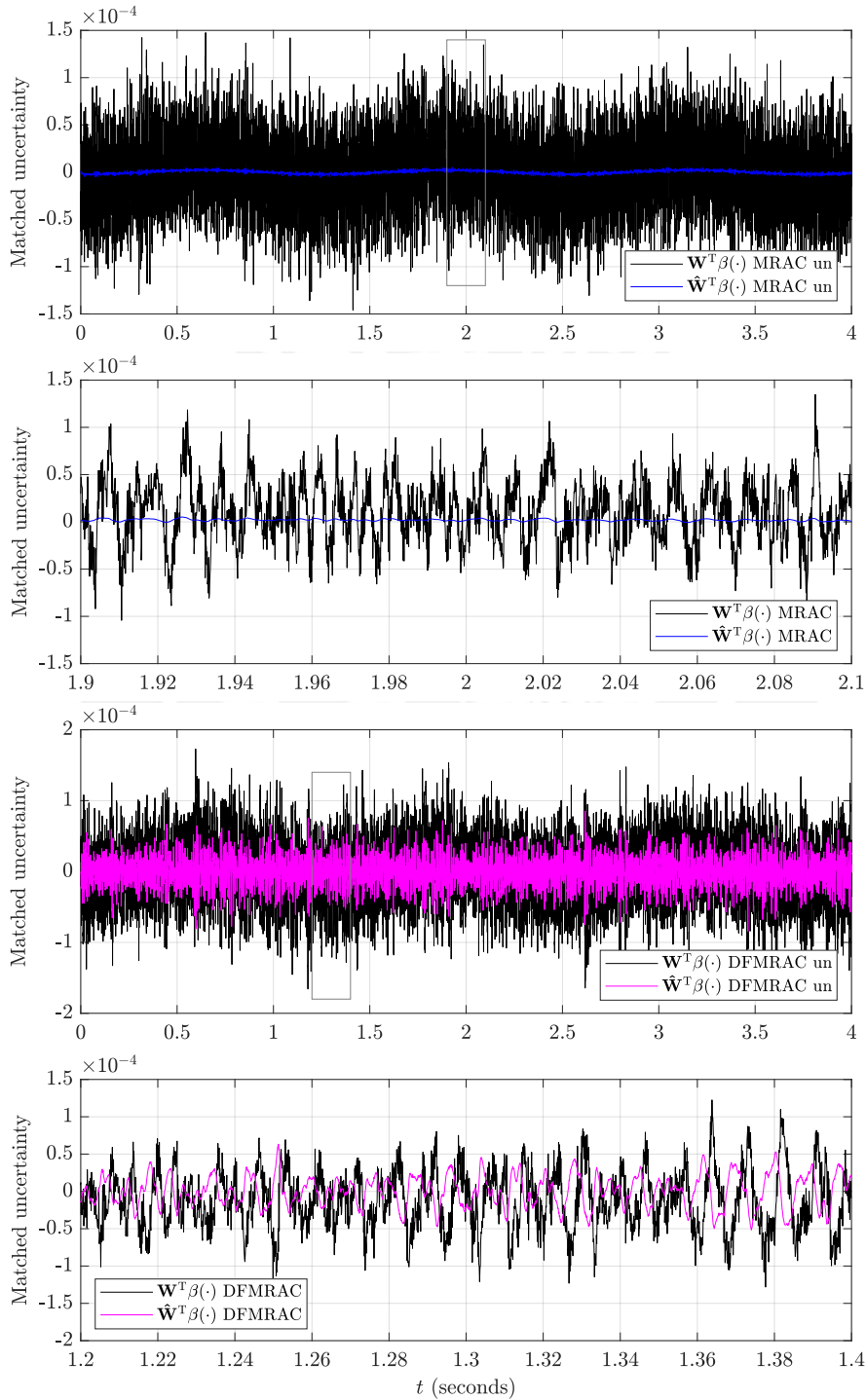


Figure 26: Ideal vs estimated matched uncertainties of the “MRAC un” and “DFMRAC un”.

Figure 21 shows the nominal and adaptive control output of the simulated controllers. The adaptive control output of the “DFMRAC un” plays a more significant role in comparison to the “MRAC un”. This could be seen also in Figure 26 when the “DFMRAC un” has a better approximation to the ideal matched uncertainty.

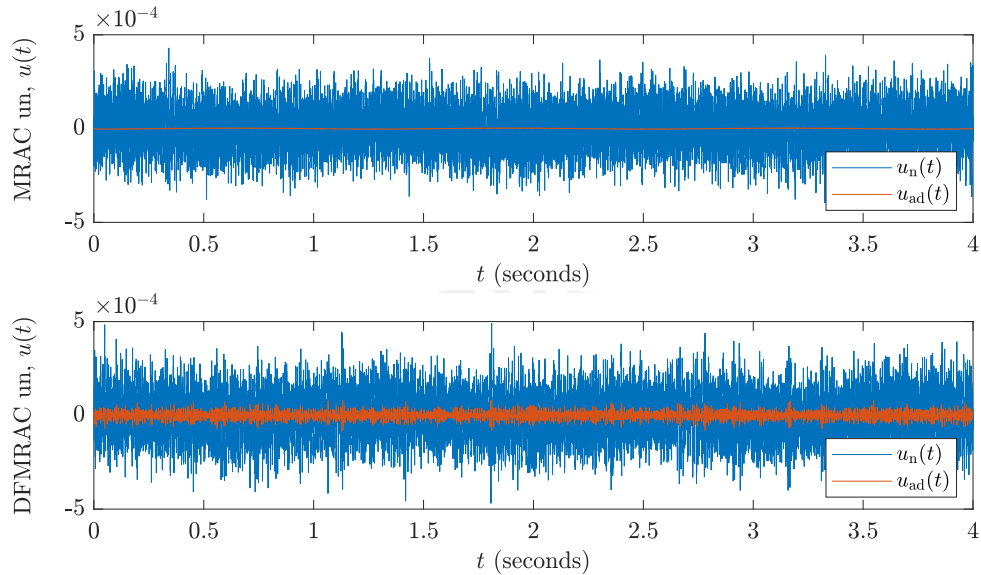


Figure 27: Nominal and adaptive control output of the “MRAC un” and “DFMRAC un” considering sensor noise.

5 Experimental results

This chapter presents the experimental results of applying the adaptive controllers in the NPMDM. First, a sine reference will be tested, in which changes in the amplitude and frequency of the sine will be applied to evaluate the performance of the adaptive controllers. Second, a smooth step reference will be performed, in which the height and the transition time of the step will be changed. Finally, a test regarding the time execution is presented. It is important to remark that all the tests include the DOB-based controller explained in Section 1.4.7.

5.1 Sine reference tests

In this first part, the adaptive controllers follow a sine reference of the form $r(t) = A_{\sin} \sin(2\pi f_{\sin} t)$, where A_{\sin} is the amplitude and it will increase from 100 nm to 4 mm, but keeping the same frequency at $f_{\sin} = 0.1$ Hz.

Test for $A_{\sin} = 100$ nm:

Since it is not visually perceptible to show the difference in the results of the three outputs when applying the old MRAC, new MRAC and DFMRAC in the same graph, only the output response obtained by the DFMRAC is plotted in Figure 28.

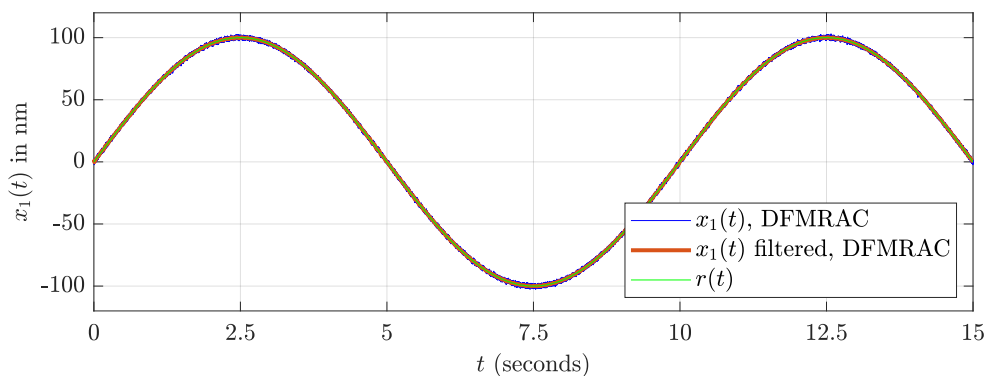


Figure 28: Output response to a $r(t) = 100 \sin(0.2\pi t)$ nm reference when applying the DFMRAC.

Nevertheless, the comparison of the mentioned controllers can be analyzed in Figure 29, which shows the closed loop system error when applying each control algorithm. When crossing the zero position, only by moving upward, it can be seen that the old MRAC is noisier than the others and clearly presents some peak errors. However, there is no significant difference between the three adaptive controllers.

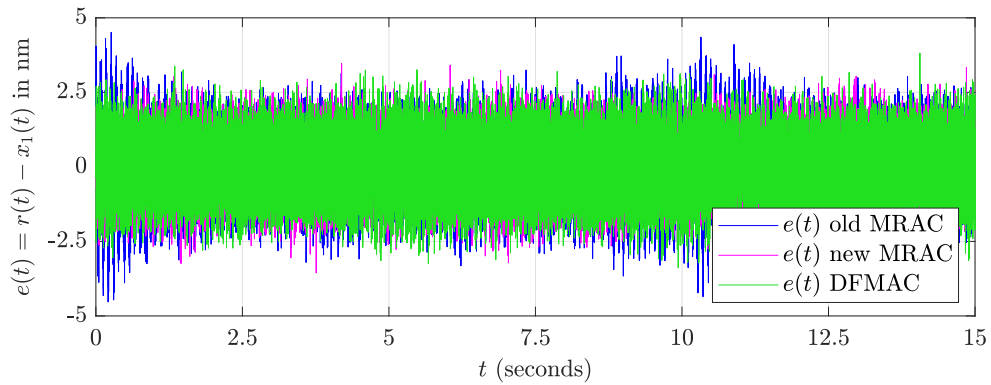


Figure 29: Error, $e(t) = r(t) - x_1(t)$, to a sine reference of 100 nm amplitude.

In Appendix A.2, Table 14 shows the maximum error results for the different amplitudes tested in this subsection. It can be seen that the new MRAC and DFMRAC achieve better results compared to the old MRAC. Considering a 100 nm amplitude, the implementation of the adaptive controllers together with the DOB-based control gives a maximum error of less than 5 nm. Also, in Appendix A.2, Table 15 shows the RMSE results. Considering a 100 nm amplitude, the new MRAC has the lower RMSE value and the RMSE remains below 1 nm for all the controllers.

The estimated parameters $\hat{\mathbf{W}}_s(t)$ are plotted to confirm if the adaptive controllers follow the same behaviour as in the simulations shown in the previous chapter. Figure 30 shows the estimated weight for the old MRAC. Similarly to the simulations, parameters $\hat{\mathbf{W}}_{s,2}(t)$ and $\hat{\mathbf{W}}_{s,3}(t)$ increase indefinitely in time due to the integration used for the calculations in the MRAC algorithm, as explained before. For the sake of completeness, it is important to comment that the vector of known parameters $\beta(x)$ in the old MRAC is defined as $\beta(x) = [1 \ x_1 \ x_2]^T$. Therefore, the order of the drifted weight parameters differs from the simulations because for this document the vector is defined as $\beta(x) = [x_1 \ x_2 \ 1]^T$.

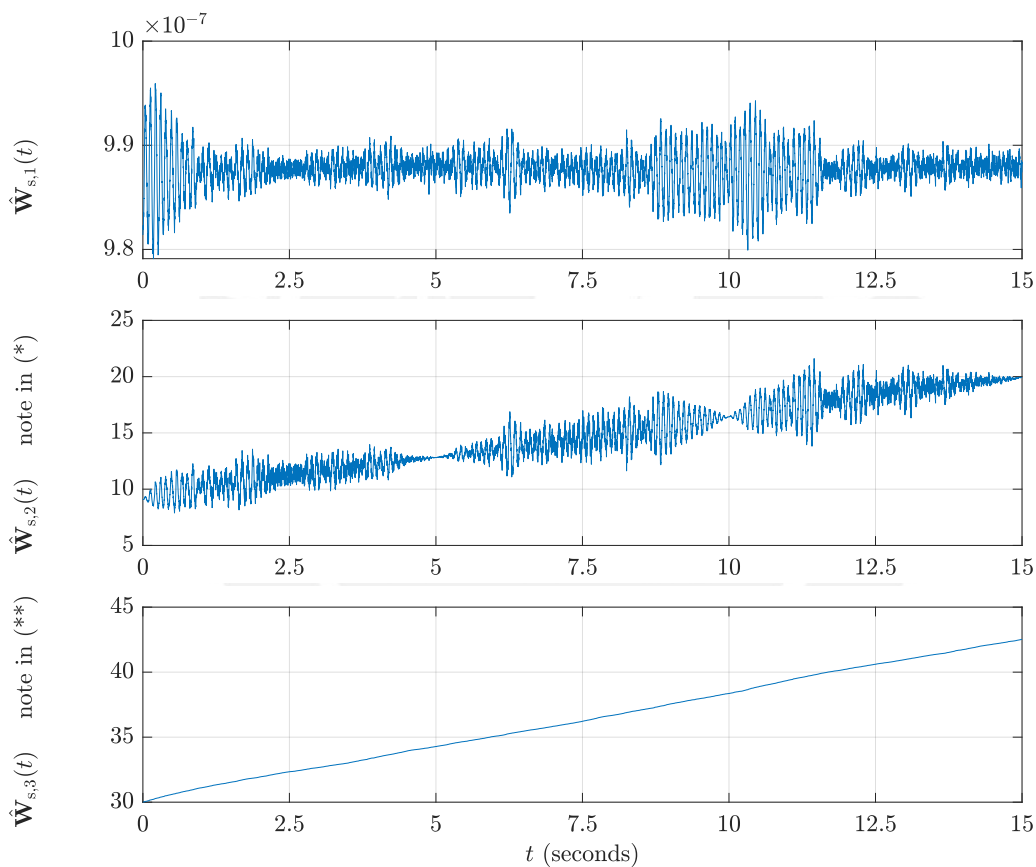


Figure 30: Estimated weight $\hat{\mathbf{W}}_s(t)$ of the old MRAC.

(*) The numbers on the y-axis correspond to the X-digits of the numbers in the following form $1.000000XX \times 10^{-6}$.

(**) The numbers on the y-axis correspond to the X-digits of the numbers in the following form $1.000XX \times 10^{-6}$.

Figure 31 shows the estimated weights for the new MRAC. Analogously to the simulations, $\hat{\mathbf{W}}_{s,1}(t)$, $\hat{\mathbf{W}}_{s,2}(t)$, $\hat{\mathbf{W}}_{s,4}(t)$ and $\hat{\mathbf{W}}_{s,5}(t)$ increase indefinitely in time. The mentioned weights have a lower value (less than 10^{-11}) in comparison to $\hat{\mathbf{W}}_{s,3}(t)$, around 10^{-7} . Therefore, it is not possible to see a drop in the performance or an instability in the system in a 15 s test despite of the drifting parameters.

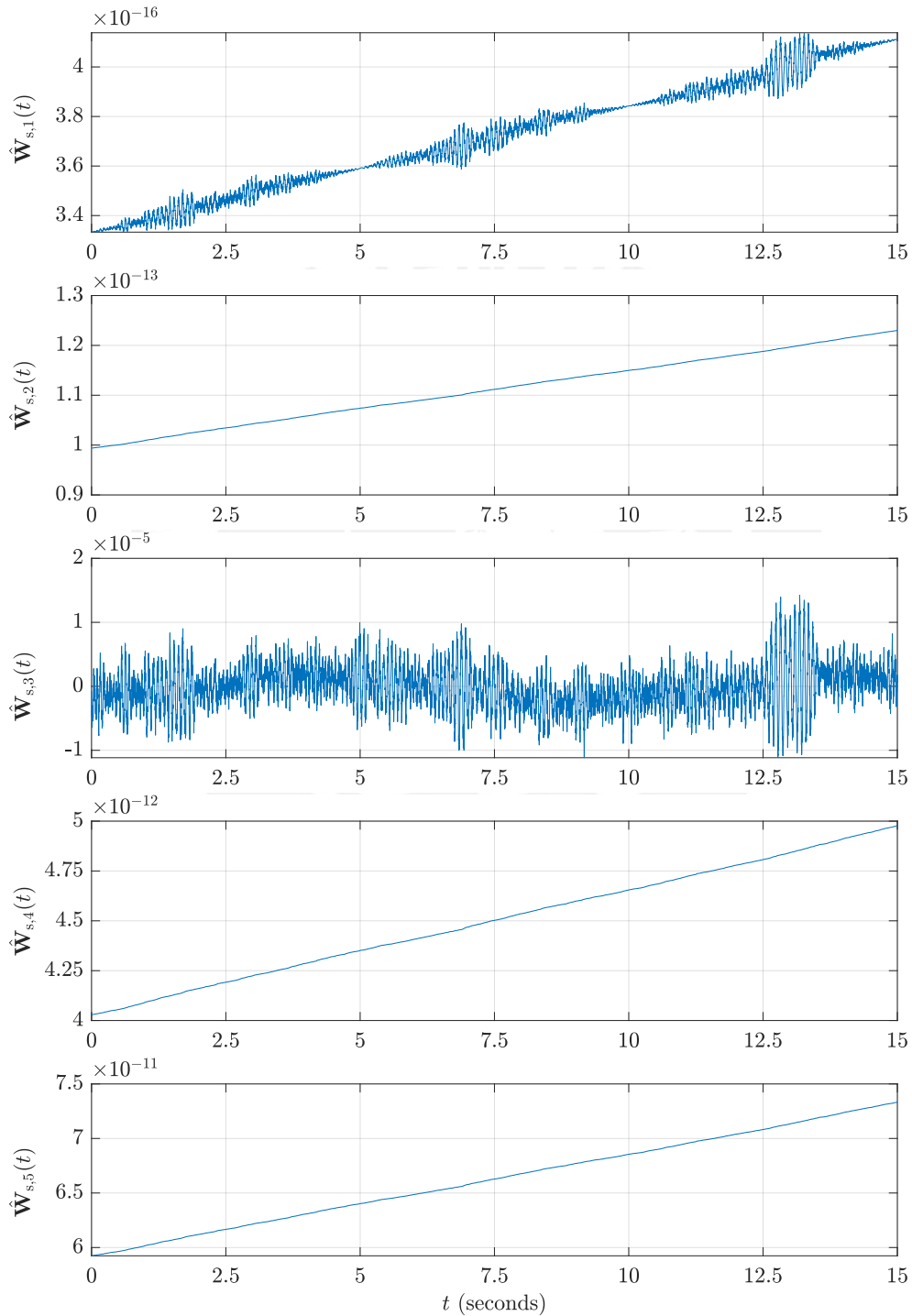


Figure 31: Estimated weight $\hat{\mathbf{W}}_s(t)$ of the new MRAC.

Figure 32 shows the estimated weights for the DFMRAC. As expected, for this controller the estimated weights $\hat{\mathbf{W}}_s(t)$ do not increase in time because they are UUB.

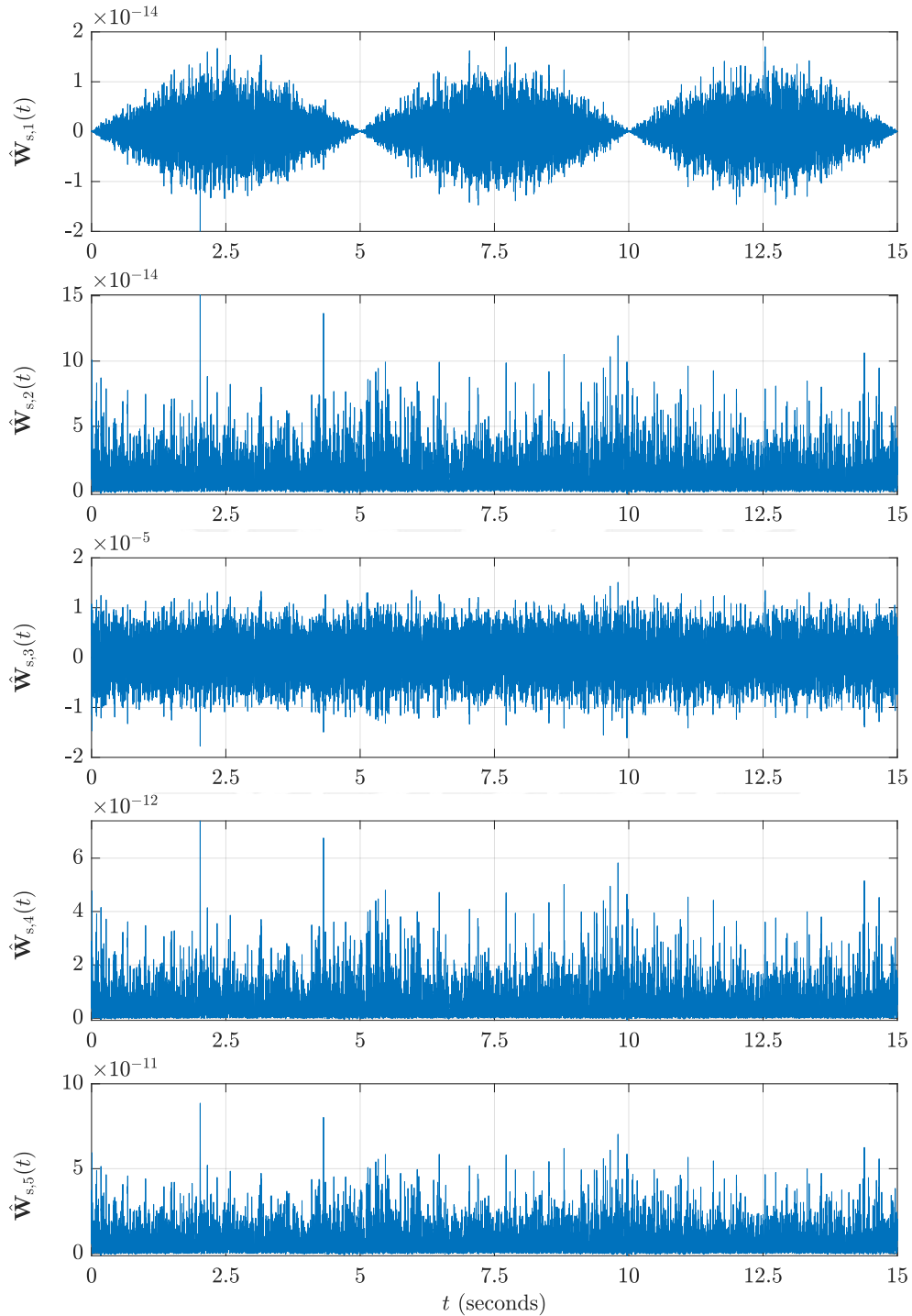


Figure 32: Estimated weight $\hat{\mathbf{W}}_s(t)$ of the DFMRAC.

Test for $A_{\sin} = 1000$ nm:

The output response is shown in Figure 62, which can be found in Appendix A.3. Figure 33 shows the closed loop system error comparison between the adaptive controllers. The results remain as above: the new controllers have a better performance than the old MRAC. In Appendix A.2, Table 14 and Table 15 show the maximum error and RMSE, respectively. It is not yet possible to observe a noticeable difference in the performance of the controllers.

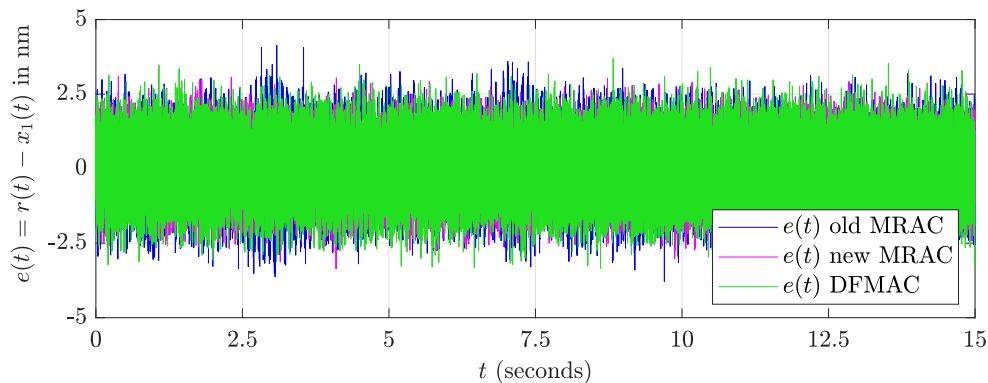


Figure 33: Error comparisons to a $r(t) = 1000 \sin(0.2\pi t)$ nm reference.

Test for $A_{\sin} = 1$ mm:

The output response is shown in Figure 63 in Appendix A.3. Figure 34 shows the error comparison between the adaptive controllers. In this test, is more evident the difference between the old MRAC, the new MRAC and DFMRAC. With a higher amplitude and keeping the frequency fixed, the velocity increases and the higher the velocity, the more dominant the friction. As the old MRAC algorithm does not con-

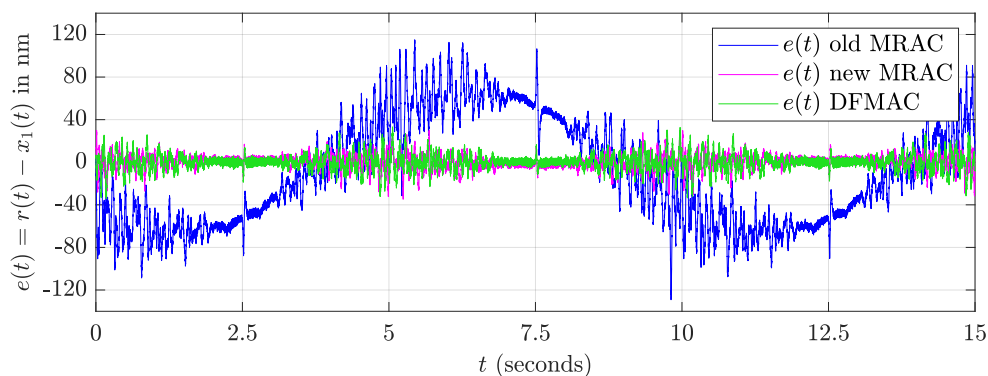


Figure 34: Error comparisons to a $r(t) = 1 \sin(0.2\pi t)$ mm reference.

sider the friction force, it can be seen undesired peaks during the trajectory, which are present when the machine reaches zero velocity (2.5, 7.5 and 12.5 s) and for high velocities (5 and 10 s). In Appendix A.2, Table 14 shows that the maximum error has reduced significantly, around 73 %, for both the new MRAC and the DFMRAC with respect to the old MRAC. In addition, Table 15 shows that the RMSE has reduced approximately 87 % for the new MRAC and 85 % for the DFMRAC with respect to the old MRAC.

Test for $A_{\sin} = 4$ mm:

The output response is shown in Figure 64 in Appendix A.3. Figure 35 shows the error comparison between the adaptive controllers. Table 14 and Table 15 show the maximum error and RMSE, respectively. The results remain similar as the previous one. The new controllers have a better performance than the old MRAC. Higher velocities produce higher error (in the old MRAC more than 650 nm, while in the new controllers less than 250 nm). Figure 35 shows that the effect of the increased velocities dominates even the effect of direction change at zero velocity (2.5, 7.5 and 12.5 s).

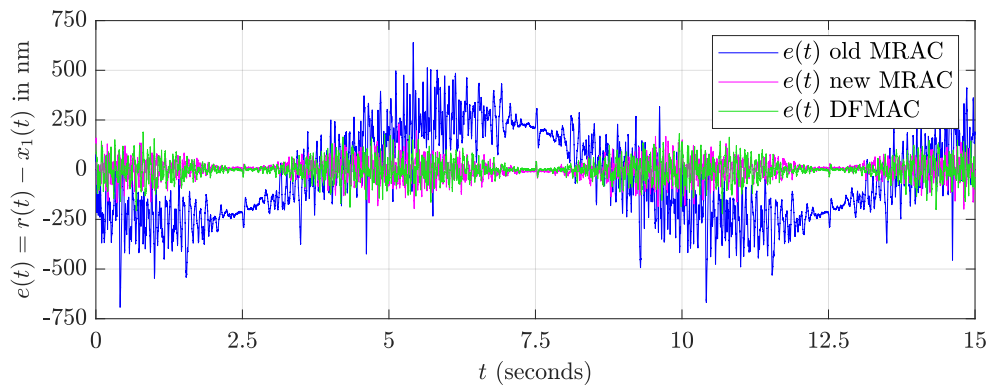


Figure 35: Error comparisons to a $r(t) = 4 \sin(0.2\pi t)$ mm.

5.1.1 Changing sine amplitude test

The results of the previous tests show that increasing the amplitude of the sine reference causes an increase in the maximum error and RMSE. To visualize these increases, a test with different sine reference amplitudes but with a fixed frequency of 0.2 Hz is developed. The application of a standard PI-SFC algorithm is also included in the test. Figure 36 shows the different sine references with a changing amplitude from 50 nm to 5 mm.

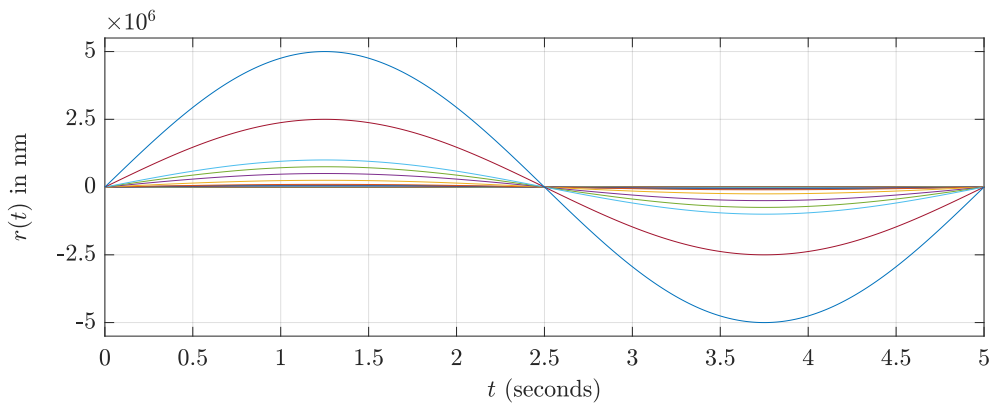


Figure 36: Sine references with different amplitudes from 50 nm to 5 mm with a fixed frequency of 0.2 Hz.

Figure 37 shows the maximum error for the PI-SFC, and the old and new adaptive controllers. Especially for larger amplitudes, the new controllers improve the control performance significantly.

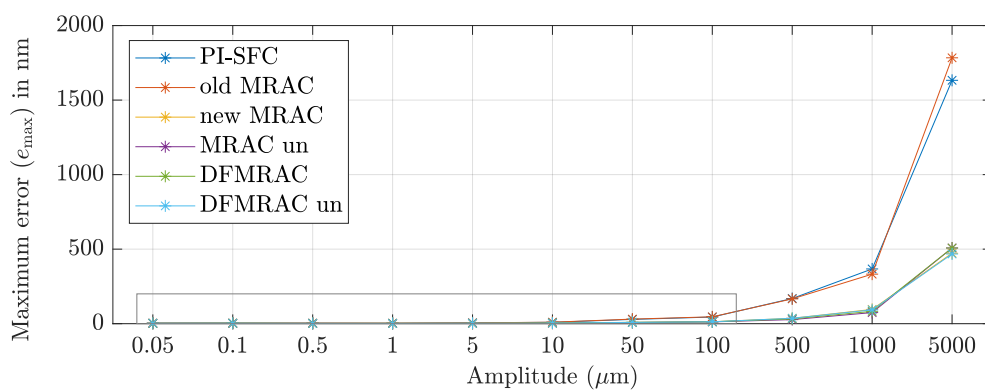


Figure 37: Maximum error of the sine reference test with different amplitudes and a fixed frequency of 0.2 Hz.

Regarding smaller amplitudes (up to $1 \mu\text{m}$), the results remain similar as illustrated in Figure 38, which is the zoomed version of Figure 37.

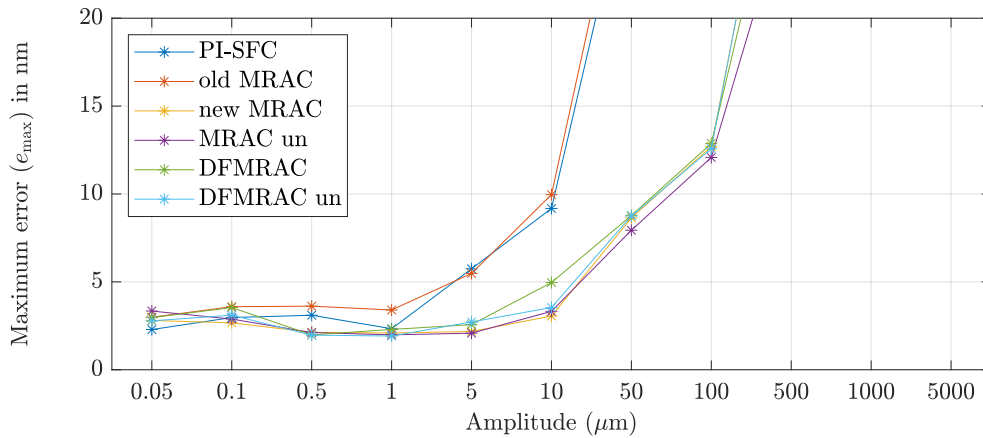


Figure 38: Maximum error of the sine reference test with different amplitudes and a fixed frequency of 0.2 Hz (zoomed version).

Table 4 shows the maximum error values of Figure 37. The best results are highlighted in green and the worst in red for each amplitude tested. The new adaptive controller has approximately 70 % less maximum error than the PI-SFC or the old MRAC over a $100 \mu\text{m}$ sine amplitude.

Table 4: Maximum error values in nm of the changing sine amplitude test.

Amp. (μm)	PI-SFC	old MRAC	new MRAC	MRAC un	DFMRAC	DFMRAC un
0.05	2.29	2.99	2.80	3.34	2.97	2.78
0.1	2.97	3.59	2.67	2.88	3.54	3.11
0.5	3.10	3.62	2.13	2.12	1.98	1.97
1	2.33	3.40	2.09	1.98	2.29	1.92
5	5.74	5.48	2.18	2.08	2.57	2.72
10	9.18	9.96	3.06	3.32	4.96	3.54
50	28.69	30.69	8.64	7.94	8.78	8.75
100	44.59	46.07	12.70	12.08	12.88	12.58
500	168.85	166.30	36.04	27.34	32.07	36.38
1000	367.23	332.33	95.79	74.42	82.75	92.77
5000	1632.70	1783.70	472.54	508.00	507.48	467.52

Figure 39 shows the RMSE of the results. Same as before, there is an improvement for larger amplitudes (greater than $1 \mu\text{m}$) and remain similar for lower amplitudes (equal or lower than $1 \mu\text{m}$), see zoomed part.

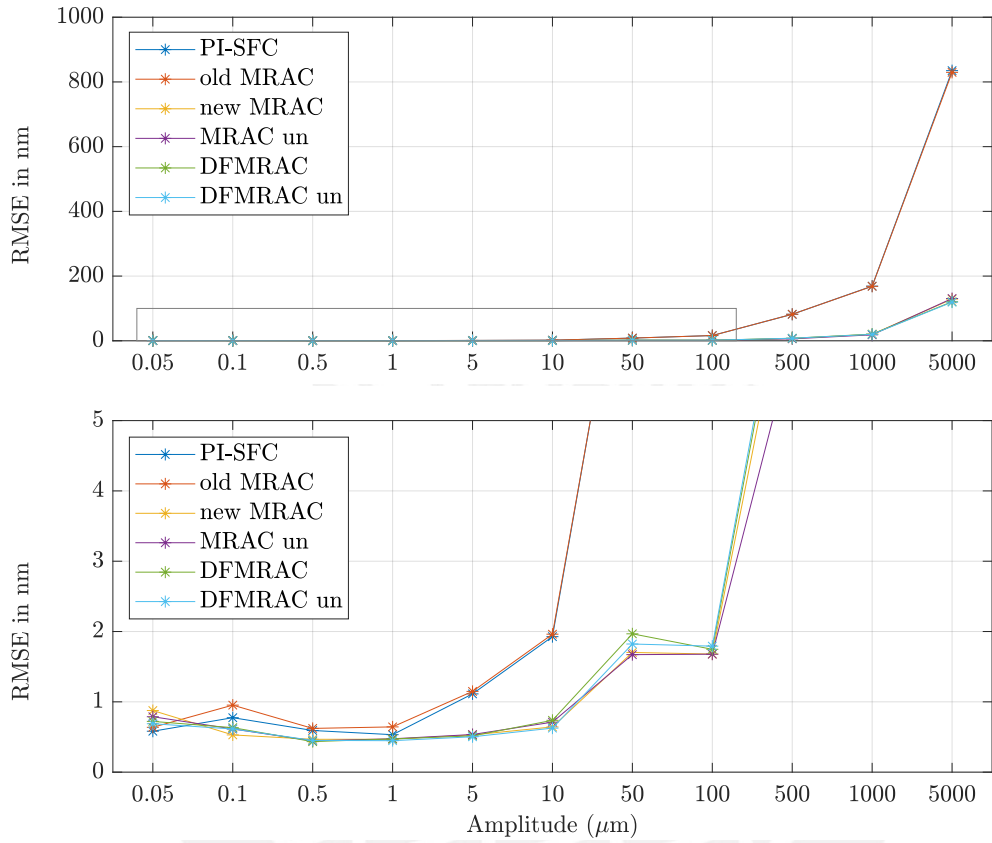


Figure 39: RMSE of the sine reference test with different amplitudes and a fixed frequency of 0.2 Hz.

Table 5 shows the RMSE values regarding Figure 39. Over 100 μm sine amplitude, the RMSE of the new adaptive controllers has been reduced by about 85% in comparison to the PI-SFC or the old MRAC.

Table 5: RMSE values in nm of the changing sine amplitude test.

Amp. (μm)	PI-SFC	old MRAC	new MRAC	MRAC un	DFMRAC	DFMRAC un
0.05	0.58	0.64	0.88	0.79	0.72	0.69
0.1	0.77	0.95	0.53	0.61	0.63	0.61
0.5	0.59	0.62	0.47	0.44	0.43	0.45
1	0.53	0.64	0.47	0.47	0.47	0.45
5	1.11	1.15	0.53	0.54	0.52	0.50
10	1.93	1.96	0.64	0.71	0.74	0.63
50	8.40	8.37	1.70	1.67	1.97	1.82
100	16.23	16.23	1.68	1.68	1.75	1.79
500	81.89	82.05	7.39	6.09	7.79	7.95
1000	168.93	168.40	20.00	18.46	20.64	19.95
5000	834.96	829.61	128.99	130.71	120.80	119.47

It is important to remark that there are no significant differences between the MRAC, DFMRAC, “MRAC un” and “DFMRAC un” for this sine reference test.

This part of the evaluation considers the results obtain by the last sine reference at 5 mm amplitude of the test. In Appendix A.3, Figure 65 shows the error $e(t) = r(t) - x_1(t)$, in which it can be seen that the new adaptive controllers in fact achieve better results. Furthermore, Figure 40 shows the output of each controller, $u(t)$. Despite noticing significant differences in performance with respect to the old controllers, it seems that the control output is quite similar between all of them, see the zoomed version. However, it is important to remark that small changes in the control output can make a significant impact to a high-precision machine.

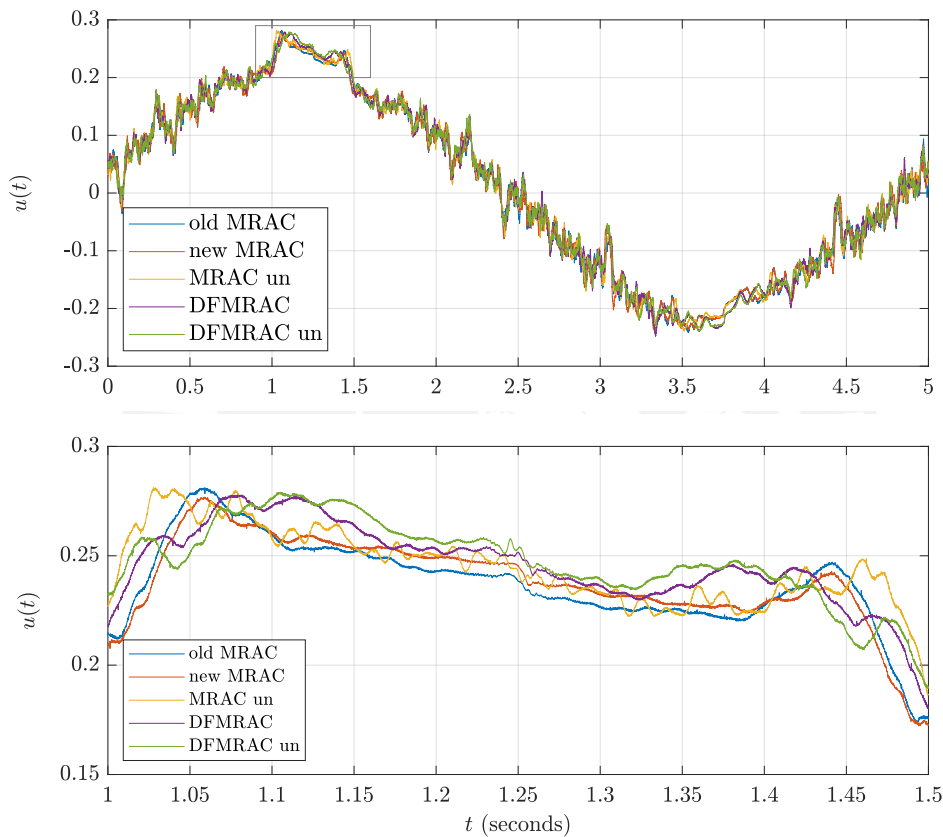


Figure 40: Control output comparison regarding the changing sine amplitude test with a 5 mm amplitude and a 0.2 Hz frequency.

Figure 41 shows the nominal $u_n(t)$, adaptive $u_{ad}(t)$ and DOB-based $u_{dob}(t)$ control output comparisons for the different applied controllers. It can be observed that the MRAC and “MRAC un” react differently with a higher participation in the adaptive control part but also changing the nominal control value. The old MRAC, DFMRAC and “DFMRAC un” seem to be inactive but they are not. Their value is small compared to the nominal or DOB-based controllers. In Appendix A.2, Figure 66 shows the zoomed version of them.

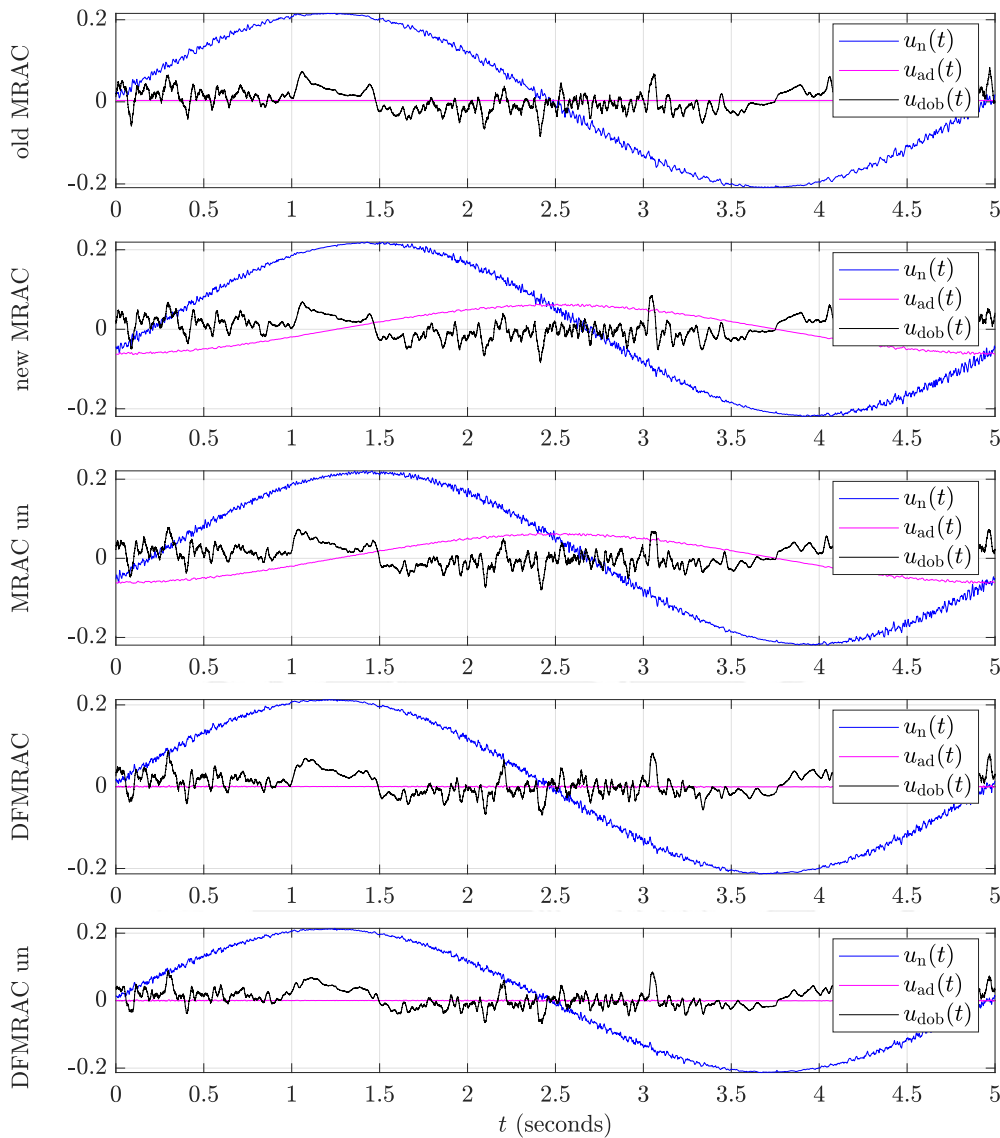


Figure 41: Nominal, adaptive and DOB-based control output comparisons regarding the changing sine amplitude test with a 5 mm amplitude and a 0.2 Hz frequency.

Now the terms that compose the adaptive control are analyzed. The adaptive control was previously defined as $u_{ad}(t) = \hat{\mathbf{W}}^T(t)\beta(\cdot)$. Therefore, depending on the dimensions of the matrices $\hat{\mathbf{W}}(t)$ and $\beta(\cdot)$, the matrix multiplication looks like this:

$$u_{ad}(t) = u_{ad,1}(t) + u_{ad,2}(t) + u_{ad,3}(t) + \dots, \quad (186)$$

where $u_{ad,1}(t) = \hat{\mathbf{W}}_1(t)\beta_1(\cdot)$, $u_{ad,2}(t) = \hat{\mathbf{W}}_2(t)\beta_2(\cdot)$, $u_{ad,3}(t) = \hat{\mathbf{W}}_3(t)\beta_3(\cdot)$ and so forth. In Appendix A.2, figures 67, 68, 69, 70 shows each term of the output adaptive control of the old MRAC, new MRAC, “MRAC un”, DFMRAC, respectively. Figures 71 and 72 shows the eleven terms regarding the “DFMRAC un”.

It can be seen in the past mentioned figures that the adaptive control terms $u_{ad,1}(t)$ and $u_{ad,2}(t)$ for the new adaptive proposals have a low value (approximately 10^9 or less) with respect to the other adaptive control terms, which raises the question of whether these terms can be deleted from the controller. Figure 42 shows that despite the fact of not using the total adaptive control terms the performance of the new controllers is not affected.

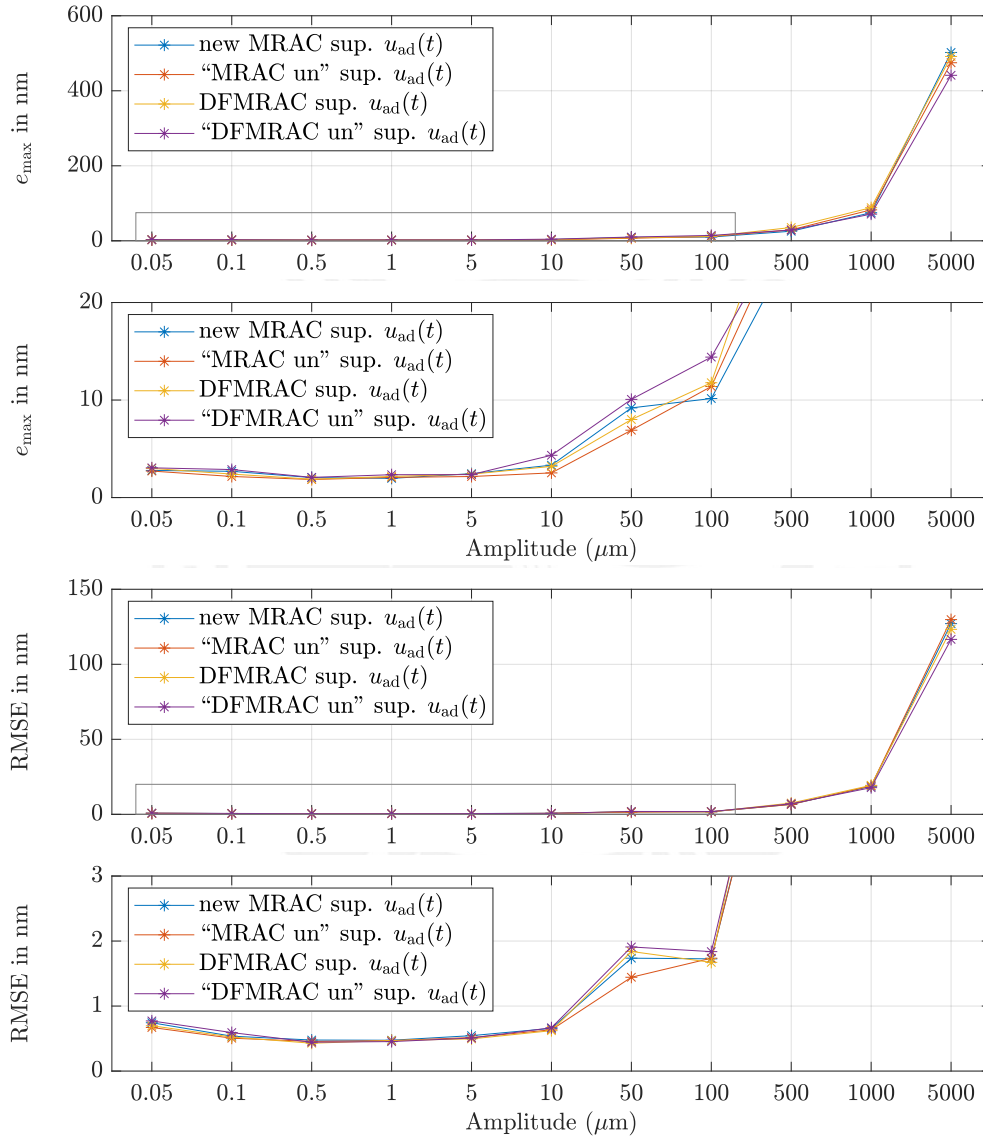


Figure 42: Maximum error and RMSE comparison for the reduced adaptive controllers regarding the changing sine amplitude test with a 5 mm amplitude and a 0.2 Hz frequency.

5.1.2 Changing sine frequency test

Increasing the frequency of the sine reference will also affect the performance of the controllers because the system will move with a higher velocity and, additionally, the directional changes will be more abrupt. In this first part of the experiment, the amplitude of the reference is set at 100 nm and the sine frequency will increase. Later on, the amplitude will be set at 1 mm. Figure 43 shows the maximum error results for a sine reference with different frequencies and 100 nm amplitude. It can be seen that for a frequency lower than 0.5 Hz the maximum error is similar for all controllers. However, from a frequency of 0.75 Hz the new adaptive controllers have a lower error.

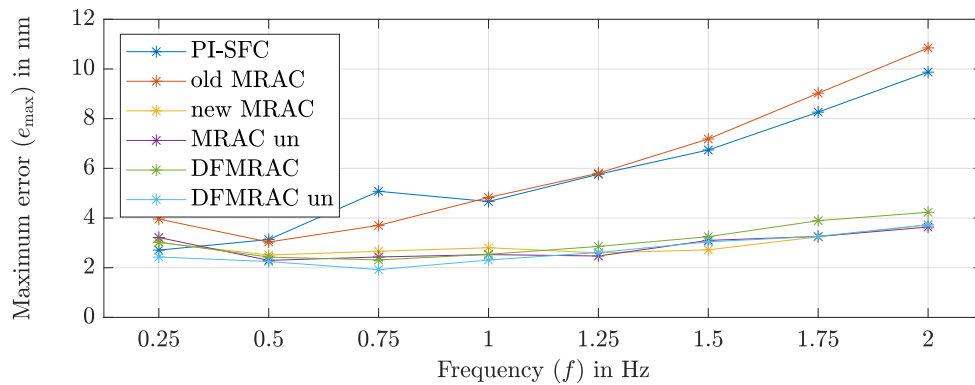


Figure 43: Maximum error of the sine reference test with different frequencies and a fixed 100 nm amplitude.

Table 6 shows the maximum error values regarding Figure 43. Same as before, the best results are highlighted in green and the worst in red for each of the frequencies tested. Considering a 2 Hz frequency for the sine reference, the maximum error for the new controllers remains below 4.5 nm, whereas for the PI-SFC and MRAC around 10 nm. The new adaptive controllers have similar results.

Table 6: Maximum error values of the sine reference test with different frequencies and a fixed 100 nm amplitude.

Freq. (Hz)	PI-SFC	old MRAC	new MRAC	MRAC un	DFMRAC	DFMRAC un
0.25	2.708	3.959	3.013	3.216	3.029	2.430
0.5	3.133	3.035	2.511	2.296	2.428	2.249
0.75	5.077	3.703	2.662	2.432	2.313	1.924
1	4.664	4.828	2.804	2.528	2.540	2.310
1.25	5.760	5.804	2.596	2.472	2.857	2.613
1.5	6.738	7.183	2.720	3.100	3.249	3.043
1.75	8.263	9.024	3.245	3.259	3.894	3.263
2	9.873	10.848	3.719	3.637	4.231	3.732

Figure 44 shows the RMSE values for this experiment. As expected, for higher frequencies the RMSE is higher. Similarly, up to a frequency of 0.5 Hz the RMSE is similar for all controllers and from a frequency of 0.75 Hz the performance is better for the new adaptive controllers.

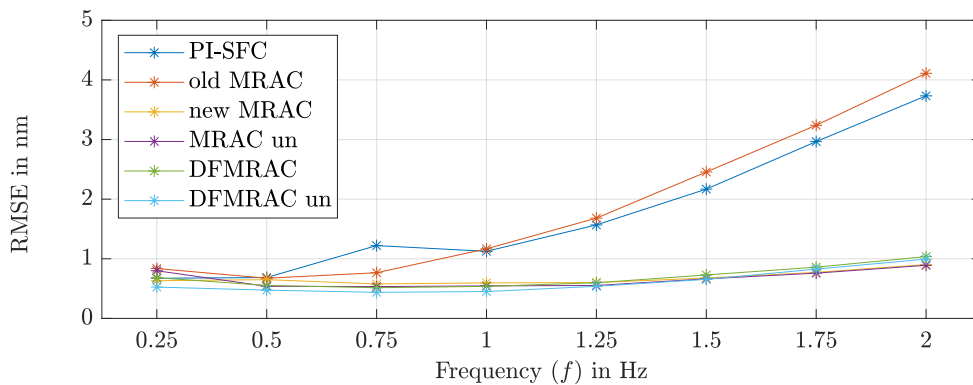


Figure 44: RMSE of the sine reference test with different frequencies and a fixed 100 nm amplitude.

Table 7 shows the RMSE values regarding Figure 44. Considering a 2 Hz frequency for the sine reference, the new adaptive controllers have a RMSE of approximately 1 nm, while the previous implemented controllers around 4 nm.

Table 7: RMSE values of the sine reference test with different frequencies and a fixed 100 nm amplitude.

Freq. (Hz)	PI-SFC	old MRAC	new MRAC	MRAC un	DFMRAC	DFMRAC un
0.25	0.67	0.84	0.63	0.80	0.68	0.53
0.5	0.69	0.67	0.65	0.54	0.55	0.47
0.75	1.22	0.77	0.58	0.53	0.51	0.44
1	1.13	1.17	0.60	0.55	0.54	0.45
1.25	1.57	1.68	0.60	0.55	0.60	0.54
1.5	2.17	2.46	0.68	0.66	0.73	0.65
1.75	2.97	3.24	0.77	0.76	0.86	0.83
2	3.73	4.11	0.90	0.89	1.04	1.00

A similar test of changing frequencies is developed with a higher amplitude of 1 mm. This test combines both scenarios, higher range of motion and higher velocity. Figure 45 shows the maximum error. The improvement of the results can be easily visualized. In the detail of Figure 45, it can be seen that the DFMRAC leads to a lower maximum error than the MRAC.

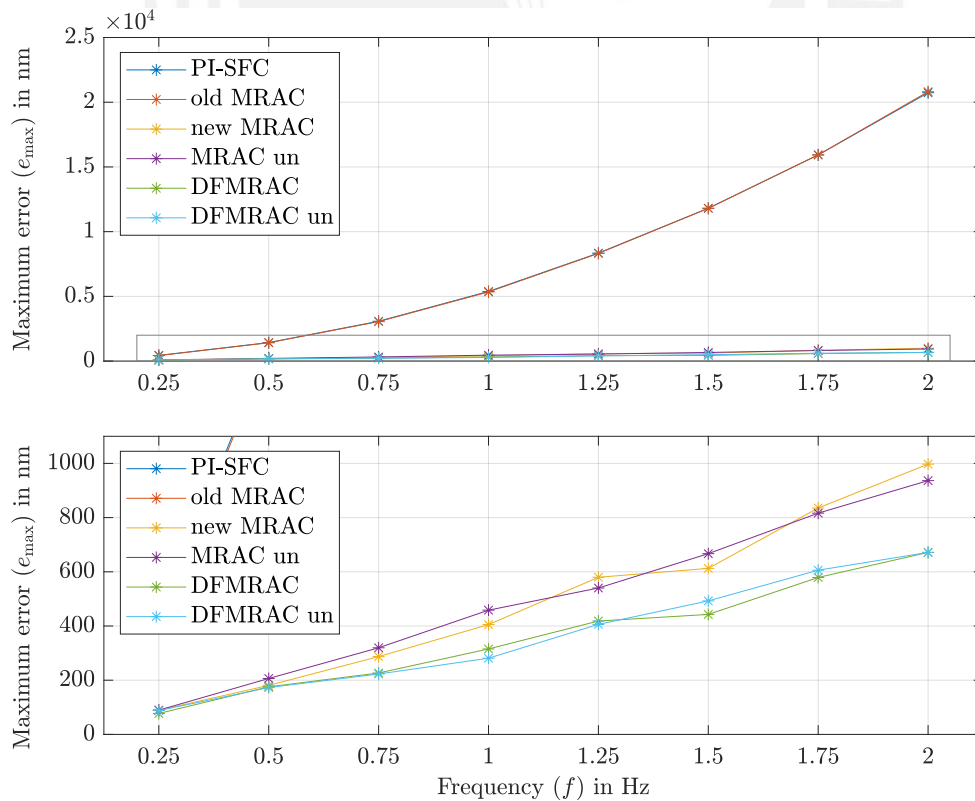


Figure 45: Maximum error of the sine reference test with different frequencies and a fixed 1 mm amplitude.

Table 8 shows the maximum error values regarding Figure 45. For certain frequencies, around a 95 % reduction of the maximum error is achieved by the new controllers compared to the old MRAC. It can be observed, highlighted in green, that the best performance is accomplished by the DFMRAC and “DFMRAC un”.

Table 8: Maximum error values of the sine reference test with different frequencies and a fixed 1 mm amplitude.

Freq. (Hz)	PI-SFC	old MRAC	new MRAC	MRAC un	DFMRAC	DFMRAC un
0.25	438.50	425.96	89.23	89.54	77.14	87.86
0.5	1429.55	1416.05	180.88	206.37	175.51	172.92
0.75	3076.52	3049.42	287.17	319.62	226.64	222.86
1	5379.28	5341.98	405.23	458.41	315.33	281.18
1.25	8342.09	8318.76	579.81	540.16	418.41	406.01
1.5	11806.81	11803.61	612.64	666.92	442.69	492.61
1.75	15927.41	15933.93	835.51	816.41	579.13	605.89
2	20733.23	20812.88	997.19	936.40	671.61	671.64

Figure 46 shows the RMSE results. The better performance is reached by the new adaptive controllers.

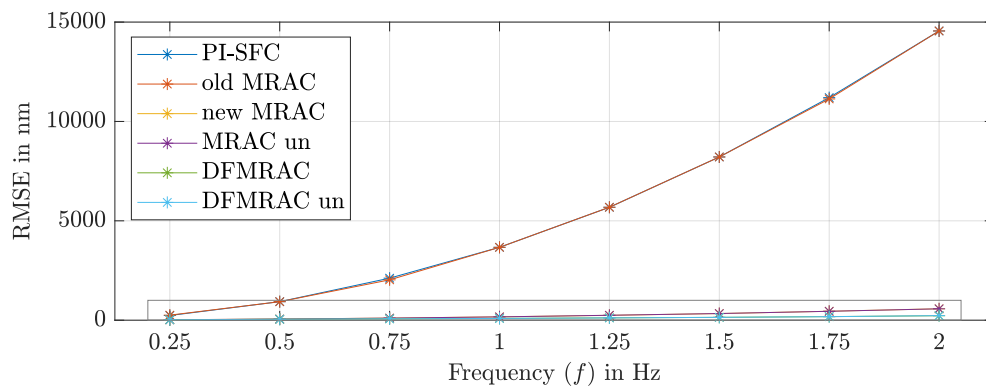


Figure 46: RMSE of the sine reference test with different frequencies and a fixed 1 mm amplitude.

Figure 47 shows the zoomed version of the previous picture. It can be observed that the DFMRAC and “DFMRAC un” obtain a lower RMSE than the MRAC and “MRAC un”.

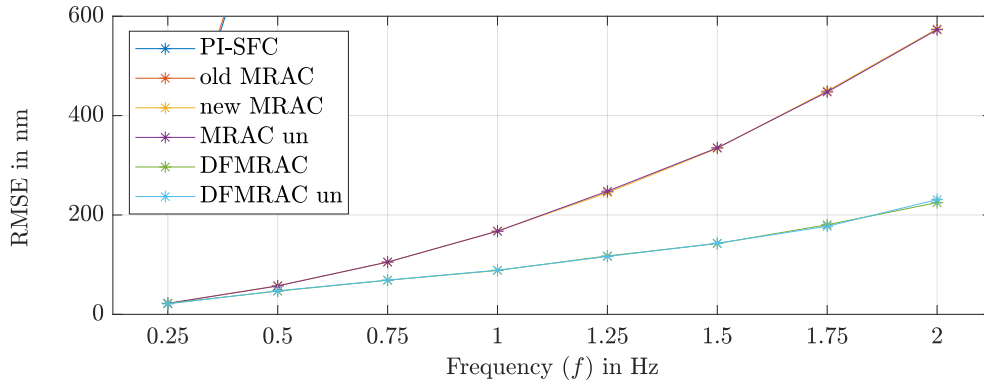


Figure 47: RMSE of the sine reference test with different frequencies and a fixed 1 mm amplitude (zoomed version).

Table 9 shows the values related to Figure 46. Approximately a 95 % reduction in RMSE compared to the old MRAC is accomplished. It is possible to observe a 98 % reduction for certain cases.

Table 9: RMSE values of the sine reference test with different frequencies and a fixed 1 mm amplitude.

Freq. (Hz)	PI-SFC	old MRAC	new MRAC	MRAC un	DFMRAC	DFMRAC un
0.5	931.85	931.47	57.67	57.16	46.75	47.39
0.25	236.23	253.62	21.74	22.21	22.06	21.11
0.75	2114.25	2030.21	105.01	105.32	68.64	68.88
1	3666.66	3666.56	167.68	167.31	88.35	88.92
1.25	5681.70	5683.03	244.84	247.83	117.59	116.45
1.5	8212.65	8212.81	334.07	335.17	142.47	143.20
1.75	11199.14	11133.06	449.70	447.56	180.38	177.22
2	14552.74	14553.96	574.45	572.89	224.91	230.78

It is important to point out in this experiment that the DFMRAC and “DFMRAC un” for the first time achieved noticeably better performance in terms of maximum error (30 % less) and RMSE (60 % less) than the new MRAC and “MRAC un”.

5.2 Step reference tests

This section presents the results of the tests performed on the NPMDM considering a step reference. The step reference trajectory has a smooth behaviour between the stationary points (initial and desired height). The transition time of the step can be change by increasing or decreasing the maximum velocity. For the first experiments, the maximum velocity is set at 1 mm/s and the step heights will be 10 μm and then 1 mm. Secondly, a multi-step test is included. Finally, the velocity will change from 1 mm/s to 5 mm/s for a fixed height of 10 mm to evaluate the performance of the controllers.

Test for a double step of 10 μm :

The reference is a double step of 10 μm and it starts from the absolute zero position. Since the difference between the output response when applying the different controllers is not visually perceptible, only the one corresponding to the DFMRAC is shown. Figure 48 shows the output response with the DFMRAC, in which the controller successfully follows the desired trajectory.

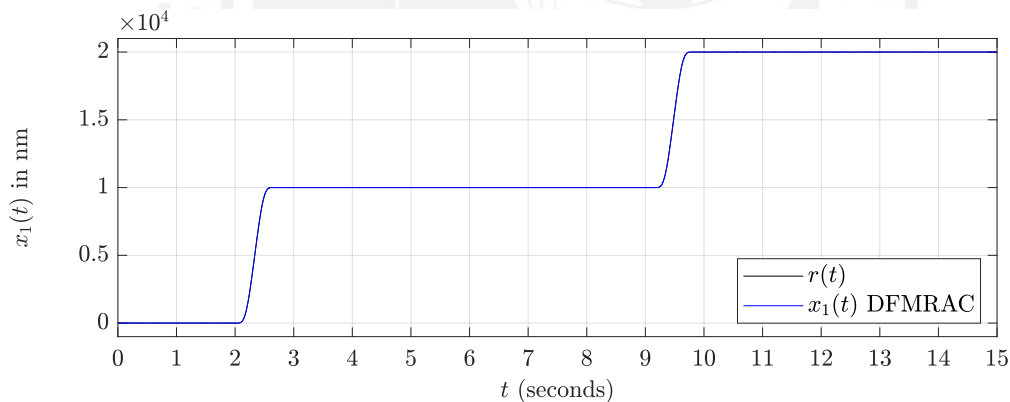


Figure 48: Output response to a 10 μm step height reference with DFMRAC.

Even though the maximum velocity is set at 1 mm/s, it can be seen in Figure 79 in Appendix A.3 that the maximum reached velocity is less than 0.05 mm/s. The reason is that the machine needs a larger step height to reach that velocity. Figure 49 shows the error comparison when applying the old MRAC, new MRAC and DFMRAC. It can be seen that the error peaks have been reduced by the new controller proposals and there is a clear improvement.

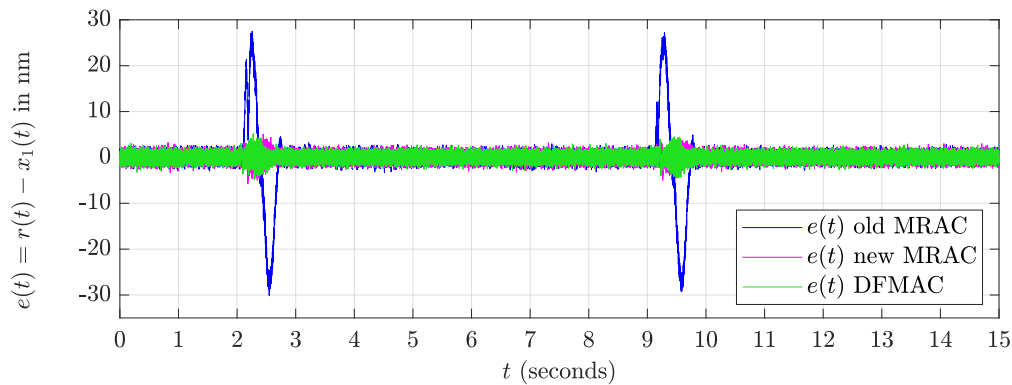


Figure 49: Error, $e(t) = r(t) - x_1(t)$, regarding a $10 \mu\text{m}$ step height reference.

In Appendix A.3, Table 16 shows the maximum error of the test, which is approximately 5 nm for the new controllers and 30 nm for the old MRAC. Furthermore, Table 17 shows that the RMSE remains below 1 nm for the new controllers and around 5 nm for the old MRAC.

Test for a double step of 1 mm:

The output response to a double step of 1 mm reference can be seen in Appendix A.3 in Figure 78. In addition, Figure 80 shows that the maximum reached velocity is below 0.75 mm/s. The maximum velocity of 1 mm/s still needs a larger height to be reached. Figure 50 shows the comparison of the error. In this test, it can be seen a remarkable improvement between the new MRAC and DFMRAC with respect to the old MRAC. The friction force has a higher impact on a larger range of motion, as the range of elastic deformation is limited. Therefore, because the old MRAC does not consider the dry friction, the output have undesired error peaks of more than 150 nm. In Appendix A.3, Table 16 shows the maximum error of the test, which remains below 50 nm for the new adaptive controllers and around 200 nm for the MRAC. Table 17 shows that the RMSE for the old MRAC is approximately 50 nm and for the new proposals is below 5 nm.

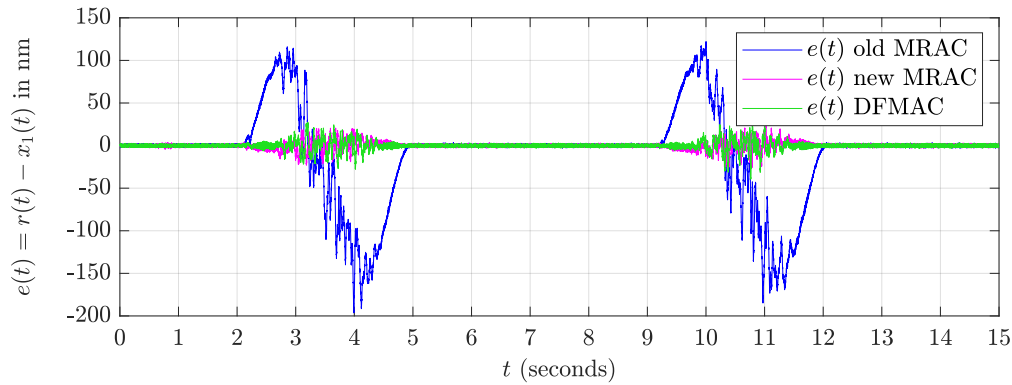


Figure 50: Error, $e(t) = r(t) - x_1(t)$, regarding a 1 mm step height reference.

5.2.1 Multi-step test

The reference trajectory combining different step positions is shown in Figure 51. The multi-step test helps to visualize the behaviour of the machine in negative positions and when starting at a position different to zero.

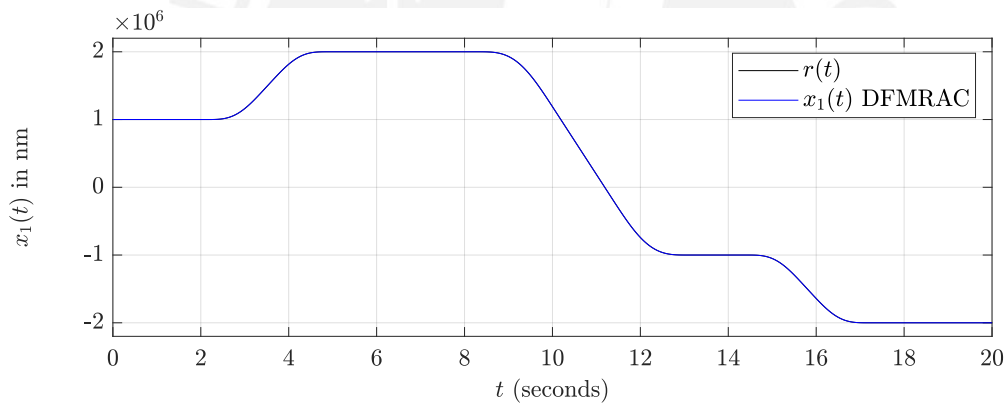


Figure 51: Output response to a multi-step reference with DFMRAC.

In Appendix A.3, Figure 81 shows that the maximum velocity of 1 mm/s was reached at approximately 10s and remains constant until 11.5s in this test. A height of 3 mm was needed to see this behaviour. Figure 52 shows the error when applying the old MRAC, new MRAC and DFMRAC. The results are analogously to the previous ones: the new controllers have a better performance. In Appendix A.3, Table 16 shows that the maximum error for the new adaptive controllers remains under 70 nm, while the old MRAC around 230 nm. Table 17 shows the RMSE, which is also better for the new controllers with less than 10 nm, whereas for the old MRAC is around 65 nm.

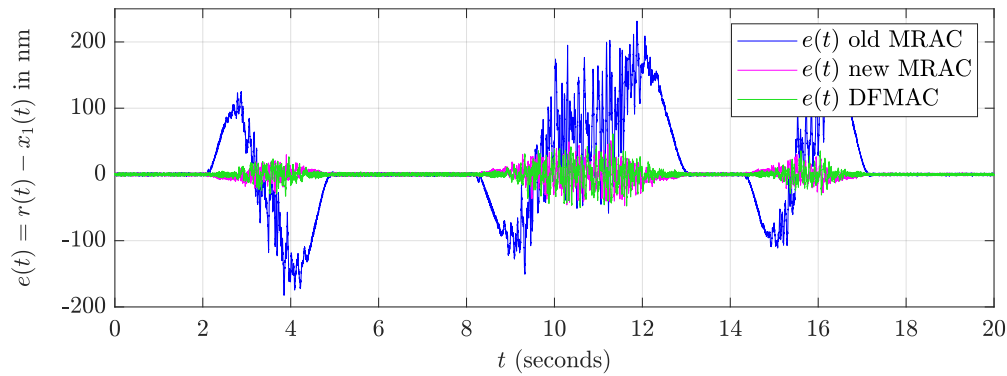


Figure 52: Comparison of the error $e(t) = r(t) - x_1(t)$ of a multi-step reference in the NPMDM.

5.2.2 Changing step maximum velocity test

In the past tests, it can be seen that a higher velocity has an impact on the performance of the controllers. In that sense, the aim of this test is to visualize the maximum error and the RMSE of a step reference with the same height of 10 mm, but decreasing its transition time and therefore increasing its maximum velocity reached. Figure 53 shows the different step references with different transition times (maximum reached velocities) that will be taken part of the test.

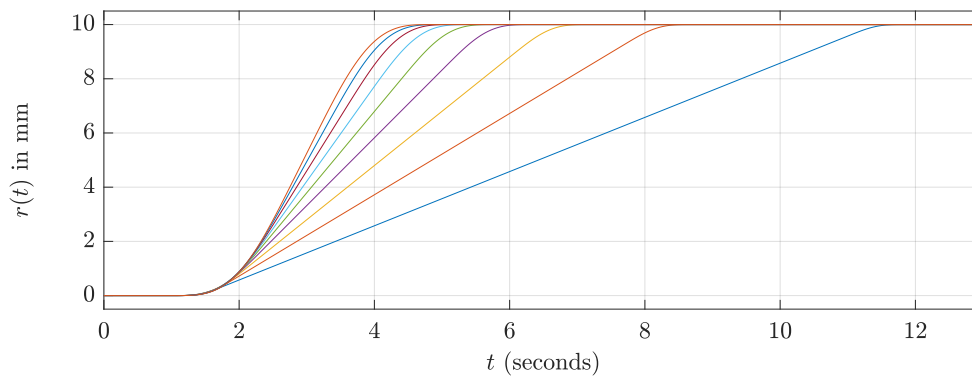


Figure 53: Step references with a fixed height of 10 mm and different transition times.

Figure 54 shows the maximum velocities reached corresponding to each transition time given in Figure 53. In both figures the same colors are used for the plots. All the maximum velocities can be achieved by a step height of 10 mm.

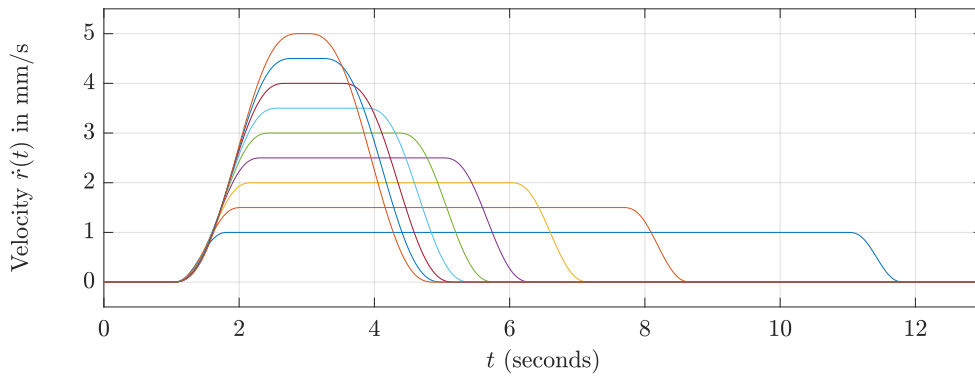


Figure 54: Different velocities plot for a 10 mm step height.

Figure 55 shows the maximum error and RMSE. Similar as before, the new adaptive controllers achieve better results. In Appendix A.3, Table 18 and Table 19 show the numeric values from the graphs. The maximum error was reduced by approximately 60 % and the RMSE by 75 % in comparison to the old controllers.

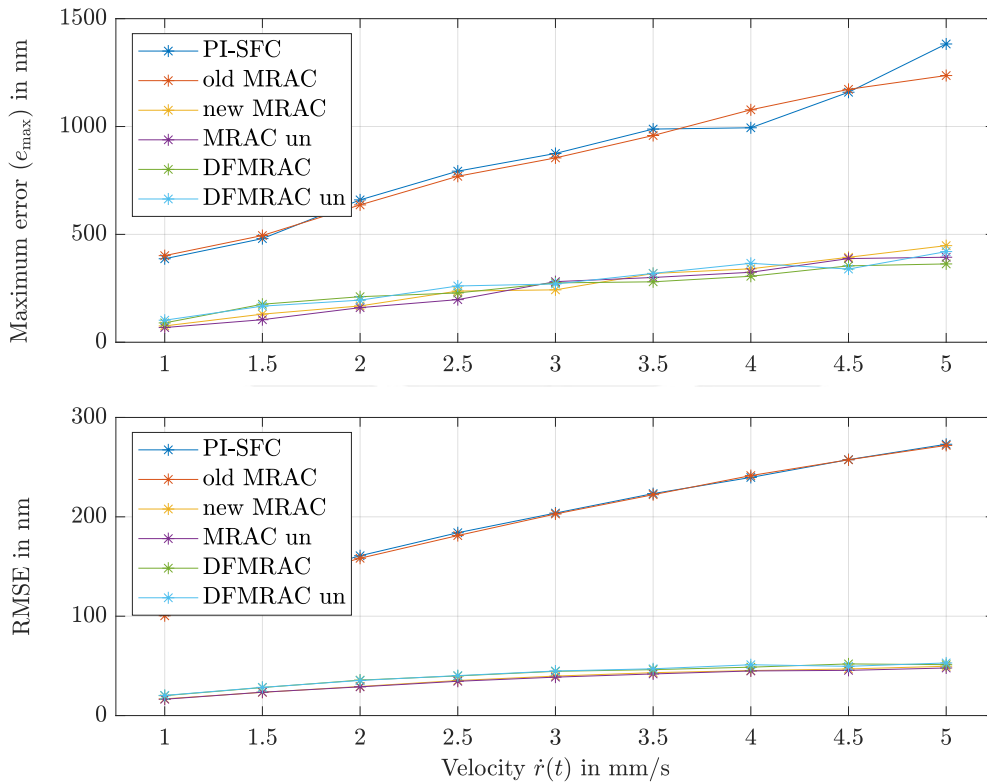


Figure 55: Maximum error and RMSE regarding a step reference at different velocities.

Then, the control output is analyzed only for the last test at 5 mm/s velocity. Figure 56 shows the nominal, adaptive and DOB-based control output comparison of the new MRAC and DFMRAC algorithms. Similar as before, for the MRAC the adaptive control part has a higher influence in the total control output, while for the DFMRAC it does not. In Appendix A.2, figures 73, 74, 75 shows the corresponding adaptive control terms ($u_{\text{uad},1}(t)$, $u_{\text{uad},2}(t)$, ...) of the old MRAC, new MRAC and DFMRAC, respectively. Figures 76 and 77 shows the eleven adaptive control terms corresponding to the “DFMRAC un”.

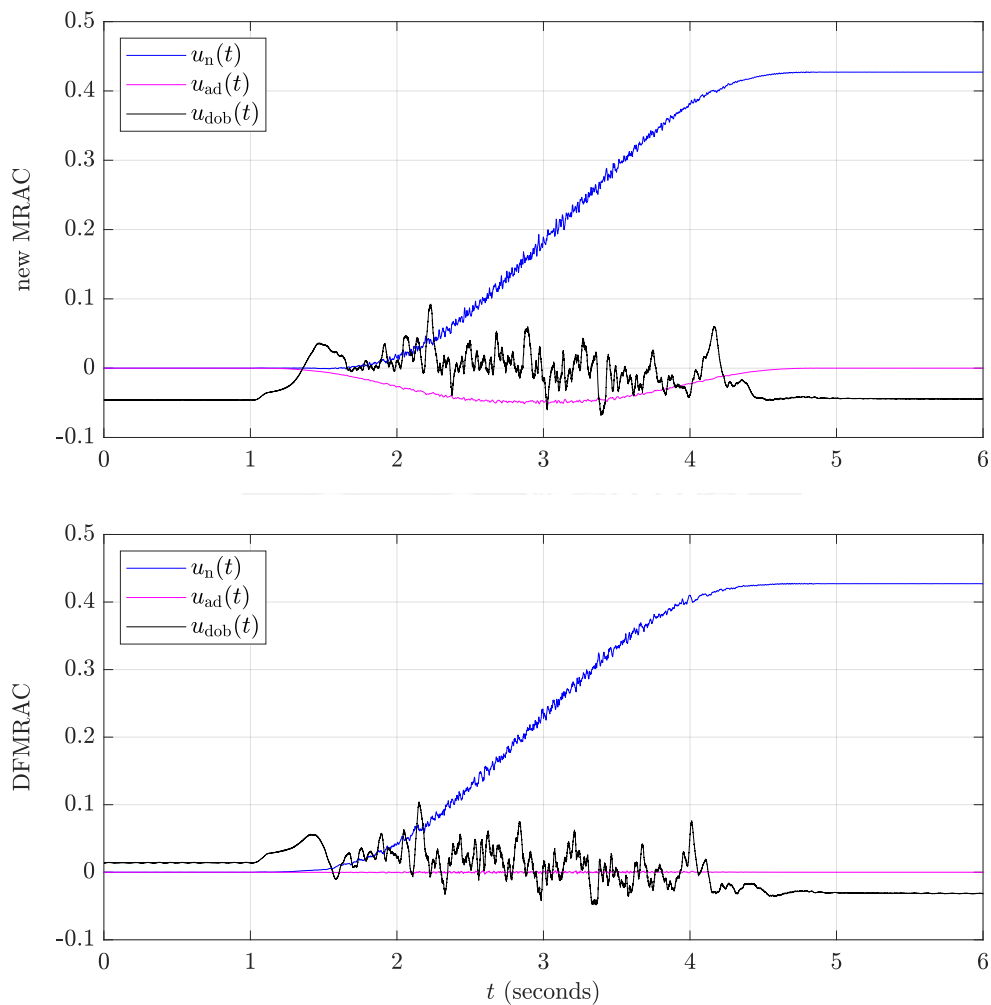


Figure 56: Nominal, adaptive and DOB-based control output comparison of the new MRAC and DFMRAC regarding the changing step maximum velocity test at 5 mm/s velocity.

Similar to Subsection 5.1.1, the adaptive control terms $u_{ad,1}(t)$ and $u_{ad,2}(t)$ for the new adaptive proposals have a low value (approximately 10^9 or less) with respect to the other adaptive control terms. Therefore, these terms are suppressed from the controller. Figure 57 shows that despite the fact of not using the total adaptive control terms the performance of the controllers is not affected.

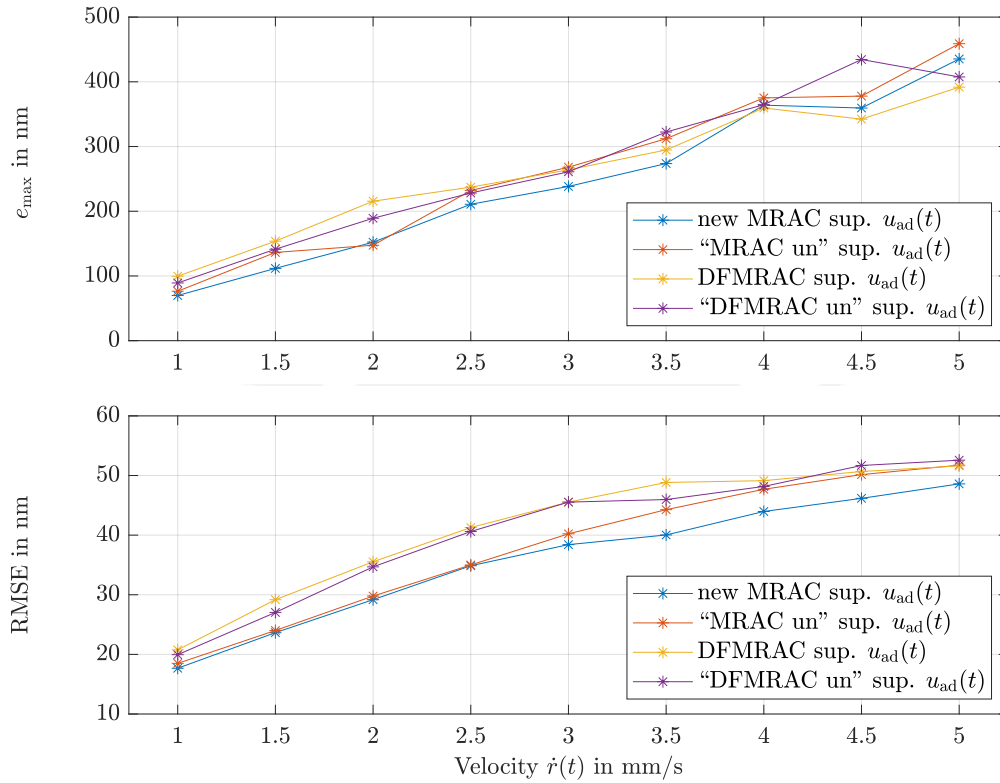


Figure 57: Maximum error and RMSE comparison for the reduced adaptive controllers regarding the changing step maximum velocity test at 5 mm/s velocity.

5.3 Execution time test

This test evaluates the execution time for the implemented controllers. Figure 58 shows the execution time for a sine reference test with a 100 nm fixed amplitude and different frequencies. It can be seen that the new adaptive controllers need slightly more time for execution, around $1 \mu\text{s}$ more. The reason for this is that the weight matrix, \mathbf{W}_s , in the new adaptive controllers has increased (previously it was of order 3×1 and now of order 5×1), which leads to an increase in computational demand. In addition, β_s has nonlinearities in $\beta_{s,4}$ and $\beta_{s,5}$, see Equation (46) and Equation (47), respectively. These terms are more difficult to operate and therefore also increase the computational cost. However, this is not critical for the system.

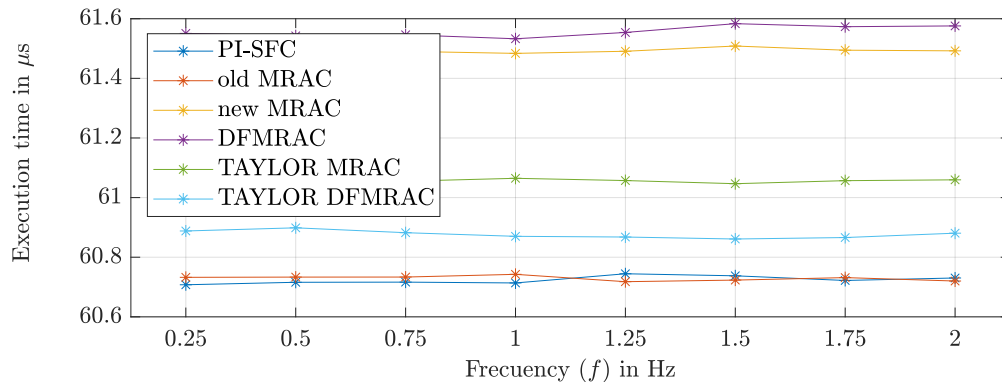


Figure 58: Execution time when applying different controllers.

The “Taylor MRAC” and “Taylor DFMRAC” is a simplified way to estimate the friction terms by employing a Taylor approximation of order 2. The extended vector of known system parameters for the Taylor approximation is shown in Equation (187). Note that extending one row in β_{taylor} will increase the dimensions of the gain matrices for the adaptive controllers. However, the operations are now simpler than before and the execution time only increases by $0.5 \mu\text{s}$.

$$\beta_{\text{taylor}}(x) = \begin{bmatrix} x_1 \\ x_2 \\ 1 \\ x_1^2 \\ x_2^2 \\ x_1 x_2 \end{bmatrix} \quad (187)$$

6 Conclusions and Outlook

The main objective of this master thesis is the implementation of a derivative-free adaptive control algorithm for the vertical axis of the nanopositioning and nanomeasuring demonstration machine. In this sense, the main objective is achieved because it is implemented a DFMRAC algorithm in real time in the experimental setup, which is developed theoretically in Chapter 3 and the experimental tests are shown in Chapter 5. Both adaptive algorithms, DFMRAC and MRAC, have been investigated with their respective extensions regarding the unknown input matrix case in Section 3.3 and Section 2.3, respectively. In Chapter 5, it can be found their implementation results.

The review in Section 1.4 of the principles of operation, sensors, actuators and control algorithms already implemented in the NPMDM provides insight into the characteristics of the new controllers to be implemented. For example, the control output signal in the simulations is saturated between -0.4 and 0.75 and the sample time for the Simulink blocks code is set at 0.0001 s. The simulation of the adaptive controllers in Matlab in Chapter 4 allows testing different controller gains to find the most suitable ones before applying the algorithms to the real system.

The results of the new implementations are compared with the old MRAC and a standard PI-SFC in Chapter 5. For that purpose, sine and step references are considered for the experiments. Referring to the sine reference tests in Subsection 5.1.1, when considering a fixed sine frequency of 0.2 Hz and an increasing amplitude greater than 100 μm , approximately 70% less maximum error is achieved by the new adaptive controllers in comparison to the old MRAC or the PI-SFC. For this experiment, the RMSE is reduced by 85% . With respect to the changing frequency sine test in Subsection 5.1.2 at a fixed 1 mm amplitude, a reduction of around 95% for both, maximum error and RMSE, is achieved. Concerning the step reference experiments, firstly a multi-step reference is tested in Subsection 5.2.1, in which the first step starts at 1 mm position (not at absolute zero) and also negative positions are reached, see Figure 51. The controllers are able to follow the desired reference and the best performance is again achieved by the new adaptive controllers, see Figure 52. In addition, in Subsection 5.2.2 a reference test changing its transition time, which indirectly increases the reached maximum velocity, is performed. When considering a fixed step height of 10 mm and velocities up to 5 mm/s, the maximum error is reduced by 60% and the RMSE by 75% . In conclusion, the addition of

the friction term in the adaptive control algorithms improves the performance of the NPMDM. Regarding all the experiments, there are no remarkable differences between the performance of the new MRAC, DFMRAC and their extensions to the unknown input matrix. This is because during the experiments and in general a high precision machine should not undergo drastic changes in its physical structure. It is also proved in simulations and experiments that the DFMRAC do not have the drifting parameters problem (see Figure 32) as the MRAC does (see Figure 31) because the estimated weight parameters $\hat{\mathbf{W}}_s(t)$ are UUB. Therefore, the DFMRAC algorithm does not need a projection method for safety purposes. Despite the enlarged weight matrix (\mathbf{W}_s of size 5×1) and additional nonlinear terms in the regressor ($\beta_{s,4}$ and $\beta_{s,5}$) the execution time only increases by $1 \mu s$, see Figure 58. Finally, it can be concluded that the DFMRAC is the controller that shows more advantages as it reaches similar performances without the need of implementing a projection method.

The NPMDM is noisy. The classical DOB, as discussed before, is not capable of removing the sensor noise in the high frequencies. In this sense, further works should consider a simple noise reduction disturbance observer (SNR-DOB), which scheme is shown in Figure 59. According to [10], in the low and high frequency ranges, $Q_n(s) = \frac{2}{\tau s + 2}$ is responsible of rejecting the input disturbance $n(t)$ while $Q_d(s) = \frac{2}{(\tau s + 2)(\tau s + 1)}$ diminishes the input control disturbances $d(t)$. Figure 60 shows the output response and the error, $e(t) = r(t) - x_1(t)$, of a simulation when applying the DFMRAC algorithm with a classical DOB and a SNR-DOB. It can be seen an improvement in the noise and disturbance suppression. The maximum error is 40.24 nm for the DOB and 27.22 nm for the SNR-DOB. The RMSE is 7.33 nm for the DOB and 5.83 nm for the SNR-DOB. Following these first simulation result, an application on the test bench seems promising.

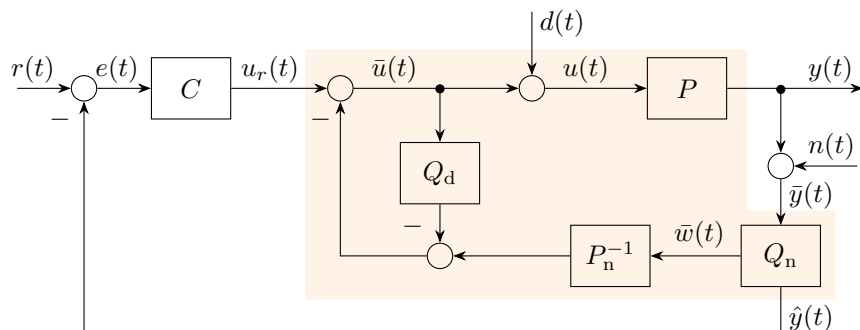


Figure 59: Noise reduction disturbance observer-based controller scheme. Extracted from [10].

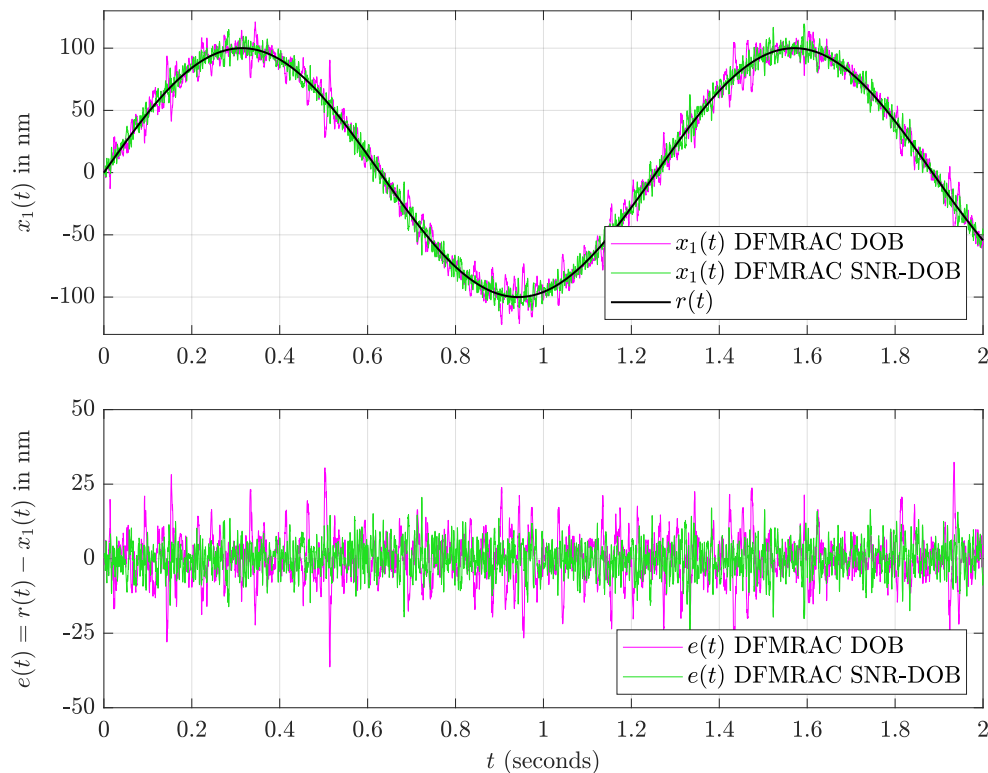


Figure 60: Output response and error, $e(t) = r(t) - x_1(t)$, comparison between DOB and SNR-DOB.

The estimation of the velocity is obtained by the second order linear filter shown in Section 1.4.3. However, this estimator adds noise to the system. For this reason, a better approach is to use the DFMRAC in output-feedback form, for example as proposed in [28]. Regarding [35], output-feedback adaptive controllers are employed when it is impossible to sense the entire state of the process. In contrast to the DFMRAC algorithm developed in this master thesis, the output-feedback form uses an observer instead of the model reference. Furthermore, according to [28], its stability analysis uses a Lyapunov-Krasovskii functional which involves the solution of a parameter dependent Riccati equation, instead of a Lyapunov equation, to show that all the error signals are UUB.

Finally, it is important to recall that two of the friction parameters are roughly estimated: the Stribeck velocity v_s and the Stribeck shape factor δ . Therefore, further works should consider identification techniques to obtain the real parameters of the friction model. It is also important to validate if the Stribeck friction model considered for this system is suitable or not.

Bibliography

- [1] Arvid Amthor. *Modellbasierte Regelung von Nanopositionier-und Nanomessmaschinen*. PhD thesis, Technische Universität Ilmenau, 2010.
- [2] Panos J Antsaklis and Anthony N Michel. *A linear systems primer*. Springer Science & Business Media, 2007.
- [3] Karl J Åström and Björn Wittenmark. *Adaptive control*. Courier Corporation, 2013.
- [4] Jae Sung Bang, Hyungbo Shim, Sang Kyun Park, and Jin Heon Seo. Robust tracking and vibration suppression for a two-inertia system by combining backstepping approach with disturbance observer. *IEEE Transactions on Industrial Electronics*, 57:3197–3206, 2010.
- [5] Wen-Hua Chen, Jun Yang, Lei Guo, and Shihua Li. Disturbance-observer-based control and related methods—an overview. *IEEE Transactions on Industrial Electronics*, 63(2):1083–1095, 2016.
- [6] TH Chiew, Z Jamaludin, AY Bani Hashim, NA Rafan, and Lokman Abdullah. Identification of friction models for precise positioning system in machine tools. *Procedia Engineering*, 53:569–578, 2013.
- [7] Zachary T Dydek, Anuradha M Annaswamy, and Eugene Lavretsky. Adaptive control of quadrotor uavs: A design trade study with flight evaluations. *IEEE Transactions on control systems technology*, 21(4):1400–1406, 2012.
- [8] Zachary T Dydek, Anuradha M Annaswamy, Jean-Jacques E Slotine, and Eugene Lavretsky. High performance adaptive control in the presence of time delays. In *Proceedings of the 2010 American Control Conference*, pages 880–885. IEEE, 2010.
- [9] Zachary T Dydek, Anuradha M Annaswamy, Jean-Jacques E Slotine, and Eugene Lavretsky. Time delay resistant adaptive control of mini-uavs. *IFAC Proceedings Volumes*, 43(2):27–32, 2010.
- [10] Jerome Han, Hongkeun Kim, Youngjun Joo, Nam Hoon Jo, and Jin Heon Seo. A simple noise reduction disturbance observer and q-filter design for internal stability. In *2013 13th International Conference on Control, Automation and Systems (ICCAS 2013)*, pages 755–760. IEEE, 2013.

- [11] IRDS. International roadmap for devices and systems. <https://irds.ieee.org/>, 2022. Accessed: 15-09-2022.
- [12] Rolf Isermann. *Digital control systems*. Springer Science & Business Media, 2013.
- [13] E Jäger, Eberhard Manske, Tino Hausotte, and H-J Büchner. Nanomessmaschine zur abbefehlerfreien koordinatenmessung (nano measuring machine for zero abbe offset coordinate-measuring). *tm-Technisches Messen*, 67(7-8):319–323, 2000.
- [14] Gerd Jäger, Eberhard Manske, Tino Hausotte, Andreas Müller, and Felix Balzer. Nanopositioning and nanomeasuring machine npmm-200—a new powerful tool for large-range micro-and nanotechnology. *Surface Topography: Metrology and Properties*, 4(3):034004, 2016.
- [15] Nam H Jo and Hyungbo Shim. Robust stabilization via disturbance observer with noise reduction. In *2013 European Control Conference (ECC)*, pages 2861–2866. IEEE, 2013.
- [16] Liu Juanxia, Lin Qing, and Liu Juhong. Derivative-free adaptive control of uav in logistics and airdrop. In *2021 China Automation Congress (CAC)*, pages 2549–2554, 2021.
- [17] Howard Kaufman, Itzhak Barkana, and Kenneth Sobel. *Direct adaptive control algorithms: theory and applications*. Springer Science & Business Media, 2012.
- [18] Hassan K Khalil. *Nonlinear control*, volume 406. Pearson New York, 2015.
- [19] Phattaradanai Kiratiwudhikul. Integration und modellbasierte regelung einer vertikalen achse zur dreidimensionalen nanopositionierung. *Fakultät für Informatik und Automatisierung*, 1(1):1–103, 2021.
- [20] Antonio Loría, Elena Panteley, and Mohamed Adlene Maghenem. Strict lyapunov functions for model reference adaptive control: Application to lagrangian systems. *IEEE Transactions on Automatic Control*, 64:3040–3045, 2019.
- [21] Eberhard Manske, Thomas Fröhlich, Roland Füßl, Ingo Ortlepp, Rostyslav Mastylo, Ulrike Blumröder, Denis Dontsov, Michael Kühnel, and Paul Köchert. Progress of nanopositioning and nanomeasuring machines for cross-scale measurement with sub-nanometre precision. *Measurement Science and Technology*, 31(8):085005, 2020.

- [22] Katsuhiko Ogata. *Ingeniería de control moderna*. Pearson Educación, 2003.
- [23] Matko Orsag, Christopher Korpela, Stjepan Bogdan, and Paul Oh. Lyapunov based model reference adaptive control for aerial manipulation. In *2013 International Conference on Unmanned Aircraft Systems (ICUAS)*, pages 966–973, 2013.
- [24] Behzad Sinafar, Amir Rikhtehgar Ghiasi, and Atousa Karimi Fazli. A new model reference adaptive control structure for uncertain switched systems with unmodeled input dynamics. *Transactions of the Institute of Measurement and Control*, 37(10):1171–1180, 2015.
- [25] Vahram Stepanyan and Krishnakumar Kalmanje. Input and output performance of m-mrac in the presence of bounded disturbances. In *AIAA Guidance, Navigation, and Control Conference*, page 7688, 2010.
- [26] James Stewart, Daniel K Clegg, and Saleem Watson. *Calculus: early transcendentals*. Cengage Learning, 2020.
- [27] M. Sunwoo, K.C. Cheok, and N.J. Huang. Model reference adaptive control for vehicle active suspension systems. *IEEE Transactions on Industrial Electronics*, 38(3):217–222, 1991.
- [28] Tansel Yucelen. *Advances in adaptive control theory: Gradient-and derivative-free approaches*. PhD thesis, Georgia Institute of Technology, 2012.
- [29] Tansel Yucelen and Anthony Calise. A kalman filter optimization approach to direct adaptive control. In *AIAA Guidance, Navigation, and Control Conference*, page 5858, 2009.
- [30] Tansel Yucelen, Anthony Calise, Wassim Haddad, and Kostyantyn Volyanskyy. A comparison of a new neuroadaptive controller architecture with the sigma-and e-modification architectures. In *AIAA Guidance, Navigation, and Control Conference*, page 6060, 2009.
- [31] Tansel Yucelen, Anthony Calise, and Nhan Nguyen. Evaluation of derivative-free adaptive controller with optimal control modification. In *AIAA Guidance, Navigation, and Control Conference*, page 6604, 2011.
- [32] Tansel Yucelen and Anthony J. Calise. Kalman filter modification in adaptive control. *Journal of Guidance Control and Dynamics*, 33:426–439, 2010.

- [33] Tansel Yucelen and Anthony J Calise. Derivative-free model reference adaptive control. *Journal of Guidance, Control, and Dynamics*, 34(4):933–950, 2011.
- [34] Tansel Yucelen and Anthony J Calise. Robustness of a derivative-free adaptive control law. *Journal of Guidance, Control, and Dynamics*, 37(5):1583–1594, 2014.
- [35] Tansel Yucelen, Kilsoo Kim, and Anthony Calise. Derivative-free output feedback adaptive control. In *AIAA Guidance, Navigation, and Control Conference*, page 6282, 2011.



A Appendix

A.1 Parameter values for the simulations and adaptive controllers

Matrices of the ideal system:

$$\mathbf{A} = \begin{bmatrix} 0 & 1 \\ -159.4667 & -5.5147 \end{bmatrix}$$

$$\mathbf{B} = \begin{bmatrix} 0 \\ 3.7333 \end{bmatrix} \quad (188)$$

$$\mathbf{C} = \begin{bmatrix} 1 & 0 \end{bmatrix}$$

Parameters of the system for the simulations:

All the friction parameters F_c , F_s , F_v , σ , δ and v_s are roughly estimated for the simulation purposes. However, only the Stribeck velocity and the Stribeck shape factor are employed for the implementation on the real system.

Table 10: Parameters of the system for the simulations

Parameter	Value	Unit
Mass and objective m	1.7	kg
Spring stiffness c	350	N/m
Damping constant d	15	N _s /m
Motor constant k_m	7.5	N/A
Electrical resistance coefficient k_r	1.2	unitless
Coulomb friction force F_c	2.5	N
Static friction force F_s	5	N
Viscous friction σ	1	N
Stribeck velocity δ	0.2	unitless
Stribeck shape factor v_s	0.2	unitless

Matrices of the system for simulations:

$$\mathbf{A}_s = \begin{bmatrix} 0 & 1 \\ -205.8824 & -8.8235 \end{bmatrix}$$

$$\mathbf{B}_s = \begin{bmatrix} 0 \\ 5.2941 \end{bmatrix}$$
(189)

Parameters of the PI-SFC:

Table 11: PI state control parameters.

\mathbf{Q}_{lqr}	$= \text{diag}(10^8, 10^3, 4 \times 10^{13})$
\mathbf{R}_{lqr}	$= 10$
\mathbf{k}^T	$= \begin{bmatrix} -42.7143 & 104.6260 \end{bmatrix}$
k_I	$= 2.0010 \times 10^6$
k_p	$= 2.0804 \times 10^4$
poles	$= -193.42, -101.35 \pm 168.38 i$

Parameters of the model reference:

$$\mathbf{A}_m = \begin{bmatrix} 0 & 1 & 0 \\ -7.7828 \times 10^4 & -396.1186 & 7.4704 \times 10^6 \\ -1 & 0 & 0 \end{bmatrix}$$

$$\mathbf{B}_m = \begin{bmatrix} 0 \\ 7.7828 \times 10^4 \\ 1 \end{bmatrix}$$
(190)

$$\mathbf{C}_m = \begin{bmatrix} 1 & 0 & 0 \\ 0 & 1 & 0 \\ 0 & 0 & 1 \end{bmatrix}$$

$$\mathbf{B}_{mf} = \begin{bmatrix} 0 & 0 & 0 \\ 7.7828 \times 10^4 & 396.1186 & 1 \\ 0 & 0 & 0 \end{bmatrix}$$

$$\mathbf{P} = \begin{bmatrix} 193.0027 & 0.1599 & -1.2445 \times 10^4 \\ 0.1599 & 0.0017 & -6.6931 \times 10^8 \\ -1.2445 \times 10^4 & -6.6931 \times 10^8 & 1.1946 \times 10^6 \end{bmatrix} \quad (191)$$

$$\mathbf{Q} = \begin{bmatrix} 1 & 0 & 0 \\ 0 & 1 & 0 \\ 0 & 0 & 1 \end{bmatrix}$$

Table 12 shows the gain parameters of the adaptive controllers for the simulations and for the implementations on the NPMDM. The gain parameter $\mathbf{\Gamma}_{old,1}$ refers to the gain of the old MRAC algorithm employed for the simulations and $\mathbf{\Gamma}_{old,2}$ refers to the gain parameter of the old MRAC algorithm previously developed on the NPMDM in [19].

Table 12: Gain parameters of the adaptive controllers

$$\begin{aligned} \mathbf{\Gamma}_{old,1} &= \text{diag}(10, 10, 2 \times 10^4) \\ \mathbf{\Gamma}_{old,2} &= \text{diag}(1, 100, 100) \\ \mathbf{\Gamma} &= \text{diag}(10, 10, 10^6, 10^2, 10^2) \\ \mathbf{\Gamma}_u &= \text{diag}(10, 10, 10^6, 10^2, 10^2, 10) \\ \mathbf{K}_2 &= \text{diag}(10, 10, 10^3, 10^2, 10^2) \\ \mathbf{K}_3 &= \text{diag}(10, 10, 10) \\ \mathbf{K}_4 &= \text{diag}(10, 10, 10) \\ \mathbf{\Omega}_1 &= \text{diag}(0.8, 0.8, 0.8, 0.8, 0.8) \\ \mathbf{\Xi}_{11} &= \text{diag}(0.8, 0.8, 0.8) \\ \mathbf{\Xi}_{21} &= \text{diag}(0.8, 0.8, 0.8) \end{aligned}$$

A 2 Simulations

T

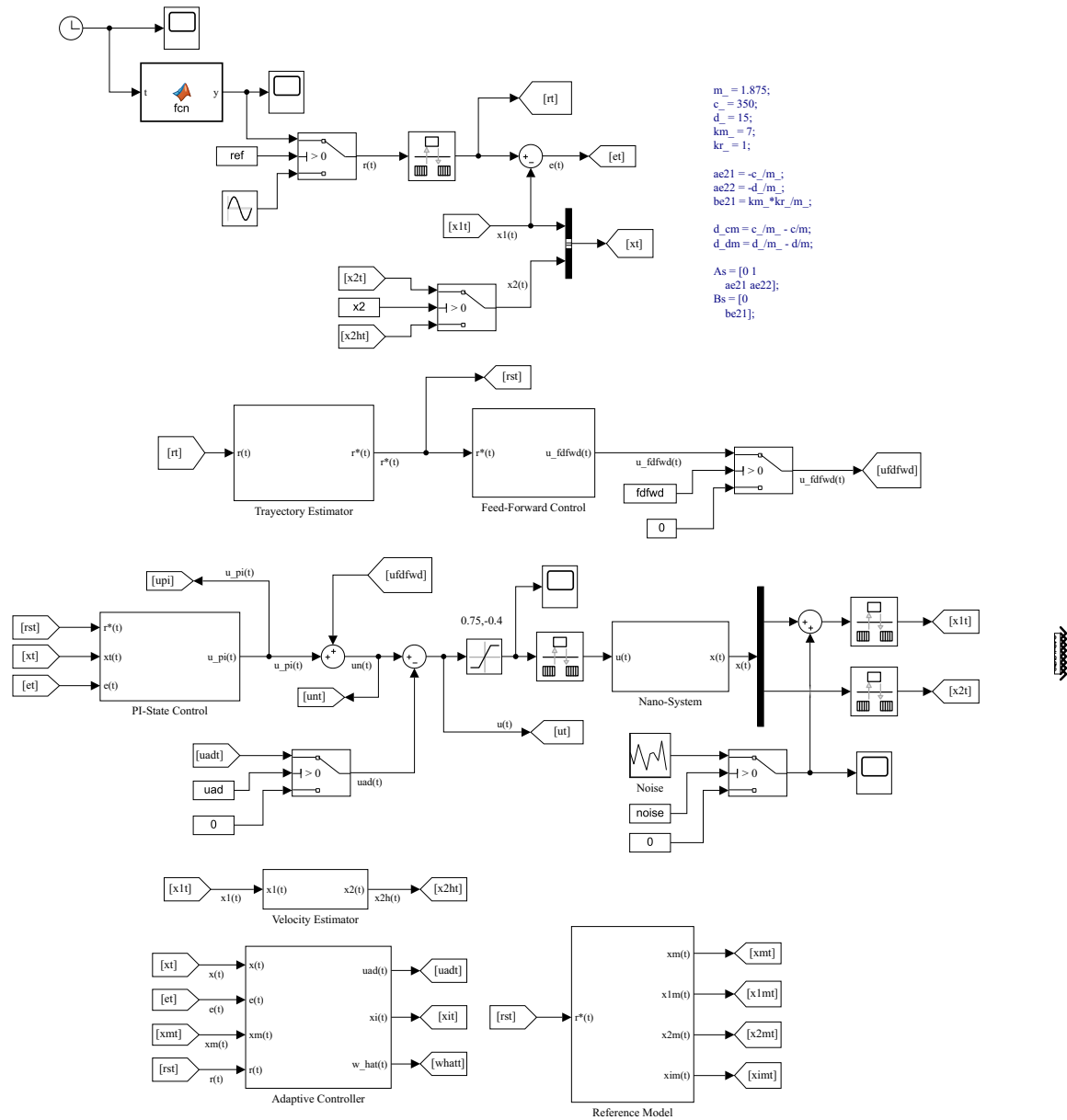


Figure 61: Simulink blocks of the system

Table 13 shows the RMSE and maximum error of the simulations of the Section 4.3.

Table 13: RMSE and maximum error for the extensions to the unknown input matrix.

Adaptive controller	RMSE (nm)	Maximum error (nm)
MRAC _{un}	3.28	14.34
DFMRAC _{un}	3.31	13.94

A.3 Experimental Results

Table 14 shows the maximum error of the experimental results considering a sine reference in the Section 5.1.

Table 14: Maximum error values in nm of the changing sine amplitude test.

A_{\sin}	old MRAC	new MRAC	DFMRAC
100 nm	4.513	3.558	3.818
1 μm	4.134	3.364	3.702
1 mm	129.167	34.758	34.268
4 mm	692.803	230.407	222.736

Table 15 shows the RMSE of the experimental results considering a sine reference in the Section 5.1.

Table 15: RMSE values in nm of the changing sine amplitude test.

A_{\sin}	old MRAC	new MRAC	DFMRAC
100 nm	0.901	0.765	0.803
1 μm	1.052	0.734	0.812
1 mm	50.598	6.536	7.361
4 mm	216.179	42.689	47.343

Sine reference test:

Figure 62 shows the output response when applying the DFMRAC algorithm to a sine reference of a 1000 nm amplitude.

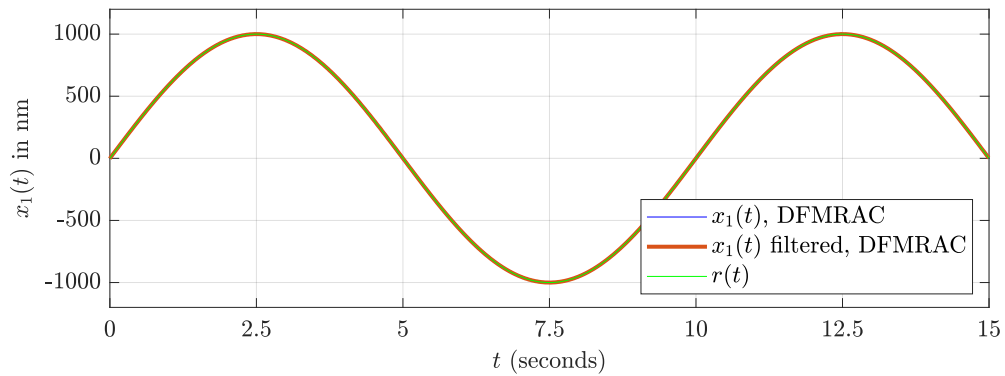


Figure 62: Output response to a $r(t) = 1000 \sin(0.2\pi t)$ nm reference when applying DFMRAC.

Figure 63 shows the output response when applying the DFMRAC algorithm to a sine reference of a 1 mm amplitude.

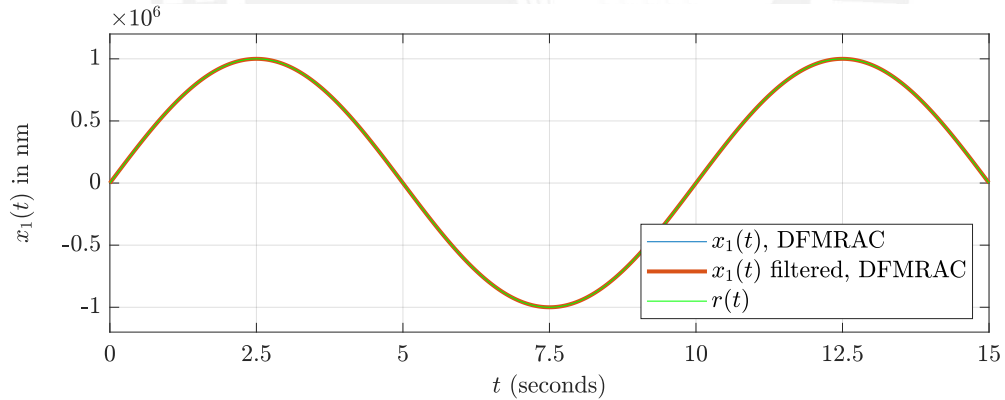


Figure 63: Output response to a $r(t) = 1 \sin(0.2\pi t)$ mm reference when applying DFMRAC.

Figure 64 shows the output response when applying the DFMRAC algorithm to a sine reference of a 4 mm amplitude.

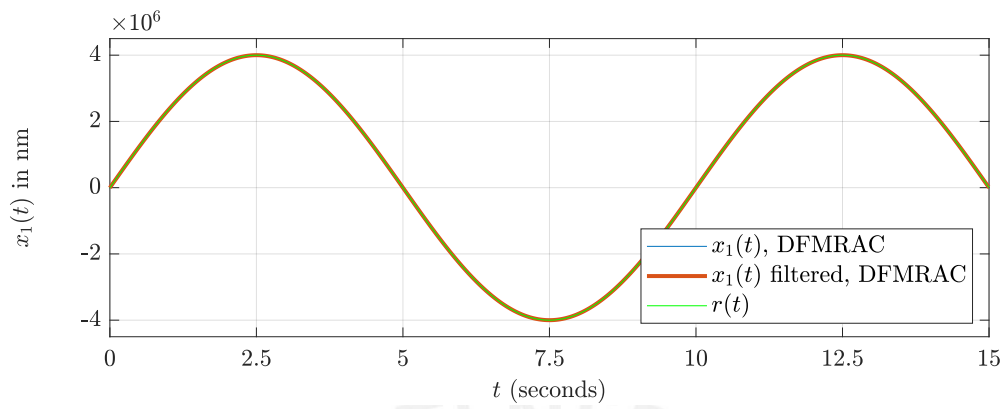
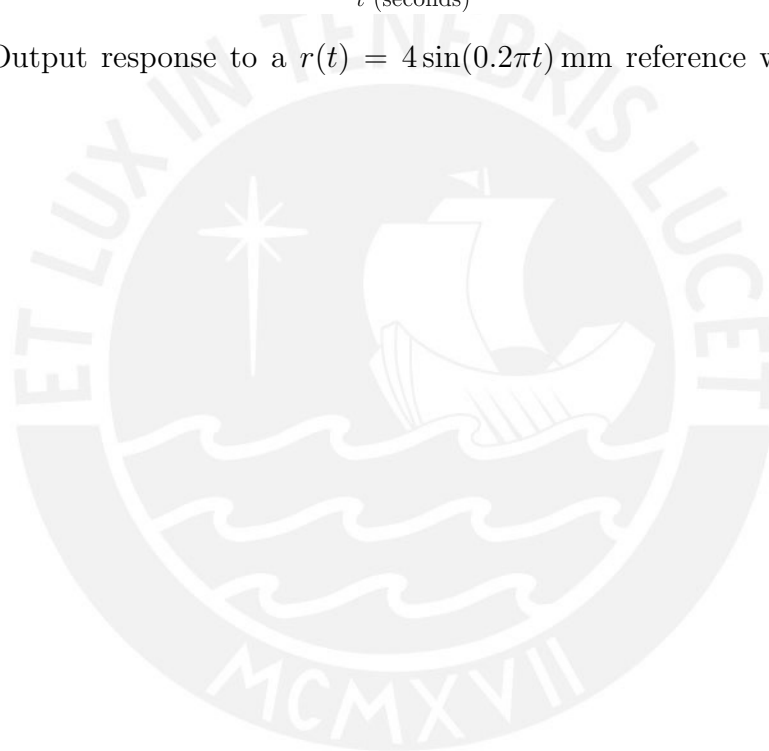


Figure 64: Output response to a $r(t) = 4\sin(0.2\pi t)$ mm reference when applying DFMRAC.



Changing sine amplitude test:

Figure 65 shows the closed loop system error comparison of the changing sine amplitude test with a 5 mm amplitude and a 0.2 Hz frequency.

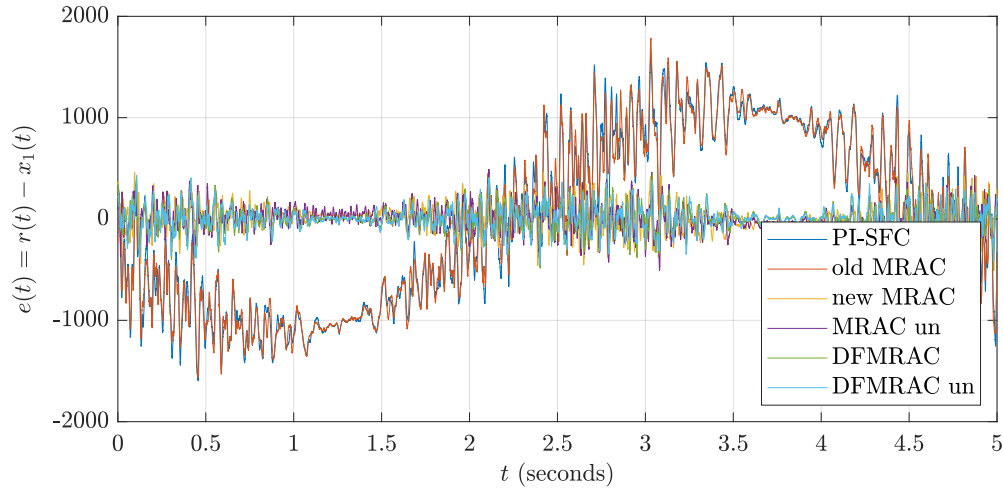


Figure 65: Error comparison regarding the changing sine test with a 5 mm amplitude and a 0.2 Hz frequency.

Figure 66 shows the adaptive control output comparison of the old MRAC, DFMRAC, “DFMRAC un” of the changing sine amplitude test with a 5 mm amplitude.

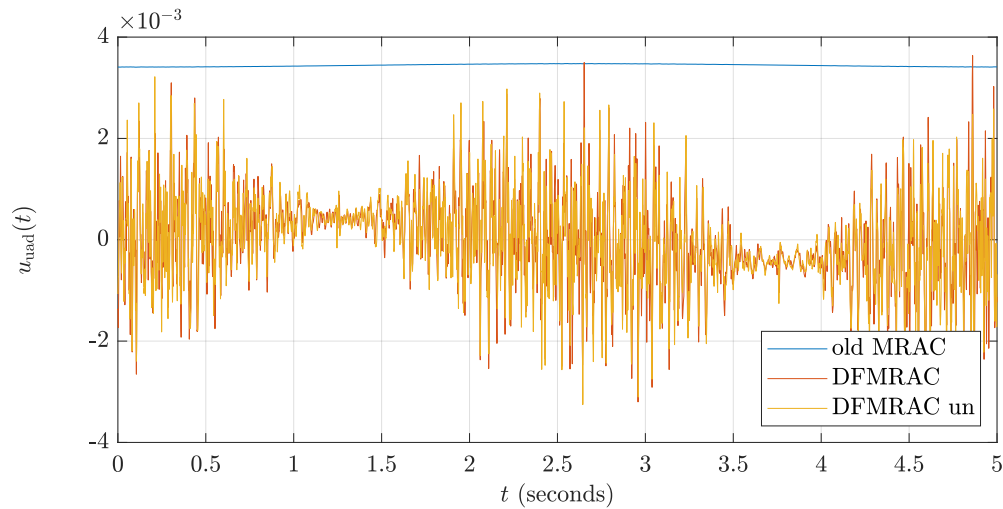


Figure 66: Adaptive control output comparison of the old MRAC, DFMRAC, “DFMRAC un” regarding the changing sine amplitude test with a 5 mm amplitude and a 0.2 Hz frequency.

Figure 67 shows the adaptive control output terms, $u_{ad,1}(t)$, $u_{ad,2}(t)$ and $u_{ad,3}(t)$ of the old MRAC.

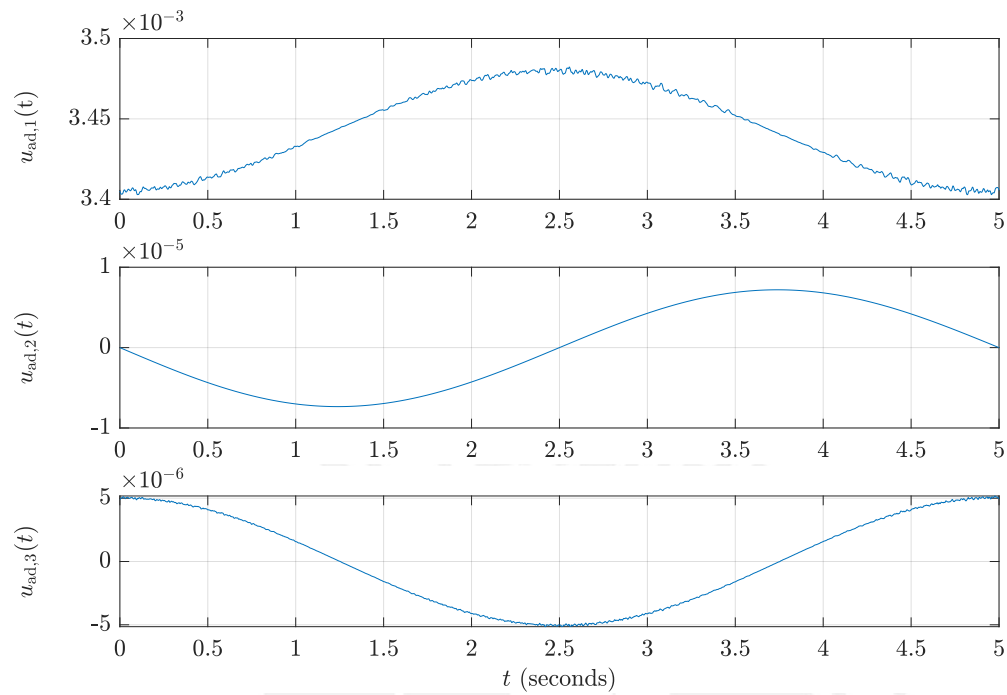


Figure 67: Adaptive control terms of the old MRAC regarding the changing sine amplitude test with a 5 mm amplitude and a 0.2 Hz frequency.

Figure 68 shows the adaptive control output terms, $u_{\text{ad},1}(t)$, \dots , $u_{\text{ad},5}(t)$ of the new MRAC.

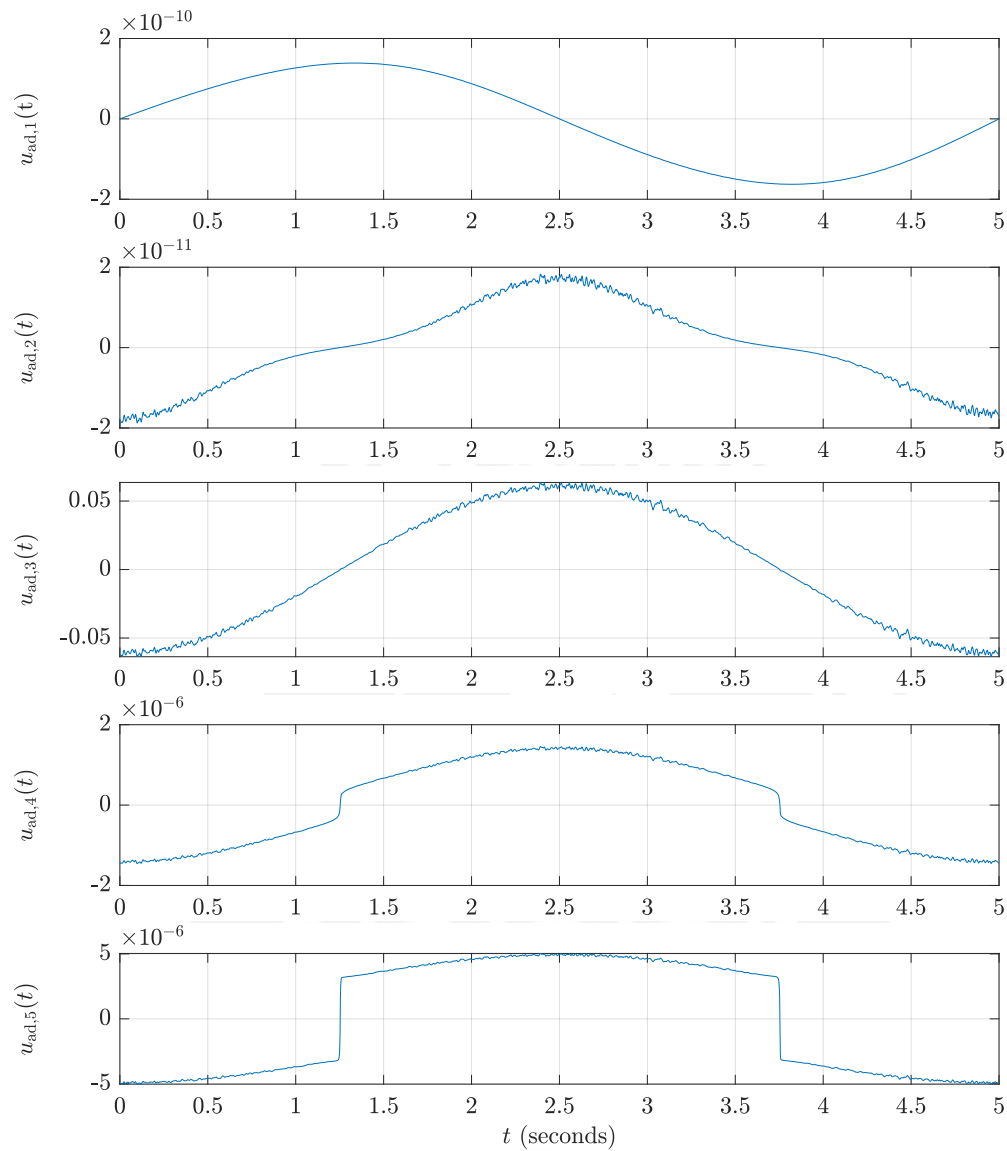


Figure 68: Adaptive control terms of the new MRAC regarding the changing sine amplitude test with a 5 mm amplitude and a 0.2 Hz frequency.

Figure 69 shows the adaptive control output terms, $u_{\text{ad},1}(t)$, \dots , $u_{\text{ad},6}(t)$ of the new “MRAC un”.

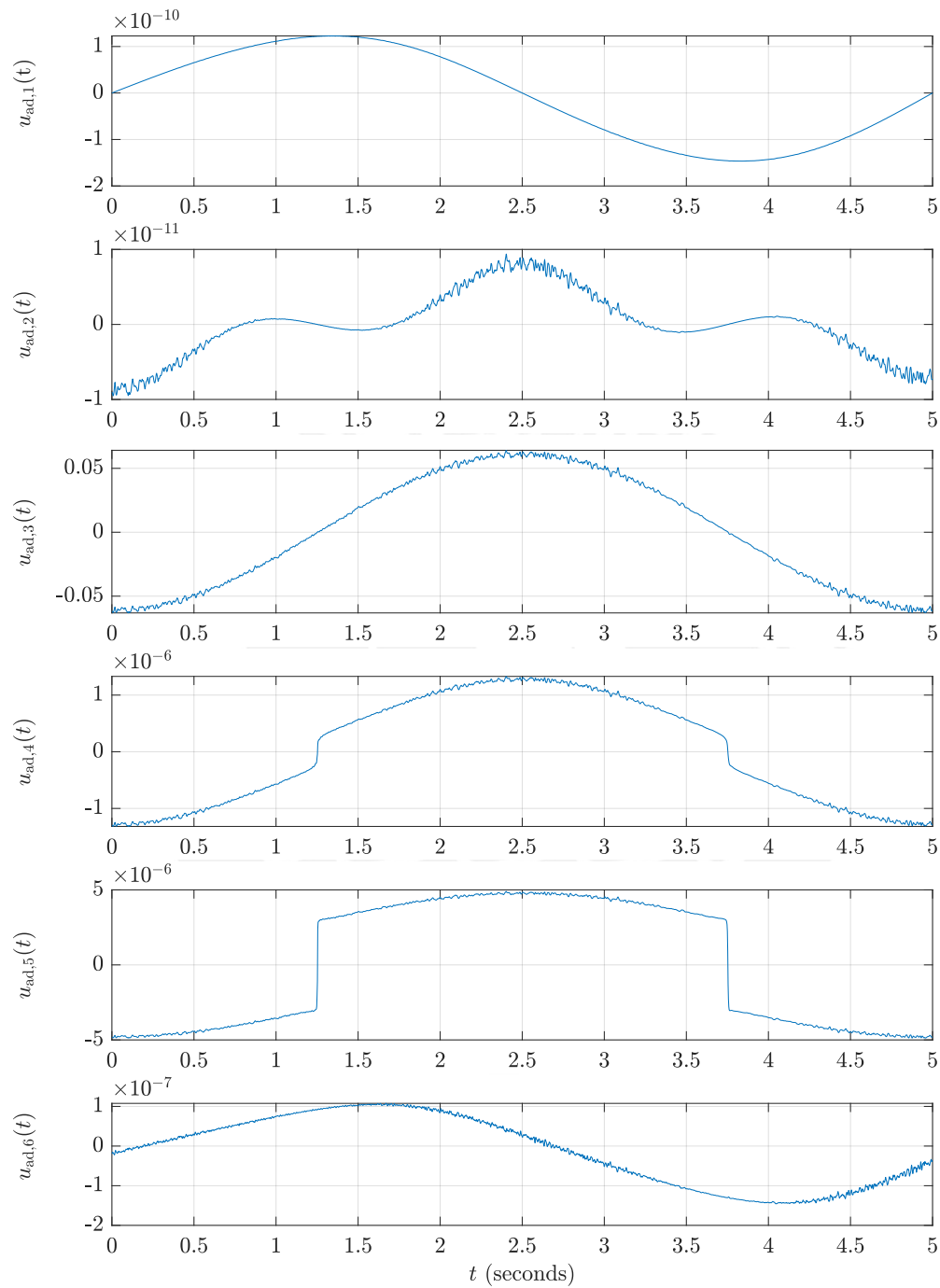


Figure 69: Adaptive control terms of the “MRAC un” regarding the changing sine amplitude test with a 5 mm amplitude and a 0.2 Hz frequency.

Figure 70 shows the adaptive control output terms, $u_{ad,1}(t)$, \dots , $u_{ad,5}(t)$ of the DFMRAC.

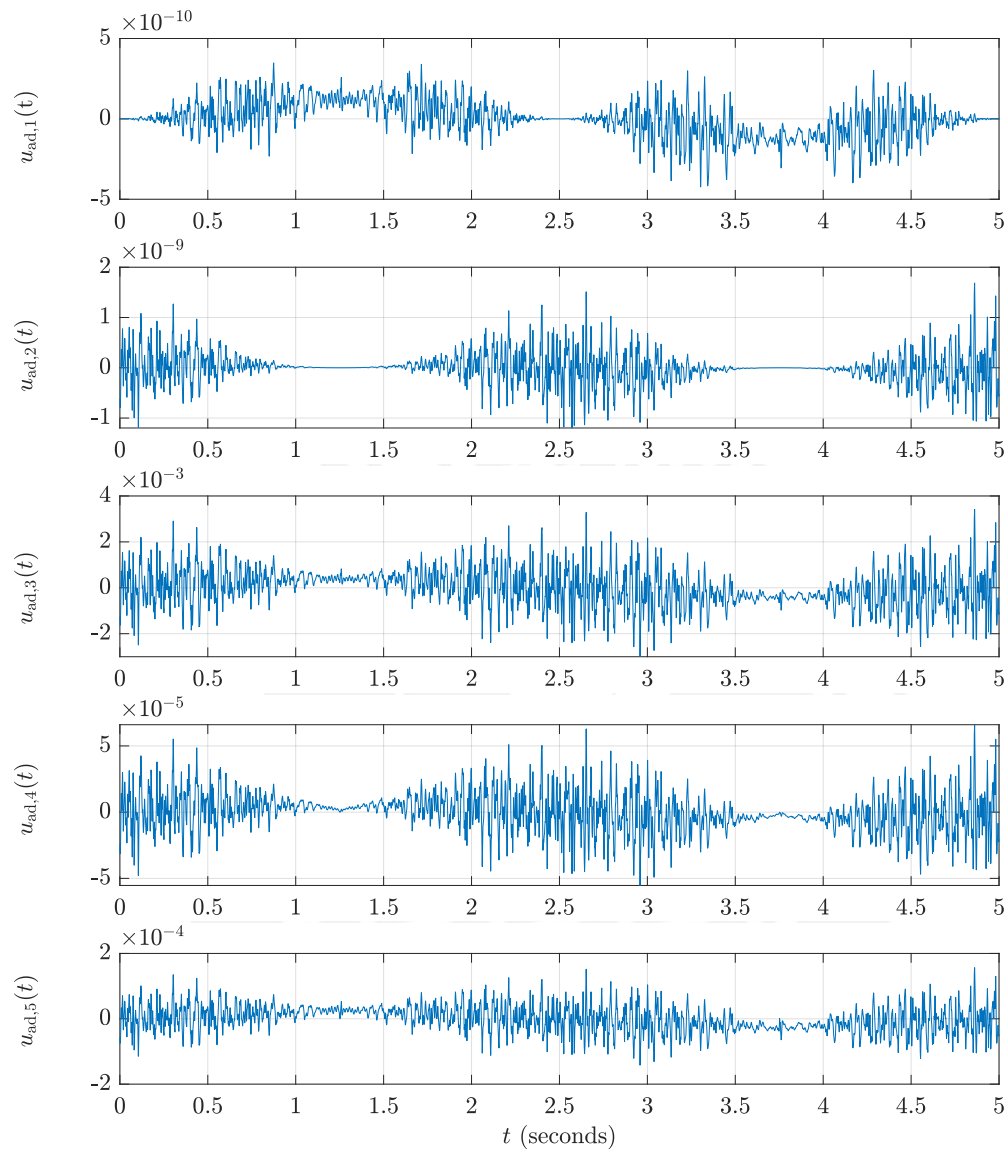


Figure 70: Adaptive control terms of the DFMRAC regarding the changing sine amplitude test with a 5 mm amplitude and a 0.2 Hz frequency.

Figure 71 shows the adaptive control output terms, $u_{\text{ad},1}(t)$, \dots , $u_{\text{ad},5}(t)$ of the “DFMRAC un”.

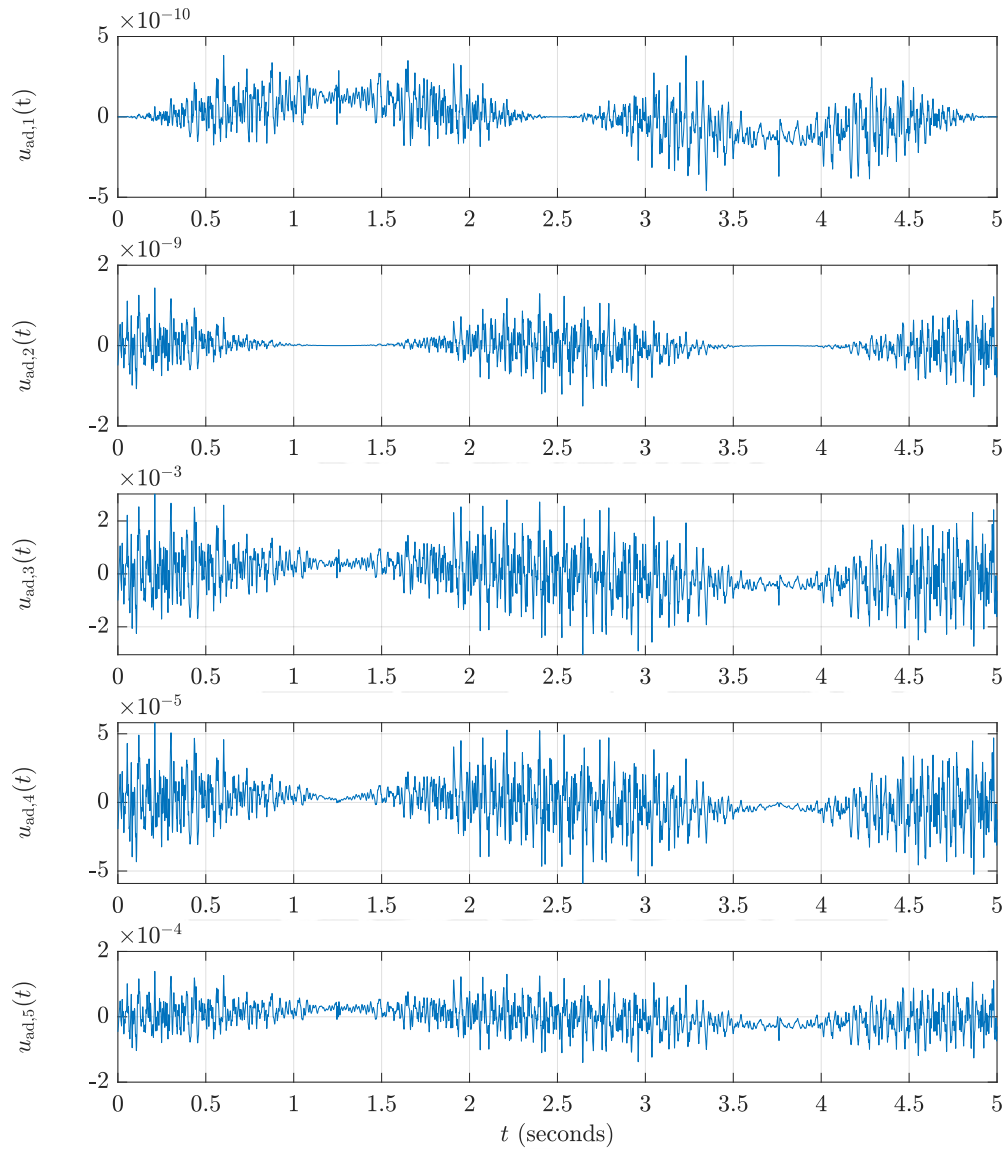


Figure 71: Adaptive control terms of the “DFMRAC un” regarding the changing sine amplitude test with a 5 mm amplitude and a 0.2 Hz frequency.

Figure 72 shows the adaptive control output terms, $u_{ad,6}(t)$, \dots , $u_{ad,11}(t)$ of the “DFMRAC un”. It can be seen that all this terms has a low value in comparison to $u_{ad,3}(t)$, $u_{ad,4}(t)$ and $u_{ad,5}(t)$ in Figure 71.

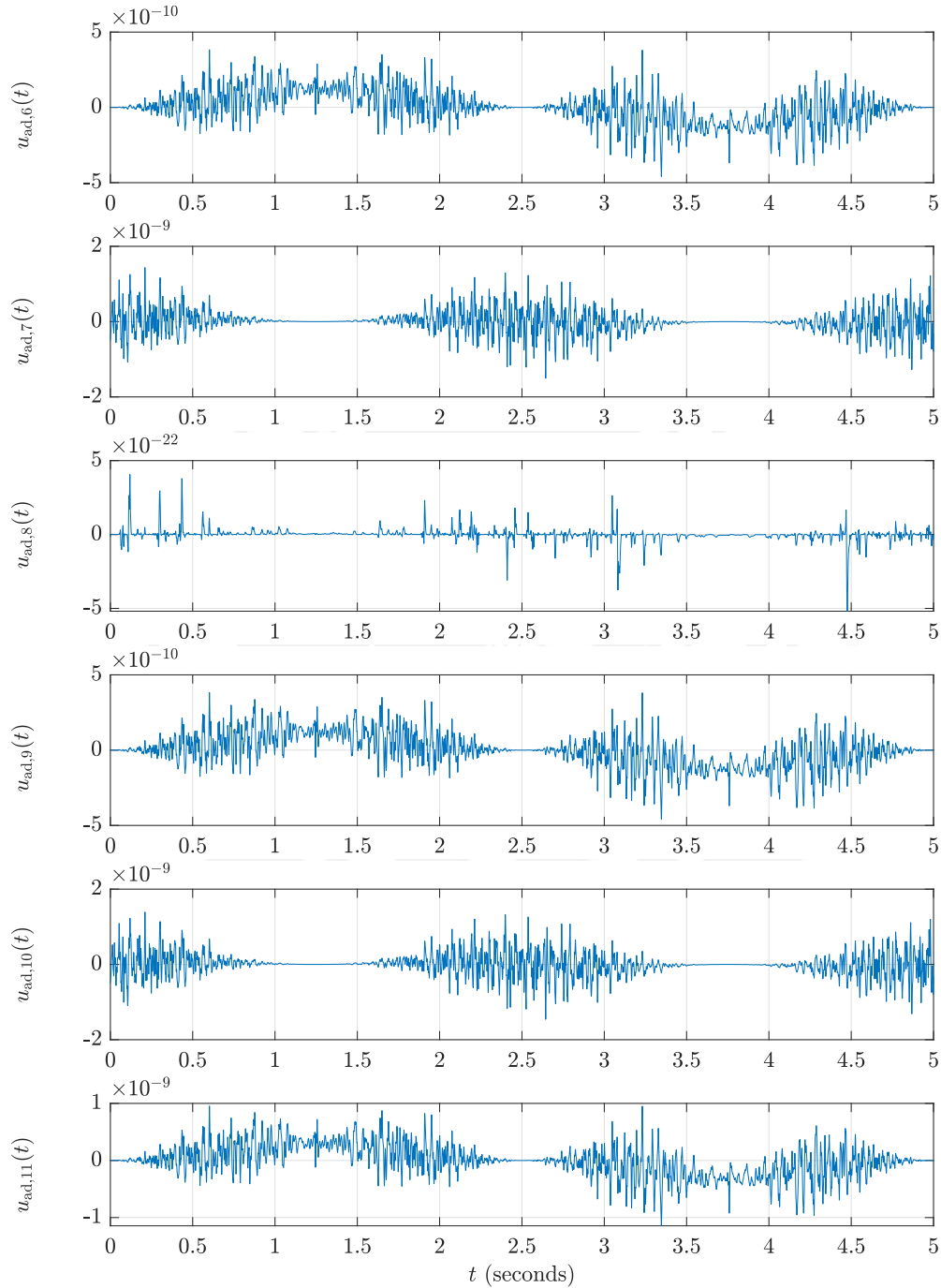


Figure 72: Adaptive control terms of the “DFMRAC un” regarding the changing sine amplitude test with a 5 mm amplitude and a 0.2 Hz frequency.

Changing step maximum velocity test:

Figure 73 shows the adaptive control output terms, $u_{ad,1}(t)$, $u_{ad,2}(t)$ and $u_{ad,3}(t)$ of the old MRAC regarding the changing step maximum velocity test at 5 mm/s velocity.

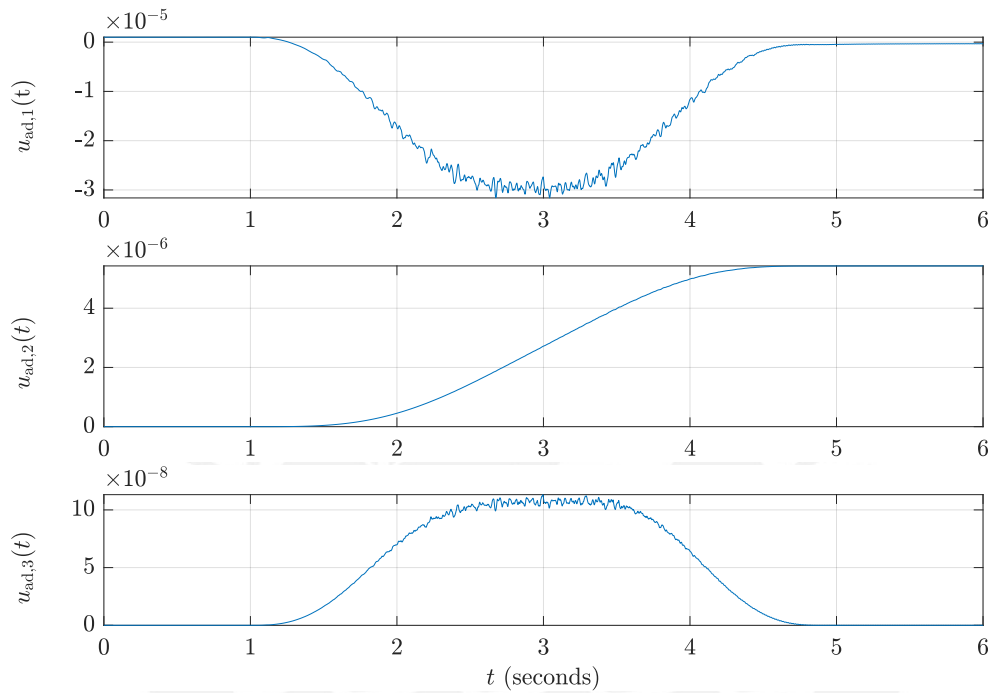


Figure 73: Adaptive control terms of the old MRAC regarding the changing step maximum velocity test at 5 mm/s velocity.

Figure 74 shows the adaptive control output terms, $u_{ad,1}(t)$, \dots , $u_{ad,5}(t)$ of the new MRAC regarding the changing step maximum velocity test at 5 mm/s velocity.

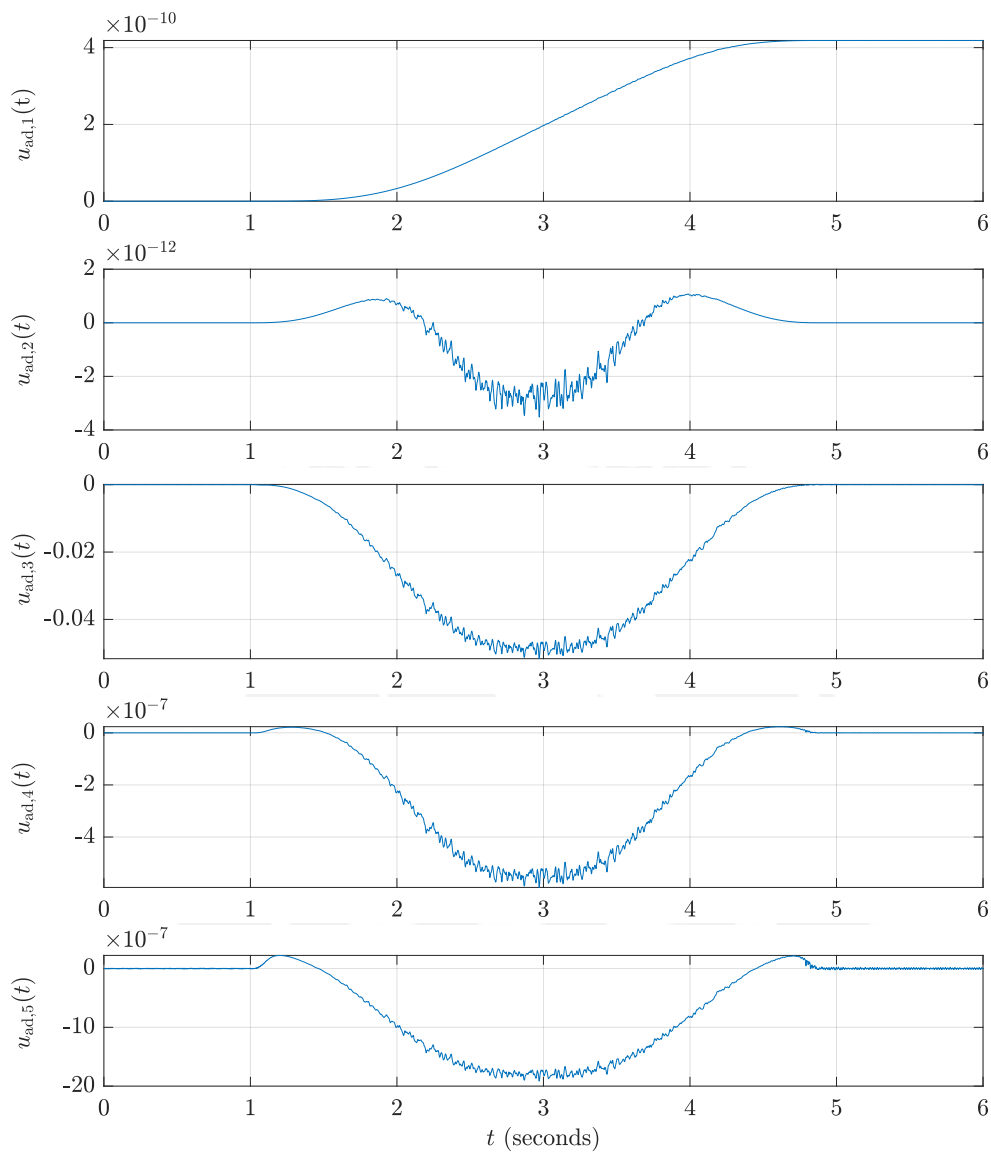


Figure 74: Adaptive control terms of the new MRAC regarding the changing step maximum velocity test at 5 mm/s velocity.

Figure 75 shows the adaptive control output terms, $u_{ad,1}(t)$, \dots , $u_{ad,5}(t)$ of the DFMRAC regarding the changing step maximum velocity test at 5 mm/s velocity.

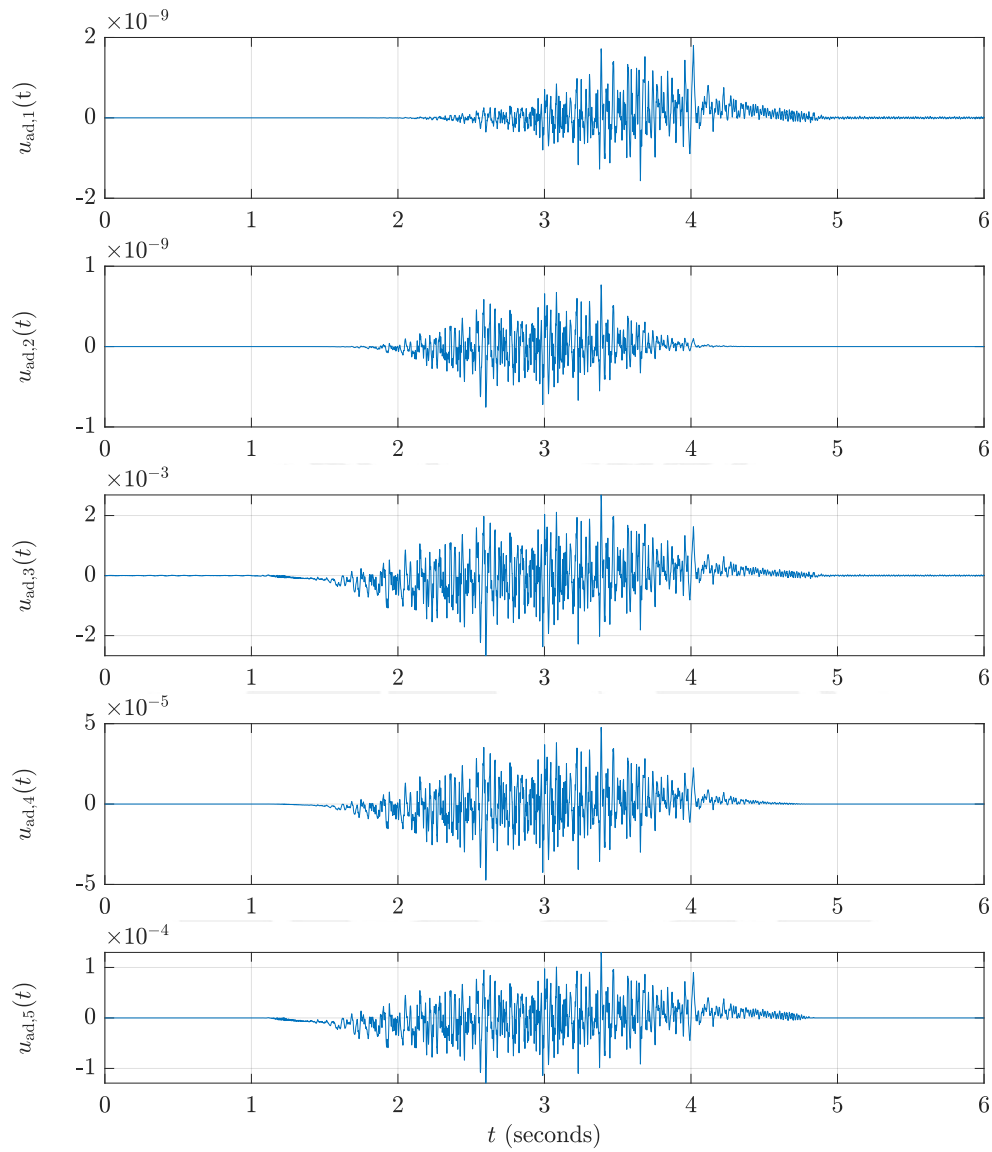


Figure 75: Adaptive control terms of the DFMRAC regarding the changing step maximum velocity test at 5 mm/s velocity.

Figure 76 shows the adaptive control output terms, $u_{ad,1}(t)$, \dots , $u_{ad,5}(t)$ of the “DFMRAC un” regarding the changing step maximum velocity test at 5 mm/s velocity.

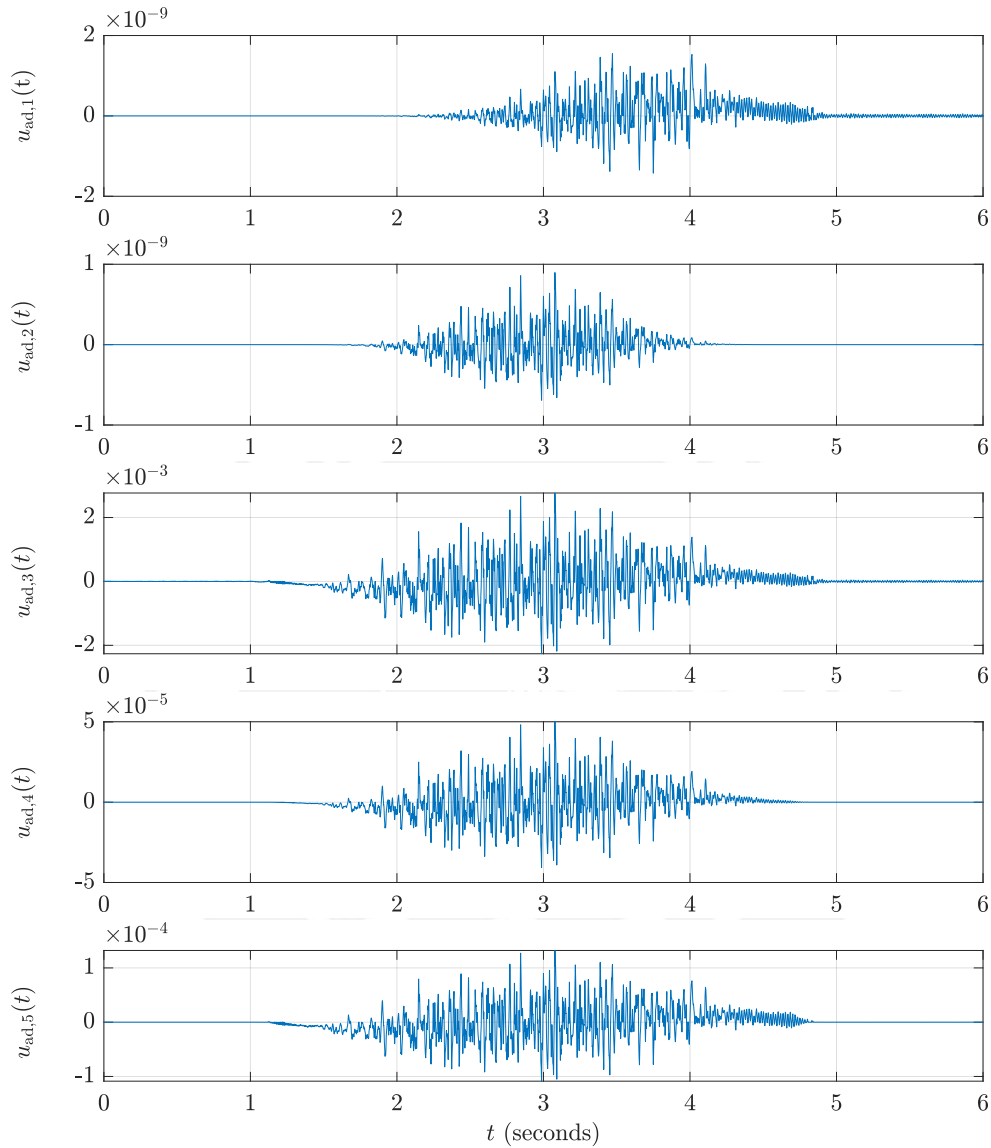


Figure 76: Adaptive control terms of the “DFMRAC un” regarding the changing step maximum velocity test at 5 mm/s velocity.

Figure 77 shows the adaptive control output terms, $u_{ad,6}(t)$, \dots , $u_{ad,11}(t)$ of the “DFMRAC un” regarding the changing step maximum velocity test at 5 mm/s velocity. It can be observed that all this terms has a low value in comparison to $u_{ad,3}(t)$, $u_{ad,4}(t)$ and $u_{ad,5}(t)$ in Figure 76.

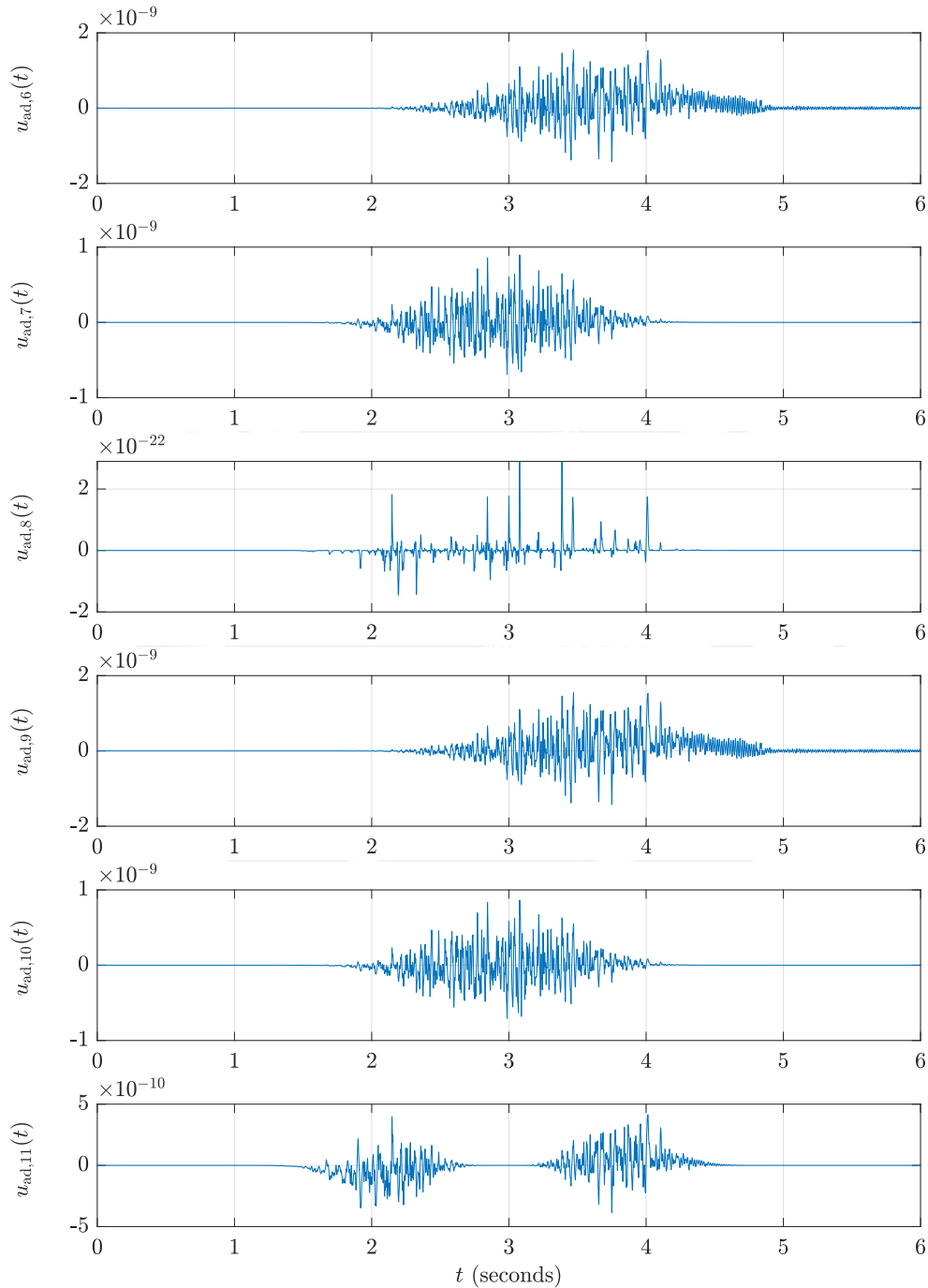


Figure 77: Adaptive control terms of the “DFMRAC un” regarding the changing step maximum velocity test at 5 mm/s velocity.

Step reference tests:

Table 16 shows the maximum error regarding the step reference test with different heights and the multi-step test.

Table 16: Maximum error values in nm from step experiment.

Type	old MRAC	new MRAC	DFMRAC
10 μm	30.124	5.750	5.185
1 mm	196.438	29.435	39.488
Multi-step	231.394	51.024	61.273

Table 17 shows the RMSE regarding the step reference test with different heights and the multi-step test.

Table 17: RMSE values in nm from step experiment.

Type	old MRAC	new MRAC	DFMRAC
10 μm	4.849	0.815	0.759
1 mm	52.383	4.156	4.593
Multi-step	65.623	7.347	8.182

Figure 78 shows the output response of the NPMDM when applying the DFMRAC algorithm to a double step reference with a step height of 1 mm.

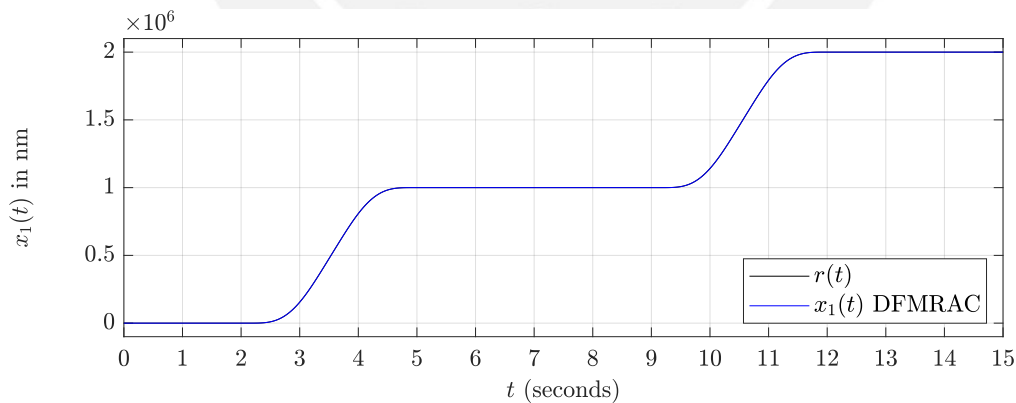


Figure 78: Output response to a 1 mm step height reference with DFMRAC.

Figure 79 shows the velocity of the double step reference test with a step height of $10\ \mu\text{m}$.

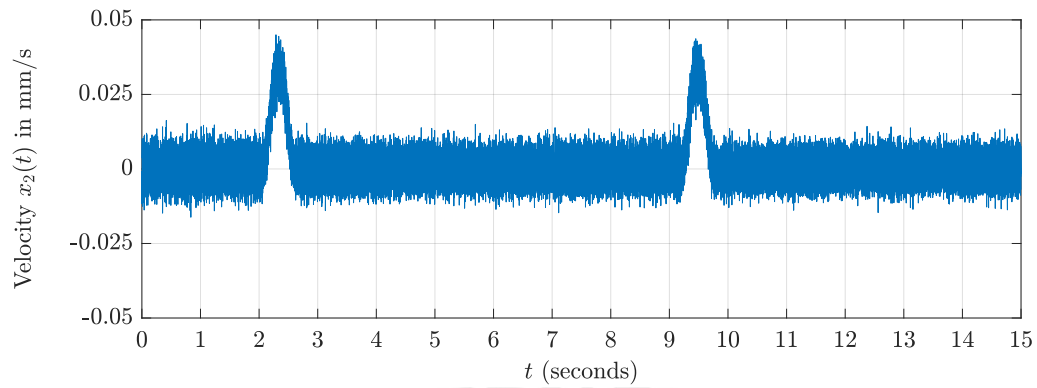


Figure 79: Velocity of the double step reference test with a step height of $10\ \mu\text{m}$.

Figure 80 shows the velocity of the double step reference test with a step height of $1\ \text{mm}$.

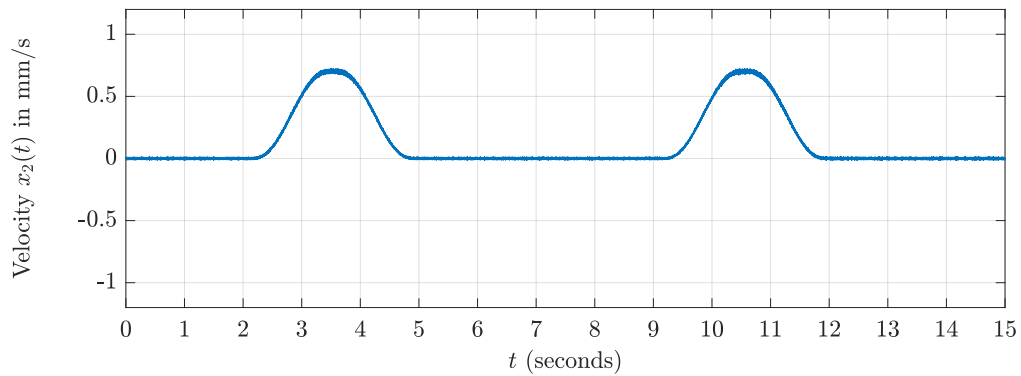


Figure 80: Velocity of the double step reference test with a step height of $1\ \text{mm}$.

Figure 78 shows the velocity of the multi-step reference test.

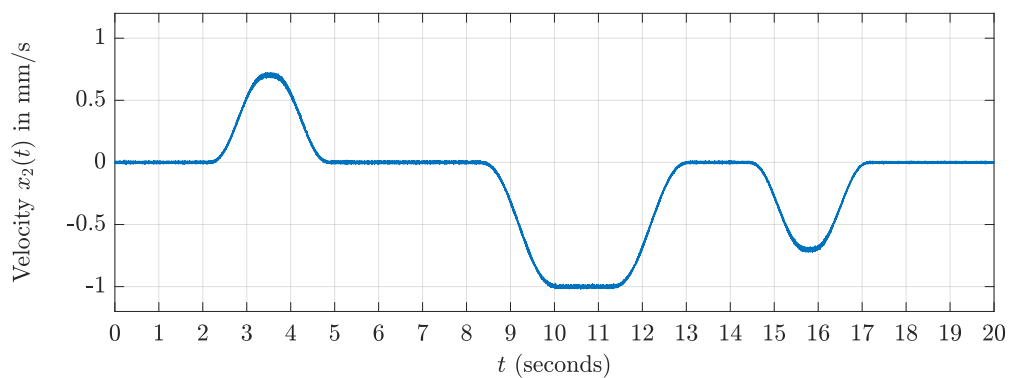


Figure 81: Velocity for the multi-step reference test.

Changing maximum velocity test:

Table 18 shows the maximum error of the step reference test for different velocities. The values from the table corresponds to Figure 55.

Table 18: Maximum error in nm when testing a step reference at different velocities.

Vel. (mm/s)	PI-SFC	old MRAC	new MRAC	MRAC un	DFMRAC	DFMRAC un
1	387.08	401.51	75.70	68.15	89.71	102.15
1.5	480.43	494.78	130.28	104.55	176.26	167.35
2	659.95	636.69	168.38	160.42	211.17	195.15
2.5	793.16	769.33	237.23	197.59	228.59	260.85
3	875.10	854.51	242.90	280.95	275.15	270.23
3.5	988.18	958.40	318.79	300.24	280.16	319.21
4	994.18	1077.50	340.54	324.34	305.86	365.86
4.5	1158.93	1172.36	393.83	387.88	354.10	339.30
5	1382.66	1236.37	447.85	394.09	363.07	420.17

Table 19 shows the RMSE of the step reference test for different velocities. The values from the table corresponds to Figure 55.

Table 19: RMSE in nm when testing a step reference at different velocities.

Vel. (mm/s)	PI-SFC	old MRAC	new MRAC	MRAC un	DFMRAC	DFMRAC un
1	104.11	100.44	16.82	16.43	20.06	20.29
1.5	133.01	131.51	23.39	23.52	28.21	28.38
2	160.84	158.29	29.29	28.91	35.68	35.36
2.5	183.99	181.15	35.28	34.51	39.91	40.21
3	203.78	202.85	39.73	38.68	44.51	44.86
3.5	223.37	222.27	43.17	41.90	46.22	47.09
4	239.63	241.51	45.30	44.90	48.70	51.15
4.5	257.54	257.41	46.91	45.51	51.98	49.56
5	273.03	271.87	49.62	47.89	51.23	52.96